

AECL-11941

Reprinted from

Nuclear Engineering and Design

Nuclear Engineering and Design 180 (1998) 113–131

CATHENA: A thermalhydraulic code for CANDU analysis

B.N. Hanna

*Safety Thermalhydraulics Branch, Atomic Energy of Canada Limited (AECL), Whiteshell Laboratories, Pinawa,
Manitoba ROE 1LO, Canada*

Received 31 January 1997, received in revised form 23 September 1997, accepted 31 October 1997



ELSEVIER

CATHENA: A thermalhydraulic code for CANDU analysis

B.N. Hanna

*Safety Thermalhydraulics Branch, Atomic Energy of Canada Limited (AECL), Whiteshell Laboratories, Pinawa,
Manitoba ROE 1LO, Canada*

Received 31 January 1997; received in revised form 23 September 1997; accepted 31 October 1997

Abstract

This paper describes the Canadian algorithm for thermal hydraulic network analysis (CATHENA) transient, thermalhydraulics code developed for the analysis of postulated upset conditions in CANDU^{®1} reactors. The core of a CANDU reactor consists of a large number of horizontal pressure tubes containing fuel bundles. As a result of the unique design of the CANDU reactor, the CATHENA thermalhydraulic code has been developed with a number of unique modelling capabilities. The code uses a one-dimensional, two-fluid, nonequilibrium representation of two-phase flow. Some of the unique features of the CATHENA code are the one-step semi-implicit numerical method used and the solid heat transfer modelling capability that allows horizontal fuel bundles to be represented in detail. The code has been used in the design and analysis of CANDU-3, CANDU-6 and CANDU-9 reactors. The code has also been used for the design and analysis of the multiple applied lattice experimental (MAPLE) class of reactors and for the analysis of thermalhydraulic experimental programs conducted by Atomic Energy of Canada Limited (AECL) © 1998 Elsevier Science S.A. All rights reserved.

1. Introduction

The Canadian algorithm for thermal hydraulic network analysis (CATHENA) thermalhydraulic code was developed by Atomic Energy of Canada Limited (AECL), Whiteshell Laboratories (WL), primarily for the analysis of postulated accident conditions in CANDU reactors. The development of CATHENA began in 1985 following from earlier thermalhydraulic codes which used equilibrium thermalhydraulic models. Thermalhydraulic modelling switched to nonequilibrium models to more accurately represent the horizon-

tal CANDU fuel channels for two-phase stratified flow conditions predicted during some postulated loss-of-coolant accidents (LOCA).

The CATHENA thermalhydraulic code was designed to be as general as possible. As a result, it has found a wide range of applications. The code is currently in use for the analysis of CANDU-6 reactors and for the designs of future CANDU reactors (i.e. CANDU-3 and CANDU-9). Because of the generality of the input structure and heat transfer models, the code can be used for circuit thermalhydraulic analysis or detailed modelling of fuel channels. The code has also been used in the design and analysis of thermalhydraulic test facilities within AECL. In addition, the code has been used for the design and analysis

¹ CANDU[®] is a registered trademark of Atomic Energy of Canada Limited (AECL)

of the multiple applied lattice experimental (MAPLE) class of research reactors being developed by AECL.

This paper describes the CATHENA thermal-hydraulic model, wall heat transfer models and system models highlighting the unique capabilities of the code required for the analysis of CANDU reactors. The final section of the paper presents the future development plans for the code.

2. Thermalhydraulic model

The thermalhydraulic model in CATHENA is a one-dimensional, non-equilibrium two fluid model similar to that found in other current state-of-the-art reactor analysis codes (TRAC-PFI/MOD1, 1986; RELAP5/MOD3 Ransom et al., 1984; CATHARE Micaelli et al., 1987). The basic thermalhydraulic model consists of six partial differential equations for mass, momentum and energy conservation—three for each phase. The conservation equations are coupled by a flow-regime dependent set of constitutive equations defining the transport of mass, momentum and energy between the phases and between each phase and the pipe walls. In addition, the gas phase may consist of a mixture of up to four noncondensable gas components and the vapour.

A number of authors Slattery (1972), Vernier and Delhay (1968) and Ishii (1978) have discussed the derivation of two-fluid model conservation equations for two-phase flow as a result of time and spatial averages of local, instantaneous conservation equations for each phase. A detailed derivation of the two-fluid model conservation equations used in CATHENA is outside the scope of this paper.

In the conservation equations presented here it is assumed that all quantities represent cross-sectional area and time average values. The mathematical averaging operator notation has been omitted for convenience of presentation.

The two-fluid model conservation equations solved in CATHENA can be written as:

Mass conservation (for phase k);

$$\frac{\partial}{\partial t} \alpha_k \rho_k + \frac{1}{A} \frac{\partial A}{\partial z} \alpha_k \rho_k C_{0k} v_k = m_{ki} - \Gamma_k \quad (1)$$

Momentum conservation (for phase k);

$$\begin{aligned} \frac{\partial}{\partial t} \alpha_k \rho_k C_{0k} v_k + \frac{1}{A} \frac{\partial A}{\partial z} \alpha_k \rho_k C_{1k} v_k^2 + \frac{1}{A} \frac{\partial}{\partial z} \alpha_k P \\ + \frac{1}{A} \beta_k \frac{\partial}{\partial z} \alpha_k = \tau_{kw} + \tau_{ki} + m_{ki} v_{ki} + P'_{ki} - \alpha_k \rho_k g_z \end{aligned} \quad (2)$$

Energy conservation (for phase k);

$$\begin{aligned} \frac{\partial}{\partial t} \alpha_k \rho_k \left[h_k + \frac{v_k^2}{2} \right] + \frac{1}{A} \frac{\partial A}{\partial z} \alpha_k \rho_k C_{0k} v_k \left[h_k + \frac{v_k^2}{2} \right] \\ - \alpha_k \frac{\partial}{\partial t} P - \alpha_k \beta_k \frac{\partial}{\partial t} \alpha_k \\ = q_{kw} + q_{ki} + \tau_{ki} v_{ki} + v_{ki} P'_{ki} + m_{ki} \left(h_{ki} + \frac{v_{ki}^2}{2} \right) \\ - \alpha_k \rho_k v_k g_z \end{aligned} \quad (3)$$

where: A is the cross-sectional area of the conduit; m_{ki} represents the interface mass transfer rate for the k th phase; Γ_k represents a source of noncondensables (zero for the liquid phase); C_{0k} and C_{1k} represent the flow profile coefficients for mass flux and momentum flux, respectively; v_k is the velocity of phase k , α_k is the fraction of the cross-section occupied by phase k ; β_k is the phase-to-interface pressure difference ($P_k - P_i$); τ_{kw} is the wall shear component for phase k ; τ_{ki} is the interface shear for phase k ; P'_{ki} is the apparent mass term; v_{ki} is the intrinsic interface velocity; q_{kw} is the wall heat transfer to phase k ; q_{ki} is the heat transfer from phase k to the interface; h_k is the enthalpy of phase k ; h_{ki} is the enthalpy of phase k at the interface; and g_z is the acceleration due to gravity in the z direction.

In addition to the phase conservation equations, a set of interface constraints or 'conservation' equations must be satisfied. For an infinitesimally thin interface and assuming the effect of surface tension is neglected, the interface constraint for mass momentum and energy can be written as,

$$\sum_k m_{ki} = 0 \quad (4)$$

$$\sum_k [\tau_{ki} + P'_{ki} + m_{ki}v_{ki}] = 0 \quad (5)$$

$$\sum_k \left[q_{wki} + q_{ki} + v_{ki}P'_{ki} + \tau_{ki}v_{ki} + m_{ki} \left(h_{ki} + \frac{v_{ki}^2}{2} \right) \right] = 0 \quad (6)$$

These constraint equations determine the form and value of the constitutive equations for the interphase transfers of mass, momentum and energy. In particular, the interface energy constraint, Eq. (6) defines the mass transfer at the interface (evaporation or condensation) as a function of the interface, q_{ki} , and direct wall-to-interface, q_{wki} energy transfer rates. In CATHENA, the choice of a single interface velocity, $v_{ki} = v_i$, and complementary forms for the virtual mass, $P'_{gi} = -P'_{fi}$, and the interface shear terms, $\tau_{gi} = -\tau_{fi}$, means that these terms do not appear in the interface mass transfer rate expression.

Four noncondensable gases may also be included as components of the gas phase. The noncondensable gas components are assumed to be in local thermal equilibrium with the vapour and are assumed to be transported at the gas velocity. For vapour and noncondensable gas mixtures, the Gibbs–Dalton law for ideal gases is assumed and therefore their thermodynamic state can be defined by a single gas temperature. An additional mass conservation equation, Eq. (7) for each noncondensable gas component is defined in terms of its mass fraction of the total gas mixture,

$$\frac{\partial}{\partial t} A\alpha_g\rho_g X'_{nc} + \frac{\partial}{\partial z} A\alpha_g\rho_g C_{0g}v_g X'_{nc} = A\Gamma'_{nc} \quad (7)$$

where X'_{nc} and Γ'_{nc} are the mass fraction and source term for the i th noncondensable gas component in the gas phase.

To close the mathematical model, the density of each phase, ρ_k , is related to the pressure, P , and the phase enthalpy, h_k . This is performed through a set of bi-quintic Hermite polynomials as described by Liner et al. (1988) that yield the phase entropy, s_k , with continuous first and second derivatives in both pressure and enthalpy. The phase density, ρ_k , and the thermodynamic properties such as phase temperature, T_k and specific heats, C_{pk} , are determined from the derivatives of the entropy function. These thermodynamic prop-

erties have been fit for both H₂O and D₂O. Noncondensable gas properties based on ideal gas approximations are available for H₂, N₂, He, Ar, CO₂ and air.

Although the two-fluid conservation equations are similar for all thermalhydraulic codes the flow regime modelling and the constitutive equations used to model the interphase mass, momentum and energy transfers are code specific. The flow regime modelling and the constitutive equations chosen determine in large part the range of application of a thermalhydraulic code. As a result, some of the constitutive models chosen are specific to CANDU geometry and conditions.

2.1. Flow regime and constitutive equations

In CATHENA, two-phase flows are divided into two flow regime categories: mixed and separated. The mixed flow category includes the disperse bubble, slug, churn and dispersed droplet flow regimes. The separated flow category includes the stratified flow regime for horizontal pipes and the annular flow regime for vertical or inclined pipes. In addition, a ‘piston’ flow regime is defined for injection fronts.

The transition between the mixed and separated flow categories is determined by a transition weighting factor, W_s , that is defined as the product of a number of transition criteria. To remove possible discontinuities in constitutive equations during flow regime transitions, the constitutive equations (for example interface shear, τ_{ki}) are determined by weighting between the values calculated from constitutive relations for mixed and separated flow categories. The weighted constitutive equations are determined from,

$$F_A = W_s F_S + (1 - W_s) F_M \quad (8)$$

where F_A is the flow regime averaged value of the constitutive equation and F_S and F_M are the separated and mixed category value of the constitutive equation, respectively.

Since flow regime transition mechanisms are dependent on the pipe cross-section geometry and orientation the transition criteria are defined separately for horizontal and inclined pipes.

2.1.1. Horizontal pipes

The flow category transition weighting factor, W_s criteria for horizontal pipes is determined as a function of five flow regime transition criteria. The limits of the flow regime transition criteria for horizontal pipes, including the horizontal fuel channels, are shown in Table 1.

The flow regime transition criteria shown in Table 1 are defined as follows:

For piping with a circular cross-section the nondimensional flux, j^* , is defined by,

$$j^* = \frac{j_f}{0.8004\Phi} \text{ for } j_f = \alpha_f v_f \quad (9)$$

where Φ is defined as,

$$\Phi = D_c^{0.4545} \text{ for } j_g < 1.0 \quad (10)$$

or

$$\Phi = D_c^{0.4545} j_g^{0.090909} \text{ for } j_g \geq 1.0 \quad (11)$$

This flow regime transition criterion approximates the stratification limit given by the Weisman et al. (1979) flow regime for horizontal circular pipes. Since CANDU fuel channels contain a string of multiple-element fuel bundles, the above flow regime transition criterion is not adequate. For the fuel channels the following non-dimensional liquid flux flow stratification criterion, replacing Eq. (9), has been developed:

$$j^* = \frac{j_f}{j_{\min}} \text{ where } j_{\min} = 0.085 \text{ m s}^{-1} \quad (12)$$

The second flow stratification criterion was determined from a characteristics analysis of the CATHENA thermalhydraulic model for stratified flow. From the analysis, the stratified flow regime

Table 1
Flow category transition criteria in horizontal pipes

n	$W_n = 1.0$ stratified	$1.0 > W_n > 0.0$ transition	$W_n = 0.0$ mixed
1c	$j^* < 1.0$	$1.0 \leq j^* < 10.0$	$j^* \geq 10.0$
1p	$ j_f < j_{f\min}$	$j_{f\min} \leq j_f < j_{f\max}$	$ j_f \geq j_{f\max}$
2	$U_r^* < 0.75$	$0.75 \leq U_r^* < 1.0$	$U_r^* \geq 1.0$
3	$\alpha_g > 0.1$	$0.1 \geq \alpha_g > 10^{-5}$	$\alpha_g \leq 10^{-5}$
4	$C_s^* < 1.0$	$1.0 \leq C_s^* < 5.0$	$C_s^* \geq 5.0$
5	$U_c^* < 1.0$	$1.0 \leq U_c^* < 11.0$	$U_c^* \geq 11.0$

is stable for relative velocities ($v_r = |v_g - v_f|$) less than the limit specified by the hydrostatic pressure difference between the phases given by,

$$U_r^* = \frac{v_r}{U_r^c} \quad (13)$$

with

$$U_r^c = \left[g \cos \theta \frac{\rho'}{\rho_g \rho_f} \left\{ \rho_f \left(\frac{F_f}{\alpha_f} - F'_f \right) - \rho_g \left(\frac{F_g}{\alpha_g} - F'_g \right) \right\} \right]^{0.5} \quad (14)$$

where the channel geometry parameters, F_k , is the distance from the centroid of a phase to the interface, F'_k is its derivative with respect to the void fraction, α_g , and θ is the angle of inclination of the channel from the horizontal. For 37-element (CANDU) and 7-element bundles² the functions F_k and F'_k are defined through tabular functions. For circular pipes the F_k and F'_k functions can be defined analytically from the geometric relationship between the stratified fluid level and the void fraction. This flow regime transition Eq. (13) criterion is similar to a Helmholtz stability limit.

The third stratification criterion is based on void fraction, α_g . For low void fractions it has been observed experimentally that stratified flow is unstable except under complete stagnation conditions.

The fourth stratification criterion is applied only under countercurrent flow conditions in circular pipes. This stratification criterion represents the flooding limit for countercurrent flow for flow downstream of an elbow in a CANDU feeder. The transition criterion is based on the flooding criterion of Ardron and Banerjee (1986) through the nondimensional parameter C_s^* defined by

$$C_s^* = \frac{|j_g| \sqrt{\rho_g}}{C_f \alpha_g^{3/2} \sqrt{g D_c (\rho_f - \rho_g)}} \quad (15)$$

The fifth stratification criterion accounts for the entrainment of liquid droplets at high relative velocities (i.e. where the gas is moving much faster than the liquid). The criterion is based on the

² 7-Element heated sections are used in some CANDU related experimental facilities.

Table 2
Flow category transition criteria in vertical or inclined pipes

n	$W_n = 1.0$ annular	$1.0 > W_n > 0.0$ transition	$W_n = 0.0$ mixed
1	$ j_d < 3.0$	$1.0 \leq j_d < 5.0$	$ j_d \geq 5.0$
2	$\alpha_g > 0.8$	$0.8 \geq \alpha_g > 0.4$	$\alpha_g \leq 0.4$
3	$U_e^* < 1.0$	$1.0 \leq U_e^* < 11.0$	$U_e^* \geq 11.0$

non-dimensional entrainment velocity, U_e^* , defined by Popov and Rohatgi (1983), given by

$$U_e^* = \frac{|v_g - v_f|}{V_r^c} \tag{16}$$

with

$$V_r^c = \frac{2.6\sigma \sqrt{\rho_d \rho_g} V_\mu^{0.8}}{Re_\delta^{0.2} \mu_r}$$

$$V_\mu = \frac{\mu_r}{\sqrt{\rho_f \sigma} \sqrt{g(\rho_f - \rho_g)}}$$

$$Re_\delta = 2 \cdot \frac{(1.0 - \sqrt{\alpha_g}) \rho_f D_c |v_f|}{\mu_r} \tag{17}$$

2.1.2. Vertical and inclined pipes

The flow category transition weighting factor, W_n , for vertical and inclined pipes is determined as a function of three flow regime transition criteria. The limits of the transition criteria for vertical and inclined pipes are shown in Table 2.

The first flow regime transition criterion accounts for the flow regime transition to churn-turbulent based on liquid superficial velocity developed by Weisman and Kang (1981). The second flow regime transition criterion accounts for the transition to the annular flow regime based on void fraction from the flow regime map of Weisman and Kang (1981). The third flow regime transition criterion accounts for the flow regime transition to the dispersed droplet flow regime as a result of droplet entrainment. This criterion has the same form as that used in horizontal pipes, shown in Eq. (16).

2.1.3. Mixed flow regimes

The mixed flow category in CATHENA includes the dispersed bubble, slug-churn and dis-

persed droplet flow regimes. To insure smooth transitions in the mixed flow category the constitutive equations are determined by the weighting relation,

$$F_m = \psi_b F_b + \psi_s F_s + \psi_d F_d \tag{18}$$

where ψ_b , ψ_s and ψ_d are the weighting factors for the disperse bubble, slug-churn and disperse droplet flow regimes, respectively. The mixed flow category flow regime weighting factors are determined from the mixed flow regime map of Taitel et al. (1980) shown in Fig. 1. This mixed flow regime map is used for both horizontal and vertical piping components.

2.2. Constitutive relations

2.2.1. Virtual mass

In any two-fluid, two-phase flow model a number of constitutive relations are required to represent the transfer of mass, momentum and energy between the phases as functions of the averaged dependent variables. In addition, constitutive relations are required for wall shear and heat transfer to fuel and piping walls. The modelling of heat transfer from fuel and piping walls will be considered after the two-phase flow model has been discussed.

Virtual or apparent mass in a two-fluid model accounts for dynamic pressure differences inte-

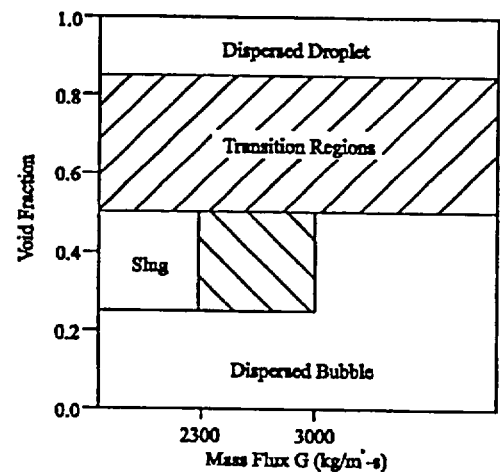


Fig. 1. Mixed category flow regime map.

grated over the interface. The concept of virtual mass has been used in fluid dynamics for a long time (Lamb, 1924) and represents the mass of fluid surrounding an object that would have to be accelerated by the immersed object. Thus, virtual mass limits the relative acceleration of the phases that would result from imposed pressure gradients by increasing the effective mass of the dispersed phase (gas bubbles or liquid droplets). Since the geometry of the interface is flow regime dependent, the magnitude of the virtual mass term is flow regime dependent.

The form of the virtual mass term used in the CATHENA is taken from Stuhmiller (1977), and is given by,

$$P'_{ki} = (-1)^k \rho_{AP} \left[\frac{\partial}{\partial t} v_r + v^* \frac{\partial}{\partial z} v_r \right] \quad (19)$$

where v^* is a convecting velocity which is normally the volumetric mixture velocity. More complex differential forms for the virtual mass term have been proposed, for example that of Drew et al. (1979), however the dominant term in Eq. (19) is the time derivative of the relative velocity. As a result, all of the proposed forms are effectively similar except in regions of high acceleration such as near a break in the circuit. For these special regions other empirical models are used to define the flow rates.

For the separated flow category, stratified and annular, the virtual mass coefficient is small since the interface is primarily parallel to the principal flow direction and therefore is assumed to be zero. For the mixed flow category, the virtual mass coefficient, ρ_{AP} , is given by an expression derived by Hanna et al. (1979) from a study of sonic velocity in two-phase flow.

2.2.2. Phase-to-interface pressure difference

The effect of surface tension has been neglected in CATHENA, however a 'static' phase-to-interface pressure difference arises from two sources:

1. the hydrostatic pressure difference in horizontal stratified flow, and
2. the integrated pressure distribution around interfaces in the flow field arising from form drag.

In the mixed flow category the phase-to-interface pressure difference is assumed to be of the form given by Stuhmiller, (1977). This function for phase-to-interface pressure difference is also used for the annular flow regime. Although no theoretical basis for the above expression exists for the annular flow regime, the form and value of the phase to-interface pressure difference insures that the CATHENA conservation equations are 'well-posed' over a wide range of relative velocities. That is, the characteristics of the resulting conservation equations are real and the equations form a hyperbolic system of equations, Hancox et al. (1980).

For the stratified flow regime, the phase-to-interface pressure difference is determined from the hydrostatic pressure variation with depth in the conduit. For a pipe of arbitrary cross section, the phase-to-interface pressure difference is given by

$$\beta_k = (P_k - P_i) = (-1)^k \rho_k g |F_k| \cos \theta \quad (20)$$

where

$$F_k = y_i - \frac{(-1)^k}{A\alpha_k} \int_{y_k}^{y_i} y f(y) dy \quad (21)$$

In Eq. (21) y_i , y_k and θ are height of the gas-liquid interface, the top and bottom of the conduit and the angle of inclination of the conduit from the horizontal, respectively. For a circular pipe the integrals, F_k , can be determined from analytical expressions in the angle ξ . The angle ξ subtends the interface at the centre of the pipe and can be determined by the solution to the transcendental relation

$$2\pi(1 - \alpha_g) = \xi - \sin \xi \quad (22)$$

For channels containing 37-element and 7-element pin bundles, the integral expressions in Eq. (21) have been evaluated as a function of the interface elevation using tabulated geometric data

2.2.3. Interface shear

The momentum transfer between the phases through interface shear forces is represented in all flow regimes by the relation

$$\tau_{ki} = (-1)^k \frac{A_i \rho_i f_i}{8} (v_g - v_i) |v_g - v_i| \quad (23)$$

where A_i , ρ_i and f_i are the interface area per unit volume, the effective interface density and the D'Arcy friction factor, respectively. For all flow regimes, the calculation of interface shear is arranged such that it remains nonzero as the relative velocity approaches zero. Since the parameters A_i , ρ_i and f_i are dependent on the interface geometry, they are flow regime dependent.

For the disperse bubble flow regime the parameters A_i , ρ_i and f_i are given by

$$f_{ib} = \frac{24(1 + 0.15Re_i^{0.687})}{Re_i} + \frac{f_{i\infty}}{(1 + 4.25 \cdot 10^4 \cdot Re_i^{-1/16})}$$

$$Re_i = \frac{\rho_{ib} D_b v_r}{\mu_f}$$

$$f_{i\infty} = 0.50$$

$$\rho_{ib} = \rho_f$$

$$A_i = \frac{6\alpha_g}{D_b} \tag{24}$$

The bubble diameter is determined from the relation of Wallis (1969) for larger void fractions ($\alpha_g \leq 0.01$) with a fixed bubble number approach being used for smaller void fractions. A smooth transition is insured by choosing the number of bubbles per unit volume, N_b , based on the transition void fraction. The friction factor in Eq. (24) is a modification of the drag coefficient for spherical particles of Clift and Gauvin (1971). The high Reynolds number drag coefficient, $f_{i\infty}$ has been increased from 0.44 to 0.5 to account for bubble deformation to hemispherical capped bubbles at higher relative velocities.

The relations for the slug-churn flow regime follows the approach of Ishii et al. (1981) and are given by

$$A_{is} f_{is} = A_{isb} f_{ib} + A_{iss} f_{iss}$$

$$f_{iss} = 8.16(1 - \alpha_g)(1 - 1.16\alpha_g)^2$$

$$A_{isb} = \max[3.6, 6.0 - 24(\alpha_g - 0.25)]\alpha_{gs} \frac{(1 - \alpha_b)}{D_b}$$

$$A_{iss} = \frac{4.5\alpha_b}{D_c}$$

$$\alpha_{gs} = 0.25 \exp\left[-10 \frac{(\alpha_g - 0.25)}{0.6}\right]$$

$$\alpha_b = \frac{(\alpha_b - \alpha_{gs})}{(1 - \alpha_{gs})}$$

$$\rho_i = \rho_f \tag{25}$$

where the interface friction factor for bubbles, f_{ib} is given by the expression in Eq. (24). For the droplet disperse flow regime, the interface shear parameters are given by,

$$A_{id} = \frac{6.0(1 - \alpha_g)}{D_d} \quad \rho_i = \rho_g \tag{26}$$

where the interface friction coefficient, f_i is defined by the relation of Clift and Gauvin (1971) for spherical particles given in Eq. (24).

For horizontal stratified flow the interface area per unit volume, hydraulic diameter and density are determined for circular pipes from

$$A_{id} = \frac{4 \sin(\xi/2)}{\pi D_c}$$

$$D_i = \frac{\alpha_g \pi D_c}{\pi + \sin(\xi/2) - \xi/2}$$

$$\rho_i = \rho_g \tag{27}$$

where ξ is the angle at the interface subtended by the interface. The expression for the interface friction factor, f_i is a weighted combination of the expressions appropriate to smooth and wavy interfaces given by Kowalski (1987). For pipes containing fuel pin bundles, the interface density is the same, however, the interface area per unit volume, A_i , is determined from tabulated functions.

In the annular flow regime, the interface shear parameters are given by the correlation modified for droplet entrainment (Wallis, 1969),

$$A_{id} = \frac{4 \sqrt{\alpha_g}}{D_c}$$

$$f_i = 0.02[1 + 150\{1 - \sqrt{\alpha + (1 - \alpha_{gc})}\}] \times \max[1.0, U_c^{2.5}]$$

$$\rho_i = \rho_g$$

$$\alpha_{gc} = 1 - \min[E\alpha_f, \alpha_f] \tag{28}$$

with the definition of U_c^* given by the annular flow regime transition relation in Eq. (16) and the entrainment factor, E , is determined by the expression of Popov and Rohatgi (1983).

2.2.4. Wall shear

In CATHENA, different approaches are used for the mixed flow and separated flow categories for the calculation of the wall shear constitutive relation. For mixed flow a two-phase friction multiplier approach is used. Four two-phase friction multipliers are available in CATHENA:

1. HTFS (Chaxton et al., 1972),
2. homogeneous,
3. Martinelli-Nelson, Jones and Dight (1962), and
4. Friedel (1979).

The HTFS (Chaxton et al., 1972) two-phase friction multiplier is the code default since it was correlated over the widest range of two-phase flow conditions. For this two-phase flow multiplier the wall friction term is defined by,

$$\tau_{kw} = -\zeta_k \left[\frac{\tau^* f_{kw}}{D_c} \rho_k |v_k| \frac{v_k}{2} + \left(\frac{k}{l} \right) \rho_m |v_m| \frac{v_m}{2} \right] \quad (29)$$

The wall friction is assumed to be split between the phases based on the void fraction (i.e. $\zeta_k = \alpha_k$) resulting in a smooth approach to the single-phase flow limits. The two-phase multiplier, τ^* , is defined through a similar approach to that used in the RELAP5/MOD2 code (Ransom et al., 1984). The term (k/l) represents the user specified loss coefficient per unit pipe length.

For the separated flow category, annular and horizontal stratified, the wall shear terms are defined individually for each phase by,

$$\tau_{kw} = - \left[\frac{A_{kw} f_{kw}}{D_c} + \alpha_k \left(\frac{k}{l} \right) \right] \rho_k \frac{|v_k|}{2} v_k \quad (30)$$

For both the mixed and separated flow categories the phase-wall friction factor, f_{kw} , is calculated from the Colebrook-White friction factor given the pipe roughness and the phase-wall Reynolds number defined by,

$$Re_{kw} = \frac{\rho_k |v_k| D_c}{\mu_k} \text{ for mixed flow}$$

$$Re_{kw} = \frac{\rho_k |v_k| D_{kw}}{\mu_k} \text{ for separated flow} \quad (31)$$

The hydraulic diameter for the phase, D_{kw} , and the wall-phase contact fraction, A_{kw} , are defined by the interfacial geometry of the separated flow category, void fraction and pipe geometry. For the horizontal-stratified flow regime, the phase-wall contact fractions are given for a circular pipe by the relations of Solbrig et al. (1978). For a stratified flow in a horizontal fuel bundle, the wall-phase contact fraction and the phase hydraulic diameter are defined from tabular functions on void fraction.

In an annular flow, the phase-wall contact fractions and phase-wall hydraulic diameters are defined by the relations of Solbrig et al. (1978). To provide a smooth transition to single-phase gas conditions from the annular flow regime a minimum film thickness of 0.1 mm is assumed.

2.2.5. Interface heat transfer

The interface heat transfer term, q_{ki} , is assumed to consist of a sensible and a latent heat transfer component and is of the form given by Yuen and Chen (1978),

$$q_{ki} = \lambda_{ki}(h_k - h_{ki}) + m_{ki}(h_k - h_{ki}) \quad (32)$$

where λ_{ki} represents a generalized heat transfer coefficient and m_{ki} is the rate of creation per unit volume of phase k . The vapour generation rate is determined by the mass and energy balance at the interface given in Eq. (6). If the kinetic energy contribution to the phase enthalpy is neglected, the resulting vapour generation rate is given by,

$$m_{gi} = \frac{\sum_k q_{wki} + \sum_k \lambda_{ki}(h_k - h_{ki})}{(h_g - h_f)} \quad (33)$$

Since the interface area per unit volume is flow regime dependent, the generalized interface heat transfer coefficients, λ_{ki} , are flow regime dependent except for the metastable states of superheated liquid and subcooled vapour. In Eq. (33), q_{wki} represents the wall heat transfer resulting in vapour generation or condensation. In addition,

the phase enthalpy at the interface, h_{ki} , is assume to be the phase saturation enthalpy, h_k^{sat} . For superheated liquid (i.e. $h_l > h_l^{sat}$)

$$\lambda_{li} = 2 \cdot 10^5 \alpha_l \alpha_g + 0.005(h_l - h_l^{sat}) \quad (34)$$

For subcooled vapour (i.e. $h_g < h_g^{sat}$)

$$\lambda_{gi} = 2 \cdot 10^4 \alpha_l \alpha_g + 0.005(h_g - h_g^{sat}) \quad (35)$$

For the mixed flow regime category the generalized interface heat transfer coefficients are calculated for the disperse-bubble, slug-churn and dispersed droplet flow regimes and weighted using Eq. (18) used previously for interface shear in the mixed flow category. For the dispersed-bubble flow regime λ_{ki} is defined by,

$$\lambda_{kib} = \frac{A_i K_k}{C_{pk} D_b} (2 + 0.5 Re_{ki}^{0.5} Pr_k^{0.3}) \quad (36)$$

For the slug-churn flow regime λ_{ki} is defined by,

$$\lambda_{kis} = A_{isb} \lambda_{kib} + A_{isa} \lambda_{kia}$$

$$\lambda_{kia} = \frac{K_k}{C_{pk} D_i} (Nu_{ki} + 0.5 Re_{ki}^{0.5} Pr_k^{0.3}) \quad (37)$$

where the liquid and gas interface Nusselt numbers, Nu_{li} and Nu_{gi} , are given by,

$$Nu_{li} = 80.0 \quad Nu_{gi} = 3.66 \quad (38)$$

The interface areas per unit volumes, A_{isb} and A_{isa} , are the same as those defined for the interface friction calculation in Eq. (25). For the dispersed-droplet flow regime λ_{ki} is defined by,

$$\lambda_{kid} = \frac{A_i K_k}{C_{pk} D_d} (2 + 0.5 Re_{ki}^{0.5} Pr_k^{0.3}) \quad (39)$$

For the separated flow category, the generalized interface heat transfer coefficient for the gas phase, λ_{gi} , is defined by the Dittus and Boelter (1930) correlation,

$$\lambda_{gi} = 0.023 \frac{A_i K_g}{C_{pg} D_i} Re_{gi}^{0.8} Pr_g^{0.4} \quad (40)$$

for both the annular and the stratified flow regimes.

The generalized interface heat transfer coefficient for the liquid, λ_{li} , is defined by different forms for the stratified and annular flow regimes. For horizontal stratified flow λ_{li} is given by,

$$\lambda_{li} = \frac{A_i K_l}{C_{pl} D_i} (1 + 0.25 Re_{li}^{0.75} Pr_l) \quad Re_{li} = 0.3 \frac{\rho_l |v_{li}| D_i}{\mu_l} \quad (41)$$

whereas in the annular flow regime λ_{li} is defined by,

$$\lambda_{li} = \max(\lambda_{li}^{Lam}, \lambda_{li}^{1urb})$$

$$\lambda_{li}^{Lam} = \frac{A_i K_l}{C_{pl} \max(\delta, 1 \cdot 10^{-5})}$$

$$\delta = 0.5 D_c (1 - \sqrt{\alpha_g})$$

$$\lambda_{li}^{1urb} = 0.065 \frac{A_i K_l}{\mu_l C_{pl}} \sqrt{\rho_l Pr_l \tau_i}$$

$$\tau_i = 0.023 \rho_g v_g^2 Re_g^{-0.2}$$

$$Re_g = \frac{\rho_g |v_g| D_c}{\mu_g} \quad (42)$$

For the special condition of subcooled liquid injection into vapour filled piping a 'piston' like flow regime can form. For this condition condensation on the liquid is reduced since the interface area available for condensation is reduced to approximately the pipe cross-sectional area.

2.2.6. Flow distribution coefficients

The two-phase flow distribution coefficients, C_{ok} and C_{ik} appearing in the mass, momentum and energy conservation equations result from the cross-sectional averaging procedure. These coefficients account for the difference between the products of the average void fraction and phase velocity and the average of the product of void fraction and phase velocities. For example under low flow conditions both the void fraction and the velocity have approximately parabolic profiles. These conditions result in significantly higher gas flow rates (and therefore lower void fractions) than would have been predicted if the profiles had been neglected. These coefficients are normally neglected in PWR codes like RELAP (Chow and Ransom, 1984) but have been included in BWR analysis codes like TRAC-BD1/Mod1 (Taylor et al., 1984). The values of the distribution coefficients used in CATHENA are defined by assuming power-law void and phase velocity profiles. After integration and simplification, the power-law profiles chosen are defined by the C_{oi} coeffi-

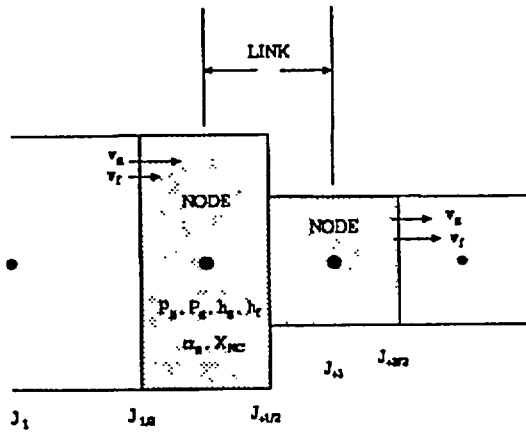


Fig. 2. CATHENA finite-difference mesh arrangement.

cient of Lellouche and Zolotar (1982) that is a function of the phase density ratio, mixture Reynolds number and channel geometry.

3. Two-fluid model numerical solution

The two-fluid thermalhydraulic model forms a set of coupled, nonlinear, first-order partial differential equations with nonlinear source terms. To solve these equations for a piping network representing a CANDU reactor—or test facility—the piping network is idealized by a system of discrete control volumes. The thermalhydraulic finite-difference equations in CATHENA are based on semi-implicit first-order, donor-cell upwind differencing over control volumes, or NODEs, within which mass, energy are conserved and separate control volumes, or LINKs, within which momentum is conserved.

This results in the staggered finite-difference mesh arrangement shown in Fig. 2, where volume average quantities (pressure, void fraction, phase enthalpies, and noncondensable mass fractions) are represented at the NODEs and the phase velocities are represented at the LINKs connecting the NODEs. As a result mass, energy and noncondensable finite-difference conservation equations are derived for the NODEs whereas the finite-difference momentum conservation equations are derived for the LINKs.

For ease of presentation, the thermalhydraulic finite-difference equations used in CATHENA can be grouped into three terms

1. χ_1 for the storage terms,
2. χ_2 for the transport terms, and
3. χ_3 for the source terms

The complete finite-difference conservation equations can then be written in the form,

$$\chi_1 + \chi_2 = \chi_3 \quad (43)$$

Since the form of the finite-difference equations for both gas and liquid phases is similar, only the equations for the gas phase will be presented.

Integration over NODE j and the time interval $t^n \leq t \leq t^{n+1} \Delta t$ of Eq. (1) yields the gas mass finite-difference conservation equation,

$$\begin{aligned} \chi_1 = & \rho_g^n (\alpha_g^{n+1} - \alpha_g^n) \\ & + \alpha_g^n \left[\frac{\partial \rho_g^n}{\partial P} (P_g^{n+1} - P_g^n) + \frac{\partial \rho_g^n}{\partial h_g} (h_g^{n+1} - h_g^n) \right] \\ & + \alpha_g^n \sum_i \left[\frac{\partial \rho_g^n}{\partial X_{nc}^i} (X_{nc}^{i,n+1} - X_{nc}^{i,n}) \right] \end{aligned} \quad (46)$$

$$\begin{aligned} \chi_2 = & \frac{\Delta t}{V_j} \sum_L (AC_{0g})_L \\ & \times \text{sgn}_L [(\alpha_g \rho_g)_j^n v_{gL}^{n+1} + \rho_g^n v_{gL}^n \alpha_g^{n+1} \\ & - (\alpha_g \rho_g)_j^n v_{gL}^n] \end{aligned}$$

$$\begin{aligned} \chi_3 = & \Delta t \left[m_{g1}^n - \Gamma_k^n + \frac{\partial m_{g1}^n}{\partial P} (P_g^{n+1} - P_g^n) \frac{\partial m_{g1}^n}{\partial h_g} \right. \\ & + (h_g^{n+1} - h_g^n) + \frac{\partial m_{g1}^n}{\partial h_f} (h_f^{n+1} - h_f^n) \\ & \left. + \sum_i \frac{\partial m_{g1}^n}{\partial X_{nc}^i} (X_{nc}^{i,n+1} - X_{nc}^{i,n}) \right] + \epsilon_g^n \end{aligned} \quad (44)$$

where the superscript, n and $n + 1$ represent quantities evaluated at time t and $t + \Delta t$, respectively and the subscripts L and J represent quantities for links (i.e. at $j \pm 1/2$) and 'upwind' nodes as determined by the link velocities, respectively. The term sgn_L determines the orientation of the link with respect to the velocity sign convention (i.e. -1 or 1) and V_j is the volume of the j th node. The mass truncation error correction term, ϵ_g^n will be defined at the end of the section.

Integration over LINK $j + 1/2$ and time interval Δt of Eq. (2) yields the gas momentum energy finite-difference conservation equation,

$$\begin{aligned} \chi_1 &= \overline{\alpha_g \rho_g^n}_{j+1/2} [v_g^{n+1} - v_g^n]_{j+1/2} \\ \chi_2 &= \Delta t \left\{ \overline{\alpha_g^n}_{j+1/2} (P_{g_j+1/2}^{n+1} - P_{g_j-1/2}^{n+1}) \right. \\ &\quad + \overline{\beta_g^n}_{j+1/2} (\alpha_{g_{j+1}} - \alpha_{g_j})^{n+1} \\ &\quad \left. + \left(\frac{\alpha_g \rho_g}{2} \right)_{j+1/2}^n [(v_g^n v_g^{n+1})_{j+1/2} - (v_g^n v_g^{n+1})_j] \right\} \\ \chi_3 &= \Delta t \Delta z [\tau_{gw}^{n+1} + \tau_{gi}^{n+1} + m_{gi}^n (v_{gi}^n - v_{gi}^{n+1}) \\ &\quad - \alpha_g \rho_g g_z]_{j+1/2} \\ &\quad - \rho_{AP}^n [\Delta z (v_g^{n+1} - v_g^n - v_f^{n+1} + v_f^n)]_{j+1/2} \\ &\quad + \Delta t v_{j+1/2}^* (v_{g_{j+1/2}} - v_{g_j} - v_{f_{j+1/2}} - v_{f_j}) \\ &\quad + \Delta P_{JNK_g} + \Delta P_{PMP_g} \end{aligned} \quad (45)$$

where the subscripts JNK_g and PMP_g represent terms added to represent piping junctions and pumps, respectively. The subscript, J refers to the 'upwind' link and the overbar notation denotes a node quantity averaged over the link.

Integration over NODE j and time interval Δt of Eq. (3) yields the gas internal energy finite-difference conservation equation,

$$\begin{aligned} \chi_1 &= [(\alpha_g \rho_g)^n (h_g^{n+1} - h_g^n) - \alpha_g^n (P_g^{n+1} - P_g^n) \\ &\quad - \beta_g^n (\alpha_g^{n+1} - \alpha_g^n)]_j \\ \chi_2 &= \frac{\Delta t}{V_j} \sum_L (AC_{0g})_L \\ &\quad \times \text{sgn}_L [-(\alpha_g \rho_g)^n v_{gL}^{n+1} (h_g^{n+1} - h_g^n) \\ &\quad + \rho_g^n (h_{gJ} - h_{gI})^n \\ &\quad \times \{ \alpha_{gI}^n (v_g^{n+1} - v_g^n)_L + v_{gL}^n (\alpha_g^{n+1} - \alpha_g^n)_J \}] \\ \chi_3 &= \Delta t \left[q_{gw}^{n+1} + \lambda_{gi}^n \left\{ h_{gi}^n + \frac{\partial h_{gi}^n}{\partial P} (P_g^{n+1} - P_g^n) \right. \right. \\ &\quad \left. \left. - h_g^{n+1} \right\} \right]_j + \Delta t Q_{PMP}^n \end{aligned}$$

The alternative form for the energy flux term, χ_2 in Eq. (46)) used in CATHENA is given by,

$$\chi_2 = \frac{\Delta t}{V_j} \sum_L (AC_{0g})_L \text{sgn}_L \{ (\alpha_g \rho_g)^n v_{gL}^n (h_g^{n+1} - h_g^n) \} \quad (47)$$

Although the form in Eq. (47) is not entirely consistent with the finite-difference form used for the mass conservation, Eq. (44), it reduces the number of entries in the global finite-difference matrix resulting in a significant reduction in the computational effort for some problems. No significant differences in the solutions have been found using Eq. (47).

In addition to the phase conservation equations a species conservation equation is required for each noncondensable constituent included in the gas phase. The noncondensable finite-difference equation is determined by the integration of Eq. (7) over NODE j and time interval Δt to yield,

$$\begin{aligned} \chi_1 &= (\rho_g X_{nc}^i)^n (\alpha_g^{n+1} - \alpha_g^n)_j \\ &\quad + \left[\frac{\partial \rho_g^n}{\partial P} (P_g^{n+1} - P_g^n) + \frac{\partial \rho_g^n}{\partial h_g} (h_g^{n+1} - h_g^n) \right. \\ &\quad \left. + \sum_{k \neq i} \frac{\partial \rho_g^n}{\partial X_{nc}^k} (X_{nc}^{k,n+1} - X_{nc}^{k,n}) \right] (\alpha_g X_{nc}^i)^n \\ &\quad + (\alpha_g \rho_g)^n (X_{nc}^{i,n+1} - X_{nc}^i)_j \\ \chi_2 &= \frac{\Delta t}{V_j} \sum_L (AC_{0g})_L \\ &\quad \times \text{sgn}_L [-2(\alpha_g \rho_g X_{nc}^i)^n v_{gL}^n + (\alpha_g \rho_g X_{nc}^i)^n v_{gL}^{n+1} \\ &\quad + (\rho_g X_{nc}^i)^n v_{gL}^n \alpha_g^{n+1} + (\alpha_g \rho_g)^n v_{gL}^n X_{nc}^{i,n+1}] \\ \chi_3 &= \Delta t \Gamma_{ncj}^n \end{aligned} \quad (48)$$

The above set of coupled, semi-implicit, finite-difference equations for all NODEs and LINKs in the thermalhydraulic network form a single sparse matrix,

$$\bar{D} \bar{x} = \bar{B} \quad (49)$$

where \bar{D} is the matrix of coefficients for the 'new time' (i.e. t^{n+1}) variables in the vector \bar{x} and \bar{B} contains all the 'old time' variable terms. This sparse finite-difference matrix equation is solved by the Harwell MA28 (Duff, 1980) sparse matrix solution subroutine library for the \bar{x} variables.

Since the density of the phases is not a linear function of pressure and phase enthalpy a truncation error in mass and energy can develop over a time step. An additional error may also result during transitions between two-phase and single-phase conditions since the void fraction must be

limited to values between zero and unity. To prevent this truncation error from accumulating, a mass correction term is calculated for each phase and applied in the subsequent time step. The truncation error for the gas mass conservation, ϵ_g^{n+1} is calculated for each NODE from,

$$\begin{aligned} \epsilon_g^{n+1} &= \alpha_g^n \overline{\rho_g^{n+1}} + \rho_g^n (\alpha_g^{n+1} - \overline{\alpha_g^{n+1}}) - \alpha_g^{n+1} \rho_g^{n+1} \\ \overline{\rho_g^{n+1}} &= \rho_g^n + \frac{\partial \rho_g^n}{\partial P} (P_g^{n+1} - P_g^n) + \frac{\partial \rho_g^n}{\partial h_g} (h_g^{n+1} - h_g^n) \\ &\quad + \sum_i \frac{\partial \rho_g^n}{\partial X_{nc}^i} (X_{nc}^{i,n+1} - X_{nc}^{i,n}) \end{aligned} \quad (50)$$

where $\overline{\alpha_g^{n+1}}$ is the solution of the finite difference equation before limiting its value to between zero and unity. This mass conservation correction algorithm is similar to that applied in the RELAP5/MOD2 code (Ransom et al., 1984).

Since all of the flux (mass, momentum and energy) terms in Eqs. (44)–(48) are treated semi-implicitly the finite-difference equations are linearly stable for all timestep sizes. This can be inferred both from Hirt's heuristic stability analysis (Roach, 1982) and a linear stability analysis. However, since the source terms—in particular the heat transfer and vapour generation rates—can be highly nonlinear a timestep control algorithm is required to ensure simulation accuracy.

The timestep control algorithm in CATHENA samples the rates of change of all dependent variables, truncation error and wall temperatures. The maximum rates of change for these variables are compared with preset limits to determine a timestep multiplier for the subsequent time step. In addition, if a maximum rate of change exceeds a preset limit, the current time step is rejected and is redone at a smaller time step. The timestep control algorithm was described in detail by Richards and McDonald (1981).

4. Wall heat transfer modelling

The wall heat transfer model within CATHENA is referred to as the generalized heat transfer package (GENHTP). GENHTP consists of three major modelling components:

1. wall-to-fluid heat transfer

2. wall-to-wall heat transfer, and
3. conduction within solid models.

Any number of GENHTP models can be coupled to one or more thermalhydraulic nodes. The GENHTP is very flexible in that the model geometry and the connection of all heat transfer surfaces to the thermalhydraulic model are specified through the input file. As a result, a very detailed heat transfer description of a CANDU fuel channel can be assembled by combining a number of GENHTP models. A simplified representation of CANDU fuel channel illustrating many of the capabilities of GENHTP is shown in Fig. 3.

The wall-to-fluid models within GENHTP include all of the flow boiling regimes encountered during postulated transients, single-phase liquid, nucleate boiling, transition boiling, film boiling, single-phase vapour convective heat transfer and condensation. Subcooled nucleate boiling can also be modelled with vapour being directly generated in the two-fluid CATHENA thermalhydraulic model. The modes of heat transfer are governed by the boiling curve as illustrated in Fig. 4. To provide user flexibility, a number of heat transfer coefficient options are available including those for CANDU conditions and longitudinally-finned MAPLE fuel.

The conduction models available within GENHTP include one-dimensional radial conduction

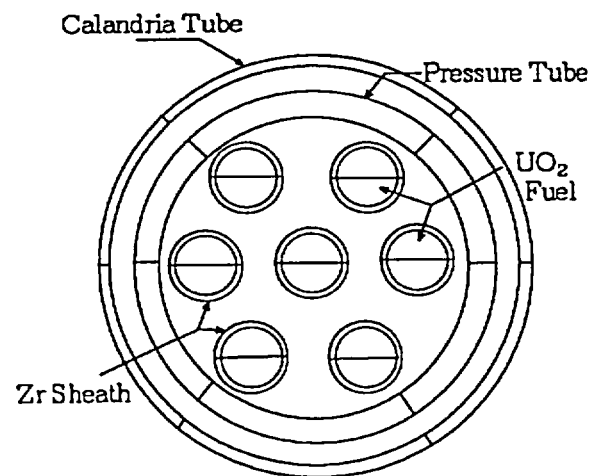


Fig. 3 Sample geometry for a fuel channel GENHTP

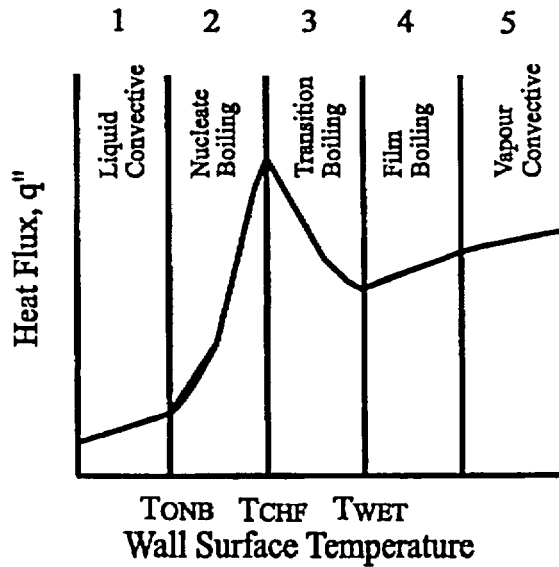


Fig. 4. Boiling heat transfer categories.

and two-dimensional radial plus circumferential conduction. A number of built-in temperature dependent material property functions are available in GENHTP for common reactor materials such as carbon steel, stainless steel, zirconium, zirconium oxide and uranium oxide. Temperature dependent material property tables for less common materials can also be specified through input. Heat generation within GENHTP models is determined by user supplied tables or through feedback from the point-reactor kinetics model in CATHENA. The heat generation models available also include the energy liberated by the zirconium-steam reaction.

The wall-to-wall heat transfer models available in GENHTP include both thermal radiation heat transfer and solid-to-solid contact conduction models. As well, GENHTP includes a fuel channel deformation model that determines pressure-tube straining into either contact with the calandria tube or pressure-tube failure.

4.1. Solid conduction models

All GENHTP models are assumed to be circular in cross-section. As a result, GENHTP calculates conduction heat transfer within fuel elements

or piping walls through the numerical solution of the conduction equation in cylindrical co-ordinates,

$$\rho C_p \frac{\partial T}{\partial t} = \frac{1}{r} \frac{\partial}{\partial r} \left(Kr \frac{\partial T}{\partial r} \right) - \frac{K}{r^2} \frac{\partial^2 T}{\partial \theta^2} + q''' \tag{51}$$

subject to a set of convective boundary conditions given by,

$$K \frac{\partial T}{\partial \eta} \Big|_{\eta} = h_{c\eta} (T_{\eta}^i - T_{\eta}^e) \tag{52}$$

where, T_{η}^i , refers to the environment temperature for the i th surface and, η is the normal direction to the i th boundary surface. Surface boundary conditions—for either heat transfer to the CATHENA thermalhydraulic node or through user specified boundary conditions to an external environment—may be applied to both inside and outside radial boundaries. In the case of radial plus circumferential conduction, boundary conditions may also be specified for individual GENHTP model sectors.

The heat conduction Eq. (51) is solved, subject to the surface boundary conditions in Eq. (52), by a finite-element, variational technique (Rayleigh–Ritz) in the radial direction with a finite-difference term for the circumferential conduction term. This technique was chosen because of earlier experience with the numerical method and that it guarantees convergence of the temperature field (average) from higher temperatures as the radial nodalization is refined.

The discussion of the heat conduction in GENHTP applies to the two-dimensional—radial plus circumferential—solution, however with the appropriate simplifications it also applies to the solution of the one-dimensional radial conduction equations. The variational approach to the solution of the heat conduction Eq. (51) is to seek a stationary value to the functional,

$$F(T) = \int_{r_1}^{r_m} \left[\frac{\partial T}{\partial r} Kr \frac{\partial T}{\partial r} - 2T_1 \left(Q' - \rho C_p \frac{\partial T}{\partial t} \right) \right] dr + r_1 (h_{c1} T^2 - 2Th_{c1} T_{\eta}) \Big|_{r_1} + r_m (h_{cm} T^2 - 2Th_{cm} T_{\eta}) \Big|_{r_m} \tag{53}$$

where the term, Q' , is given by sum of the heat generation per unit volume and the circumferential heat conduction term or,

$$Q' = q''' + \frac{K}{r} \frac{\partial^2 T}{\partial \theta^2} \quad (54)$$

The first variation of the functional, $F(T)$, is taken using $\delta(\partial T/\partial r) = \partial(\delta T)/\partial r$. After partial integration,

$$\begin{aligned} \delta F(T) &= \int_{r_1}^{r_m} \delta T \left[-\frac{\partial}{\partial r} \left(Kr \frac{\partial T}{\partial r} \right) - r \left(Q' - \rho C_P \frac{\partial T}{\partial t} \right) \right] dr \\ &+ 2r_1 \delta T \left(-K \frac{\partial T}{\partial r} + h_{c1}(T - T_a) \right) \Big|_{r_1} \\ &+ 2r_m \delta T \left(K \frac{\partial T}{\partial r} + h_{cm}(T - T_{fm}) \right) \Big|_{r_m} \quad (55) \end{aligned}$$

At the stationary point, $\delta F(T)$ is equal to zero for an arbitrary δT . This implies that each of the three bracketed terms in Eq. (55) has to be identically zero. To find the stationary point of $F(T)$, a trial function, ψ , is defined for an estimate of the radial temperature field as a linear combination of functions of the radius, r , by

$$T(r) = \psi(r) = \sum_{i=1}^N c_i \beta_i(r) \quad (56)$$

where c_i and β_i are the undetermined coefficients and the independent co-ordinate functions. The stationary point of $F(T)$ is obtained by taking,

$$\frac{\partial F(\bar{C})}{\partial c_i} = 0 \quad \text{where } i = 1, 2, \dots, N \quad (57)$$

This generates the matrix transient heat conduction equation

$$\bar{A}_1 \frac{d\bar{C}}{dt} + \bar{A}_2 \bar{C} = \bar{B} \quad (58)$$

which is solved by an implicit finite-difference scheme,

$$(\bar{A}_1^* + \Delta t \bar{A}_2^*) \bar{C}^{n+1} = \Delta t \bar{B}^n + \bar{A}_1^* \bar{C}^n \quad (59)$$

Thus we can solve for the coefficients of the trial function, c_i^{n+1} , yielding the radial temperature field through back-substitution into Eq. (56). The trial function, ψ , is defined by assuming a

linear temperature profile between radial nodes as,

$$\psi(r) = \left[\frac{(r_{i+1} - r)}{\Delta r_i} \right] \psi_i + \left[\frac{(r - r_i)}{\Delta r_i} \right] \psi_{i+1}$$

for $r_i \leq r \leq r_{i+1}$ where $\Delta r_i = r_{i+1} - r_i$ (60)

From Eq. (60), the node temperatures ψ_i are the undetermined coefficients, c_i , used in Eq. (56).

4.2. GENHTP wall-to-fluid heat transfer

Strong coupling between wall heat transfer and the fluid model is extremely important in a thermalhydraulic code. This coupling is particularly important during refill of superheated piping and fuel channels by subcooled liquid because the local pressure is controlled by the balance between subcooled vapour generation at the hot wall and the condensation of vapour on the subcooled water. As a result, a semi-implicit wall-to-fluid heat transfer algorithm was developed for CATHENA. Wall heat transfer for the N surfaces is determined from,

$$q_{kw}^{n+1} = \sum_{j=1}^N [hc_k A_k]^n (T_w^{n+1} - \overline{T_k^{n+1}})^j + q_{ck}^n \quad (61)$$

where hc_k and A_k are the heat transfer coefficient and phase contact area for the j th surface for phase k , respectively. Since the phase temperatures, T_k^{n+1} are not dependent variables in the thermalhydraulic model, they are determined from the first-order Taylor series expansions,

$$\overline{T_k^{n+1}} = T_k^n + \frac{(h_k^{n+1} - h_k^n)}{C_{Pk}} \quad (62)$$

The energy conservation correction term q_{ck}^n in Eq. (61) is necessary since the heat transfer from the wall surfaces is determined based on the time n fluid and saturation temperatures.

A unique feature of the wall-to-fluid heat transfer algorithm is the ability to account for thermal stratification in a horizontal fuel channel that may occur at near zero flow. The model is necessary under low flow conditions since the upper fuel pins may be exposed to superheated steam at the same time that the lower fuel pins are exposed to subcooled liquid. For example, if the gas phase heat transfer calculation was based on the average

gas phase temperature, the fuel sheath temperatures would be underestimated. While multi-dimensional flow and temperature calculations are possible they are not currently feasible in an integrated thermohydraulic simulation of a reactor. To account for this temperature variation in a one dimensional model, a linear temperature profile is assumed based on the liquid level and the surrounding wall temperatures.

4.3. GENHTP wall-to-wall heat transfer

For analyses where Emergency Coolant is either delayed or is not available in a CANDU the principal heat sink is the reactor's heavy water D₂O moderator that surrounds the fuel channels. For these conditions thermal radiation heat transfer between fuel and the pressure tube is the dominant heat transfer mechanism. In addition, contact heat transfer between fuel bundle bearing pads and the pressure tube also contributes to the heat removal from the fuel.

As a result, thermal radiation and solid-solid contact heat transfer can be included within or between GENHTP models. For radiation heat transfer, the media (gas and liquid) are assumed transparent and the surfaces specified by the user are assumed to be grey, diffuse and the temperature of each surface is assumed to be uniform. The radiation view factors for the surfaces are calculated, prior to the simulation, by the auxiliary code MATRIX. For the solid-solid contact heat transfer, the user specifies the fractional contact between GENHTP surfaces and a contact conductance either as a constant or as a function of other system variables (i.e. surface temperature, pressure, etc.) through the CATHENA control models.

To complete the channel heat transfer modelling, the possible plastic deformation of the Zr-Nb pressure tube can be included during a simulation. The pressure-tube deformation model of Shewfelt and Godin (1986) is included in GENHTP. The model determines the nonuniform, transverse creep of the pressure tube either into contact with the calandria tube or up to the point of rupture as a function of the internal pressure and calculated temperature distribution.

5. Component models

To complete the modelling of a CANDU reactor, or a test loop such as RD-14M (Ingham et al., 1986) a number of component models are available in CATHENA. These component models include, T-junctions, tanks, abrupt area changes, break-discharge, junction resistances, point kinetics, pumps, separators, and valves.

To provide flexibility the component models in CATHENA have been developed to be as general as is practical. For example, the generalized tank model Aydemir (1994) contains a two-region, two-fluid model and multiple loop piping connections may be specified at any elevation with the tank. The tank model also includes bubble rise, droplet rain-out and inter-region heat and mass transfer models. The point kinetics model includes either core-wide or channel-by-channel reactivity worth averaging to account for asymmetrical cores such as in the MAPLE class of reactor. The kinetics model also includes Xe and I reactivity feedback and the ability to calculate the decay power generation as a function the reactor operating history. The valve model provides flow resistances either derived from the orifice equation with a two-phase flow multiplier or through a proprietary Fisher valve model developed for New Brunswick Power.

6. Control system modelling

The operation of regulating and safety control systems in CANDU reactors is an integral part of many of the analyses performed. For example, the operation of the two, independent reactor shutdown systems depends on a number parameters measured during reactor operation. In addition, the modelling of thermohydraulic test loops requires the use of control models to determine the behaviour of components such as valves and pumps to enable an integral representation of the system behaviour.

Flexibility was a basic requirement in the development of the CATHENA control system. This was required for the code to be applicable to CANDU reactors, research reactors such as

MAPLE and to the variety of thermalhydraulic and channel heat transfer research facilities operated by AECL. This flexibility was also required since the code is used in design assist calculations in the development of new reactor designs. Because of this desired range of application, it is not possible to design a pre-programmed control system for all applications.

The CATHENA system control models can be divided into four categories, those allowing the user to input data, manipulate 'signals' through calculation models, operational control models, and user output models. Unique user assigned model names are used throughout the control system input description to interconnect models resulting in the capability of describing complex control algorithms. In addition, an interface to the proprietary New Brunswick Power reactor control (LEPCON Richards and Girard, 1992) is included in CATHENA. Over 200 types of thermalhydraulic, heat transfer and control variables are available as signals for the control system.

The input data models allow the user to include tabular data or polynomial functions. Calculation models allow the user to manipulate signals through either a calculator-like input format or a FORTRAN-like programming language. Operational control models provide PID (proportional, integral and derivative) controllers, trip and logical functions. User defined output models allow the writing of user-formatted output files for plotting or further analysis. In addition, user defined tables and plots can be generated from data in the simulation restart file by the post-processing utilities included in the code.

7. Code development and validation programs

7.1. Development program

The overall goal in the continued development of CATHENA is to provide the ability to perform integral or 'all effects' simulations of CANDU reactors and other facilities.

Some of the tasks in progress within the CATHENA development program toward this goal are:

- inclusion of the ELOCA (Arimescu, 1991) code for the detailed modelling of fuel thermal-mechanical behaviour including its feedback on the thermalhydraulic model through changes in flow area,
- inclusion of a multi-dimensional, two-fluid model for components like CANDU headers,
- inclusion of the transient flow regime model of Aydemir (1997) to predict the evolution of interface area per unit volume,
- inclusion of a direct interface to a multi-dimensional reactor kinetics codes
- including the effects of changing geometries and surface properties on radiation heat transfer calculations during a simulation,
- inclusion of a model for the release of noncondensables carried in liquid solution, and
- the development of a graphical user interface (GUI) for input model preparation and the viewing of simulation results

7.2. Validation

Along with the development program, an extensive CATHENA validation program following an established phenomenology validation matrix of Moeck et al. (1996) exists to assess the code over a wide range of experimental conditions. The validation program consists of a large number of simulations that can be grouped into three categories:

1. separate effect experiment simulations designed to assess single phenomena where direct measurements are available,
2. component experiment simulations to assess the ability of the code to simulate components of similar scale and thermalhydraulic conditions to those in a CANDU reactor, and
3. integral experiment simulations to assess the ability of the code to simulate the combined thermalhydraulic phenomena in a loop of similar scale to a CANDU reactor (e.g. RD-14 or RD-14M Ingham et al., 1986).

In addition to the phenomenology based validation program, a representative sample of the validation cases forms an acceptance test suite that is simulated with every code version release to the code user community.

8. Summary

The CATHENA transient, one-dimensional, two-fluid code has been developed as a versatile tool for CANDU and other AECL reactor thermalhydraulic analyses. Some of the unique features of the code including its flexible heat transfer package, GENHTP, have been highlighted. The code development and validation program continues to extend its range of application to integrated analyses of CANDU reactors.

Appendix A. Nomenclature

A	cross-sectional area	f_{id}	bubble in slug-churn flow regime interface friction factor for disperse droplet flow regime
A_i	interface area per unit volume	g_z	gravitation component in the z direction
A_{isb}	interface area per unit volume for bubbles in slug-churn flow regime	h_k	phase k specific enthalpy
A_{iss}	interface area per unit volume for Taylor bubbles in slug-churn flow regime	h_{ck}	phase k wall heat transfer coefficient
\vec{B}	vector of source terms for the finite-difference equations	h_{cn}	heat transfer coefficient for the n th surface
C_{0k}	volume flux distribution coefficient, $\langle \alpha_k v_k \rangle = C_{0k} \langle \alpha_k \rangle \langle v_k \rangle$ where $\langle \rangle$ represents the cross-section area average operator	j_k	phase k volumetric flux
C_{1k}	momentum flux distribution coefficient, $\langle \alpha_k v_k^2 \rangle = C_{1k} \langle \alpha_k \rangle \langle v_k \rangle^2$	j^*	nondimensional volumetric flux
C_P	wall specific heat	K	wall thermal conductivity
C_{Pk}	phase k specific heat at constant pressure	K_k	phase k thermal conductivity
C_s^*	nondimensional countercurrent flooding parameter, defined in Eq. (15)	(k/l)	minor loss per unit length
\vec{D}	matrix of finite difference coefficients	m_{ki}	mass transferred from phase k to the interface
D_e	pipe hydraulic diameter	Nu	Nusselt number
D_i	interface hydraulic diameter	P_k	phase k pressure
D_{bd}	interface hydraulic diameter for dispersed bubble or droplet flow regimes	P'_{ki}	apparent or virtual mass term
F_A	averaged constitutive relation value	Pr	Prandtl number
F_M	constitutive relation value in the mixed flow category	q_{ki}	heat transfer from phase k to the interface
F_S	constitutive relation value in the separated flow category	q_{kw}	heat transfer from a wall to phase k
f_i	interface Darcy friction factor	q_{wi}	wall heat transfer resulting in interface mass transfer
f_{ib}	interface friction factor for disperse bubble flow regime	q'''	heat generation per unit volume
f_{is}	interface friction factor for Taylor	Q'	circumferential conduction plus heat generation terms
		r	radial coordinate direction
		v_k	phase k velocity
		v_m	mixture velocity, $v_m = \sum_k \alpha_k \rho_k v_k / \rho_m$
		v_{ki}	phase k interface velocity
		Re	Reynolds number
		t	time
		T	wall temperature
		U_r^*	critical relative velocity ratio, defined in Eq. (13)
		U_c^*	nondimensional entrainment velocity, defined in Eq. (16)
		W_s	weighting fraction between mixed and separated flow categories
		X'_{nc}	mass fraction for the i th noncondensable gas component
		\hat{x}	vector of dependent variables in finite-difference equation matrix
		z	spatial coordinate
		$(-1)^k$	1 for gas phase (g) and -1 for liquid phase (f)

α_k	area fraction of phase k {k = g (gas) or f (liquid)}
β_k	pressure difference between phase k and the interface
ϵ_k	phase k mass conservation correction term
ρ	wall density
ρ_k	density of phase k
ρ_m	mixture density, $\rho_m = \sum_k \alpha_k \rho_k$
ρ_{AP}	apparent mass density
η	normal direction to a surface
μ_k	phase k molecular viscosity
θ	circumferential direction or angle of inclination of a pipe from the horizontal
τ^*	two-phase flow friction multiplier
τ_{kw}	friction term for phase k contact with the wall
τ_{ki}	interface friction term for phase k
λ_{ki}	generalized interface heat transfer coefficient for phase k
Γ_k	phase k volumetric sink for noncondensables
Γ_{nc}^i	volumetric source for the <i>i</i> th noncondensable gas component
σ	surface tension
$\psi_{b,s,d}$	weighting fractions for the dispersed bubble, slug and dispersed droplet flow regimes
ξ	angle subtended by the interface for stratified flow
ζ_k	phase k wall contact fraction for wall shear

References

- Ardron, K.H., Banerjee, S., 1986. Flooding in an elbow between a vertical and a horizontal or near-horizontal pipe, Part II. Theory. *Int. J. Multiphase Flow* 12 (4), 543–558.
- Arimescu, V.I., 1991. An elasto-plastic model for mechanical contact between the pellets and sheath in candu nuclear fuel elements. In: Proc. 41 st Annual International Conference Of The Canadian Nuclear Association Canadian Nuclear Society, Saskatoon, Sask., Canada, AECL-10426.
- Aydemir, N.U., 1994. A generalized non-equilibrium tank model for CATHENA with noncondensables and wall heat transfer. In Proc. Int. Conf. New Trends in Nuclear System Thermalhydraulics, 1, Pisa, Italy.
- Aydemir, N.U., 1997. A one-dimensional, transient interfacial area model: description and preliminary assessment. In: Proc. Int. Symp. Advances in Computational Heat Transfer, Cesme, Turkey.
- Chaxton, K.T., Collier, J.G., War, A.J., 1972. HTFS correlation for two-phase pressure drop and void fraction in tubes, AERE-R7162.
- Chow, H., Ransom, V.H., 1984. A simple interphase drag model for two-fluid modelling of two-phase flow systems, CONF-840614-98.
- Clift, R., Gauvin, W.H., 1971. Motion of entrained particles in a gas stream. *Can. J. Chem. Eng.* 49, 439–448.
- Dittus, F.W., Boelter, L.M.K., 1930. Heat transfer in automobile radiators of tubular type. Publications in Engineering, 443, University of California, Berkeley, CA.
- Drew, D., Cheng, L., Lahey Jr., R.T., 1979. The analysis of virtual mass effects in two-phase flow. *Int. J. Multiphase Flow* 5, 233–242.
- Duff, I.S., 1980. MA28—A set of FORTRAN subroutines for sparse unsymmetric linear equations. AERE-8730.
- Hancox, W.T., Ferch, R.L., Liu, W.S., Neiman, R.E., 1980. One-dimensional models for transient gas-liquid flows in ducts. *Int. J. Multiphase Flow* 6, 25–40.
- Hanna, B.N., Raithby, G.D., Nicoll, W.B., 1979. Sound speed and critical discharge in twophase flows. Two-Phase Momentum Heat and Mass Transfer in Chemical. Proc. Energy Eng. Syst. Hemisphere 1, 33–46.
- Friedel, L., 1979. Improved friction pressure drop correlations for horizontal and vertical two-phase pipe flow. European Two-Phase Flow Group Meeting, Ispra, Italy, Paper E2.
- Ingham, P.J., Krishnan, V.S., Sergejewich, P., Ardon, K.H., 1986. Scaling laws for simulating the CANDU heat transport system. In: Proc. 2nd Int. Conf. Simulation Methods in Nuclear Engineering, Montreal, Ontario, Canada.
- Ishii, M., 1978. Thermo-Fluid Dynamic Theory of Two-Phase Flow. Eyrolles, Paris.
- Ishii, M., Misima, K., Kataoka, I., Kocamustafaogullari, G., 1981. The importance of the interfacial area in two-phase flow analysis. In: Proc. 9th US Appl. Mech. Conf. ASME.
- Jones, A.B., Dight, D.G., 1962. Hydrodynamic stability of a boiling channel, Part 2. KAPL-2208, Knolls Atomic Power Laboratory.
- Kowalski, 1987. Wall and interfacial shear stress in stratified flow in a horizontal pipe. *AIChE J.* 33 (2), 274–281.
- Lamb, H., 1924. Hydrodynamics, 5th ed. Cambridge University Press, Cambridge.
- Lellouche, G.S., Zolotar, B.A., 1982. Mechanistic model for predicting two-phase void fraction for water in vertical tubes, channels and rod bundles. EPRI NP-2246-SR.
- Liner, Y., Hanna, B.N., Richards, D.J., 1988. Piecewise approximation of the thermodynamic properties of heavy water. Proc. Int. Sym. Fundamentals of Gas-Liquid Flow, vol 72, pp. 99–103.
- Micaelli et al., 1987. Numerical methods used for thermalhydraulics in the reactor safety code CATHARE. Proc. Int. Topical Meeting on Advances in Reactor Physics, Mathematics and Computations, Paris, France, April 27–30.

- Moeck, E.O., Luxat, J.C., Simpson, L.A., Petrilli, M.A., Thompson, P.D., 1996. Generic Validation of Computer Codes for Safety Analyses of CANDU Power Plants, Can Nucl. Soc. Bull. 17 (2), 23–29.
- Popov, N.K., Rohatgi, U.S., 1983. Effect of interfacial shear and entrainment models on flooding predictions. AIChE Symposium Series, Heat Transfer, Seattle.
- Ransom, V.H., et al., 1984. RELAP5/MOD2, code manual volume 1, system models and solution methods. EGG-SAAM-6377.
- Richards, D.J., McDonald, B.H., 1981. A dynamic grid-point allocation scheme for the characteristic finite-difference method. OECD Specialist Meeting, Pasadena, California, AECL-7147.
- Richards, D.J., Girard, R., 1992. Integrating CATHENA with CANDU plant controllers. In: Proc. 13th Annu. CNS Conf. Saint John, N.B., Canada, June 7–10.
- Roach, P.J., 1982. Computational Fluid Mechanics, Hermosa, Albuquerque.
- Shewfelt, R.S.W., Godin, D., 1986. Ballooning of thin-walled tubes with circumferential temperature variations. AECL-8317, Res. Mech. 28, 21–33.
- Slattery, J.C., 1972. Momentum, Energy and Mass Transfer in Continua, McGraw-Hill, New York.
- Solbrig, C.W., McFadden, J.H., Lyczkowski, R.W., Hughes, E.D., 1978. Heat transfer and function correlations to describe steam-water behaviour in nuclear safety studies AIChE Symp. Series 74, Heat Transfer Research and Applications.
- Stuhmiller, J.H., 1977. The influence of interfacial pressure forces on the character of twophase flow model equations. Int. J. Multiphase Flow 3 (6), 551–560.
- Taitel, Y., Barnea, D., Dukler, A.E., 1980. Modelling flow pattern transitions for steady upward gas-liquid flow in vertical tubes. AIChE J. 26 (3), 345–354.
- Taylor, D.D., et al., 1984. TRAC-BD1/Mod1: An advanced best estimate computer program for boiling water reactor transient analysis. NUREG/CG-3633.
- TRAC-PFI/MOD1, 1986. An advanced computer program for pressurized water reactor thermalhydraulic analysis. NUREG/CR-3858.
- Vernier, P., Delhay, J.M., 1968. General two-phase flow equations applied to the thermodynamics of boiling nuclear reactors. Energy Prmaire 4.
- Wallis, G.B., 1969. One-Dimensional Two-Phase Flow. McGraw-Hill, New York.
- Weisman, J., Duncan, D., Gibson, J., 1979. Effect of fluid properties and pipe diameter on two-phase flow patterns in horizontal lines. Int. J. Multiphase Flow 5 (6), 437–462.
- Weisman, J., Kang, S.Y., 1981. Flow pattern transitions in vertical and upwardly inclined lines. Int. J. Multiphase Flow 7 (3), 271–291.
- Yuen, M.C., Chen, L.W., 1978. Heat transfer measurements of evaporating liquid droplets. Int. J. Heat Mass Transfer 21, 537–542.

PREDICTED AND MEASURED FLOW AND TEMPERATURE DISTRIBUTIONS IN A FACILITY FOR SIMULATING IN-REACTOR MODERATOR CIRCULATION

L.N. Carlucci, V. Agranat, G.M. Waddington, H.F. Khartabil, J. Zhang*

*Atomic Energy of Canada Ltd., Chalk River Laboratories
Chalk River, Ontario, Canada, K0J 1J0*

**Atomic Energy of Canada Ltd, Mississauga, Ontario
E-mail: carluccib@aecl.ca*

ABSTRACT

The Computational Fluid Dynamics code, MODTURC_CLAS, has been validated against experimental data obtained in the Moderator Test Facility at the Chalk River Laboratories of Atomic Energy of Canada Limited. The MTF is an integral scaled facility built to investigate moderator behaviour, having the key characteristics of a full-scale CANDU® nuclear reactor calandria vessel. Predicted three-dimensional fluid flow and temperature distributions within the MTF vessel are in good agreement with the experimental data, which represent a range of operating conditions of the moderator in the recent CANDU 9 design.

INTRODUCTION

The core of a typical CANDU nuclear reactor consists of a large cylindrical vessel filled with a matrix of several hundred parallel fuel channels arranged in a square array. The use of heavy water as coolant and moderator is a characteristic of all CANDU designs. Low-pressure moderator, surrounding the channels, is used to slow down fast neutrons to thermal speeds, thereby enabling the nuclear-fission reaction to be maintained with natural uranium fuel. Most (>95%) of the heat generated by the fission reaction is removed by high-pressure coolant circulated inside the individual channels.

In the recent CANDU 9 design (Figure 1), the moderator is introduced into the calandria vessel through a system of twelve downward-pointing nozzles located symmetrically on both sides of the calandria shell, at about the 10.45 o'clock position. Each nozzle is fitted with fan-shaped, multicompartment diffusers that emit flat, spreading jets of fluid in the reflector region, approximately parallel to the calandria wall. These jets meet at the bottom of the core at approximately the vessel's

vertical plane of symmetry (the 6 o'clock position), and turn upward to flow through the core region to remove the heat generated by direct deposition of neutron and gamma energy to the moderator. The hot moderator fluid is removed via four outlet ports, symmetrically located on the vessel wall at approximately the 11:00 o'clock position, passed through external heat exchangers, and returned to the inlet nozzles.

Knowledge of the moderator flow and temperature distributions within the calandria vessel is particularly important for the safety analysis of certain postulated accident scenarios where the moderator is required to provide a backup heat sink to the emergency core cooling system. The Computational Fluid Dynamics (CFD) computer code, MODTURC_CLAS, is employed by the CANDU industry to predict moderator flow and temperature distributions in a range of CANDU moderator designs. It is based on the commercial general-purpose CFD code, TASCflow, developed by AEA Technology Engineering Software Ltd (formerly Advanced Scientific Computing Ltd) [1].

This paper describes the validation of the MODTURC_CLAS code (version 2.2.1a) against data from the Moderator Test Facility (MTF), designed to simulate representative CANDU 9 steady-state and transient moderator flow conditions.

MODEL DESCRIPTION

MTF: Scaling Considerations

To validate the MODTURC_CLAS code, it is desirable to use the data from experiments that relate, as far as possible, to the actual geometry and processes occurring within the moderator. The MTF was designed and built to conduct such experiments. It is an integral test facility, having all the key characteristics of a typical CANDU reactor calandria vessel, with all linear dimensions being ¼ of the corresponding physical values in the CANDU 9 reactor.

® CANDU = CANada Deuterium Uranium, registered trademark of AECL

The scale was arrived at by balancing two competing requirements. It had to be large enough to ensure turbulence throughout the vessel, so that all the governing phenomena in the full-scale reactor calandria play essentially the same role in the reduced scale. At the same time, the size had to be economically viable in terms of capital and operating costs, particularly in aspects related to power and flow requirements, which can increase dramatically with increased scale.

Once the scale was chosen, dimensionless groups, derived by non-dimensionalizing the governing equations, were used to select the appropriate MTF operating conditions, simulating the corresponding full-scale reactor conditions. The dimensionless volumetric heat source, Q^* , and the Archimedes number, Ar , were matched for the MTF and the CANDU 9 calandria vessel, as they were identified to be the primary similarity parameters in the MTF scaling. In particular, Ar compares two significant forces acting on the fluid: the buoyancy force caused by the fluid density variation (mostly within the heated core) and the inertia force caused by the forced convection of coolant injected through the nozzles. This parameter is calculated as being $Ar = g\beta \Delta T_r D / V_i^2$, where V_i is the magnitude of the inlet velocity, ΔT_r is the reference temperature difference, D is the vessel diameter, g is the acceleration due to gravity and β is the thermal expansion coefficient of the fluid. The Reynolds number, $Re = V_i D / \nu$, where ν is the kinematics viscosity of fluid, is considered to be a secondary similarity parameter and is not matched. Its values are high enough for both the MTF and the CANDU 9 calandria to obtain turbulent flow conditions where the fluid flow sensitivity to variations in Re is low.

MODTURC_CLAS: Models and Grid

The MODTURC_CLAS equations, governing the mixed convection flow in the MTF, are the time-averaged conservation equations (mass, momentum and energy) coupled with the standard k - ϵ turbulence model equations for the turbulent kinetic energy, k , and its dissipation rate, ϵ . The governing equations are not discussed here, as they are well described in the TASCflow documentation [1]. The user-specified models are the models for hydraulic resistance, buoyancy force and heat generation, which produce the source terms for the above conservation equations.

The effect of fuel channels on the moderator flow is modelled by using a uniform isotropic porosity ($\gamma = 0.83$) to account for the flow-volume reduction, and an empirically based friction-factor correlation [2] to

model the distributed hydraulic resistance to the mean fluid flow in the tube bank. The hydraulic resistance correlation [2] was obtained from the tube bank tests for a range of local tube Reynolds numbers, Re_t , from 2000 to 9000, and for the pitch-to-diameter ratios of 2.16 (in-line tube bank flow) and 3.06 (staggered tube bank flow). According to its implementation in the MODTURC_CLAS code, the cross-flow pressure loss coefficient varies with Re_t to the power of -0.166 . Re_t is defined as $d|V|/\nu$, where d is the tube diameter and V is the local fluid velocity vector calculated by MODTURC_CLAS

The buoyancy force is modelled using the Boussinesq approximation, which results in the following buoyancy force per unit volume in the vertical direction z : $S_{bz} = -\gamma\beta\rho_r(T-T_r)g_z$, where ρ_r and T_r are the reference fluid density and temperature, respectively. In the present work, β and ρ_r were taken at the water temperature of 50°C, which was considered to be the volume-averaged temperature, and T_r was equal to the inlet water temperature, T_i .

The nuclear heating of the moderator was simulated in the MTF by the electrical heating of the individual channels or calandria tubes that comprise the core. The heat generation in the MTF core region is modeled with a separate pre-processor module of MODTURC_CLAS, which calculates the volumetric heat source for the fluid energy equation.

Boundary conditions are as follows: at the inlets, the uniform fluid velocity, temperature, k and ϵ are specified; at the outlets, the pressure is given; and at the vessel walls, the no-slip adiabatic conditions are used. The values of k and ϵ at the inlets are expressed in terms of the inlet turbulence intensity and the eddy length scale, taken as being 0.05 and 0.005 m, respectively.

The computational grid used is the butterfly design grid (see Figure 2). The base grid applied in most simulations comprises $69 \times 82 \times 24 = 135\,792$ nodes, with 69 being the number of cross-sectional planes in the axial direction, and $82 \times 24 = 1968$ being the number of nodes in each cross-sectional plane. The base grid size was chosen based on the results of grid independence tests conducted by AEA Technology Engineering Software Ltd.

The MODTURC_CLAS equations are solved by iterations until the convergence criterion is satisfied.

RESULTS AND DISCUSSION

In all, the MTF was used to carry out five steady-state and two transient integral tests. The steady-state tests covered a range of possible steady-state operating

conditions, including isothermal, nominal flow and power for two outlet-to-inlet temperature differences, nominal flow and power with inlet flow asymmetry, and reduced flow and power with inlet flow asymmetry to simulate one-pump operation. The transient tests were designed to simulate the main features of two postulated loss-of-coolant accident scenarios. Measurements during the steady-state tests included local velocities (magnitudes and turbulence intensities) and temperatures throughout the vessel using moveable probes, whereas measurements during the transients were limited to coolant temperatures throughout the vessel using fixed probes

Figures 3 and 4 compare predicted and measured temperature distributions and velocity vectors in the middle cross-section of the MTF vessel for the steady-state test with nominal flow and power conditions. The figures illustrate the typical patterns of flow and temperature distributions in the MTF core: the fluid flow is predominantly vertical and the temperature distribution is stratified; i.e., the fluid temperature increases with elevation. The asymmetry in the velocity measurements at the vessel bottom is attributed to a combination of the highly unsteady nature of the turbulent jets and possible geometric misalignments of the inlet nozzles due to manufacturing tolerances. Code predictions do not show this asymmetry because the k-epsilon model accounts for only the mean behaviour of the turbulent flow and not its unsteady nature, and the nozzle geometries on each side of the vessel were assumed symmetric.

Overall, results from the validation of MODTURC_CLAS against the MTF data for representative CANDU 9 steady-state and transient conditions indicate good agreement between the code predictions and measurements, specifically:

- The measurements and code predictions of velocity and temperature fields confirm the stability of the CANDU 9 moderator system over a wide range of conditions, including significant flow asymmetry resulting from one-pump operation.
- The measurements and code predictions show the temperature to be monotonically increasing from the bottom to the top of the core (Figure 3). In general, there is good agreement between the measured and predicted temperatures. There is a slight tendency to underpredict temperatures at the bottom of the vessel, possibly due to insufficient jet entrainment, as modelled by the code. However, agreement improves near the top, where

the maximum temperature is reached. The difference between the predicted and measured maximum temperatures is less than 1°C.

- The measurements and code predictions indicate that the overall flow and temperature patterns are determined primarily by the forced flow induced by the inlet jets, as they flow and entrain core liquid toward the bottom of the vessel, collide, and induce a stable upward flow through the core, assisted by buoyancy forces (Figure 4).
- The measurements and code predictions indicate that the temperature field and, to a lesser extent, the velocity field are largely two-dimensional in the core cross-section, with decreasing axial variation as the top of the core is reached

CONCLUSIONS

- The CFD code, MODTURC_CLAS, has been validated against MTF data representing a range of CANDU 9 nuclear reactor conditions.
- Good quantitative agreement between the code predictions of three-dimensional water temperature distribution in the MTF vessel and the temperature measurements has been obtained for both steady-state and transient simulations
- The predicted and measured flow and temperature distribution patterns in the MTF vessel have confirmed the stability of the CANDU 9 moderator system.

ACKNOWLEDGEMENTS

The authors would like to acknowledge the contributions of A.O. Banas in the initial stage of the project, J.K. Szymanski of Ontario Power Generation for providing details of the resistance model and assistance in running MODTURC_CLAS, and M. Ivanovic of AEA Technology Engineering Software Ltd. for conducting the grid independence tests.

REFERENCES

1. "TASCflow Theory Documentation", Version 2.2, 1993 April, Advanced Scientific Computing Ltd., Waterloo, Ontario, Canada
2. G.I. Hadaller, R.A. Fortman, J.K. Szymanski, W.I. Midvidy and D.J. Train, "Frictional Pressure Drop for Staggered and In-Line Tube Banks with Large Pitch to Diameter Ratio", Proceedings of the 17th Annual CNS Symposium on Reactor Dynamics and Plant Control, Kingston, Ontario, Canada, 1992 August.

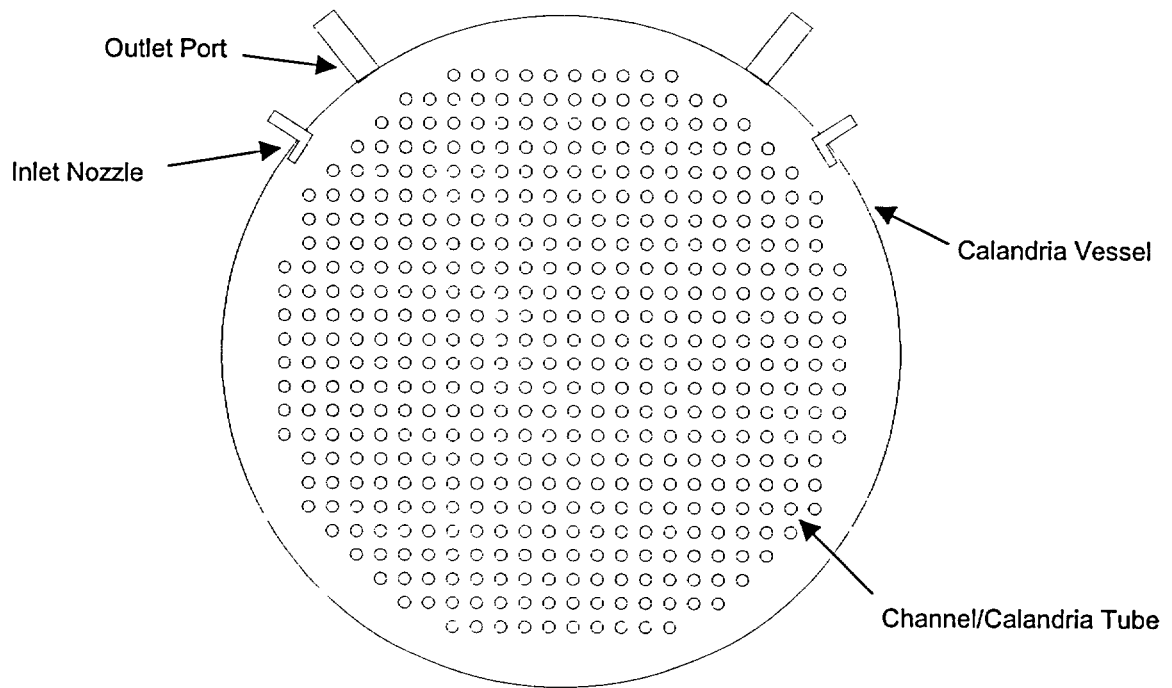


Figure 1: Simplified cross-sectional view of a CANDU 9 calandria vessel

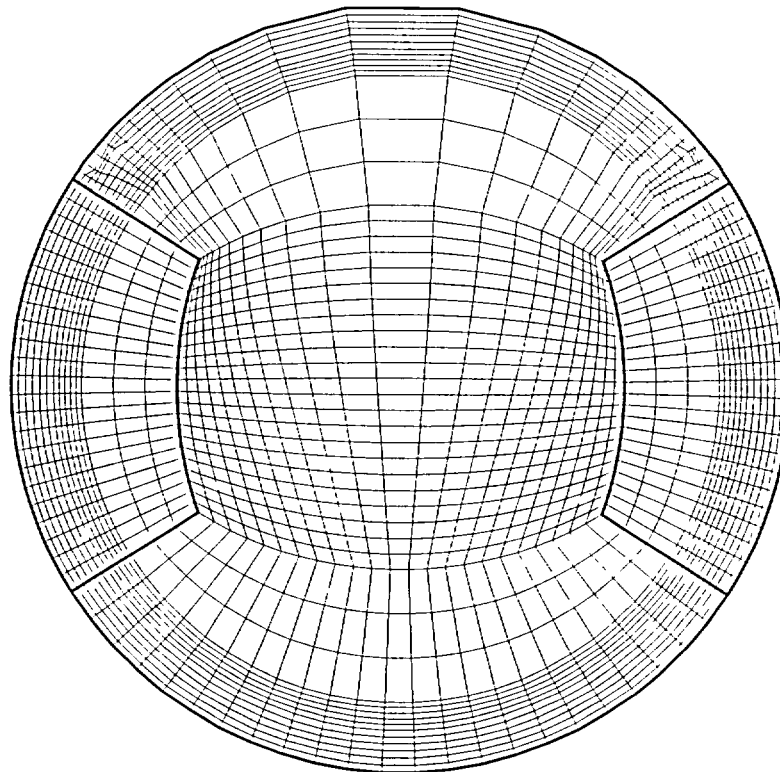


Figure 2: Cross-section of base grid at inlet nozzle plane

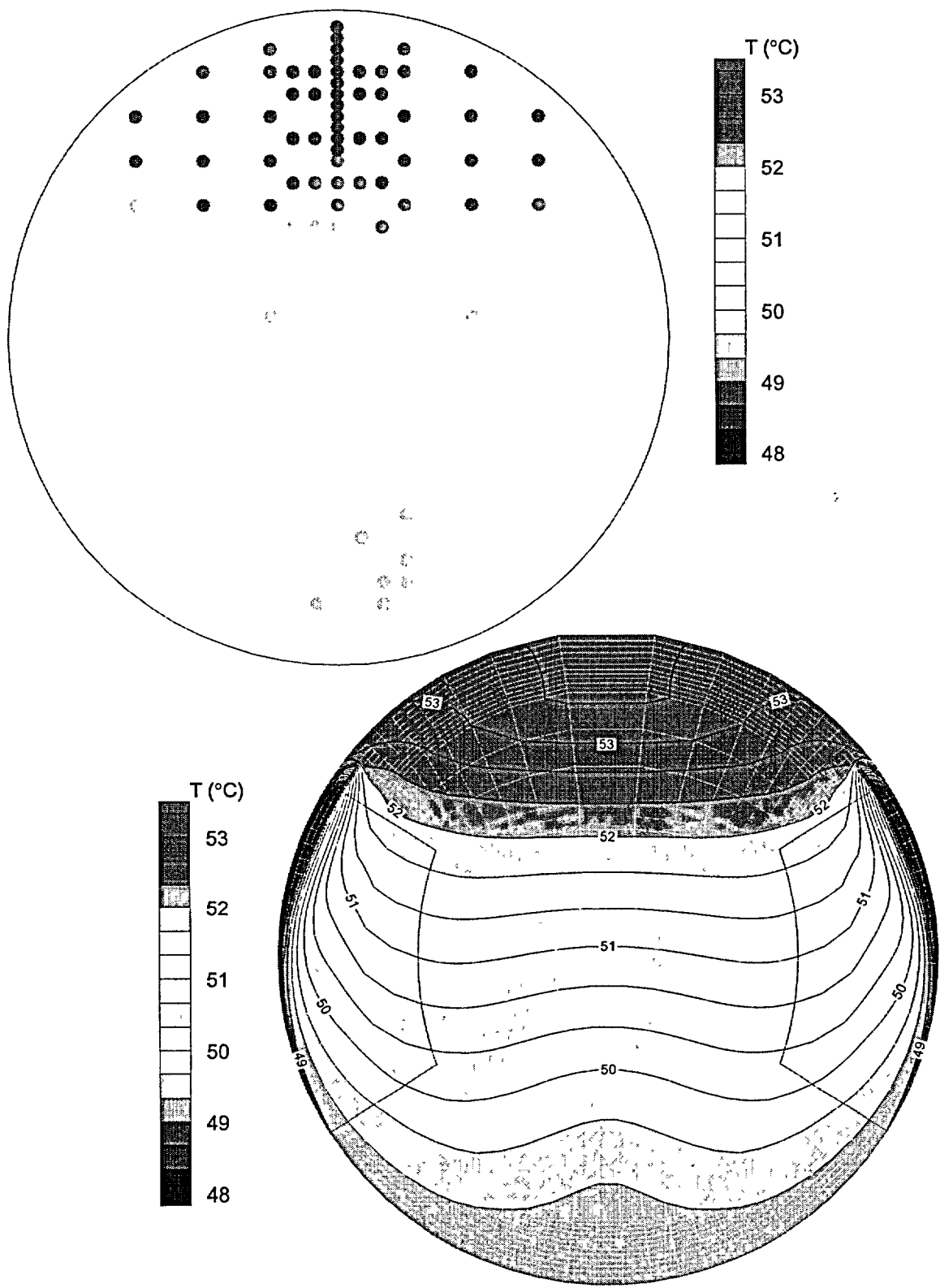


Figure 3: Comparison of predicted (lower) and measured (upper) temperature distributions in middle cross-section for nominal flow and power conditions

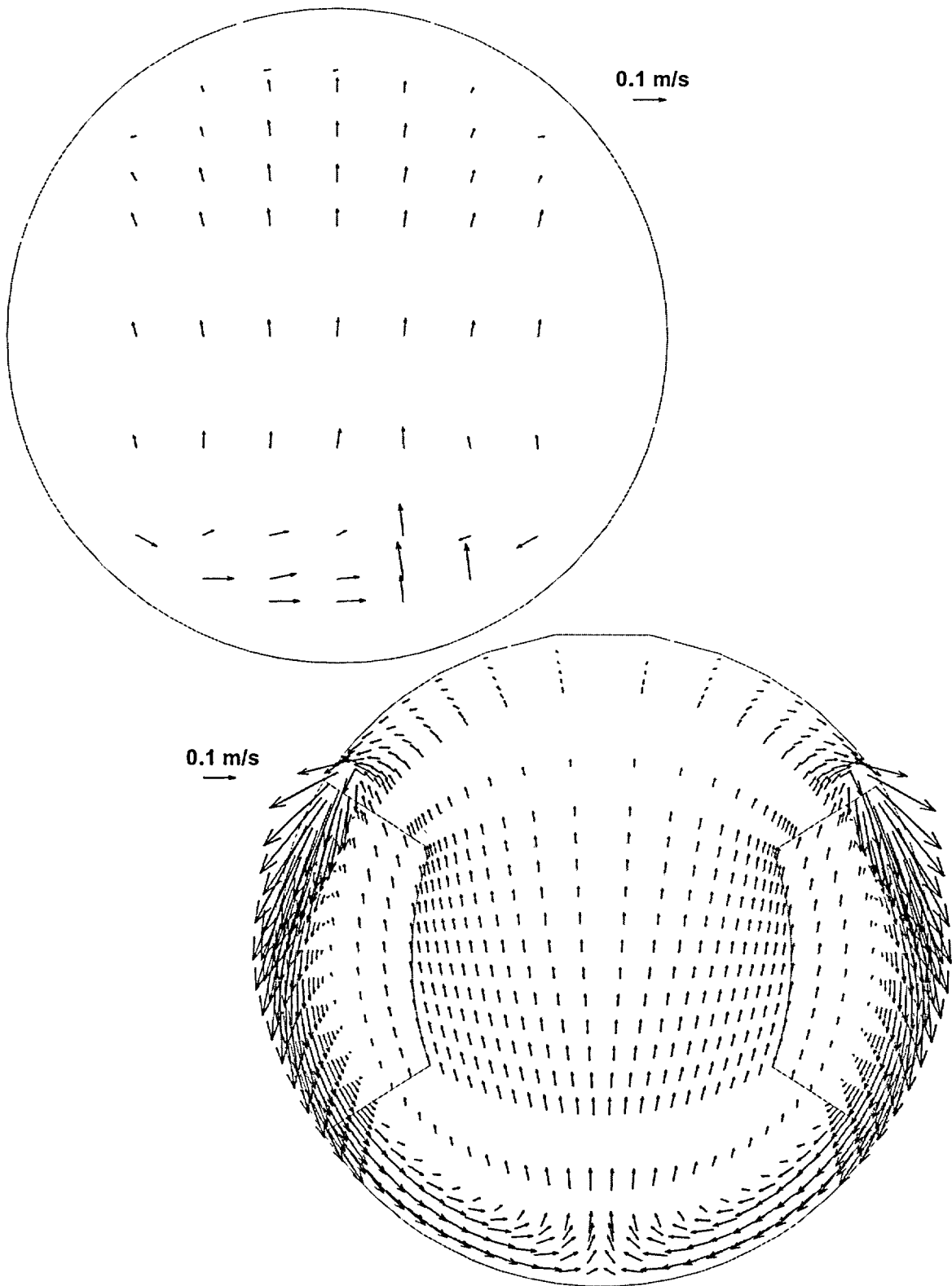


Figure 4: Comparison of predicted (lower) and measured (upper) velocity vectors in middle cross-section for nominal flow and power conditions

A GENERALIZED PREDICTION METHOD FOR CRITICAL HEAT FLUX IN CANDU FUEL-BUNDLE STRINGS

Laurence K.H. Leung and Dé C. Groeneveld

Chalk River Laboratories
Atomic Energy of Canada Limited
Chalk River, Ontario K0J 1J0
Canada

Guy Hotte

Hydro-Québec
1000 de la Gauchetière, west
14th floor, Office 1400
Montreal, Quebec H3B 4W5
Canada

ABSTRACT

A generalized prediction method has been derived for critical heat flux (CHF) in CANDU[®] fuel-bundle strings. It is set up in the form of a look-up table (referred to as the bundle CHF table) and is primarily based on the tube CHF table of Groeneveld et al. (1996). Three correction factors have been introduced to account for (1) the enthalpy imbalance within the bundle, (2) the difference in characteristic diameter of the CANDU bundles from a 8-mm tube, and (3) the orientation effect from vertical to horizontal flow.

The capability of the bundle CHF table in the prediction of bundle dryout power has been assessed with data of horizontal light-water flow and both vertical and horizontal Freon-12 flow. These data were obtained with 37-element bundle simulators having either uniform or non-uniform (primarily a downstream skewed-cosine flux shape) axial-flux distributions. Using the bundle CHF table in the calculations, the measured CANDU bundle dryout power was predicted with good accuracy.

1. INTRODUCTION

Critical heat flux (CHF) is often used as the criteria for determining the operating margin during normal reactor operation. It is the maximum heat flux for which efficient cooling can be sustained on the heated surface. Beyond CHF, the rate of heat transfer to the coolant is reduced. This results in a rapid increase in surface temperature and can cause damage to the heated surface. Therefore, an accurate prediction of CHF in fuel bundles is essential for the safe operation of a reactor. It is the objective of this study to derive a generalized prediction method for CHF in CANDU fuel-

bundle strings, applicable over a wide range of flow conditions (such as those encountered in postulated loss-of-regulation and loss-of-coolant accidents).

2. A GENERALIZED PREDICTION METHOD FOR BUNDLE CHF

Most prediction methods currently in use are based on correlations expressing CHF as functions of pressure, mass flux and dryout quality. Coefficients and exponents included in the empirical correlations were optimized with CHF data obtained with bundle simulators. The bundle CHF databases, however, cover only a limited range of flow conditions. For flow conditions outside the database, the correlations may not have the correct asymptotic and parametric trends. This limits the extent of extrapolation of the correlations to conditions outside the database.

The tube CHF databases, on the other hand, cover a much wider range of flow conditions than the bundle CHF databases. The combined AECL-IPPE tube CHF database consists of over 30 000 points (Groeneveld et al. 1996). Their parametric trend can be used to extend the prediction method for bundle CHF to conditions outside the bundle CHF database.

The present approach employs a tube-based prediction method and extends it to bundle geometries by accounting for the separate effects. Among various prediction methods, the 1995 tube CHF table (Groeneveld et al. 1996) provides a much better prediction accuracy than other look-up tables and correlations. In addition, it represents closely the parametric trend of the tube CHF database. Therefore, it is selected as the base method for predicting bundle CHF.

CANDU[®] (CANada Deuterium Uranium) is a registered trademark of Atomic Energy of Canada Limited (AECL)

The differences between vertical tube CHF values and horizontal bundle CHF values (in the CANDU fuel channels) are assumed to be caused by (1) the enthalpy imbalance within the bundles, $(x_{DO})_{mb}$, (2) the differences in geometric characteristics (hydraulic diameter, shape, narrow gap, etc.) between tubes and bundles, K_{geom} , and (3) the orientation effect between horizontal and vertical channels, K_{orient} . Three correction factors have been derived to account for these effects. They are primarily based on observed trends in simple geometries. The bundle CHF data have not been used in the development of these correction factors, but are used to validate the proposed methodology.

2.1 Enthalpy Imbalance in Bundles

A detailed analysis of the enthalpy imbalance within a bundle requires a subchannel code such as ASSERT (Carver et al. 1990). There is no specific methodology available to estimate the degree of enthalpy imbalance in bundles based on the cross-sectional average flow parameters, especially at CHF conditions. Recently, an analysis of the pressure-drop data showed a large difference in thermodynamic quality at the point of onset of significant void (OSV) between tubes and bundles. Based on a similar form of the Saha and Zuber correlation (1974), the thermodynamic quality at the OSV point is correlated for tubes as

$$(x_{OSV})_{tube} = -218 Bo Re^{0.2} (\rho_l / \rho_v)^{0.5} \quad (1)$$

where ρ_l and ρ_v are the densities of the liquid and vapour, respectively, in kg/m^3 . The boiling number is expressed as

$$Bo = \frac{q}{GH_f} \quad (2)$$

where q is the surface heat flux in W/m^2 , G is the mass flux in $kg/m^2 \cdot s$ and H_f is the latent heat of vaporization in J/kg . The Reynolds number is expressed as

$$Re = \frac{GD_w}{\mu} \quad (3)$$

where μ is the dynamic viscosity of liquid in $kg/m \cdot s$. The hydraulic equivalent diameter is calculated with

$$D_w = \frac{4A_f}{P_w} \quad (4)$$

where A_f is the flow area in m^2 and P_w is the wetted perimeter in metres. A similar equation, with different coefficients and exponents, was derived to predict the OSV point in 37-element bundles. Equation (1) is valid only for convective-dominated heat transfer. When conduction becomes dominant, the thermo-dynamic quality at

the OSV point is calculated with the Saha and Zuber correlation, which is expressed as

$$(x_{OSV})_{cond} = -0.0022 \frac{q D_w C_{p_l}}{H_f k_f} \quad (5)$$

where C_{p_l} is the specific heat capacity of liquid in $J/kg \cdot K$, and k_f is the thermal conductivity of liquid in $W/m \cdot K$. To ensure a smooth transition, the maximum thermodynamic quality at the OSV point between conduction (i.e., Equation (5)) and convection (i.e., Equation (1)) is used,

$$(x_{OSV})_{tube \& \ bundle} = \text{Max.} ((x_{OSV})_{conv}, (x_{OSV})_{cond}) \quad (6)$$

The dimensionless enthalpy imbalance between tubes and bundles at the OSV point is expressed as

$$(x_{OSV})_{imb} = \text{Max.} ((x_{OSV})_{tube} - (x_{OSV})_{bundle}, 0) \quad (7)$$

The enthalpy imbalance becomes zero at a vapour quality of 1.0, but the exact variation of enthalpy imbalance with vapour quality is unknown. To ensure a correct asymptotic trend, it is assumed that the enthalpy imbalance is maximum at the OSV point and linearly reduces to zero as the quality approaches 1 (as illustrated in Figure 1). Hence, the enthalpy imbalance between tubes and bundles at the CHF point is

$$(x_{DO})_{imb} = \frac{1 - (x_{DO})_{bundle}}{1 - (x_{OSV})_{bundle}} (x_{OSV})_{imb} \quad (8)$$

where x_{DO} is the cross-sectional average dryout quality in bundles. The tube-equivalent dryout quality is calculated with

$$(x_{DO})_{equiv. \ tube} = (x_{DO})_{bundle} + (x_{DO})_{imb} \quad (9)$$

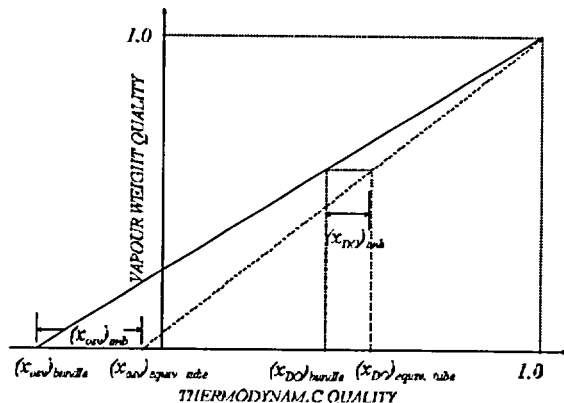


Figure 1 Definition of enthalpy imbalance within a bundle.

and is used to evaluate the CHF value with the tube CHF table. Since heat flux is required in calculating the thermodynamic qualities at the OSV point, an iterative procedure is used to solve for the CHF.

2.2 Correction Factor for Diameter Effect

Groeneveld et al (1996) showed that the effect of tube diameter on CHF follows generally the relationship.

$$\frac{CHF_D}{CHF_{D=0.008m}} = \left(\frac{D}{0.008} \right)^n \quad (10)$$

A value of $-1/2$ appears to be most appropriate as the exponent in Equation (10), when compared against the tube CHF database. Several studies, however, observed a more complex tube-diameter effect on CHF than that represented by this simple formulation (e.g., Wong (1997)).

Wong (1997) observed a much more complex effect of tube diameter on CHF, which is a function of pressure, mass flux, and quality. Considering only the pressure effect on the exponent, the effect of diameter appears significant at low-pressure conditions and diminishes as the pressure increases. A value of $-1/2$ appears to be valid for pressures up to 8 MPa, while a value of -0.2 is more appropriate for a pressure of 12 MPa. The average value of the exponent appears to approach zero for pressure values close to the critical pressure (beyond 18 MPa).

Based on the tube data of Wong (1997), the exponent value in Equation (10) is modified to account for the pressure effect. It is expressed as

$$n = -0.5 (1 - \exp(-0.95 (\log(p/p_c))^2)) \quad (11)$$

In most analyses, the hydraulic equivalent diameter is often used as the characteristic diameter of a 37-element bundle. It is calculated in the traditional manner (i.e., using Equation (4)). Several studies of CHF in annuli (Doerffer et al 1994) and bundles (Heron et al 1969), however, showed that this approach is not appropriate. Modifications are required to improve the prediction accuracy of a tube-based correlation for annuli or bundle geometries.

A recent analysis of the pressure-drop data obtained over a full-scale bundle string showed that the equivalent-annuli definition of the hydraulic diameter is more appropriate for the 37-element bundle (Leung and Hotte 1997).

$$D_{hy,annuli} = D_o - D_i \quad (12)$$

where D_o is the inside diameter of the outer tube in metres and D_i is a characteristic dimension of the outside diameter of the inner tube in metres. After examining three definitions, Leung proposed the use of the weighted-average value of the pitch-circle diameter in the bundle as the equivalent inner-tube diameter. It is defined as

$$D_i = D_{rod} + \frac{6D_p + 12D_{ir} + 18D_{or}}{36} \quad (13)$$

where D_{rod} is the element diameter in metres, and D_{ir} , D_{or} and D_{or} are the pitch-diameter values from the centre of the bundle to the centre of the element in the inner ring, middle ring and outer ring, respectively, in metres. This definition has been used in pressure-drop calculations for bundles of four and 37 elements. It may be extended to similar bundle geometries having the same-size elements distributed in rings (typical of a CANDU-type bundle). However, modifications may be needed to extend its application to other bundle geometries.

The correction factor for the bundle effect is expressed as

$$K_{geom} = \frac{CHF_D}{CHF_{D=0.008m}} = \left(\frac{D_{hy,annuli}}{0.008} \right)^n \quad (14)$$

with the exponent, n , evaluated with Equation (11). Figure 2 shows the variation of the geometric correction factor with respect to pressure.

The equivalent-annuli diameter (i.e., Equation (12)) is not applied to the calculations of thermodynamic quality at the OSV point and the friction factor, which were empirically derived with the traditional definition of hydraulic-equivalent diameter of the bundle.

2.3 Correction Factor for Orientation Effect

The correction factor for orientation effect on CHF, as suggested by Wong et al (1990) for tubes, is used. It is expressed as

$$K_{orient} = \frac{CHF_h}{CHF_v} = 1 - \exp\left(-\left(\frac{T_1}{3}\right)^{0.5}\right) \quad (15)$$

The ratio of inertia to gravitational forces in two-phase flow, T_1 , is defined as

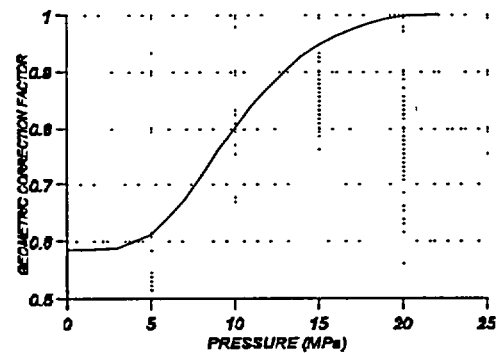


Figure 2: Variation of the geometric correction factor with pressure

$$T_1 = \frac{f_l (1 - x_g)^2 G^2}{(1 - \alpha)^2 g D_{hydraulic} \rho_f (\rho_f - \rho_g) \alpha^{0.5}} \quad (16)$$

where g is the acceleration due to gravity in m/s^2 and α is the void fraction. The actual vapour quality, x_g , was included to account for non-equilibrium effects in the subcooled-boiling region. The friction factor for the liquid phase, f_l , is calculated with a Blasius-type correlation derived for the 37-element bundles

$$f_l = a Re_l^{-b} \quad (17)$$

where Re_l is the liquid Reynolds number,

$$Re_l = \frac{(1 - x_g) G D_{hy}}{\mu_f} \quad (18)$$

The friction factor correlation was derived with the traditional definition of hydraulic equivalent diameter. Hence, the same definition is used in the present calculations.

As suggested by Wong et al. (1990), the void fraction is calculated with the correlation of Premoli et al. (1970) and the actual vapour quality is evaluated with the Saha and Zuber correlation (1974).

At low-flow conditions (mass fluxes below $500 \text{ kg/m}^2\text{s}$) where fully stratified flow may occur and CHF becomes zero, the mass flux threshold values are evaluated with the methodology recommended by Osamusali et al. (1990)

3. BUNDLE CHF TABLE

A bundle CHF table is set up using the 1995 tube CHF table of Groeneveld et al. (1996) and the correction factors (described in previous sections). The bundle CHF values in a reference channel are evaluated with the following equation

$$CHF_{bundle} = CHF_{tube} K_{geom} K_{orient} \quad (19)$$

where $CHF_{tube} = f(P, G, (x_{DO})_{tube})$, K_{geom} and K_{orient} are the correction factors for the geometric and orientation effects. Both the pressure, P , and mass flux, G , are the cross-sectional average value at a specific location. The tube-equivalent dryout quality is calculated by correcting the bundle dryout quality, $(x_{DO})_{bundle}$, which is the cross-sectional average value based on a heat balance, with the enthalpy imbalance, $(x_{DO})_{imb}$ (i.e., Equation (9)). All calculated table entries are examined to ensure correct parametric trends (i.e., CHF increases with decreasing quality, increasing mass flux, or decreasing pressure). Some of them are adjusted to eliminate irregular fluctuations. A section of the bundle CHF table is shown in Appendix I. As stated above, this table is based only on the proposed prediction method and not on any bundle experimental data

4. ASSESSMENT OF THE BUNDLE CHF TABLE

The bundle CHF table is assessed with the CHF data (of both water and Freon flow) to ensure that the methodologies, which are not based on any bundle CHF data, are valid. This assessment is performed by comparing the predicted dryout power against the measurements for the same inlet flow conditions in various experiments (without a prior knowledge of the dryout location and quality)

4.1 Bundle CHF Data

A number of full-scale bundle tests were performed using electrically heated simulators of a 37-element segmented bundle string equipped with spacers and bearing pads. Both the axial and radial heat-flux distributions of the bundle strings were simulated by using tubes with varying wall thicknesses. The radial heat-flux distribution of the bundle corresponds to the natural-uranium profile. Two axial heat-flux distributions have been simulated: uniform and downstream skewed-cosine profiles.

Loop conditions at both inlet and outlet ends of the bundle string were monitored with differential-pressure cells and Chromel-Alumel (K-Type) thermocouples. In addition, pressure taps were installed at various locations along the bundle string to obtain pressure-drop data. Spring-loaded thermocouples mounted on sliding carriers were installed inside the elements. They were moved axially and radially to obtain surface-temperature measurements on various locations of each element. Dryout was assumed to occur when the surface temperature increased rapidly (about 5°C).

The light-water data were obtained with four different bundle strings. Two uniform-bundle strings (with six and three metres heated-length values) and one non-uniform-bundle string (with six metres heated length) were tested in the U-1 loop at Chalk River Laboratories (CRL), and one non-uniform-bundle string (with six metres heated length) was recently tested at Stern Laboratories (SL). The Freon-12 data were obtained with two bundle strings in the MR-3 loop at CRL. These bundle strings were heated over a six-metre length with either uniform or stepped downstream-skewed-cosine profiles.

4.2 Effect of Axial-Flux Distribution on CHF

The effect of axial-flux distribution on CHF must be accounted for, in the comparison against data of the non-uniform bundle string. In the present study, the boiling-length-average (BLA) heat-flux approach is used. However, the BLA heat flux is evaluated from the point of OSV, rather than from the saturation point (as suggested by Bertoletti et al. 1964). The OSV point is a more realistic transition between single- and two-phase flow, due to the enthalpy imbalance within a 37-element bundle. A subsequent comparison shows that the prediction accuracy is not sensitive to the transition point in calculating the BLA heat flux.

4.3 Fluid-to-Fluid Modelling of CHF

In the comparison against the Freon data, the local flow conditions are converted into water equivalent values via the fluid-to-fluid modelling parameters (Groeneveld et al 1986). The pressure is modelled via the liquid-to-vapour density ratio,

$$\left(\frac{\rho_f}{\rho_g} \right)_{Freon} = \left(\frac{\rho_f}{\rho_g} \right)_{H_2O} \quad (20)$$

the mass flux is based on the Weber number,

$$\left(\frac{G^2 D_w}{\sigma \rho_f} \right)_{Freon} = \left(\frac{G^2 D_w}{\sigma \rho_f} \right)_{H_2O} \quad (21)$$

where F is the surface tension in N/m , and the thermodynamic quality is based on

$$x_{q, Freon} = x_{q, H_2O} \quad (22)$$

The local CHF value is evaluated with the bundle CHF table based on the light-water equivalent flow conditions, and the equivalent-CHF value of Freon flow is converted with the boiling number

$$\left(\frac{CHF}{G H_{fr}} \right)_{Freon} = \left(\frac{CHF}{G H_{fr}} \right)_{H_2O} \quad (23)$$

The same modelling relationships (i.e., Equations (20) to (23)) are used to extend the light-water-based prediction methods to heavy-water analyses (heavy water is the coolant used in CANDU reactors)

For vertical channels, the CHF values evaluated with the table (derived for horizontal flow) are converted to vertical bundle CHF values with the orientation correction factor, i.e.,

$$CHF_{vertical\ bundle} = \frac{CHF_{bundle\ table}}{K_{geom}} \quad (24)$$

4.4 Prediction Accuracy of the Bundle CHF Table

Table 1 summarizes the prediction accuracy of the bundle CHF table for dryout power. Overall, the table predicts the data with an average error of 0.76% and a root-mean-square (rms) error of 5.71%. This verifies the appropriateness of the present methodology for extending the vertical CHF value of an 8-mm tube to a horizontal 37-element bundle. The best prediction accuracy is shown for the SL non-uniform bundle data, and the worst for the CRL non-uniform bundle data. The average error is defined as

Table 1. Prediction accuracy of the bundle CHF table.

Test strings	No of Data	Error (%)	
		Avg	Rms
SL non-uniform bundle	407	0.22	4.90
CRL uniform bundle	256	-1.47	5.63
CRL non-uniform bundle	108	1.14	8.42
Freon flow	634	1.95	5.65
All bundle data	1405	0.76	5.71

$$Average\ Error = \frac{1}{N} \sum_{i=1}^N (Error)_i \quad (25)$$

and the rms error is

$$Rms\ Error = \sqrt{\frac{1}{N} \sum_{i=1}^N (Error)_i^2} \quad (26)$$

where

$$Error = \frac{Pred.\ Power - Expt.\ Power}{Expt.\ Power} \quad (27)$$

Figure 3 shows the distributions of data at various error ranges (e.g., -1 to 1%, 1 to 3%, 3 to 5%, etc.) for high-pressure water flow. The number of data within various ranges of prediction error generally follows the normal error distribution. However, a small bias towards underprediction is observed (i.e., within -3% to -1%). Similar prediction accuracies were obtained for both water and Freon data, even though the presented methodologies were derived mainly with tube data obtained in water. This demonstrates that the fluid-to-fluid modelling approach is also appropriate for 37-element bundle analyses.

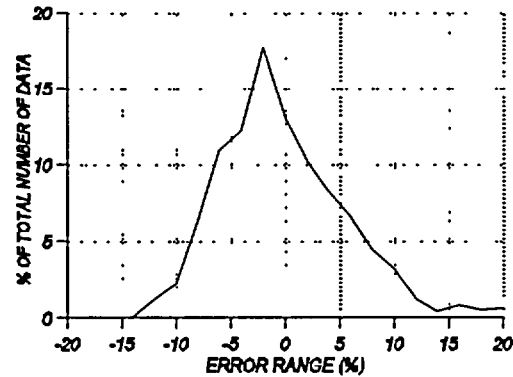


Figure 3 The distributions of data within various ranges of prediction error for the bundle CHF tables.

5. CONCLUSIONS AND FINAL REMARKS

- ! A CHF look-up table has been developed for the CANDU 37-element bundle string. It is based on the tube CHF table and three correction factors to account for the enthalpy imbalance, geometry and channel orientation.
- ! The prediction accuracy of the bundle CHF table has been assessed with data of full-scale bundle strings having either uniform or non-uniform axial heat-flux distributions. Overall, the average error is 0.76% and the rms error is 5.71% for 1405 points of either Freon or water flow.
- ! The 1997 bundle CHF table is valid only for aligned bundles, which were simulated in the full-scale bundle tests. It is anticipated that it will underpredict the CHF values for a string of misaligned bundles, because the bundle junction increases the mixing and reduces the enthalpy imbalance.
- ! For bundle strings having a radial heat-flux distribution different from that of natural-uranium fuel, the correction factor recommended by Yin et al (1991) should be used.
- ! The present study has demonstrated that CHF in CANDU fuel-bundle geometries can be predicted accurately with a generalized methodology that is not dependent on bundle CHF data. This provides a much wider range of application than correlations.
- ! Further improvements in the prediction accuracy can be made by updating the table entries using the experimentally measured bundle CHF values.

6. REFERENCES

- Bertoletti, S., Gaspari, G.P., Lombardi, C., Soldaini, G. and Zavattarelli, R., 1964, Heat Transfer Crisis in Steam-Water Mixtures - Experimental Data in Round Tubes and Vertical Upflow Obtained during the CAN-2 Program, CISE-R-90
- Carver, M.B., Tahir, A., Kiteley, J.C., Banas, A.O., Rowe, D.S. and Midvidy, W.I., 1990, Simulation of the Distribution of Flow and Phases in Vertical and Horizontal Bundles Using the ASSERT-4 Subchannel Code, *Nuclear Engineering and Design*, vol 122, pp 12-23.
- Doerffer, S., Groeneveld, D.C., Cheng, S.C. and Rudzinski, K.F., 1994, A Comparison of Critical Heat Flux in Tubes and Annuli, *Nuclear Engineering Design*, vol 149, pp 167-175.
- Groeneveld, D.C., Leung, L.K.H., Kirillov, P.L., Bobkov, V.P.,

Smogalev, I.P., Vinogradov, V.N., Huang, X.C. and Royer, E., 1996, The 1995 Look-Up Table for Critical Heat Flux in Tubes, *Nuclear Engineering and Design*, vol 163, pp 1-23

Groeneveld, D.C., Kiameh, B.P. and Cheng, S.C., 1986, Prediction of Critical Heat Flux (CHF) for Non-Aqueous Fluids in Forced Convective Boiling, *Proc of the 8th Int Heat Transfer Conf.*, San Francisco, U.S.A., vol. 5, pp. 2209-2214

Heron, R.A., Kinneir, J.H., Stevens, G.F. and Wood, R.W., 1969, Burn-Out Power and Pressure Drop Measurements on 12 ft 7-Rod Clusters Cooled by Freon-12 at 155 PSIA, AEEW-R 655

Leung, L.K.H. and Hotte, G., 1997, A Generalized Prediction Method for Single-Phase Pressure Drop in a String of Aligned CANDU-Type Bundles, *Proc of the 20th CNS Simulation Symposium*, Sept 7-9, Niagara-on-the-Lake, Ontario, vol II

Osamusalu, S.I., Groeneveld, D.C. and Cheng, S.C., 1990, Onset of Flow Stratification in Horizontal Rod Bundles, *Proc. of the 3rd Int Conf. On Simulation Methods in Nuclear Engineering*, April 18-20, Montreal, Canada

Premoli, A., Francesco, D. and Prina, A., 1970, An Empirical Correlation for Evaluating Two-Phase Mixture Density under Adiabatic Conditions, *Proc of the European Two-Phase Flow Group Meeting*, Milan.

Saha, P. and Zuber, N., 1974, Point of Net Vapour Generation and Vapour Void Fraction in Subcooled Boiling, *Proc of the 5th International Heat Transfer Conf.*, Tokyo, vol 4, pp 175-179

Wong, W.C., 1997, Effect of Tube Diameter on Critical Heat Flux in Vertical Steam-Water Flow, M.A.Sc. Thesis, University of Ottawa

Wong, Y.L., Groeneveld, D.C. and Cheng, D.C., 1990, CHF Prediction for Horizontal Tubes, *Int. J Multiphase Flow*, vol 16, no 1, pp 123-138

Yin, S.T., Groeneveld, D.C. and Wakayama, M., 1991, The Effect of Radial Flux Distribution on Critical Heat Flux in 37-Rod Bundles, *Proc 12th National Heat Transfer Conf.*, July 28-31, Minneapolis, USA, vol. 5, pp 277-283

7. ACKNOWLEDGMENTS

The authors would like to thank W.C. Wong for providing the data on the diameter correction factor, and test engineers at Ontario Hydro and Stern Laboratories for providing data from the recent full-scale 37-element bundle tests

APPENDIX I: Section of the bundle CHF table** for light-water flow (CHF values in $\text{kW}\cdot\text{m}^{-2}$).

Pressure (kPa)	Mass Flux ($\text{kg}\cdot\text{m}^{-2}\cdot\text{s}^{-1}$)	Thermodynamic Quality																							
		-0.5	-0.4	-0.3	-0.2	-0.15	-0.1	-0.1	0	0.05	0.1	0.15	0.2	0.25	0.3	0.35	0.4	0.45	0.5	0.6	0.7	0.8	0.9	1	
3000	0	1588	1576	1182	788	591	262	129	0	0	0	0	0	0	0	0	0	0	0	0	0	0	0	0	
3000	50	1591	1588	1585	1582	1579	265	132	0	0	0	0	0	0	0	0	0	0	0	0	0	62	58	41	0
3000	100	1594	1591	1588	1585	1582	268	265	0	0	0	0	0	0	0	238	235	229	223	218	206	182	87	51	0
3000	300	1597	1594	1591	1588	1585	1577	1471	1320	1241	1224	1201	1165	1097	982	893	722	625	482	275	186	90	54	0	0
3000	500	2835	2832	2829	2642	2520	2387	2235	2115	2029	1926	1815	1696	1507	1329	951	725	628	485	278	189	93	57	0	0
3000	1000	3897	3366	3316	3130	3027	2918	2811	2703	2557	2330	2164	2037	1836	1343	954	728	631	488	281	192	96	60	0	0
3000	1500	4415	3905	3514	3184	3181	3178	3175	3069	2931	2333	2167	2040	1839	1346	957	731	634	491	284	195	99	63	0	0
3000	2000	4418	4061	3517	3187	3184	3181	3178	3072	2934	2336	2170	2043	1842	1349	960	734	637	494	287	198	102	66	0	0
3000	2500	4421	4064	3520	3190	3187	3184	3181	3075	2937	2339	2173	2046	1845	1352	963	737	640	497	290	201	105	69	0	0
3000	3000	5006	4607	4031	3345	3190	3184	3181	3078	2940	2342	2176	2049	1848	1355	966	740	643	500	381	262	106	66	0	0
3000	3500	5951	5426	4813	4027	3614	3353	3187	3081	2943	2345	2179	2052	1851	1358	969	743	678	610	505	275	107	66	0	0
3000	4000	8684	7843	5175	4410	3907	3480	3215	3084	2946	2348	2182	2055	1854	1361	972	746	720	663	561	305	124	67	0	0
3000	4500	9212	8253	7391	4943	4362	3773	3352	3087	2949	2351	2185	2058	1857	1364	975	831	766	732	576	316	127	68	0	0
3000	5000	9722	8664	7738	5518	4924	4231	3526	3090	2952	2354	2188	2061	1860	1367	1030	911	832	746	619	338	141	68	0	0
3000	5500	10216	9060	8070	6073	5458	4663	3732	3237	2955	2357	2191	2064	1863	1370	1119	995	897	803	652	350	162	96	0	0
3000	6000	10692	9439	8396	7322	5879	5197	3994	3418	2958	2360	2194	2067	1866	1425	1236	1110	959	841	669	381	188	103	0	0
3000	6500	11159	9857	8705	7578	6240	5683	4280	3538	2961	2363	2197	2070	1869	1526	1373	1206	1035	870	684	411	216	120	0	0
3000	7000	11615	10238	8999	7816	7066	6025	4534	3652	2964	2366	2200	2073	1872	1632	1429	1273	1109	922	696	441	242	134	0	0
3000	7500	12067	10615	9283	8046	7286	6199	4781	3749	2968	2369	2202	2076	1953	1746	1530	1335	1167	994	720	474	272	152	0	0
3000	8000	12518	10980	9555	8260	7497	6337	5284	4065	3191	2563	2527	2483	2354	2068	1662	1449	1265	1074	766	510	297	168	0	0
5000	0	1278	1271	953	635	262	259	126	0	0	0	0	0	0	0	0	0	0	0	0	0	0	0	0	0
5000	50	1281	1278	1275	1272	265	262	129	0	0	0	0	0	0	0	0	0	0	0	0	0	0	50	38	0
5000	100	1284	1281	1278	1275	268	265	262	0	0	0	0	0	0	0	220	218	213	203	194	181	84	48	0	0
5000	300	1287	1284	1281	1278	1275	1272	1233	1108	1035	1023	1020	1009	981	938	890	718	608	479	272	183	87	51	0	0
5000	500	2219	2216	2213	2043	1920	1835	1782	1775	1758	1681	1594	1522	1464	1279	924	721	611	482	275	186	90	54	0	0
5000	1000	2736	2605	2483	2376	2326	2278	2236	2195	2106	2013	1929	1844	1677	1282	927	724	614	485	278	189	93	57	0	0
5000	1500	3588	3169	2956	2732	2657	2579	2505	2431	2356	2210	2063	1962	1680	1285	930	727	617	488	281	192	96	60	0	0
5000	2000	4149	3719	3267	2941	2820	2654	2536	2451	2382	2213	2066	1965	1683	1288	933	730	620	491	284	195	99	63	0	0
5000	2500	4418	4061	3517	3003	2939	2810	2610	2480	2400	2216	2069	1968	1686	1291	936	733	623	494	287	198	102	66	0	0
5000	3000	4635	4289	3791	3198	3056	2911	2731	2517	2415	2219	2072	1971	1689	1294	939	736	626	497	278	259	103	63	0	0
5000	3500	4971	4570	4093	3445	3226	3009	2763	2559	2418	2222	2075	1974	1692	1297	942	739	638	607	502	272	104	63	0	0
5000	4000	5648	5149	4630	3941	3445	3130	2796	2562	2421	2225	2078	1977	1695	1300	945	742	679	645	558	302	121	64	0	0
5000	4500	6108	5532	4975	4290	3695	3307	2909	2588	2436	2228	2081	1980	1698	1303	948	828	758	729	573	313	124	65	0	0
5000	5000	6585	5936	5321	4649	4018	3544	3059	2623	2452	2231	2084	1983	1701	1306	1027	908	799	743	616	335	138	80	0	0
5000	5500	6957	6233	5587	4913	4343	3783	3279	2861	2487	2234	2087	1986	1704	1309	1116	992	894	800	649	347	159	93	0	0
5000	6000	7606	6778	6061	5388	4821	4214	3654	3102	2569	2246	2090	1989	1707	1368	1233	1107	956	838	666	378	185	100	0	0
5000	6500	8079	7176	6391	5644	5247	4567	3919	3256	2642	2256	2093	1992	1721	1523	1370	1203	1032	867	681	408	213	117	0	0
5000	7000	9059	8031	7113	6230	5565	4846	4120	3361	2692	2277	2120	2026	1808	1629	1426	1270	1106	919	693	438	239	131	0	0
5000	7500	9500	8405	7409	6473	5819	5116	4327	3487	2788	2368	2199	2073	1950	1743	1527	1332	1164	991	717	471	269	149	0	0
5000	8000	9880	8729	7651	6694	6050	5350	5281	3712	2949	2560	2524	2480	2351	2065	1659	1446	1262	1071	763	507	294	165	0	0
6000	0	1196	1156	867	262	259	126	123	0	0	0	0	0	0	0	0	0	0	0	0	0	0	0	0	0
6000	50	1199	1196	1193	265	262	129	126	0	0	0	0	0	0	0	0	0	0	0	0	0	0	47	35	0
6000	100	1202	1199	1196	268	265	262	259	0	0	0	0	0	0	0	210	209	205	197	153	137	81	45	0	0
6000	300	1205	1202	1199	1196	1193	1190	1162	1049	976	962	959	944	920	898	861	634	480	354	269	180	84	48	0	0
6000	500	1935	1900	1897	1803	1681	1584	1518	1505	1501	1470	1405	1363	1318	1195	906	637	483	357	272	183	87	51	0	0
6000	1000	2554	2439	2294	2155	2089	2027	1992	1943	1875	1810	1763	1742	1557	1198	909	640	486	360	275	186	90	54	0	0
6000	1500	2812	2809	2628	2431	2356	2286	2216	2146	2072	1907	1821	1763	1560	1201	912	643	489	363	278	189	93	57	0	0
6000	2000	3412	3055	2939	2687	2532	2372	2275	2189	2085	1910	1824	1766	1563	1204	915	646	492	366	281	192	96	60	0	0
6000	2500	3893	3577	3285	2949	2772	2591	2402	2286	2088	1913	1827	1769	1566	1207	918	649	495	369	284	195	99	63	0	0
6000	3000	4431	4101	3623	3195	2975	2747	2562	2300	2091	1916	1830	1772	1569	1210	921	652	498	459	375	227	100	60	0	0
6000	3500	4820	4441	3965	3442	3162	2865	2587	2303	2094	1919	1833	1775	1572	1213	924	655	635	604	499	262	101	60	0	0
6000	4000	5319	4869	4353	3700	3370	2993	2588	2306	2097	1922	1836	1778	1575	1216	927	739	664	636	555	299	118	61	0	0
6000	4500	5640	5134	4586	3914	3563	3174	2737	2366	2100	1925	1839	1781	1578	1219	930	825	725	717	570	310	121	62	0	0
6000	5000	6041	5481	4872	4156	3780	3374	2919	2509	2169	1942	1852	1784	1581	1222	1024	905	786	733	613	332	135	77	0	0
6000	5500	6532	5882	5241	4532	4076	3594	3094	2625	2252	1991	1874	1802	1612	1273	1113	989	874	797	646	344	156			

6000	6500	7710	6879	6083	5201	4677	4331	3651	2987	2412	2078	1922	1849	1684	1520	1367	1200	1029	864	678	405	210	114	0
6000	7000	8820	7852	6911	5204	4834	4590	3858	3132	2512	2151	1992	1917	1805	1626	1423	1267	1103	916	690	435	236	128	0
6000	7500	9103	8085	7089	6116	5533	4847	4069	3306	2689	2365	2196	2070	1947	1740	1524	1329	1161	988	714	468	266	146	0
6000	8000	9471	8386	7335	6386	5791	5281	5278	3474	2825	2557	2521	2477	2348	2062	1656	1443	1259	1068	760	504	291	162	0

FULL SCALE WATER CHF TESTING OF THE CANFLEX BUNDLE

G.R. Dimmick and W.W. Inch, (AECL), J.S. Jun and H.C. Suk, (KAERI)
G.I. Hadaller, R. Fortman and R. Hayes, (Stern Laboratories)

Fuel Channel Thermalhydraulics Branch
Chalk River Laboratories
Atomic Energy of Canada Limited
Chalk River, Ontario
CANADA K0J 1J0

Abstract

CANFLEX is a 43-element CANDU fuel bundle that uses two diameters of elements, 13.5 mm for the inner eight, and 11.5 mm for the remainder. The thermalhydraulic performance of the CANFLEX bundle has been improved over the current 37-element design by both the increased fuel subdivision and by the use of patented CHF enhancing buttons attached to the elements.

To quantify the improved performance, a series of CHF and pressure drop measurements with an electrically heated assembly simulating a string of twelve aligned CANFLEX bundles in a 5.1% crept CANDU fuel channel, were undertaken at Stern Laboratories. The heated part of the string was nominally 6 m long and was equipped with spacer planes, bearing pads, button planes and simulated end plates to mimic the geometry of a string of aligned CANFLEX bundles. The axial heat flux profile was a cosine skewed towards the outlet end of the fuel string and the radial profile simulated that for natural uranium fuel. The five downstream bundles were equipped with moveable internal thermocouples to measure the surface temperature and to detect CHF. As one of the applications of CANFLEX is to alleviate the eroding operating margins due to reactor aging, the string was tested in a flow tube that simulated a 5.1% crept pressure tube.

Both single- and two-phase pressure drop, and CHF data were taken. The flow conditions covered the ranges from 6 to 11 MPa outlet pressure, 10 to 25 kg/s flow, and 200 to 290°C channel inlet temperature. For the same channel inlet conditions both the single- and two-phase pressure drops were very similar to 37-element fuel. Thus, there should be no significant effect on overall reactor operation during transition refueling. For the parameter region around the normal reactor operating conditions, the channel dryout power for CANFLEX was at least 10% higher than that for the 37-element design, based on similar channel inlet conditions. The focus of this paper is on the experimental hardware and the procedures used to obtain high quality thermalhydraulic data.

1. INTRODUCTION

The primary objective of the tests was to obtain CHF and pressure drop data for CANFLEX over the range of flow conditions of interest for reactor operation. The bundle design, experimental procedures, data acquisition, QA etc., all built on previous experimental campaigns conducted at Stern Laboratories with a 37-element bundle [1]. A key concern in this program was ensuring repeatability and demonstrating the validity of the data. Also, because this was the first testing for CHF of a CANFLEX bundle in water, the CHF behaviour e.g. preferred dryout locations, was unknown. Thus, a number of single and two phase tests were used to both understand the thermalhydraulic behaviour of the bundle, and to ensure data

validity. These consisted of heat balances, single phase rotational temperature scans, Onset of Nucleate Boiling (ONB), Onset of Significant Void (OSV), and single- and two-phase pressure drop measurements. The emphasis in this paper is on the experimental hardware and the procedures used to obtain high quality thermalhydraulic data. The details of the data themselves are reported in [2].

2. EXPERIMENTAL FACILITY

2.1 Fuel String Simulation

The fuel string simulation is an electrically heated, 43-element, segmented design with a nominal 6 metre heated length and a non-uniform, downstream skewed cosine, axial heat flux distribution, as shown in Figure 1. The fuel string external geometry was constructed in accordance with general fuel design drawings and was intended to provide an exterior surface that as close as possible simulated a fully aligned string of 12 CANFLEX fuel bundles. The design maximum operating power level is 13.5 MW at 240 volts DC with a design pressure of 13.5 MPa and a maximum local sheath surface temperature of 650°C.

The fuel string consists of twelve simulated fuel bundles, each 495.3 mm long cold (480.1 mm actual heated length), with fully aligned elements and end plates, representative of the CANFLEX design. The simulated spacers, bearing pads and buttons are a hollow design to minimize local current mal-distributions. The diameter of the inner eight heater tubes is 13.5 mm and the diameter of the remaining heater tubes is 11.5 mm.

The twelve fuel bundles are identified as "A" through "L", where "A" is located at the inlet, or upstream end, and "L" is located at the outlet, or downstream end. The bundle cross-section showing the orientation of the end plates, and the element nomenclature, as viewed looking downstream, is given in Figure 2. The radial flux distribution, expressed in terms of local linear element power ratio with respect to the average, is 1.034/ 1.081/ 0.873/ 1.056 from center to outer ring element, which simulated a natural uranium fueled CANFLEX bundle.

2.2 Test Section

The test section comprises the pressure housing, ceramic liners which form the flow channel and provide electrical isolation of the fuel string, "tee sections" at each end with electrical isolating flanges, sealing flanges at each end for the electrode extensions which provide for relative motion due to differential thermal expansion, pressure tap instrumentation, thermal insulation and structural supports. Suitable leads are included at each end to connect the heater electrode extensions to the power supplies.

The ceramic liners, which form the flow channel and simulate the inside surface of the reactor pressure tube, are made from high purity alumina (Al_2O_3). At the inlet and outlet of the channel the liners are "uncrept" and have a uniform inside diameter of 103.86 mm (104.11 mm hot, at 303°C). The liners for the crept portion of the flow channel have inside diameters machined to provide non-uniform axial profiles to simulate crept pressure tubes with maximum diametral creep of 5.1%. The axial creep profile is shown along with the axial flux profile in Figure 1.

Each liner segment is approximately 0.25 metres long with interconnecting steps at each end for alignment. The inner surface is very smooth (roughness less than 1.5 micron rms, new, prior to use). To minimize flow bypass in the annulus between the liners and the pressure housing, the diametral clearance between the liners and the housing is small (nominally 0.23 mm, at operating conditions) and special "piston ring" seals are installed between liners at various locations along the length of the test section.

The pressure boundary is fabricated from identical short (1 m) length spools made from 410 stainless steel forgings with integral flanges. The clamped connections are sealed with metal "O-rings" and have interconnecting steps at each end to ensure alignment. The tee sections at each end incorporate calming regions with re-entrant geometries to minimize flow mal-distribution. The test section is mounted on pipe rollers to allow for thermal expansion, with the downstream flange fixed.

2.3 Test Loop

The primary test loop [3], shown in Figure 3, consists of a main circulating pump, the channel inlet and outlet feeder piping, a preheater (normally used for pressure drop tests), two heat exchangers, a steam/water separator, a condenser, a filter, and various valves and controllers to control flow, pressure and temperature.

Heat rejection from the primary loop is accomplished by passing flow through the heat exchangers and by feed and bleed using the separator and condenser. The secondary water for the heat exchangers and condenser is recirculated by pumps through two cooling towers.

The flow through the test section is controlled by pneumatically operated globe valves in the inlet feeder piping. Some flow is normally maintained through the loop bypass line to condense steam in the outlet line before entering the separator. The system pressure is maintained by controlling the rate of bleed from the separator and the temperature is adjusted by controlling the rate of feed of the cold makeup water in conjunction with control of the primary flows through the heat exchangers.

A high pressure chemical feed pump is used to inject hydrazine into the primary loop water at the circulating pump inlet to control the pH level of the water between 7.2 and 8.0. This serves to maintain the dissolved oxygen content below 5 ppb to minimize corrosion of the test loop components which are mainly carbon steel. The electrical conductivity of the loop water is also monitored and generally held below 5 mho.cm^{-1} to prevent appreciable electrolytic corrosion in the test section. A low pressure (for initial startup) loop bypass cartridge filter and a high pressure (for continuous use) loop bypass cartridge filter are installed across the main circulating pump to remove any particulate matter in the loop water during operation.

2.4 Power Supplies

The electrical power to the fuel string is provided by seven individually controlled rectifiers, with a total rated output capacity of 13.6 Megawatts DC (i.e. 56,666 amps @ 240 volts). The power supplies are connected to the fuel string with the positive terminals grounded at the downstream end and the negative terminals floating at the upstream end. The specified maximum allowable output ripple of the power supplies is 3% of output power, over the range of 25% to 100% output power. The ripple frequency is 720 Hz.

The seven power supplies are remotely controlled using the data acquisition system computer. Using custom, keyboard driven software, the computer outputs a control setpoint, handles the current sharing among the power supplies, and provides incremental control, ramping, etc. of each power supply. Incremental steps of 25 kilowatts (total of all supplies) are typically used for power increases and decreases. Steps of 5 kilowatts may be used for small increases as the onset of CHF is approached.

2.5 Instrumentation

The test section is fully instrumented to measure temperature, pressure and differential pressure at the locations shown in Figure 4.

The fluid temperatures at the test section inlet and outlet, and at the flow meters, are measured using Resistance Temperature Detectors (RTD). Two RTD's are located at the test section inlet and outlet tees, for redundant measurements, and one RTD is located at the flow measurement location. The primary coolant flow to the test section is measured using two calibrated orifice meters in series, each with an estimated measurement uncertainty of $\pm 0.3\%$ (2σ) of full scale.

Absolute pressures are measured at the fuel string inlet and outlet with two pressure transmitters at each location for redundant measurement. Differential pressures are measured along the flow channel over a 0.4953 metre length (equivalent to 1 fuel bundle). The pressure taps are located on the sides of the channel, slightly below the horizontal centerline to minimize trapped vapour in the sense lines, and upstream of the bundle centre-plane appendages to avoid flow disturbances.

The overall power provided to the fuel string is calculated from the measured total current (using a Hall effect transducer installed around the test section) and the voltage potential between the inlet and outlet closure flanges (direct measurement). In addition, the electrical power from individual supplies is calculated from the measured current (shunt meter) of each supply and the voltage potential measured between the inlet and outlet flanges. The sum of these individual power measurements provides a redundant check of the total power.

The CHF detection instrumentation consists of two hundred and fifty-eight (258) thermocouples that are mounted in movable carriers inside most of the heater elements in the downstream half of the fuel string. The thermocouple tips are spring loaded to contact the inner surface of the heaters. The carriers can be rotated and moved axially, by a remotely controlled drive mechanism, to measure the inside wall temperature over most of the surface of the downstream heater elements. CHF detection thermocouples are installed in Bundles "H" through "L". The thermocouple carrier design, utilizes Macor material with grooves surrounding the thermocouple tip and slits in the sides to reduce conduction and minimize any temperature offset effects during transient and post-dryout testing. A thermocouple drive mechanism which is remotely controlled by a Programmable Logic Controller (PLC) device is used to position the bundle thermocouples. It can move all of the instrument strings together axially and rotate each instrument string independently. The axial speed of the drive is adjustable from 0.03 to 1.1 $\text{cm}\cdot\text{s}^{-1}$ and the rotational speed is adjustable from approximately 0.01 to 0.07 $\text{rev}\cdot\text{s}^{-1}$.

2.6 Data Acquisition System

The data acquisition system consists of a MicroVAX 4000-100 mini-computer (running under a VAX/VMS operating system) with four CPI scanners (120 A/D input channels each), a MicroMAC digital input/output system, various magnetic disk storage units, a 1 Gb/650 Mb R/W optical disk storage unit, various graphics terminals, text display terminals, video display monitors, and graphics printers.

The individual instrumentation signals are connected, via signal conditioning devices, to the data acquisition system. Prior to each series of testing, the instrumentation devices are connected via patch cabling and connection devices to the CPI scanners and the input signal paths are verified by exciting each instrument (as close to each instrument as possible) and observing an appropriate change in the engineering value displayed by the data acquisition system.

During testing, the data acquisition system uses in-house custom software to scan and digitize approximately 370 instrument signals at the rate of 5 or 10 samples per second per channel. A unique test point number is automatically incremented and assigned each time a data file is saved. The signals are converted into engineering units and selected data are continuously displayed on terminals and video displays for on-line monitoring by test personnel.

The data acquisition system computer also provides on-line monitoring of the fuel string thermocouples for CHF detection (dryout). The operators can select on-line, via keyboard entry, up to 10 thermocouple signals for real time display on each of two special graphics display terminals. Temperature changes of the order of 1°C are readily detectable on the screen and dryout behaviour is easily distinguished on the monitored thermocouple traces. A typical display is shown in Figure 5.

For the steady-state CHF tests, all of the thermocouples signals are continuously scanned by the data acquisition system and the standard deviation of each signal is calculated. If the standard deviation of any of the bundle thermocouples exceeds 0.5°C, the channel number and identification for that thermocouple is flashed onto the video screen to alert the test operators. It can then be selected for real-time viewing and for visual confirmation of dryout by the test engineers. This criterion, using the standard deviation, or noise, of the thermocouple signals to indicate dryout, was selected based on past experience. It gives good agreement with the visual observations and generally avoids "false" indications of dryout that can occur during changes in power or during bundle thermocouple rotation if the criterion was based on changes in absolute temperature.

In addition to the above automatic dryout detection system, each thermocouple signal (corrected for the temperature rise across the heater wall) is compared to the average of 10 upstream thermocouple signals. If the temperature for any individual thermocouple is 10 degrees or more above this average, the channel number of that thermocouple is flashed onto the video screen to alert the operators. Thus, the test operators are alerted if any of the 258 bundle thermocouples goes into a post-dryout condition, where the temperature can become relatively steady and hence may not be picked up by the previous temperature noise dryout detection system.

For steady-state tests, all of the data signals are recorded for a 30 second period, typically 300 samples per channel, at an operator selected appropriate time. For time-history recordings, the signals are recorded continuously for a selected period (typically 30 to 45 minutes). All of these data are stored and are retrievable for post-test processing, such as plotting selected data channels versus time, converting the as-measured heater temperatures to heater tube outer surface temperatures, etc. Also, via Ethernet communication links, the data are transferred to IBM compatible PC's for insertion of the steady-state data into database summary files and for further analyses, such as preparation of contour plots of the heater tube outer surface temperatures.

3. TEST PROCEDURES

Because of electricity costs, all testing was done during weekends when off-peak power was available. A typical test weekend consisted of loop startup at zero power on Friday morning with a series of single-phase pressure drop runs being performed at up to 260°C, the loop temperature being reached using pump heat. The loop was maintained hot (with zero power on the test section) for both the Friday and Saturday night periods when CHF testing was not ongoing. Maintaining the loop hot during the weekend, put less stress on the bundle and loop components, and also allowed more efficient data production as warmup times were eliminated. With this procedure a whole testing campaign could be completed in about 5 weekends. Besides the CHF tests, a number of tests were performed to both monitor the correct operation of the loop and bundle, and also to provide a fuller understanding of the thermalhydraulics within the bundle. These other tests are detailed below.

3.1 Heat Balances

Heat balances at 2 and 8 MW were performed prior to the start of each weekends testing. Additional heat balances were also performed on the Saturday evening, Sunday morning and at the end of the weekend to

ensure that all the loop instrumentation continued to perform correctly. Typical heat losses were between 25 and 50 kW, i.e. less than 1%, and could be ascribed to a combination of heat loss through the test station insulation and loss to the cooling systems for the end seal flanges.

3.2 Temperature Rotational Scans

During all of the 2 MW heat balances, the test section thermocouples were positioned axially just upstream of the mid-plane bearing pads and fully rotated while recording the readings. This resulted in a complete temperature map of all the rods at that axial location. An example of one of these maps is given in Figure 6, where the local temperatures are depicted by various colours. It is immediately obvious that the upper part of the bundle is significantly cooler than the lower part. This confirms that the bundle was physically sitting on the bottom of the flow tube with the large bypass gap (as a result of the 5.1% creep) at the top of the bundle. An additional observation is that line of symmetry is not completely vertical but passes through approximately rods 2 and 13. This slight tilt was caused by the large magnetic forces attracting the bundle to a slightly off center steel floor beam. The tilt will have no significant effect on the CHF results and was monitored throughout the tests to ensure that it did not change.

3.3 Onset of Nucleate Boiling (ONB)

Measurement of the ONB in individual subchannels provides a method of estimating the enthalpy distribution throughout the bundle. In these tests the thermocouples were oriented towards the subchannels and starting from single-phase conditions and with constant flow, inlet temperature and pressure, the power was increased in small steps while recording the thermocouple temperatures. An example of these data is shown in Figure 7. Initially, before boiling occurs, the temperatures are below saturation and rise relatively steeply with power. When the ONB point for each thermocouple is reached, the thermocouple traces flatten out and the temperature is close to saturation and relatively independent of power. In Figure 7 only a few of the bundle thermocouples are plotted but they show that the rods on the upper half of the bundle require about twice the power to reach nucleate boiling compared to rods on the bottom of the bundle. This dramatically illustrates the large bypass flow that exists with a 5.1% crept liner.

3.4 Onset of Significant Void (OSV)

Measurement of the pressure drops along the bundle during the ONB tests gives information on the OSV. The data for the last six pressure taps in the bundle for the test in Figure 7 are given in Figure 8. The flat portion of the curve is the single-phase pressure drop and the knee in the DP curves is where significant void first occurs in the bundle at that location. The single-phase pressure drop for DP8 to DP11 are very similar as these are in the region of maximum creep. At the DP12 and DP13 locations the pressure tube diameter is changing rapidly back to the uncrept value which accounts for the higher single-phase pressure drop. The progressive movement of the OSV point up the bundle with increasing power is evident.

3.5 Single- and Two-Phase Pressure Drop

A series of single-phase pressure drop measurements were made prior to starting CHF testing each weekend. These were used to monitor the condition of the bundle for buildup of crud deposits on the heater surfaces. An example of the pressure profile along the heater string in single phase is shown in Figure 9. The profile deviates from a straight line due to the varying axial creep profile which affects the bundle flow area and hence pressure gradient along the bundle length. Generally it was found that the single phase pressure drop would rise by about 1 to 2% as a result of the crud deposited during one weekend's CHF testing. In addition to the specific single phase pressure drop runs, the pressure transducer signals were automatically recorded whenever a computer scan was taken, e.g. during OSV or CHF tests and this resulted in a large number of two-phase pressure drop data. A typical axial pressure gradient in two-phase is

also shown in Figure 9. Comparison with a single phase pressure gradient measurement at the same loop flow shows that the two-phase started at about bundle H. From these data the two-phase multipliers can be extracted.

3.6 CHF Tests

Approximately 90 CHF points were taken during the campaign of testing with the 5.1% crept pressure tube. The procedure used was to fix the inlet temperature, flow and outlet pressure at the desired conditions, and then slowly increase the bundle power until CHF was detected. It was, of course, essential to be sure that the first indication of dryout anywhere on the bundle for each CHF test had been found. Thus, after the initial indication of dryout, the power would be increased by typically 100 kW and the thermocouples axially slid and rotated to ensure that there was not an earlier CHF at any other location. If an earlier CHF was found, the thermocouples were moved to that location, the power reduced and the CHF value for the new location determined. This procedure was repeated until it was certain that the first indication of dryout anywhere on the bundle had been found and this then became the CHF point. Following recording of the CHF data, the test-section power was increased gradually to up to 5% overpower until additional thermocouples indicate the CHF condition. Typically one or more additional thermocouples would come into dryout with less than a 1% power increase. A number of CHF points taken, usually on a prior weekend, were repeated. The repeatability was excellent, CHF generally being detected within 100 kW (~1%) of the previous value.

An example of the CHF data taken at 11 MPa is shown in Figure 10 plotted as power against inlet temperature. The data follow the normal trends of the dryout power increasing with increasing flow and decreasing inlet temperature. The data are very well behaved and follow conventional trends by being approximately linear when cross plotted as power versus flow, as shown in Figure 11. At 17 kg/s and above, the data are essentially linear, with some deviation occurring at 13.5 kg/s and 10 kg/s due to flow stratification effects.

The initial dryouts were generally in bundles J or K (sometimes both simultaneously) on the outer rods in the lower part of the bundle. The radial position on the rod varied depending on the axial location. If the dryout was just upstream of the mid-plane spacers, it generally occurred facing an inner subchannel, e.g. on rod #3 facing the subchannel formed by rods 3, 23 and 2. If it was just upstream of the downstream button plane, the dryout tended to be in the subchannel formed by two outer rods and the pressure tube, i.e. immediately upstream of the button. These dryout locations show that the button planes provide significant protection against CHF immediately downstream. At the lowest flow, 10 kg/s, initial dryout occasionally occurred at the downstream end of bundle J on rod 37, i.e. in the inner part of the bundle.

3.7 Onset of Dry Sheath (ODS)

In a number of CHF tests the power was incremented in small steps beyond the initial CHF point to obtain the post-dryout temperature versus power profile. These measurements allowed the determination of the ODS power, i.e. the power at which the sheath temperature exceeds the critical point of water, 374°C. The data for one test is shown in Figure 12. Initial dryout was at 6050 kW and the ODS point is at about 6160 kW, a power increase of 1.8%.

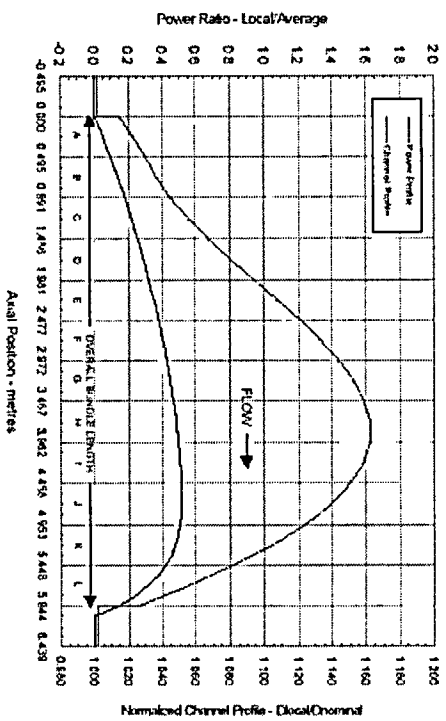
4. SUMMARY

A full scale electrically heated simulation of a CANFLEX fuel string has been constructed and tested in a high pressure water loop at representative reactor thermalhydraulic conditions. The primary objective of the experiments was to obtain CHF and single- and two-phase pressure drop for CANFLEX fuel. In addition a

number of secondary data were obtained which both provided an understanding of the thermalhydraulic behaviour within the bundle, and also provided confidence in the quality of the CHF data. The data exhibited the conventional trends of CHF increasing with increasing flow and decreasing inlet temperature. Repeat CHF points taken at random during the testing program showed that the repeatability of the data was excellent

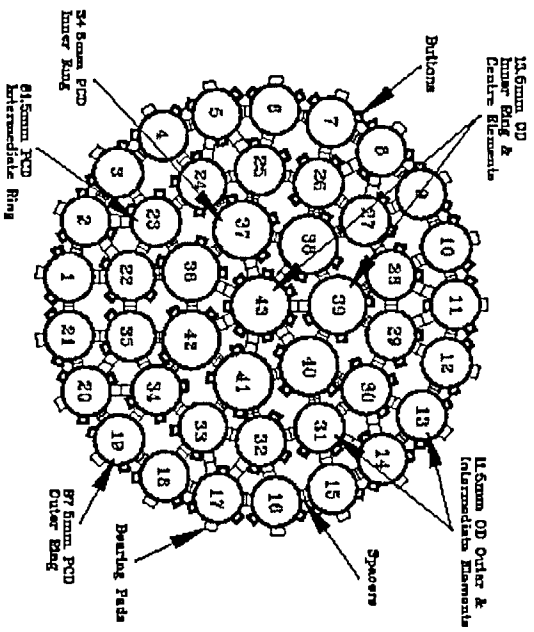
5. REFERENCES

- 1 Fortman, R.A., Hadaller, G.I., Hayes, R C., Stern, F., (Stern Laboratories), Midvidy, W.I. (Ontario Hydro), "Heat Transfer Studies with CANDU Fuel Simulators", ICONES 1997 May 26-30, Nice, France.
- 2 Leung, L.K.H. et al., "Critical Heat Flux and Pressure Drop for a CANFLEX Bundle String Inside an Axially non-uniform Flow Channel", 6th Int. Conf on CANDU Fuel, Niagara Falls, Canada, 1999 September 26-30
- 3 Fortman, R.A. et al., "A New Facility for the Determination of Critical Heat Flux in Nuclear Fuel Assemblies", INC93, Toronto, Canada, 1993 October 3-6.



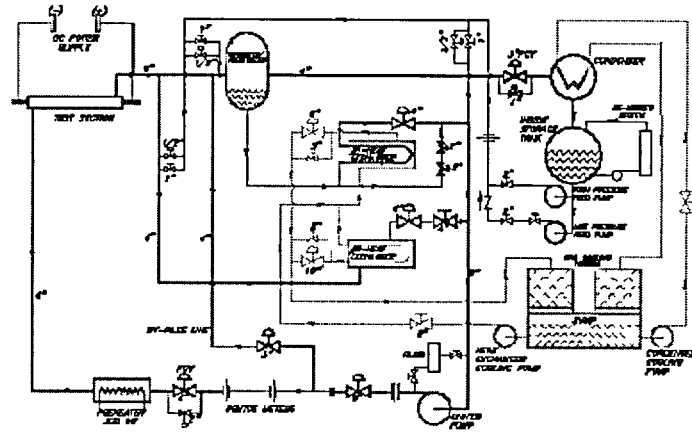
Axial Power and Flow Channel Profiles

Figure 1



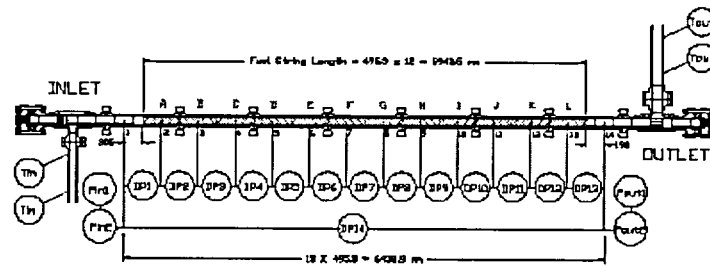
CANFLEX Bundle Cross Section
(Looking Downstream)

Figure 2



CHF Test Loop

Figure 3



CANFLEX Test Section

Figure 4

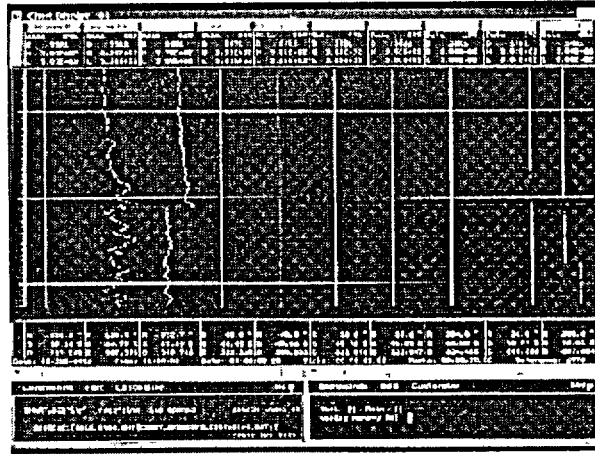
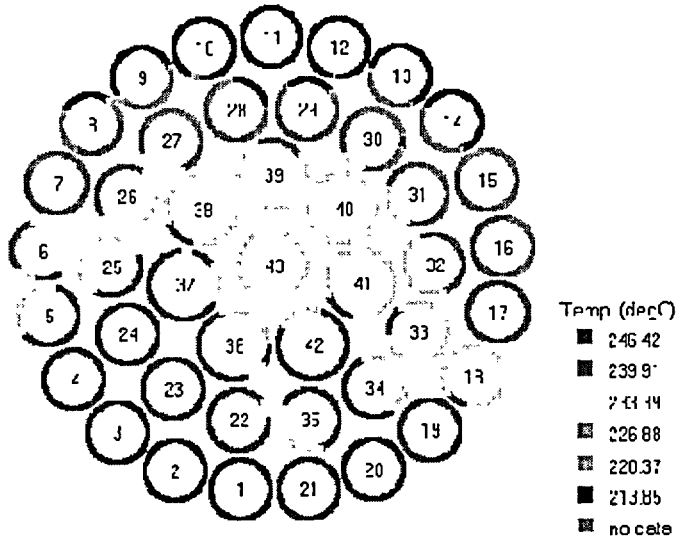


Chart Display for Dryout Detection

Figure 5

PROFILE MAP



Scale 06" = 1 unit
 255 mm to 265 mm
 Plane J

Temperature Map from Profile Scan (#611J)

Figure 6

Figure 7 Onset of Nucleate Boiling

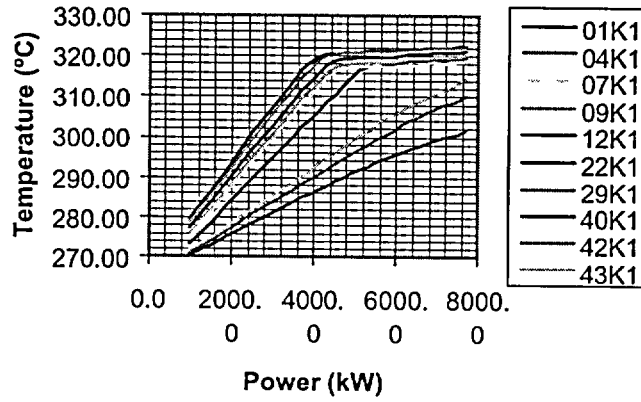
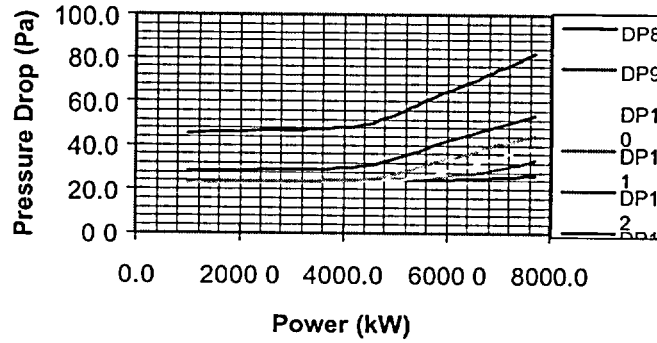
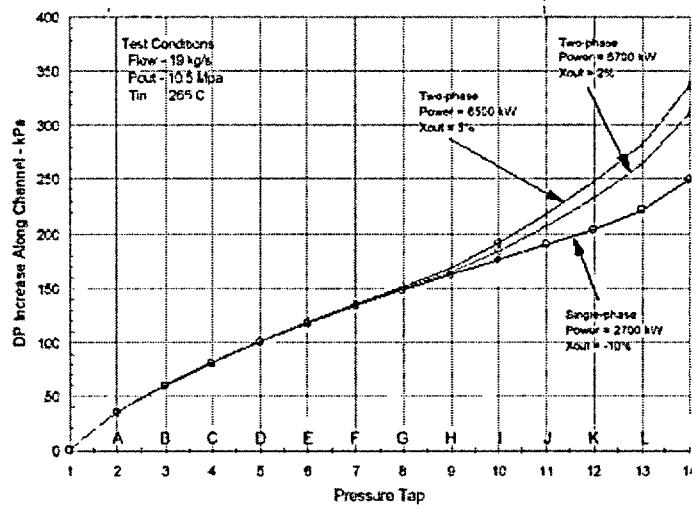


Figure 8 Onset of Significant Void





Pressure Gradient Along Flow Channel

Figure 9

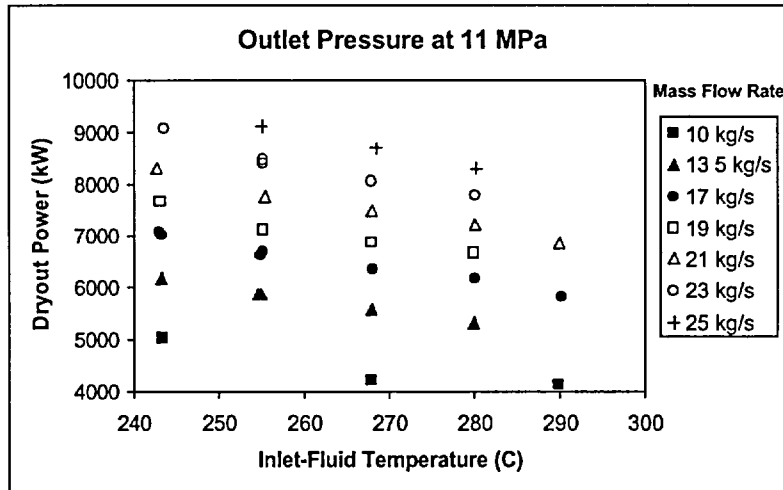


Figure 10 CANFLEX CHF Data

CANFLEX CHF at 11 MPa

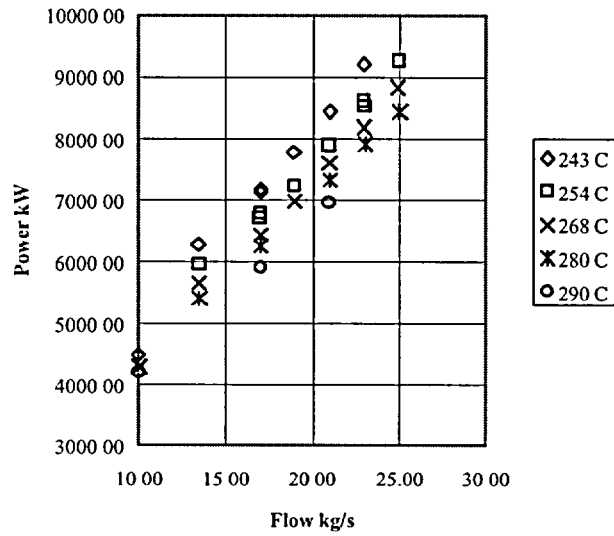
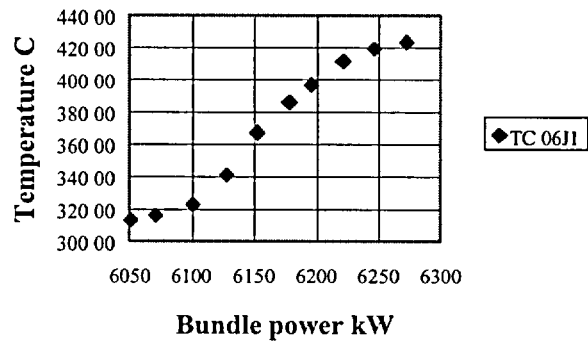


Figure 11

Figure 12 Onset of Dry Sheath



CRITICAL HEAT FLUX AND PRESSURE DROP FOR A CANFLEX BUNDLE STRING INSIDE AN AXIALLY NON-UNIFORM FLOW CHANNEL

L.K.H. LEUNG, D.C. GROENEVELD, G.R. DIMMICK, D.E. BULLOCK AND W.W. INCH

Fuel Channel Thermalhydraulics Branch
Chalk River Laboratories
Atomic Energy of Canada Limited
Chalk River, Ontario
CANADA K0J 1J0

Abstract

Experimental data of dryout power and pressure drop have been obtained with a simulated string of twelve aligned, full-scale, CANFLEX[®] fuel bundles. The bundle string consisted of 43 elements and was equipped with junction and appendages simulations. It was installed inside three flow tubes simulating three different creep profiles: one had a uniform inside diameter of 103.86 mm and the other two had axially varying inside diameters, with a peak of either 107.29 mm or 109.16 mm (3.3% and 5.1% larger than the uniform tube). Pressure variations along the fuel string were obtained with differential-pressure cells connected to a number of pressure taps. Sliding thermocouples were used to obtain surface-temperature measurements and detect dryout. A wide range of steam-water flow conditions was covered in the current tests: an outlet-pressure range from 6 to 11 MPa, a mass-flow-rate range from 7 to 25 kg/s, and an inlet-fluid-temperature range from 200 to 290°C. This paper focuses primarily on data obtained at normal operating pressures with the axially non-uniform channel that had a maximum diameter 5.1% larger than the reference pressure tube.

Local and boiling-length-average (BLA) critical-heat-flux values were derived from the dryout-power data for various flow conditions. Unlike the traditional BLA approach, the averaging process was initiated from the onset of significant void (OSV), instead of from the saturation point. This allowed the extension of the BLA approach to subcooled dryout conditions. The OSV values were evaluated from the pressure distribution along the bundle string. Comparisons of various parameters were made between the 37-element and CANFLEX bundles. Overall, the dryout-power values were consistently higher for the CANFLEX bundle than the 37-element bundle. At inlet-flow conditions of interest, the dryout-power measurements were, on average, 17% higher for the CANFLEX bundle than the 37-element bundle. The fuel-string pressure drop was similar between the CANFLEX and 37-element bundle strings.

1. INTRODUCTION

A new design of the CANDU^{®(1)} fuel bundle has recently been completed jointly by Atomic Energy of Canada Limited (AECL) and the Korea Atomic Energy Research Institute (KAERI), to deliver improved power and safety margins to reactor operators. It is called the CANFLEX[®] (CANDU Flexible) bundle and consists of 43 fuel pins containing about the same amount of uranium in weight as the 37-element bundle. Figure 1 shows a CANFLEX fuel bundle prior to loading into the CANDU reactor at Point Lepreau nuclear station for demonstration irradiation. Unlike its predecessors, the fuel pins of a CANFLEX bundle are separated into two groups with different outer diameters. Each pin is equipped with innovative, patented, no-load-bearing heat-transfer-enhancement devices called the buttons. Previous analyses and tests focusing on separate effects concluded that the buttons provide a significant improvement in critical heat flux (CHF) with minimal effect on pressure drop, compared to other heat-transfer-enhancing devices. A similar conclusion was made when the dryout-power and pressure-drop measurements were compared between the 37-element and CANFLEX bundle strings cooled with Freon-134a flow. This implies that the critical channel power of the CANDU reactor can be further improved by replacing the current 37-element bundles with a string of CANFLEX bundles.

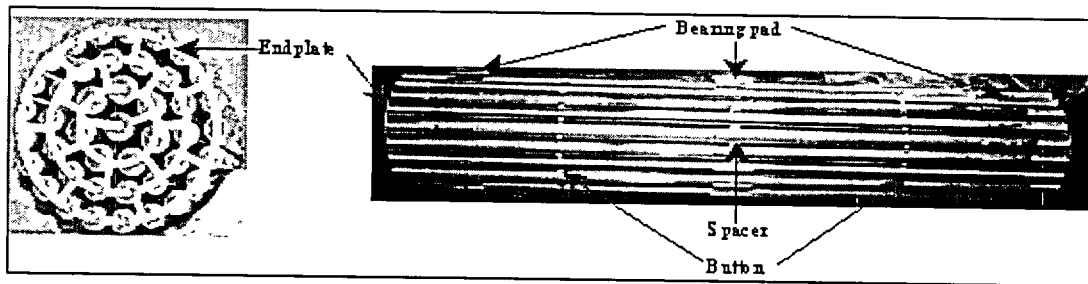


FIGURE 1: VIEWS OF A CANFLEX BUNDLE.

To confirm the improvement in critical channel power, a full-scale CANFLEX bundle test was recently completed to provide data on steady-state dryout power and fuel-string pressure drop. The test covered a wide range of flow conditions and three different flow tubes. This paper focuses primarily on data obtained at normal operating pressures with an axially non-uniform channel that had a maximum inside diameter 5.1% larger than a reference pressure tube. It presents the results of (i) an analysis of the data for dryout power, CHF and fuel-string pressure drop, and (ii) a comparison of these values between 37-element and CANFLEX bundle strings.

2. FULL-SCALE CANFLEX BUNDLE TESTS

Full-scale CANFLEX bundle tests were performed to obtain licensing data in the high-pressure steam-water loop at Stern Laboratories (Dimmick et al. 1999). The test string consisted of a 6-m-long, 43-element bundle simulator. The elements were constructed with Inconel tubes of two different outer diameters (13.5 and 11.5 mm). Bundle segmentation was simulated with

⁽¹⁾ CANDU[®] and CANFLEX[®] are registered trademarks of Atomic Energy of Canada Limited (AECL).

specially designed spool pieces that imitated the radial and cross webs of the endplate in a fuel bundle. Corresponding elements in the upstream and downstream bundles of the spool pieces were aligned axially. Appendages (i.e., spacers, bearing pads and AECL-patented non-load-bearing buttons) were spot-welded at various locations, as specified in the bundle design. Power was applied to the bundle string through Joule heating. The sheath thicknesses of the elements were varied along the axial length and from ring to ring. This provided accurate simulations of non-uniform radial and axial heat-flux distributions. The radial heat-flux distribution simulated a bundle with natural-uranium fuel, and the axial heat-flux distribution corresponded to a downstream skewed-cosine profile. A ceramic flow tube insulated the bundle string from the metal pressure boundary. Three different flow tubes were used in the test: one had a uniform inside diameter of 103.86 mm and the other two had axially varying inside diameters, with a peak of 107.29 mm and 109.16 mm (3.3% and 5.1% larger than the uniform tube). The uniform flow tube simulated a reference uncrept pressure tube, while others simulated pressure tubes with various degrees of diametral creep.

Figure 2 shows the set-up of the test station. Fourteen taps were installed along the test section; they were connected to differential-pressure (DP) cells to provide pressure-drop measurements over the bundle string. The taps at the inlet and outlet ends were also connected separately to other DP cells to measure the absolute pressures at those locations. K-type thermocouples and resistor temperature devices (RTDs) were used to monitor the fluid temperature at the inlet and outlet ends. The inside surface temperature of the heated sheath was measured with thermocouple-slider assemblies located inside the element. The sliders in all elements were moved axially and rotated at various locations to map out the surface-temperature distributions. Dryout occurrence was assumed for a sharp surface-temperature rise of about 5°C from the nucleate-boiling temperature. Details of the experimental set-up and test procedure are described in Dimmick et al. (1999).

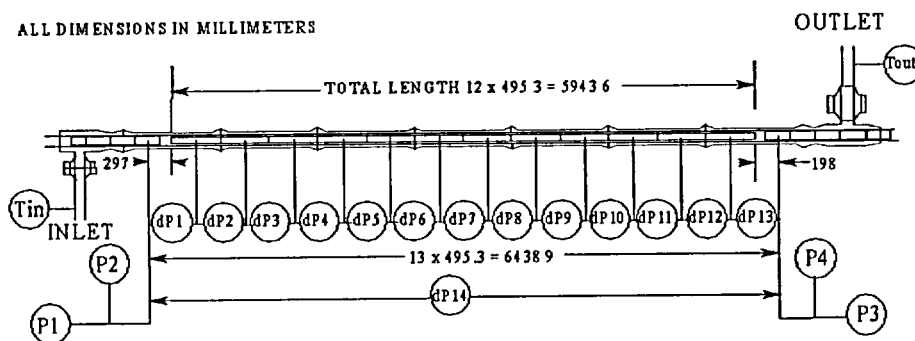


FIGURE 2: A SCHEMATIC DIAGRAM OF THE TEST STATION IN THE HIGH-PRESSURE STEAM-WATER LOOP AT STERN LABORATORIES.

A wide range of steam-water flow conditions was covered in the CHF experiment: an outlet-pressure range from 6 to 11 MPa, a mass-flow-rate range from 7 to 25 kg/s, and an inlet-fluid-temperature range from 200 to 290°C. The majority of the data are directly relevant to analyses of the regional overpower trip (ROPT) set point in the reactor. In addition, single-phase and two-phase pressure-drop tests were performed at lower pressures and fluid temperatures, as well as at

higher mass-flow rates. These data corresponded closely to those previously obtained with a simulated string of 37-element bundles at the same test facility.

3. DRYOUT POWER FOR THE CANFLEX BUNDLE STRING

The dryout power represents the total power applied to the bundle string at which the onset of intermittent dryout (OID) occurs. This corresponds to only a single point at the sheath of an element, where the liquid film has broken down, while a continuous liquid contact is maintained at the remaining surfaces of the bundle string. Because of the high heat-transfer rate due to convection (at high flow velocity) and conduction (from the dry spot to the surrounding wet area), a gradual temperature rise is associated with this type of dryout.

Figure 3 illustrates the variation in dryout power with inlet-fluid temperature and mass-flow rate at a constant outlet pressure of 11 MPa. Similar to the trends observed in tubes and 37-element bundles, the dryout power increased with decreasing inlet-fluid temperature and increasing mass-flow rate. Overall, the trends of dryout power followed a linear variation with these flow parameters over the test conditions. Several repeat points were obtained at various stages of the experiment (as indicated with multiple points at the same flow conditions). As shown in Figure 3, the repeatability of the measurements (multiple points at the same conditions) was excellent in the experiment. At conditions of interest (i.e., a mass-flow rate of 21 kg/s and an inlet-fluid temperature of 265°C), the dryout power for the CANFLEX bundle string was about 7.7 MW.

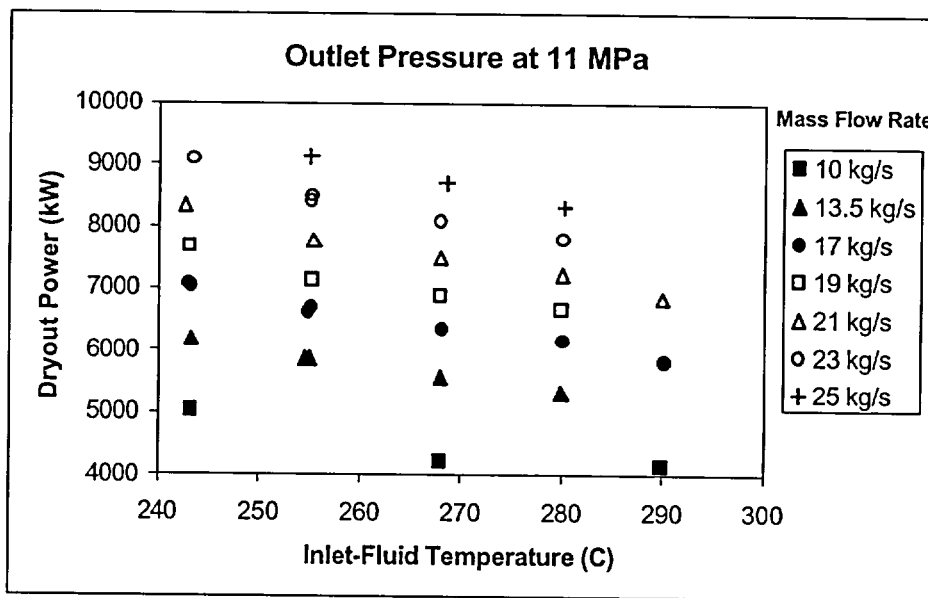


FIGURE 3: DRYOUT-POWER MEASUREMENTS FOR A CANFLEX BUNDLE STRING.

4. CHF FOR THE CANFLEX BUNDLE STRING

The evaluation of critical channel power using a system code requires an accurate CHF correlation. Currently, there are three types of CHF correlation, based on local heat flux, boiling-length-average (BLA) heat flux, or critical quality. Overall, the BLA CHF correlation provides the best prediction accuracy in both CHF and dryout location for various types of channels.

The concept of boiling length was introduced by Bertoletti et al. (1964) to account for the effect of axial heat-flux distribution on CHF over the annular film-dryout region in tubes. Strictly speaking, the boiling length is measured from the onset-of-nucleate-boiling (ONB) point to the location of interest. However, due to the uncertainty in predicting the ONB point, the saturation point has traditionally been assumed to be the initiating point for flow in tubes. Furthermore, the dryout quality is often much larger than the qualities at either the ONB or saturation points (i.e., the boiling length is much greater than 0), and hence the impact of the assumption is reduced.

The traditional approach, as used in tube flow, to initiate boiling length from the saturation point is inappropriate for analyses based on the cross-sectional average flow conditions in a tightly spaced bundle. Imbalances in flow and enthalpy distributions in the bundle have led to the initiation of boiling (i.e., ONB point) at highly subcooled flow conditions (cross-sectional average values). These imbalances increase with increasing bundle eccentricity from the concentric position; a portion of flow diverges to the open area, bypassing the heated bundle. Hence, the assumption of a small difference between the ONB and saturation points is no longer justified, and the boiling length must be redefined.

In the CHF analysis for a 37-element bundle string, Leung et al. (1996) defined the boiling length from the onset-of-significant-void (OSV) point to the location of interest. The OSV point was determined from the pressure distribution based on the pressure-drop measurements at each set of inlet-flow conditions. The determination of the OSV point in a CANFLEX bundle string is described in Section 6. Leung et al. (1996) employed the OSV point rather than the ONB point because the pressure-drop data covered a much wider range of conditions than the surface-temperature measurements. Furthermore, the difference between the ONB and OSV points was observed to be small in the 37-element bundle string (Fortman et al. 1999).

Local and BLA CHF values were evaluated with the dryout-power measurements and axial heat-flux distribution. The BLA CHF is calculated with

$$CHF_{BLA} = \frac{1}{z_{DO} - z_{OSV}} \int_{z_{OSV}}^{z_{DO}} q_{local} dz$$

where z_{DO} and z_{OSV} are the locations at the dryout and OSV points, respectively, q_{local} is the local heat flux in W/m^2 , and z is the axial distance in metres. Figure 4 compares the CHF values evaluated with either the local or BLA approach. The variation among the BLA CHF values is much less than that for the local CHF values with increasing dryout quality. Therefore, the BLA CHF values provide a better correlation than the local CHF values.

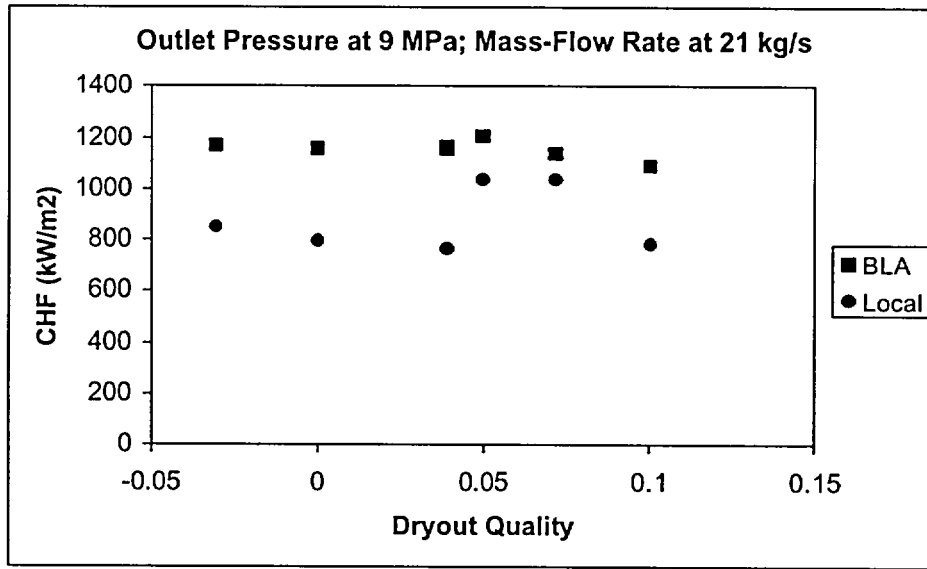


FIGURE 4: DIFFERENCES IN CHF BETWEEN THE BLA AND LOCAL APPROACHES.

Figure 5 compares the BLA CHF values for the CANFLEX bundle string at various dryout qualities and mass-flow rates. In general, the BLA CHF increases with decreasing dryout quality and increasing mass-flow rate. The same trend was observed in data obtained with tubes and the 37-element bundle string. As indicated in Figure 5, a number of data were obtained at the cross-sectional-average subcooled conditions (negative thermodynamic quality). Based on the current BLA approach, however, the data follow the same trend exhibited in the saturated dryout data. With respect to dryout quality, the variation of BLA CHF is larger at low mass-flow rates than at high mass-flow rates.

The BLA CHF values obtained at the outlet pressure of 9 MPa exhibit the same trends as those at 11 MPa (Figure 6). However, all data points, but one, lie at the saturated conditions. The trend of BLA CHF values with respect to dryout quality is similar for various mass-flow rates.

5. PRESSURE DROPS OVER THE CANFLEX BUNDLE STRING

Pressure drops were measured with DP cells connected to taps installed along the CANFLEX bundle string (see Figure 2). They were used to establish the pressure distribution and hydraulic parameters (such as friction factor in single-phase flow, OSV and two-phase multiplier in two-phase flow). The distance over neighboring taps was equivalent to a bundle length (i.e., 0.495 m), and hence effects due to skin friction, bundle junction, mid-spacer plane, button plane and bearing-pad plane could not be isolated. Figure 7 illustrates the measured pressure distribution along the unheated bundle string. The non-linear variation of pressure is caused by the change in the flow-tube diameter with axial distance.

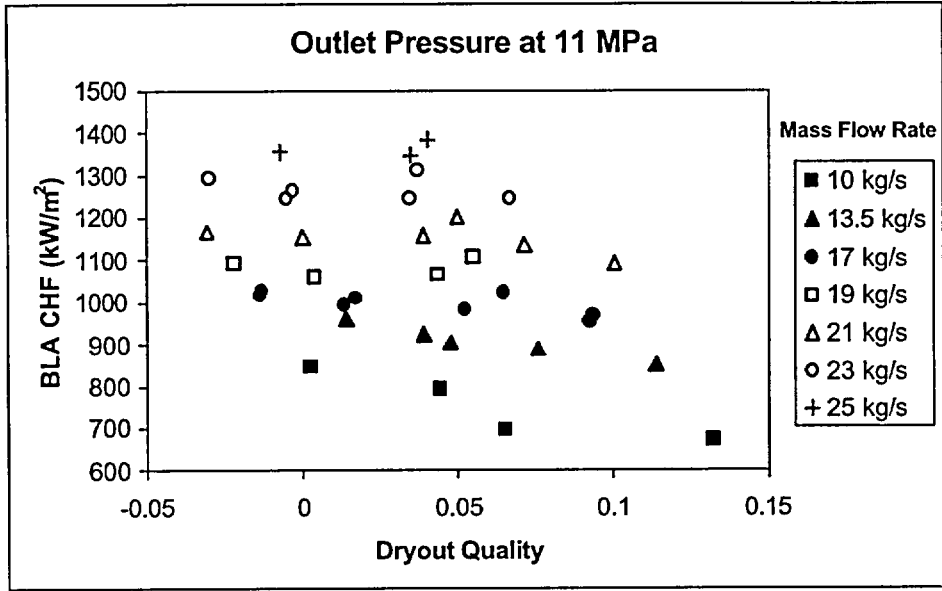


FIGURE 5: CALCULATED BLA CHF VALUES FOR THE CANFLEX BUNDLE AT AN OUTLET PRESSURE OF 11 MPa.

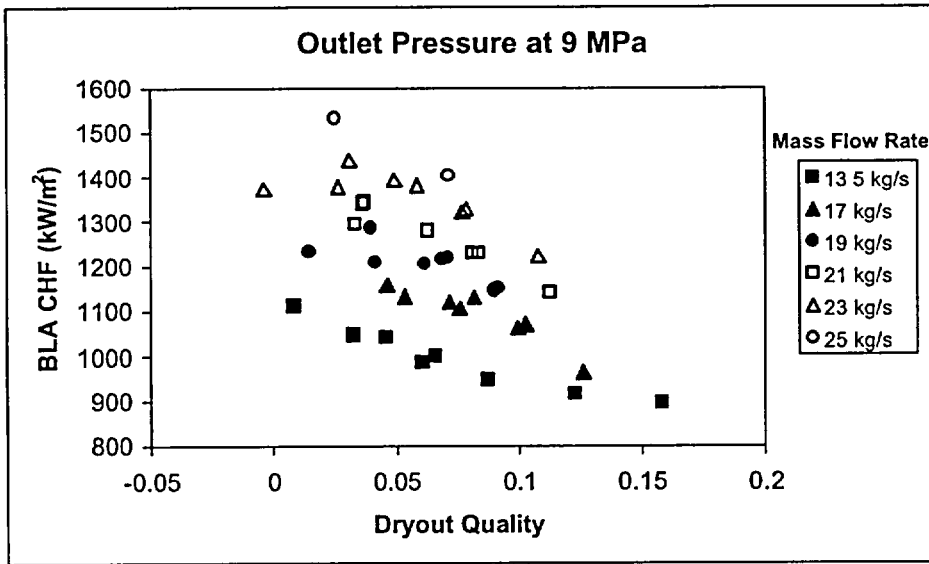


FIGURE 6: CALCULATED BLA CHF VALUES FOR THE CANFLEX BUNDLE AT AN OUTLET PRESSURE OF 9 MPa.

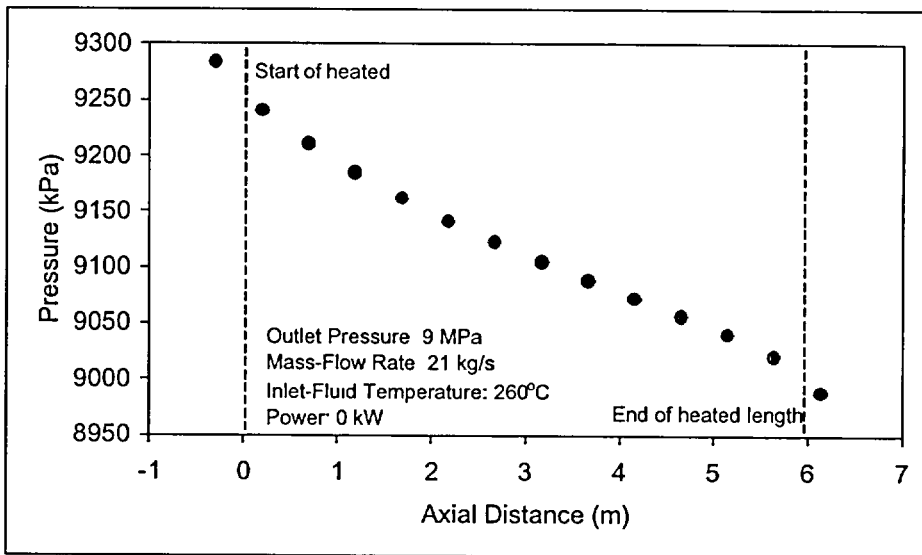


FIGURE 7: PRESSURE DISTRIBUTION ALONG THE UNHEATED BUNDLE STRING.

Figure 8 shows the axial pressure drops over various portions of the bundle string with reference to the outlet pressure tap at several power levels. The pressure-drop trend at low powers (i.e., 986 and 1972 kW) appears to be independent of the heating effect and follows closely the pressure distribution shown in Figure 7. This signifies that only single-phase liquid was flowing inside the channel and that boiling was suppressed. The channel pressure drop increased with increasing power and the pressure distribution varied strongly at the downstream end where boiling was encountered.

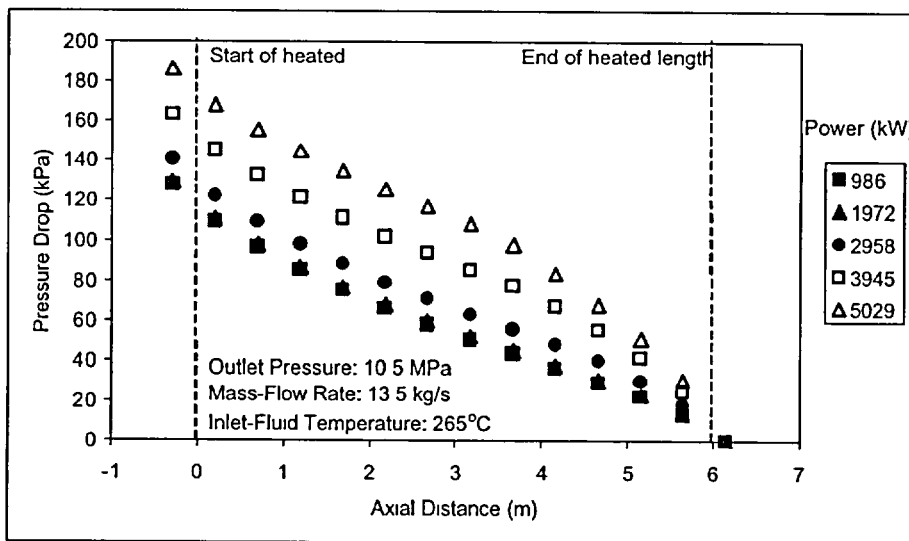


FIGURE 8: PRESSURE DROPS ALONG THE HEATED BUNDLE STRING.

6. ONSET OF SIGNIFICANT VOID IN A CANFLEX BUNDLE STRING

The OSV is often assumed to be the transition point between single-phase and two-phase flows. This is different from the ONB point, where bubbles are sustainable at the near-wall region only and would collapse when departing from the heated surface. While the pressure drop increases slightly at the region between the ONB and OSV points, the increase becomes considerably larger beyond the OSV point. Therefore, the OSV point is often determined from the pressure distribution along the channel. In a uniform channel, the single-phase pressure drop varies linearly, while the two-phase pressure drop varies non-linearly, with axial distance. Hence, the location at which the pressure gradient changes is considered to be the OSV point. In an axially non-uniform channel (i.e., varying flow area with distance), however, both the single-phase and two-phase pressure drops vary non-linearly and the turning point is difficult to establish (see Figure 8).

Leung and Hotte (1997) derived a single-phase pressure-drop model for CANDU fuel bundles, which was based primarily on correlations developed for simple channels (such as tubes and annuli). The model was validated against data obtained with both 4-rod and 37-rod bundle strings. It was used to calculate the single-phase pressure drop over the CANFLEX channel. By subtracting the predicted single-phase pressure drops from the measurements, the pressure drop over the single-phase region was eliminated, while the pressure variation over the two-phase region maintained a non-linear relation with axial distance. Figure 9 illustrates the modified pressure distribution along the CANFLEX bundle string. A slight variation in pressure with axial distance is still shown in the single-phase region; it is caused by the uncertainty in the pressure-drop model. Nevertheless, the transition between single-phase and two-phase flow is identified in the figure. Two polynomial equations were optimized separately with the data over the two pressure-drop regions. The OSV point was determined by solving these equations and locating the intersecting point.

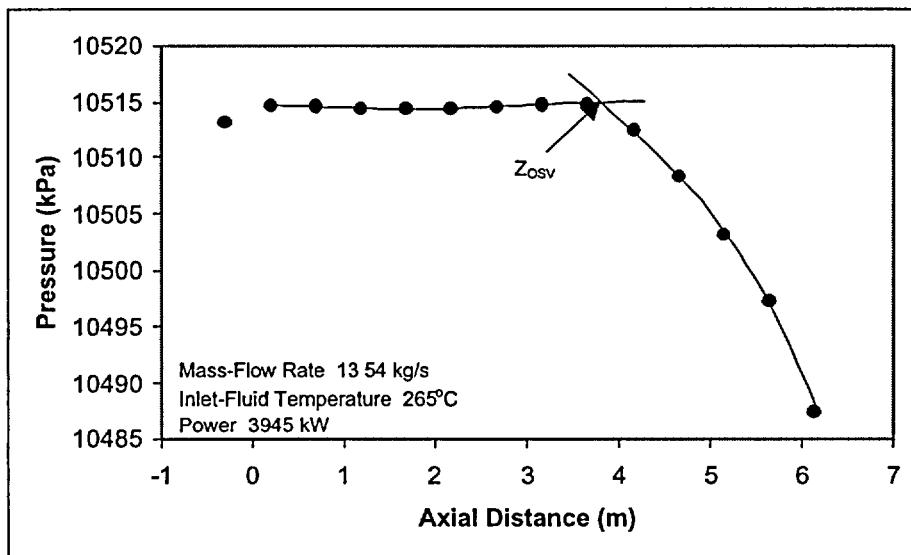


FIGURE 9: LOCATION OF OSV IN THE CANFLEX BUNDLE STRING.

7. COMPARISONS OF VARIOUS PARAMETERS BETWEEN CANFLEX AND 37-ELEMENT BUNDLE STRINGS

A similar experiment was previously completed with a simulated 37-element bundle string in the same test facility at Stern Laboratories. It covered a similar range of flow conditions and provided measurements on dryout power and pressure drop. Due to its proprietary nature, only a relative comparison of data between CANFLEX and 37-element bundles is presented here.

Figure 10 shows the dryout-power enhancement of the CANFLEX bundle string (i.e., the ratio of dryout power between CANFLEX and 37-element bundle strings) at similar inlet-fluid conditions. The dryout power for the 37-element bundle string is calculated with an optimized equation derived from the database. The overall average optimization error is 0.09% and the root-mean-square (rms) error is 3.29% for 86 data points. As Figure 10 shows, the dryout power is systematically higher for the CANFLEX bundle string than the 37-element bundle string. On average, the enhancement is about 17% for all data points. The effects of the inlet-fluid temperature and mass-flow rate on the enhancement are small over the present range, but a minor effect of pressure seems to be noticeable. The enhancement is slightly larger for data at 11 MPa than at 9 MPa.

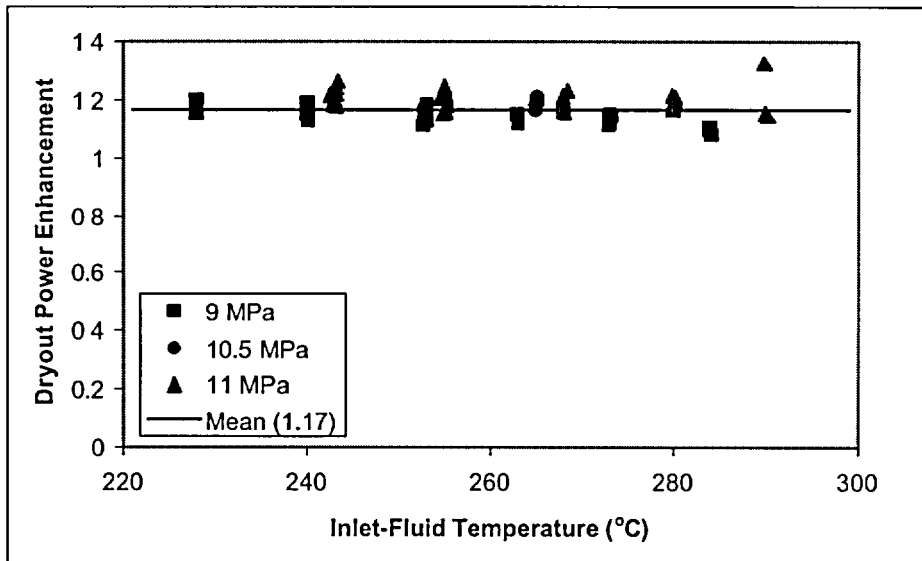


FIGURE 10: DRYOUT-POWER ENHANCEMENT FOR THE CANFLEX BUNDLE STRING INSIDE AN AXIALLY NON-UNIFORM CHANNEL WITH A MAXIMUM DIAMETER OF 5.1% GREATER THAN THE REFERENCE VALUE.

Figure 11 compares the pressure-drop characteristics between the CANFLEX and 37-element bundle strings at similar inlet-flow conditions and power (i.e., the same rate in enthalpy rise over the channel). Overall, the pressure-drop characteristics are similar for both bundle strings. A slightly higher fuel-string pressure drop is shown for the CANFLEX bundle string, and the difference is about 2.1%. This is probably caused by the uncertainty in the simulation of the bundle junction and appendages.

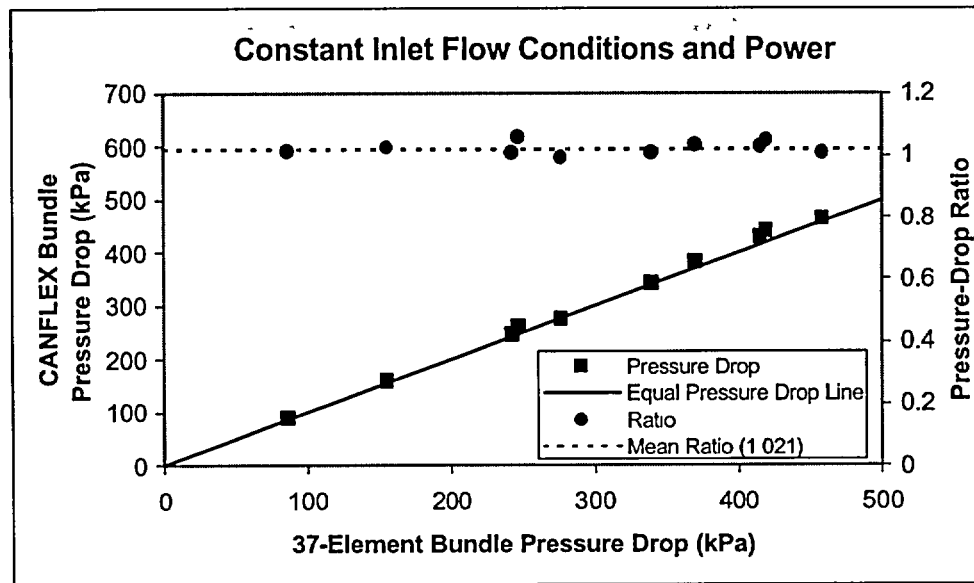


FIGURE 11: COMPARISON OF PRESSURE-DROP CHARACTERISTICS BETWEEN THE CANFLEX AND 37-ELEMENT BUNDLE STRINGS.

8. CONCLUSIONS AND FINAL REMARKS

- A set of data on dryout power and pressure drop has been obtained with a CANFLEX bundle string. The data are consistent and follow established parametric trends with various flow parameters.
- Local and BLA CHF values have been calculated with the dryout-power data.
- The OSV point has been determined using the pressure-drop measurements along the CANFLEX bundle string at various flow conditions.
- The dryout-power data are higher for the CANFLEX bundles than for the 37-element bundles. On average, the enhancement is about 17% for the range of conditions of interest at the same inlet-fluid temperature.
- The overall pressure drop is about the same for both bundle strings (the fuel-string pressure drop for the CANFLEX bundle is similar to that for the 37-element bundle at the same flow conditions and power).

9. REFERENCES

BERTOLETTI, S., GASPARI, G.P., LOMBARDI, C., PETERLONGO, G. AND TACCONI, F.A., "Heat Transfer Crisis With Steam-Water Mixtures", CISE-R-99, 1964.

DIMMICK, G.R., INCH, W.W.R., JUN, J.S., SUK, H.C., HADDALLER, G., FORTMAN, R. AND HAYES, R., "Full-Scale Water CHF Testing of the CANFLEX Bundle", Paper accepted for presentation at the 6th Int. Conf. on CANDU Fuel, Niagara Falls, Ontario, Canada, Sept. 26-30,

1999.

FORTMAN, R.A., HAYES, R.C. AND HADALLER, G.I., "37-Element CHF Program: Steady-State CHF, Transient CHF and Post-Dryout Tests with Uniform and Diametral Crept Flow Tubes", Unpublished proprietary report of the CANDU Owners Group (COG), 1999.

LEUNG, L.K.H., GROENEVELD, D.C. AND HOTTE, G., "Prediction Method To Account For The Effect Of Pressure-Tube And Diametral Creep On Critical Heat Flux And Pressure Drop For A 37-Element Bundle String", Proc. of the 19th CNS Simulation Symposium, Hamilton, Ontario, October 16-17, 1996.

LEUNG, L.K.H. AND HOTTE, G., "A Generalized Prediction Method For Single-Phase Pressure Drop In A String Of Aligned CANDU-Type Bundles", Proc. of the 20th CNS Simulation Symposium, Niagara-on-the Lake, Sept. 7-9, 1997.

10. ACKNOWLEDGEMENT

The authors would like to thank the test engineers at Stern Laboratories for performing the experiment and providing the experimental data.

Introduction of the New Fuel Bundle "CANFLEX" into an Existing CANDU Reactor

Prepared for

12th Pacific Basin Nuclear Conference

October 29 (Sun) - November 2 (Thur), 2000

Seoul, Korea

by

Wayne W.R. Inch
Atomic Energy of Canada
Limited Canada

Paul D. Thompson
Point Lepreau Generating Station,
New Brunswick Power, Canada

Ho Chun Suk
Korea Atomic Energy Research
Institute, Korea (R.O.K.)

Introduction of the New Fuel Bundle "CANFLEX" into an Existing CANDU Reactor

by

Wayne W.R. Inch Atomic Energy of Canada Limited Canada	Paul D. Thompson Point Lepreau Generating Station, New Brunswick Power, Canada	Ho Chun Suk Korea Atomic Energy Research Institute, Korea (R.O.K.)
--	--	--

ABSTRACT

The CANFLEX® fuel bundle is the latest design in the evolution of CANDU® fuel. Its 43-element fuel-bundle assembly and its patented critical-heat-flux (CHF) enhancement appendages offer higher operating and safety margins than those of current fuel, while maintaining full compatibility with operating CANDU reactors. The greater element subdivision and the use of two element sizes lower the peak linear-element rating. Therefore, the bundle is well suited for use in advanced fuel cycles, particularly those that can attain high fuel burnup. The higher operating and safety margins offer the potential of reactor power uprating, which would further increase the economic competitiveness of the CANDU reactor.

Since 1991, Atomic Energy of Canada Limited has partnered with the Korea Atomic Energy Research Institute to complete the development, qualification testing, and analysis of the CANFLEX fuel bundle. In 1994, New Brunswick Power became interested in CANFLEX as part of an overall program on plant life management. Because of the increase in critical channel power with CANFLEX, the utility recognized that it could use CANFLEX to recover some of the heat transport system operation margins, which had decreased because of reactor aging. International cooperation between AECL & KAERI, driven by specific utility requirements, has been a key factor in CANFLEX coming to fruition.

The CANFLEX bundle has undergone extensive design analysis, performance and qualification testing, as well as an independent review within the Canadian nuclear industry and independently in Korea. Final confirmation of CANFLEX compatibility involved a 24-bundle demonstration irradiation at the Point Lepreau Generating Station (PLGS) in New Brunswick, Canada. The demonstration irradiation objectives were to confirm the compatibility and the irradiation performance of the CANFLEX bundles, and to confirm the fuel fabrication processes for this new bundle design.

In 1998 September, the demonstration irradiation at PLGS was started when 8 CANFLEX bundles were loaded into channel Q20 and 8 bundles were loaded into channel S08, using standard on-power refueling. Since then, an additional 8 bundles were loaded into the reactor and all 24 fuel bundles have been discharged into the fuel bays. Twenty of the twenty-four bundles were examined in the fuel-bays to verify bundle integrity and condition. Two of those bundles have been destructively examined in post-irradiation examinations in the hot cells at the Chalk River Laboratories.

While CANFLEX was being demonstrated at PLGS, the thermalhydraulic licensing data were being established by water CHF testing. Experimental data of dryout power and pressure drop were obtained with a simulated string of 12 aligned, full-scale, CANFLEX fuel bundles in 3 different flow channels with axial variation of the inside diameter. Pressure drops over the fuel string were obtained. A wide range of steam-water flow conditions was covered in the current tests, an outlet-pressure range from 6 to 11 MPa, a mass-flow-rate range from 7 to 25 kg/s and an inlet-fluid-temperature range from 200 to 290°C. The enhancement in critical channel power was confirmed to be from 5 to 8%, depending on specific conditions.

This paper describes the results of the demonstration irradiation at PLGS, as well as the results of the thermalhydraulics test program. It summarizes the benefits involved in implementing this new technology in existing operating stations.

CANFLEX® (CANDU FLEXible) is a registered trademark of Atomic Energy of Canada Limited (AECL) and the Korea Atomic Energy Research Institute (KAERI).

CANDU® (Canada Deuterium Uranium) is a registered trademark of Atomic Energy of Canada Limited

INTRODUCTION

Since the early 1990's, Atomic Energy of Canada Limited (AECL) and the Korea Atomic Energy Research Institute (KAERI) have pursued a collaborative program to develop, verify, and prove a new fuel design that would introduce advanced fuel cycles such as slightly enriched uranium (SEU), recycled uranium (RU) and others into CANDU reactors and provide enhanced performance with natural uranium (NU) fuel through higher operating margins in existing CANDU reactors.

In 1998 September, New Brunswick Power (NBP), at the Point Lepreau Generating Station (PLGS), began a two-year demonstration irradiation of CANFLEX fuel bundles, as final verification of the CANFLEX design as a prerequisite to full-core conversion. Recently, the Korean Electric Power Corporation (KEPCO) announced a program in Korea to prepare for a demonstration irradiation in Wolsong Unit 1 and then potentially implement CANFLEX full-core. This document provides a summary of the CANFLEX qualification and performance assessment program and discusses the benefits existing plants can derive from using this fuel design.

CANFLEX BUNDLE DESIGN

The CANFLEX design is a 43-element fuel-bundle assembly offering improved operating and safety margins, compared with those of the standard 37-element fuel bundle, for operating CANDU reactors [1-4]. The CANFLEX bundle design includes critical heat flux (CHF) enhancement devices leading to 5 to 8% higher critical channel power (CCP) in a full-length fuel channel, compared with that of 37-element fuel bundles. The lower heat rating of the CANFLEX fuel elements at current bundle powers leads to lower fuel temperatures. Hence less fission-product gap-inventory is produced under normal operating conditions compared with the fission-product gap-inventory produced in standard 37-element fuel elements at a similar bundle power. The CANFLEX bundle consists of 2 fuel element sizes: small-diameter elements in the outer and intermediate rings, and larger-diameter elements in the inner and centre rings (Figure 1). Special buttons are attached to the elements at 2 planes, to provide improved heat-transfer and hence CHF enhancement. To maintain compatibility of the new bundle design with the design of existing CANDU 6 reactor and fuel handling systems, the basic overall dimensions of the CANFLEX fuel bundle were designed to be the same as those of the 37-element fuel bundle. The small-diameter elements of the outer ring result in a slightly larger end-plate diameter compared with end-plate diameter of the standard 37-element bundle. Consequently, the bearing pad heights of the bundle are designed to be larger than those of the 37-element bundle. This feature makes the CANFLEX bundle fully compatible with the sidestop/separator assembly of the CANDU 6 fuelling machine. The sidestop/separator assembly is an important component in the fuelling machine. The fuel bundle dimensions must be compatible with this assembly.

CANFLEX fuel is designed to have hydraulic and neutronic characteristics that are similar to those of the existing fuel. This feature allows operators to introduce CANFLEX bundles during normal on power refuelling. The fuel bundle, in all other respects, is designed to be equivalent to the 37-element bundle - that is it should be "transparent" to all reactor systems. To verify this, tests were performed for pressure drop, bundle strength under a number of situations such as radial cross-flow, and a test of the long-term fretting performance.

CANFLEX QUALIFICATION AND PERFORMANCE ASSESSMENT

The CANFLEX bundle has undergone an extensive verification program [5,6]. The verification program has been conducted following the strategy laid out in the Design Verification Plan (DVP). The verification work consisted of analysis and testing, drawing on the capabilities of AECL's facilities in Canada and KAERI's facilities in Korea. The DVP identifies the performance requirements, specifies the test or analysis required to verify that the requirement is met, and identifies responsibility and procedures. All testing and analysis conformed to the quality standard CAN/CSA-N286.2 or equivalent [7]. The DVP called for preparation of a Test Specification, Test Procedure, and Acceptance Criteria and identified the required documentation.

Thermalhydraulic Testing of CANFLEX to Establish Thermalhydraulic Performance Data

Full-scale CANFLEX bundle tests [8,9] were performed to obtain licensing data in a high-pressure steam-water loop. The test string consisted of a 6-m-long, 43-element, bundle simulator. A wide range of steam-water flow conditions was covered in the CHF experiment: an outlet-pressure range from 6 to 11 MPa, mass-flow-rate range from 7 to 25 kg/s, and inlet-fluid-temperature range from 200 to 290°C. Single- and two-phase pressure-drop measurements along the string were performed at lower pressures and fluid temperatures, as well as at higher mass-flow rates (Figure 2). The data corresponded closely to those previously obtained with a simulated string of 37-element bundles at the same test facility. The dryout power enhancement of CANFLEX over 37-element fuel ranges from 8 to 18% for the range of conditions of interest at the same inlet-fluid temperature (Figure 3). The water CHF data have been used to derive a CHF correlation for the NUCIRC computer code [10], which is used to calculate critical channel powers in CANDU reactors.

NUCIRC applies the correlations to the range of channel geometries, power shapes and operating conditions specific to a given reactor. Pre-release versions of NUCIRC with the CANFLEX correlations show that a typical CANDU 6 reactor will operate with 5 to 8% higher critical channel powers when fuelled with CANFLEX compared to the standard 37-element bundles. NUCIRC Version 2.01, which will contain the CANFLEX calculation options, is currently being verified and should be formally released late in fiscal year 2000/01.

Out-reactor Flow Testing

AECL and KAERI have subjected the CANFLEX fuel bundle to a set of out-reactor flow tests to simulate reactor conditions and verify that the design is compatible with existing reactor hardware. These tests include Strength Test, Impact Test, Cross flow tests, Fuelling Machine Compatibility and a 3000 h Flow Endurance Test.

In-reactor Testing

CANFLEX bundles, AJK, AJM and AJN, were irradiated in the U-1 and U-2 loops in the NRU research reactor to demonstrate performance under expected in-reactor conditions. Typical power changes during refuelling and peak outer element midplane powers exceeding 70 kW/m were used for the irradiation conditions in the NRU tests. For the high burn-up NRU irradiations, burn-ups of greater than 480 MWh/kgU were achieved. Once the bundles were removed, detailed post-irradiation examinations

(PIE) were performed. The irradiation in NRU reactor confirmed the performance of the CANFLEX bundles under in-reactor operating conditions.

Reactor Physics Testing and Analysis

The ZED-2 facility at CRL was used to measure the fine-structure, reaction rates, and reactivity coefficients for CANFLEX natural-uranium bundles, to validate the reactor physics lattice code WIMS-AECL. The data showed excellent agreement with code predictions. A fuel management computer code was used to simulate reactor operation over 600 full-power days, to determine peak bundle powers, power changes during refuelling, burnups, and residence times. Various fuel schemes were studied. Fuel performance requirements were established for NRU irradiation tests. The analysis showed that the CANFLEX bundle meets or exceeds all power requirements.

Structural Analysis

The CANFLEX design was analyzed for sheath strains, fission-gas pressure, end-plate loading, thermal behaviour, mechanical fretting, element bow, end-flux peaking, and a range of other mechanical characteristics. The CANFLEX design met the acceptance criteria.

Formal Design Review and Licensing

In Canada, AECL's Chief Engineer conducted a formal design review to assess the CANFLEX verification and qualification program, and the bundle's readiness for full-core implementation. Industry experts from New Brunswick Power, Hydro Québec, Ontario Power Generation, the two domestic fuel fabricators, and subject-area experts reviewed the CANFLEX Fuel Design Manual and other CANFLEX documentation. Reviewers provided written comments that the Design Team addressed. Closure was achieved for most issues. Actions are underway to complete outstanding items, such as PIE of the DI bundles and completion of the thermalhydraulic licensing report.

In Korea, KAERI prepared a Fuel Design Report on CANFLEX-NU, and submitted it to the Korea Institute of Nuclear Safety (KINS) in July 1996 to obtain approval of the fuel design and fabrication method, as part of the Korean licensing process. In August 6, 1999, the Korean Government Approval of the CANFLEX-NU fuel design and fabrication method was released to KAERI. However, as outlined in the previous paragraph, several actions were also assigned for the completion of outstanding work- these included submissions of the PIE reports of the fuel irradiations in the NRU reactor and a CANDU power reactor and the water CHF test report of the fuel bundle string

Demonstration Irradiation Plan

The principle objective of a demonstration irradiation is to show compatibility with all reactor systems [11,12]. The PLGS applied its standard process for special fuel irradiations for the CANFLEX demonstration irradiation [13]. This process involves preparation of an Information Report that is the basis on which both management and regulatory approvals are built. The demonstration irradiation plan called for Zircatec Precision Industries to manufacture 26 CANFLEX bundles to the Quality Assurance levels normally applied to 37-element fuel supplied to PLGS- 24 bundles for fuelling in PLGS and 2 for archiving. All configurations of CANFLEX bundles mixed with 37-element bundles in a single channel during transition and full-core refuelling were to be tested. On discharge and transportation to the PLGS

spent fuel bays, the CANFLEX bundles were to be visually examined. Two bundles would be selected and shipped to the CRL for PIE. The demonstration irradiation will be fully documented, including station data and PIE reports.

CANFLEX Demonstration Irradiation Status

Once Canadian Nuclear Safety Commission (formerly the AECS) approval for the DI was secured in the late summer of 1998, PLGS fuel engineers selected channel S08 for the high-power channel (Figure 4) and channel Q20 for the low-power channel. As part of the routine on-power fuelling in 1998 September, 8 CANFLEX bundles were fuelled into each of the 2 channels. In 1999 March, the low-power channel Q20 was refuelled and the first 4 DI CANFLEX bundles were discharged into the fuel bays. The PLGS had planned a fuel-channel inspection in channel S08 during a summer maintenance shutdown, and it was decided to leave the CANFLEX fuel in the channel during the shutdown to demonstrate its compatibility with all maintenance handling systems and operations. Thus the high-power channel S08 was refuelled after reactor start-up in 1999 August, discharging 4 CANFLEX fuel bundles and establishing a full channel of 12 CANFLEX fuel bundles. In 2000 January, the final fuelling in channel Q20 was successfully completed, discharging 4 CANFLEX bundles and restoring the channel to full 37-element configuration. In 2000 February, channel S08 was refuelled, discharging 8 CANFLEX bundles and leaving 4 CANFLEX bundles to complete their irradiation. In 2000 August the last of the DI bundles was discharged thereby completing the irradiation of 24 CANFLEX bundles at PLGS.

The power history of bundles irradiated in the high power channel S08 (Figure 5) show a relatively high burnup of over 220 MWh/kgU, compared with a more standard burn-up of 175 MWh/kgU. From an operational perspective, the CANFLEX fuel behaved exactly as 37-element fuel would have: there were no differences in any monitored aspect of station behaviour that could be attributed to CANFLEX fuel.

Irradiated Fuel In-bay Inspection

Of the 24 CANFLEX bundles irradiated, 20 bundles have been visually inspected in the fuel bays at PLGS (the remaining 4 bundles discharged in August require 2 months of cooling before a full inspection can be made). The inspection team included fuelling experts from the station, a member of the CANFLEX design team and a member of the AECL fuel inspection group - who will conduct the PIE in the cells. The examination was done using an underwater periscope; photography was achieved using a television camera attached to the periscope and digital imaging. The inspection team concluded that the bundles were in very good condition. All observations, photographs and irradiation data have been sent to the design team for review and disposition.

Full inspection reports have been prepared and the design team's disposition of the findings documented for inclusion in the Demonstration Irradiation Report. In conclusion, the 20 bundles irradiated to date have shown good performance, confirming the acceptability and compatibility of this new design.

Post-irradiation Examination

Two CANFLEX DI fuel bundles were shipped to CRL for post-irradiation examination (PIE). Bundle FLX019Z, irradiated in channel Q20 position 8, was shipped to CRL on 1999 December. Bundle FLX019Z reached a calculated bundle burnup of 144 MWh/kgU and reached a peak outer-element linear power (OELP) of 38 kW/m. Bundle FLX007Z, irradiated in channel S08 position 8, was shipped

to CRL on 2000 March 30 from PLGS. Bundle FLX007Z reached a calculated bundle burnup of 221 MWh/kgU and reached a peak OELP of 45 kW/m.

The visual and non-destructive examinations have been completed for both bundles and the destructive examinations are in progress. The following is a brief summary of the PIE results to date:

- No unusual features or anomalies were found visually.
- Outer element straightness was found to be consistent with that of irradiated 37-element bundles.
- Bearing and spacer pad wear, and end plate distortion was minor and also consistent with irradiated 37-element fuel.
- Typical pellet-interface ridging was found for FLX007Z but it was not distinctive for the lower power bundle FLX019Z (Figure 6).
- Element gamma scans are normal, and no Cs migration to the pellet-interface was evident (Figure 7), consistent with lower internal fission gas release.
- Fission gas volumes (1.4 to 1.7 mL at STP) and release (less than 0.1%) were small.
- No unusual features or anomalies have been found in the metallographic and ceramographic examination of bundle FLX019Z (e.g., typical fuel microstructure Figure 8).

The plant data, fuel-bay examinations, PIE, and assessment work will be documented in a full report in 2001. This action will conclude the demonstration irradiation program for the CANFLEX bundle.

CANFLEX DEMONSTRATION IRRADIATION IN KOREA

With the successful completion of the demonstration irradiation of CANFLEX fuel in PLGS, KEPCO has initiated a program to use CANFLEX fuel in Wolsong Unit 1, which has been operating since 1983. Korea Electric Power Research Institute (KEPRI) of KEPCO and KAERI starting in September 2000 is conducting an industrialization program for the use of CANFLEX fuel in the Wolsong reactor jointly. This 3-year program will be under Korea's Nuclear Energy R & D Mid- and Long-Projects that have been financially supported and operated by the Korea Ministry of Science and Technology since 1992. The program mainly involves a small-scale irradiation of 24 CANFLEX-NU bundles in the Wolsong reactor and production of a safety assessment report for full-core implementation of CANFLEX-NU fuel. The CANFLEX fuel is expected to be loaded in Wolsong Unit 1 in the later part of 2001. Successfully demonstrating the irradiation of CANFLEX fuel in the Wolsong power reactor will lead the way towards the full-core implementation of CANFLEX fuel in Korean CANDU reactors.

INCREASING CANDU OPERATING MARGINS WITH CANFLEX FUEL

Implementing CANFLEX fuel in existing CANDU 6 reactors will increase the critical channel powers (CCP) by 5 to 8%. The actual CCP gain depends on individual channel conditions such as channel creep shape, power shape and local flow conditions. Critical Channel Power is calculated using the computer code NUCIRC. The increase in CCP margin can be used by station operations to offset the margin reductions resulting from reactor aging, such as the effect of heat transport system fouling and of diametral creep of the pressure tubes. Alternatively, the increase in margin could be utilized to increase the core power output, particularly in a new reactor.

The ~20% reduction in the linear element rating of the CANFLEX bundle (compared with the 37-element bundle) results in a substantial reduction of the fission product inventory in the fuel-to-sheath gap (i.e., gap-inventory). For example, at the same maximum bundle power, the iodine gap-inventory in the maximum-rated element in a CANFLEX bundle is estimated to be 3 times lower than for the maximum-rated element in a 37-element bundle. This reduction provides several benefits. For accidents in which a number of fuel elements are predicted to fail and their fission-product gap-inventory released, the radiological consequences will be reduced with the use of the CANFLEX bundles. This further enhances the safety performance of the reactor. The lower gap-inventory and lower power will also lead to lower activity burden in the heat transport circuit in the event of fuel failures during normal operation. While the performance of CANDU fuel has been excellent, and the fuel failure rate has been very low, on-power fuelling and failed fuel detection and location systems are designed to provide the means for an operator to locate and remove failed fuel. The lower gap-inventory will also reduce the radiological contamination in the heat transport circuit arising from activity release from failed fuel. Consequently, the man-rem exposure during reactor maintenance is expected to be less, resulting in occupational health and cost benefits.

CONCLUSIONS

The CANFLEX fuel design has been verified through extensive testing by AECL and KAERI and has been critically reviewed under a Formal Design Review. Results from the 24 CANFLEX bundles irradiated to date in PLGS confirm the compatibility of this fuel type with existing reactor systems. After the successful demonstration irradiation of CANFLEX fuel in PLGS, KEPRI and KAERI will jointly conduct a 3-year industrialization program on the use of CANFLEX-NU fuel in Wolsong reactors starting with plans for a demonstration irradiation in the later part of 2001. Successfully demonstrating the irradiation of CANFLEX fuel in the Wolsong power reactor will lead the way towards the full-core implementation of CANFLEX-NU fuel in Korea. The economic analysis based on the CHF-enhancement data indicates a significant payback to utilities operating CANDU reactors. The utilities now have an alternative fuel that can be deployed with confidence to provide greater operating margins.

REFERENCES

1. I.J. Hastings, A.D. Lane and P.G. Boczar, "CANFLEX - An Advanced Fuel Bundle for CANDU", Int. Conf. Availability Improvements in Nuclear Power Plants, Madrid, Spain, 1989 April 10-14, and also AECL Report, AECL-9929, 1989.
2. A.D. Lane, G.R. Dimmick, J.H.K. Lau, H.C. Suk, C.H. Chung and C.B. Choi, "CANFLEX: A New CANDU Fuel Bundle with Expanded Operating Capabilities", Proc. 11th KAIF/KNS Annual Conference, Seoul, Korea, 1996 April 11-12.
3. H.C. Suk, K.S. Sim, B.G. Kim, C.B. Choi, C.H. Chung, A.D. Lane, D.F. Sears, J.H.K. Lau, I.E. Oldaker and P.G. Boczar, "CANFLEX as a CANDU Advanced Fuel Bundle", presented at the Fifth International Topical Meeting on Nuclear Thermalhydraulics, Operations and Safety, Beijing, China, 1997 April.
4. K-S. Sim and H.C. Suk, "Some Considerations in the CANFLEX-NU Fuel Design", presented at the Fifth International Conference on CANDU Fuel, Canadian Nuclear Society, Toronto, Canada, 1997 September 21-25.

5. P. Alavi, I.E. Oldaker, C.H. Chung and H.C. Suk, "Design Verification of the CANFLEX Fuel Bundle - Quality Assurance Requirements for Mechanical Flow Testing", presented at the Fifth International Conference on CANDU Fuel, Canadian Nuclear Society, Toronto, Canada, 1997 September 21-25.
6. C.H. Chung, S.K. Chang, H.C. Suk, I.E. Oldaker and P. Alavi, "Performance of the CANFLEX Fuel Bundle under Mechanical Flow Testing", presented at the Fifth International Conference on CANDU Fuel, Canadian Nuclear Society, Toronto, Canada, 1997 September 21-25.
7. Design Quality Assurance for Nuclear Power Plants, CAN/CSA-N286.2-96, Canadian Standards Association, Rexdale, Ontario.
8. G.R. Dimmick, W.W.R. Inch, J.S. Jun, H.C. Suk, G.I. Haddaller, R. Fortmann and R. Hayes, "Full-Scale Water CHF Testing of the CANFLEX Bundle", Proc. 6th CANDU Fuel Conference, Niagara Falls, Canada, 1999 September 26-30.
9. L.K.H. Leung, D.C. Groeneveld, G.R. Dimmick, D.E. Bullock and W.W.R. Inch, "Critical Heat Flux and Pressure Drop for a CANFLEX Bundle String Inside an Axially Non-Uniform Flow Channel", Proc. 6th International CANDU Fuel Conference, Niagara Falls, 1999 September 26-30.
10. G.D. Harvel, M. Soulard, R.F. Dam, P. White, R. Moffet, G. Hotte, "NUCIRC Simulations of a CANDU-Type Header Manifold Model", 5th CNS International Conference on Simulation Methods in Nuclear Engineering, Montreal Quebec, 1996.
11. W.W.R. Inch, P. Thompson, P. Reid and H.C. Suk, "Demonstration Irradiation of CANFLEX in CANDU 6 Power Reactor", Proc. 14th KAIF/KNS Annual Conference, Seoul, Korea, 1999 April 8-9.
12. W.W.R. Inch, P.D. Thompson, M.A. Cormier, and H.C. Suk, "Demonstration Irradiation of CANFLEX in a CANDU 6 Power Reactor", Proc. 15th KAIF/KNS Annual Conference, Seoul, Korea, 2000 April 18-20.
13. P.J. Reid, R.G. Steed, R.A. Gibb, R.W. Sancton, "A Standard Approach to Special Fuel Irradiations at Point Lepreau Generating Station", Proc. 19th Annual Conference of the Canadian Nuclear Society, Toronto, Ontario, Canada, 1998 October 18-21.



Demonstration Irradiation of CANFLEX in a CANDU 6 Power Reactor

by

Wayne W.R. Inch
Atomic Energy of Canada Limited, Canada

Paul D. Thompson
Point Lepreau Generating Station, New Brunswick Power, Canada

Mike A. Cormier
Atomic Energy of Canada Limited, Canada

Ho Chun Suk
Korea Atomic Energy Research Institute, Korea (R.O.K.)

Demonstration Irradiation of CANFLEX in a CANDU 6 Power Reactor

by

Wayne W.R. Inch, Atomic Energy of Canada Limited, Canada
Paul D. Thompson, Point Lepreau Generating Station, New Brunswick Power, Canada
Mike A. Cormier, Atomic Energy of Canada Limited, Canada
Ho Chun Suk, Korea Atomic Energy Research Institute, Korea (R.O.K.)

ABSTRACT

The CANFLEX[®] fuel bundle is the latest design in the evolution of CANDU[®] fuel. Its 43-element fuel bundle assembly and its patented critical-heat-flux (CHF) enhancement appendages offer higher operating and safety margins than the standard 37-element bundle; in addition, it is fully compatible with operating CANDU reactors. Since 1991, Atomic Energy of Canada Limited has partnered with the Korea Atomic Energy Research Institute to complete the development, qualification testing and analysis of the CANFLEX fuel bundle.

A 2-channel, 24-bundle demonstration irradiation of CANFLEX was started on 1998 September 03 at New Brunswick Power's Point Lepreau Generating Station. All 24 bundles have been loaded into the reactor and 16 bundles have completed their planned irradiation. The irradiated bundles will be examined to verify bundle integrity and condition. The irradiation data and in-bay photographs are expected to show that the in-reactor performance of the CANFLEX fuel has met all design criteria and that it is fully compatible with existing CANDU reactors. These results will be important in supporting the use of CANFLEX as the production fuel in CANDU 6 reactors. Several bundles irradiated in this demonstration irradiation will be destructively examined in post-irradiation examinations in the hot cells at Chalk River Laboratories of Atomic Energy of Canada Limited.

CANFLEX fuel development is part of an overall strategy on plant ageing, which recognized that certain processes were taking place within the heat-transport system which, if left unabated, could result in a decrease in the margin to fuel-sheath dryout. Because of the increase in critical channel power brought about by the improved CANFLEX design, it was recognized that this new fuel, when used in combination with other remedial actions, could counterbalance the adverse effects of ageing within the heat-transport system. Water CHF tests have been completed to firmly establish the thermalhydraulic performance of this fuel.

This paper will report on the results of the demonstration irradiation and present the CANFLEX thermalhydraulic performance data. The paper will discuss the licensing challenges in implementing this new fuel in an existing reactor. Finally, it will show potential economic and safety benefits of this new fuel concept and identify future developments and their potential economic impact.

CANFLEX[®] (CANDU FLEXible) is a registered trademark of Atomic Energy of Canada Limited and Korea Atomic Energy Research Institute.

CANDU[®] (Canada Deuterium Uranium) is a registered trademark of Atomic Energy of Canada Limited (AECL).

INTRODUCTION

Since the early 1990's, Atomic Energy of Canada Limited (AECL) and the Korea Atomic Energy Research Institute (KAERI) have pursued a collaborative program to develop, verify, and prove a new fuel design that would introduce advanced fuel cycles into CANDU reactors and provide enhanced performance with natural uranium (NU) fuel to provide higher operating margins in existing CANDU reactors.

In 1998 September, New Brunswick Power (NBP), at the Point Lepreau Generating Station (PLGS), began a two-year irradiation of CANFLEX fuel bundles, as final verification of the CANFLEX design in preparation for full-core conversion. This paper describes the CANFLEX program, the results of the demonstration irradiation (DI) and the thermalhydraulics performance testing program, and preparations for full-core implementation.

CANFLEX FEATURES

The principal features of CANFLEX fuel are enhanced thermalhydraulic performance and more balanced radial power distribution, providing CANDU plant operators with greater operating flexibility through improved operating margins [1-5]. Critical heat flux (CHF) enhancement appendages on the CANFLEX bundle enable a higher bundle power before CHF occurs, leading to a net gain in the critical channel power, typically up to 10% over the existing 37-element fuel. The maximum linear-element rating in a CANFLEX bundle is 20% lower than that of a 37-element bundle, reducing the consequences of most design-basis accidents. The lower element rating is achieved by adding extra elements and using larger-diameter elements in the two center rings and smaller-diameter ones in the outer two rings.

CANFLEX fuel is designed to have hydraulic and neutronic characteristics that are similar to those of the existing fuel. This feature allows operators to introduce CANFLEX bundles during normal on-power refuelling. No hardware changes are required to switch to CANFLEX fuel, because it is fully compatible with existing fuel-handling equipment. Fuel channels containing both CANFLEX and 37-element fuel, in any combination that can occur with normal fuelling, have improved or unchanged operating margins. Transition to CANFLEX fuel can be gradual, with no waste of existing fuel.

In addition to providing greater operating margins, the CANFLEX bundle facilitates the use of slightly enriched uranium (SEU) and/or recovered uranium (RU) [6,7]. CANFLEX-SEU and -RU offer lower fuelling costs and provide a means of raising reactor power within a fixed core size. The use and economics of SEU and RU are being assessed in a collaborative program with KAERI, SEU and RU suppliers.

CANFLEX VERIFICATION PROGRAM

The CANFLEX bundle has undergone an extensive verification program [7,8]. The verification program has been conducted following the strategy laid out in the Design Verification Plan (DVP). The verification work consisted of analysis and testing, drawing on the capabilities of AECL's facilities in Canada and KAERI's facilities in Korea.

The DVP identifies the performance requirements, specifies the test or analysis required to verify that the requirement is met, and identifies responsibility and procedures. All testing and analysis conformed to the quality standard CAN/CSA-N286.2 [11] or equivalent. The DVP called for preparation of a Test Specification, Test Procedure, Acceptance Criteria and identified the required documentation. The verification program was described in a Korea Atomic Industrial Forum Inc. (KAIF) paper in 1998 [12].

The CANFLEX-NU design report prepared by KAERI for the use of CANFLEX bundles in Korea was submitted to the Korea Institute of Nuclear Safety (KINS) in 1996 July for approval of the fuel design and manufacturing method, as part of the Korean licensing process. KINS completed its review of the report in 1999 July and the Korean Ministry of Science and Technology issued a license for the CANFLEX-NU fuel design and manufacturing method in 1999 August. KEPCO (Korea Electric Power corporation) has intensively reviewed a proposed use of the CANFLEX fuel in the Wolsong Unit 1 reactor. A small number of CANFLEX-NU fuel bundles could be irradiated in the reactor in 2001.

In 2000 February, AECL's Chief Engineer conducted a formal design review to assess the CANFLEX verification and qualification program, and the bundle's readiness for full-core implementation. Industry experts from New Brunswick Power, Hydro Quebec, Ontario Power Generation, the two domestic fuel fabricators, and subject-area experts reviewed the CANFLEX documentation. While closure was achieved for the majority of the issues, several actions were assigned for the completion of outstanding work, such as post irradiation examination (PIE) of the DI bundles and completion of the thermohydraulics licensing report. All issues raised in the design review will be addressed within the planned program

CANFLEX DEMONSTRATION IRRADIATION

Demonstration Irradiation Plan

The DI plan was outlined in a KAIF paper in 1999 [12]. It called for 26 CANFLEX bundles to be fabricated, 24 to be irradiated at PLGS and two to be kept for archive purposes. Sixteen bundles were to be irradiated in a high-powered channel and eight in a low-powered channel. The fuelling sequence for each channel is shown in Figures 1 and 2. As CANFLEX bundles were discharged and transported to the bays, they were to be visually examined. Three bundles were to be shipped to AECL's Chalk River Laboratories (CRL) for PIE. The DI will be fully documented, including station data and PIE reports.

CANFLEX Demonstration Irradiation Status and Schedule

Once Atomic Energy Control Board (AECB) approval for the DI was secured in the late summer of 1998, PLGS fuel engineers selected channel S08 for the high-power channel and channel Q20 for the low-power channel. As part of the routine on-power fuelling in 1998 September, eight CANFLEX bundles were fuelled into each of the two channels. In 1999 March, the low-power channel Q20 was refuelled and the first four DI CANFLEX bundles were discharged into the fuel bays. PLGS had planned a fuel-channel inspection in S08 during a summer maintenance shutdown, and it was decided to leave the CANFLEX fuel in the channel during the shutdown to demonstrate its compatibility with all maintenance handling and operations. Thus the high-power channel S08 was refuelled after reactor start-up in 1999 August, discharging four CANFLEX fuel bundles and establishing a full channel of 12 CANFLEX fuel bundles. In 2000 January, the final fuelling in Q20 was successfully completed, discharging four CANFLEX bundles and restoring the channel to full 37-element configuration. In 2000 February, S08 was refuelled, discharging eight CANFLEX bundles and leaving four CANFLEX bundles to complete their irradiation. At present, 20 CANFLEX bundles of the 24-bundle DI have successfully completed the planned irradiation. The remaining four bundles in S08 are expected to be discharged in 2000 September, bringing the irradiation work to completion

Demonstration Irradiation Results

The first bundles discharged (four from S08 and four from Q20) were irradiated to the power histories shown in Figures 3 and 4. S08 had a relatively high burnup of over 250 MWh/kgU, compared to a more standard burn-up of 175 MWh/kgU. The bundles in the low-power channel Q20 had lower burnup and linear powers. From an operational perspective, the CANFLEX fuel behaved exactly as 37-element fuel would: there were no significant differences in any monitored aspect of station behaviour which could be attributed to CANFLEX fuel. During the above-mentioned summer shutdown, channel S08 underwent Spacer Location And Repositioning (SLAR) and Channel Inspection and Gauging Apparatus for Reactors (CIGAR) inspection. The fuel handling associated with these procedures was uneventful and the results of the CIGAR inspection did not indicate any unusual wear in the channel.

The eight CANFLEX bundles and the two adjacent downstream 37-element fuel bundles were examined in the PLGS bays in 1999 October. The inspection team included fuelling experts from the station, a member of the CANFLEX design team and a member of the AECL fuel inspection group, who will conduct the PIE in the cells. The examination was done using an underwater periscope and photography was achieved using a television camera attached to the periscope and digital imaging. The inspection team concluded that the bundles were in very good condition. All observations, photographs and irradiation data have been sent to the design team for review and disposition.

In 2000 March, the 12 bundles discharged in the January and February fuelling were examined in the PLGS fuel bays. Again, the team found that the irradiated fuel was in very good condition. Thus the 20 bundles irradiated to date have shown good performance, verifying the acceptability and compatibility of this new design.

In 2000 January, one bundle from Q20 was shipped to CRL for PIE (Figure 5). The PIE will consist of:

- visual examination, bundle profilometry;
- disassembly and element profilometry;
- gamma scanning;
- fission-gas and void volume measurements;
- end-plate weld and button-weld strength tests;
- metallography and ceramography;
- chemical burnup analysis (high-performance liquid chromatography);
- alpha, beta and gamma autoradiography; and
- hydrogen analysis of sheath, button and end plate;

Figure 6 displays a typical gamma scan where the pellet interfaces are clearly shown and are consistent with previous fuel examinations. The examination continues.

A bundle from S08 will be shipped in 2000 April, and a third bundle in the fall of 2000. PIE on these bundles will complete the DI inspection and assessment work. All 24 CANFLEX bundles will be discharged by the fall of 2000. The plant data, fuel-bay examinations, PIE and assessment work will be documented in a full report in 2001, concluding the DI.

THERMALHYDRAULIC TESTING OF CANFLEX TO ESTABLISH LICENSING DATA

The principal performance benefit of CANFLEX fuel for existing CANDU reactors is higher critical channel powers. To secure licensing approval for CANFLEX for the DI, CHF experiments were performed in Freon-134a in the MR-3 facility at CRL, on both the 37-element and the CANFLEX simulated

fuel strings. The pressure-drop characteristics of the CANFLEX bundle were determined in both Freon tests and hot and cold water tests, and reported in a KAIF 1999 paper [13].

Full-scale CANFLEX bundle tests have been performed to obtain licensing data in the high-pressure steam-water loop at Stern Laboratories [14]. The test string consisted of a 6-m-long, 43-element, bundle simulator. The elements were constructed with Inconel tubes of two different outer diameters (13.5 and 11.5 mm). Bundle segmentation was simulated with specially designed spool pieces that imitated the radial and cross webs of the end plate in a fuel bundle. Corresponding elements in both the upstream and downstream bundles of the spool pieces were aligned axially. Appendages (i.e., spacers, bearing pads and AECL-patented non-load-bearing buttons) were spot welded at various locations as specified in the bundle design. Power was applied to the bundle string through Joule heating. The sheath thickness of the elements was varied along the axial length and from ring to ring. This provided accurate simulations of non-uniform radial and axial heat-flux distributions. The radial heat-flux distribution simulated a bundle with the NU fuel, and the axial heat-flux distribution corresponded to a downstream skewed-cosine profile. A ceramic flow tube was introduced to insulate the bundle string from the metal pressure boundary. Three different liners were used in the test: one had a uniform inside diameter of 103.86 mm and the other two had axially varying inside diameters with a peak of 107.29 mm and 109.16 mm (3.3% and 5.1% larger than the uniform tube). The uniform liner simulated a reference uncrept pressure tube, while the others simulated pressure tubes with various degrees of diametral creep.

A wide range of steam-water flow conditions was covered in the CHF experiment: an outlet-pressure range from 6 to 11 MPa, mass-flow-rate range from 7 to 25 kg/s, and inlet-fluid-temperature range from 200°C to 290°C. Most of the data are directly relevant to analyses of the regional overpower trip (ROPT) set point in the reactor. In addition, single- and two-phase pressure-drop tests were performed at lower pressures and fluid temperatures, as well as at higher mass-flow rates. The data corresponded closely to those previously obtained with a simulated string of 37-element bundles at the same test facility.

The dryout power represents the total power applied to the bundle string at which the onset of intermittent dryout (OID) occurs. This corresponds to only a single point at the sheath of an element, where the liquid film has broken down, while continuous liquid contact is maintained at the remaining surfaces in the bundle string. Figures 7 and 8 show the dryout power of the CANFLEX fuel bundle relative to the 37-element bundle. The dryout power data are consistently higher for the CANFLEX bundles than for the 37-element bundles. On average, the enhancement is about 17% for the range of conditions of interest at the same inlet-fluid temperature.

The water CHF experimental program is now complete and analysis is underway [15]. The water CHF data have been used to derive a CHF correlation for the NUCIRC computer code, which is used to calculate critical channel powers. A similar correlation has been derived for the 37-element bundle and implemented in the most recent release of NUCIRC. Figure 7 compares the CHF predictions derived from the correlations for the CANFLEX and 37-element bundles. At the time of writing, implementation of the CANFLEX correlations in NUCIRC was ongoing, so direct comparison of critical channel powers for the two fuel bundles can not be provided in this paper; it will be presented at the conference.

CANFLEX FULL-CORE IMPLEMENTATION

The successful DI of CANFLEX fuel will lead to a consideration of full-core implementation. Switching from the existing 37-element fuel to CANFLEX fuel will be largely driven by the economic benefits to be realized. The economic benefits are directly dependent on the thermalhydraulic performance. Implementing a new fuel type will require revisions to safety analysis and licensing documents and, ultimately, approval by the regulatory body.

Economic Model of CANFLEX Implementation

To provide an economic basis for implementation, an economic model has been prepared to include all investments, effects on annual utility revenues and annual operating costs. Both the net present value (NPV) and internal rate of return are calculated for a range of implementation strategies and assumptions.

The economic model can assess the changes in revenue, operating costs, and investments that result from implementation of various plant-life-extension strategies available to offset the anticipated decline in reactor power due to ageing effects. The analysis must include all fiscal-year revenues, and all investment costs are calculated to yield the annual projected cash flows. The differences between the cash flows are discounted to the decision date and are summed over the time period of application.

Implementation of CANFLEX fuel involves an initial investment in revising the safety analyses and operating procedures, leading to technical reviews and licensing submissions to obtain regulatory approval. The incremental costs of CANFLEX fuel are captured by the model. The resultant NPV quantifies the economic benefit of using a range of CANFLEX implementation strategies, to establish the sensitivity to various parameters. These various cases guide reactor management in selecting the most appropriate implementation strategy. Each reactor has unique and proprietary cost factors. The model accepts the reactor-specific costs as input assumptions and calculates the CANFLEX benefit. Current analysis using the latest thermalhydraulic performance data shows that the improvements in revenue from the CANFLEX Mk4 bundle far outweigh the additional costs associated with its introduction and production. Each utility will implement CANFLEX according to its unique situation. AECL is working with utilities in Canada to determine implementation strategies for CANFLEX.

Safety Analysis and Licensing

The PLGS Power Reactor Operating License stipulates that only fuel of an approved design may be irradiated in the reactor. Use of any fuel type other than 37-element in the reactor therefore requires regulatory approval. This approval depends on the existing safety report and supporting documentation to demonstrate that the change in fuel type does not compromise the safe operation of the reactor.

For the demonstration irradiation, a safety assessment was completed, which showed that the presence of up to 24 CANFLEX fuel bundles in the core would not have a negative impact on the safe operation of the reactor. For full-core CANFLEX implementation, further assessment is required. In addition, the assessment must consider the transition between an all 37-element core and an all CANFLEX core, since this process takes place over an extended period (about two years). However, the safety assessment in support of full-core CANFLEX implementation can build on the results of the assessment that was performed for the DI. AECL is working with CANDU utilities in Canada to establish the licensing program requirements and the various roles and responsibilities

CONCLUSIONS

CANFLEX fuel has been under development for over 10 years. CANFLEX fuel is a prime example of the benefits that can be achieved through collaborative ventures between Canada and Korea. CANFLEX fuel has been verified through extensive testing by AECL and KAERI. Results from the 20 CANFLEX bundles irradiated to date in PLGS verify the compatibility of this fuel type with existing reactor systems. The economic analysis based on the CHF-enhancement data indicates a significant payback to utilities operating older CANDU reactors. The utilities now have an alternative fuel that can be deployed with confidence in a CANDU design to provide a greater operating margin.

REFERENCES

1. I.J. Hastings, A.D. Lane and P.G. Boczar, "CANFLEX - An Advanced Fuel Bundle for CANDU", Int. Conf. Availability Improvements in Nuclear Power Plants, Madrid, Spain, 1989 April 10-14, also AECL Report, AECL-9929, 1989.
2. A.D. Lane, D.F. Sears, I.E. Oldaker, B.M. Townes, A. Celli, H.C. Suk, C.H. Chung and K-S. Sim, "Recent Achievements in the Joint AECL/KAERI Program to Develop the CANFLEX Fuel Bundle", Proc. 10th KAIF/KNS Annual Conference, Seoul, Korea, 1995 April 6-7.
3. A.D. Lane, G.R. Dimmick, J.H.K. Lau, H.C. Suk, C.H. Chung and C.B. Choi, "CANFLEX: A New CANDU Fuel Bundle with Expanded Operating Capabilities", Proc. 11th KAIF/KNS Annual Conference, Seoul, Korea, 1996 April 11-12
4. H C. Suk, K.S. Sim, B.G. Kim, C.B. Choi, C.H. Chung, A.D. Lane, D F. Sears, J.H.K. Lau, I.E. Oldaker and P.G. Boczar, "CANFLEX as a CANDU Advanced Fuel Bundle", presented at the Fifth International Topical Meeting on Nuclear Thermalhydraulics, Operations and Safety, Beijing, China, 1997 April.
5. K-S. Sim and H.C. Suk, "Some Considerations in the CANFLEX-NU Fuel Design", presented at the Fifth International Conference on CANDU Fuel, Canadian Nuclear Society, Toronto, Canada, 1997 September 21-25.
6. I.J. Hastings, P.G. Boczar and A.D. Lane, "CANFLEX - An Advanced Bundle Design for Introducing Slightly-Enriched Uranium into CANDU", presented at Int. Symp. on Uranium and Electricity (The Complete Nuclear Fuel Cycle), Saskatoon, Saskatchewan, 1988 September 18-21, Canadian Nuclear Society, also AECL Report, AECL-9766 (1988).
7. P.G. Boczar et al., "Recovered Uranium in CANDU: A Strategic Opportunity", presented at the INC Conf., Toronto, Canada, 1993 October 3-6
8. P. Alavi, I.E. Oldaker, C.H. Chung and H C. Suk, "Design Verification of the CANFLEX Fuel Bundle - Quality Assurance Requirements for Mechanical Flow Testing", presented at the Fifth International Conference on CANDU Fuel, Canadian Nuclear Society, Toronto, Canada, 1997 September 21-25.
9. P. Alavi, I.E. Oldaker, C.H. Chung and H.C. Suk, "Design Verification of the CANFLEX Fuel Bundle - Quality Assurance Requirements for Mechanical Flow Testing", presented at the Fifth International Conference on CANDU Fuel, Canadian Nuclear Society, Toronto, Canada, 1997 September 21-25.
10. C.H. Chung, S.K. Chang, H.C. Suk, I.E. Oldaker and P. Alavi, "Performance of the CANFLEX Fuel Bundle under Mechanical Flow Testing", presented at the Fifth International Conference on CANDU Fuel, Canadian Nuclear Society, Toronto, Canada, 1997 September 21-25.
11. Design Quality Assurance for Nuclear Power Plants, CAN/CSA-N286.2-96.
12. W.W.R. Inch, P. Thompson and H.C Suk, "CANFLEX From Development Concept To A Proven Fuel", Proc. 13th KAIF/KNS Annual Conference, Seoul, Korea, 1998 April 14-16

13. W.W.R. Inch, P. Thompson, P. Reid and H.C. Suk, "Demonstration Irradiation of CANFLEX in CANDU-6 Power Reactor", presented at the 14th Annual KAIF/KNS Conference, Seoul, Korea, 1999 April 8-9.
14. G.R. Dimmick, D.E. Bullock, A. Hameed and J.H. Park, "Thermalhydraulic Performance of CANFLEX Fuel", presented at the Fifth International Conference on CANDU Fuel, Canadian Nuclear Society, Toronto, Canada, 1997 September 21-25.
15. G.R. Dimmick, W.W.R. Inch, J.S. Jun, H.C. Suk, G.I. Haddaller, R. Fortmann and R. Hayes, "Full-Scale Water CHF Testing of the CANFLEX Bundle", presented at the CANDU Fuel Conference, Niagara Falls, Canada, 1999 September 26-30.
16. L.K.H. Leung, D.C. Groeneveld, G.R. Dimmick, D.E. Bullock and W.W.R. Inch, "Critical Heat Flux and Pressure Drop for a CANFLEX Bundle String Inside an Axially Non-Uniform Flow Channel", presented at the CANDU Fuel Conference, Niagara Falls, 1999 September 26-30.

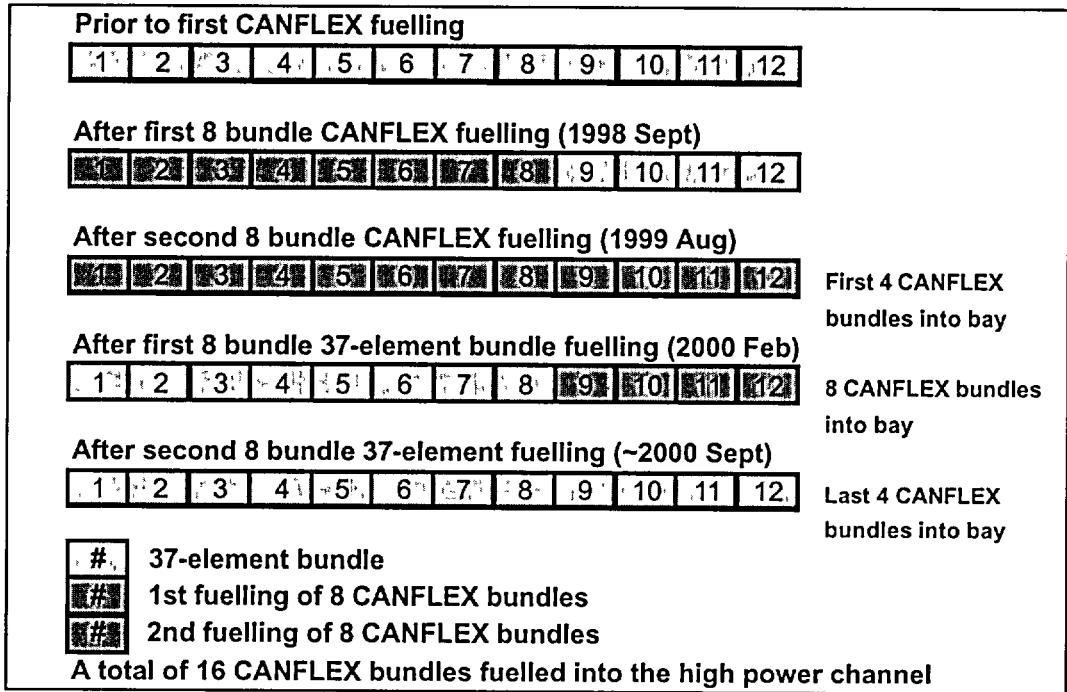


Figure 1: Planned Fuelling History for High-power Channel

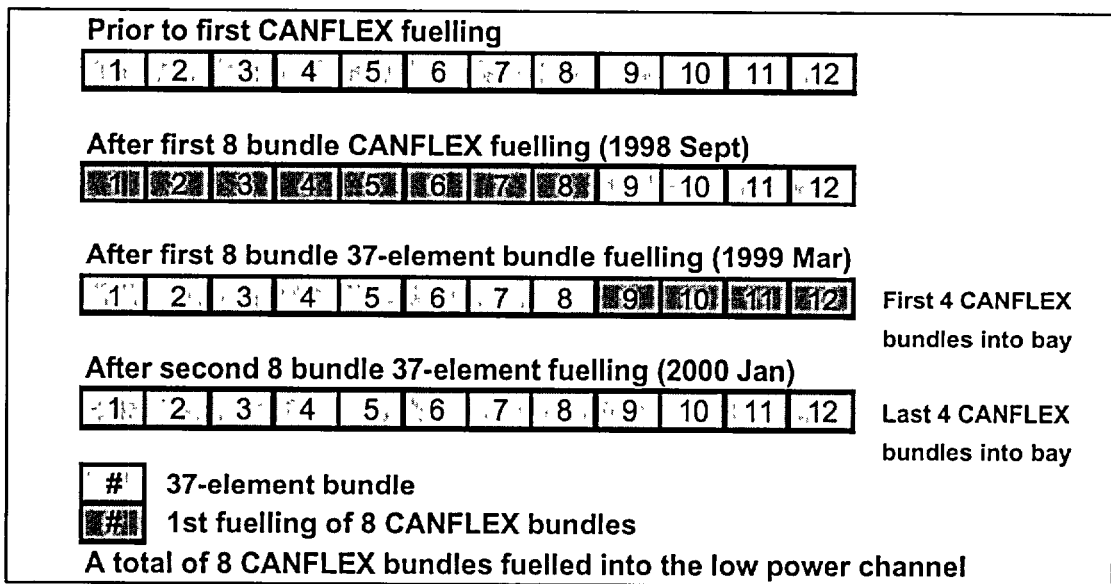


Figure 2: Planned Fuelling History for Low-power Channel

CANFLEX (Q20-06) Power History

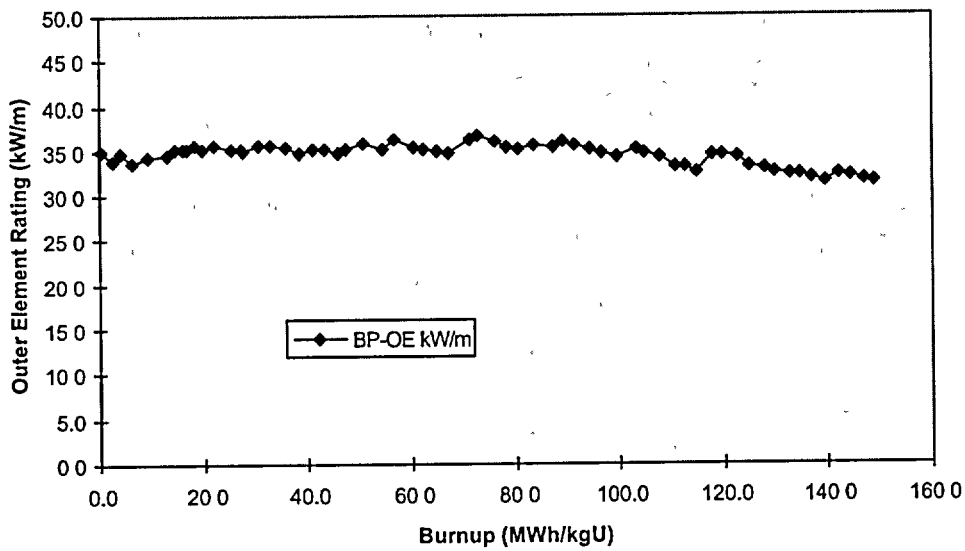


Figure 3: Power History for the DI CANFLEX Bundle From Position 6 in Low Power Channel Q20 Discharged 1999 March

CANFLEX (S08-06) Power History

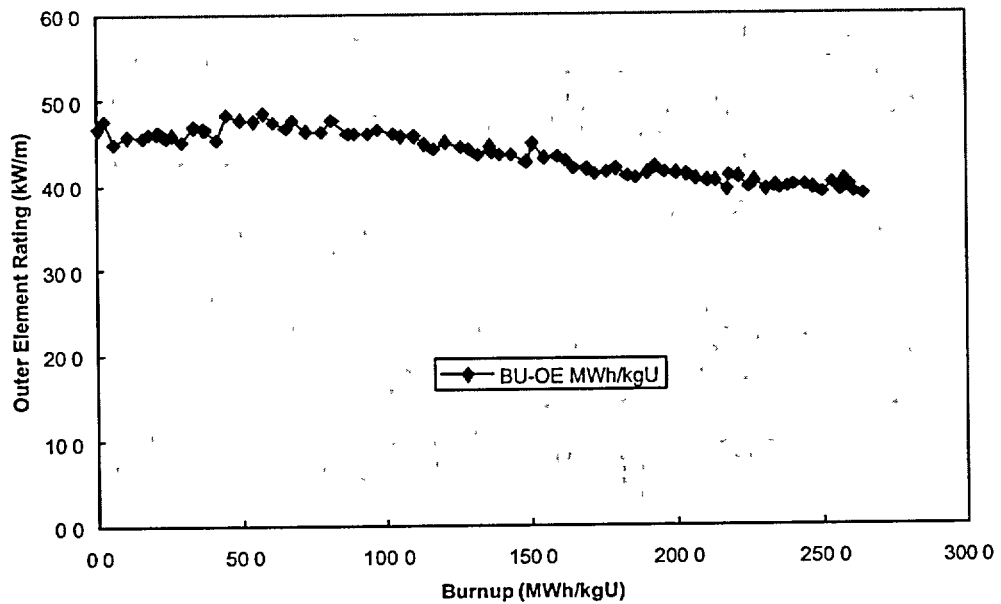


Figure 4: Power History for the DI CANFLEX Bundle From Position 6 in High Power Channel S08 Discharged 1999 September

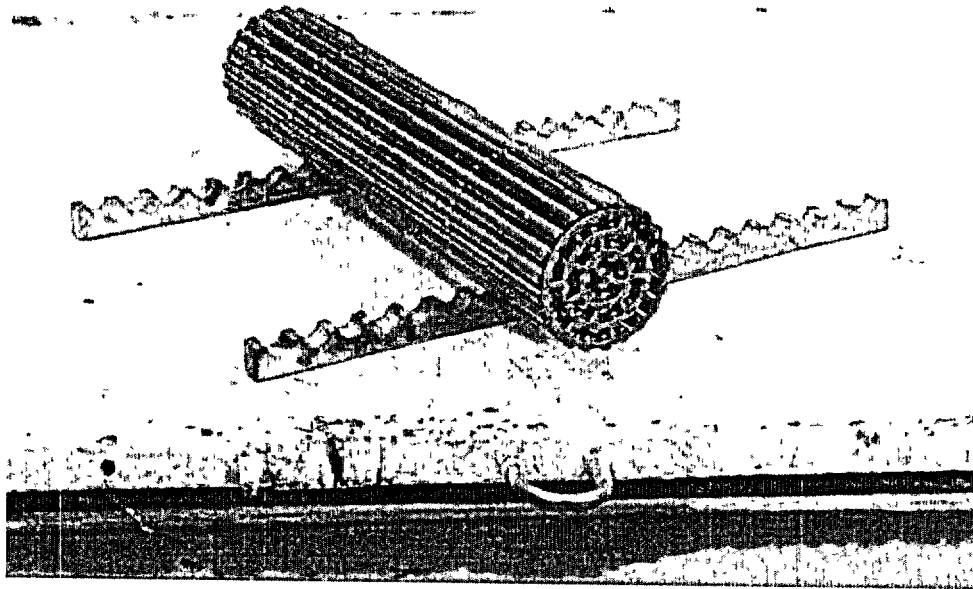


Figure 5: CANFLEX Irradiated Bundle from PLGS - Photo Taken in Hot Cells During PIE Non-Destructive Examination

Lepreau Canflex Bundle FLX019Z Element 07, 2000 Jan 27.

(2mm x 25mm slot aperture, 1mm to 500mm, 1mm increment, 60 second scans with rotation)

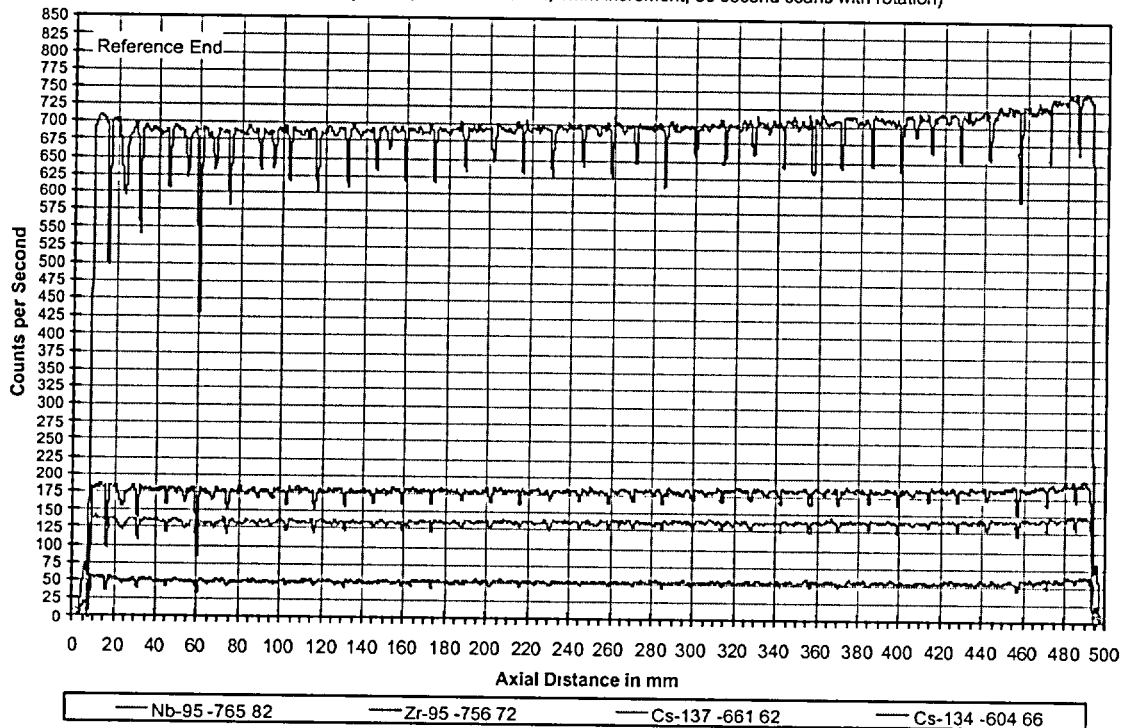


Figure 6: Typical CANFLEX Gamma-Scan Results

Comparison of CANFLEX vs 37-Element Dryout Power

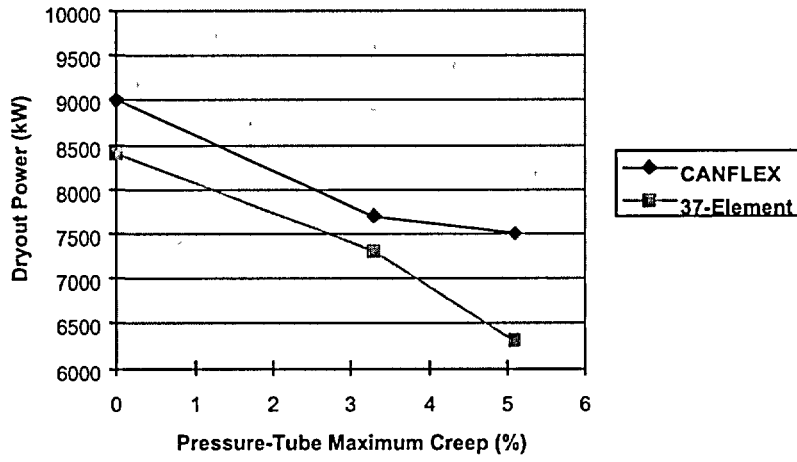


Figure 7: CANFLEX Thermalhydraulic Performance

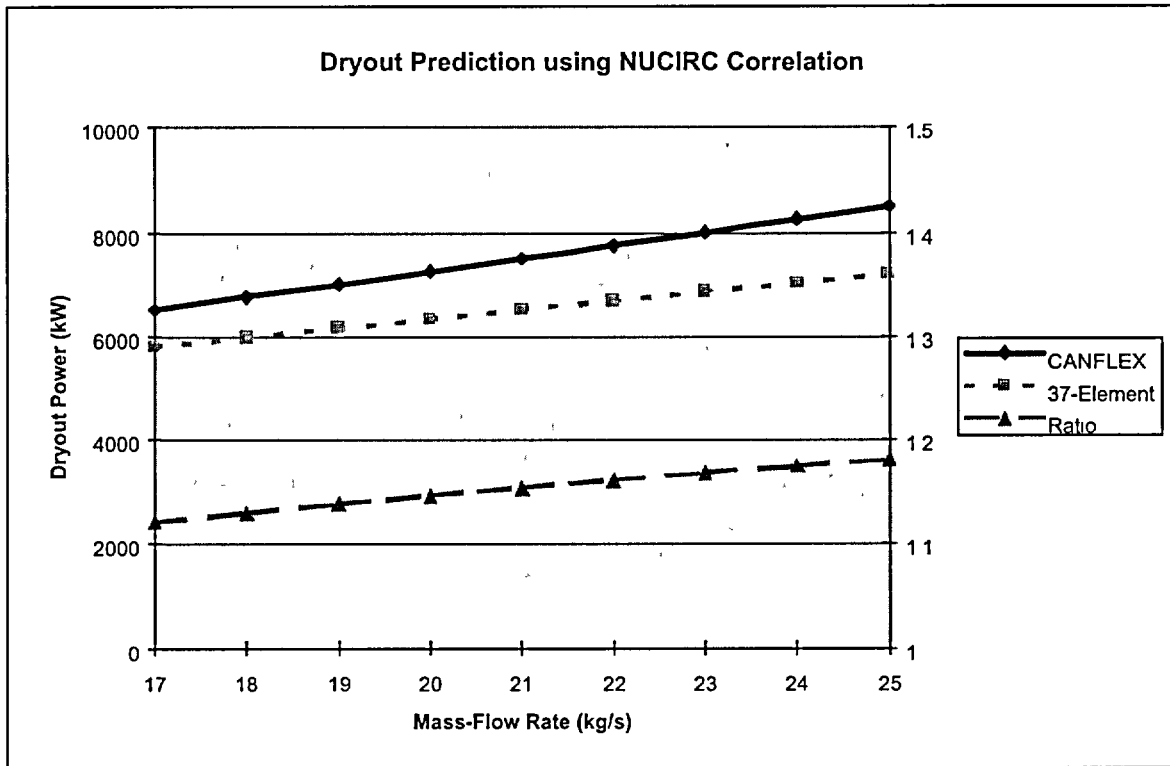


Figure 8: Cross-Correlation Comparison 5.3% (crept) data

THE DRYOUT-POWER IMPROVEMENT OF CANFLEX SEU BUNDLES IN CANDU REACTORS

L.K.H. Leung and K.F. Rudzinski
Atomic Energy of Canada Ltd.
Fuel Channel Thermalhydraulics Branch
Chalk River Laboratories
Chalk River, Ontario K0J 1J0

P.S.W. Chan
Atomic Energy of Canada Ltd.
Reactor Core Physics Branch
2251 Speakman Drive
Mississauga, Ontario L5K 1B2

ABSTRACT

An assessment of the impact on dryout power has been completed for a string of CANFLEX bundles containing 0.9% slightly enriched uranium (SEU) fuel with either a 2-bundle-shift or 4-bundle-shift fuelling scheme. The effect of radial heat-flux distribution on dryout power for the CANFLEX bundles has been shown to be small (about a 0.5% difference) between natural uranium (NU) and 0.9% SEU fuel with the same axial heat-flux distribution (AFD). On the other hand, the variation in AFD for the SEU fuel has a large impact on the dryout power, compared to the NU fuel. Based on the calculated results, the introduction of CANFLEX 0.9% SEU fuel bundles and a 2-bundle-shift fuelling scheme in a CANDU fuel channel would lead to a dryout-power enhancement of 8% to 27% over the complete range of pressure-tube creep (having the downstream-skewed profile), compared to the current 37-element NU fuel bundles using the 8-bundle-shift fuelling scheme. The enhancement is slightly higher (10% to 29%) for a 4-bundle-shift fuelling scheme.

1. INTRODUCTION

The CANFLEX[®] fuel-bundle design allows the use of various levels of enrichment in a CANDU[®] reactor. AECL is currently assessing all aspects associated with the use of slightly enriched uranium (SEU) of enrichment around 0.9% in the CANFLEX bundle. Recycled uranium (RU) from the reprocessing of spent pressurized-water reactor fuel is a potential source of enrichment. The use of SEU fuel would lead to a change in the radial heat-flux distribution (RFD) from the natural uranium (NU) fuel bundle, while the fuelling scheme would result in a change in the axial heat-flux distribution (AFD) from that currently encountered in CANDU reactors. Both changes would have a beneficial impact on the critical channel power (CCP), and hence raise the reactor operating power. This study examined the potential improvement in dryout power for a CANFLEX bundle string using 0.9% SEU fuel with either a 2-bundle-shift or a 4-bundle-shift fuelling scheme.

The current carrier of NU fuel in CANDU reactors is the 37-element bundle. It has a center-depressed RFD that does not vary significantly over the resident period inside the reactor. Previous studies have shown that the variation in RFD due to burnup has little impact on critical heat flux (CHF) (or dryout power and CCP) for NU fuel, but that the variation can be significant for SEU fuel (Yin et al. 199 1). The fuelling scheme changes the AFD of the bundle string inside the fuel channel; this in turn has a strong impact on the dryout power (and CCP). Groeneveld et al. (1992) showed that the dryout power of a bundle string with a non-uniform AFD is generally higher if its peak heat-flux point is located at the upstream end rather than the downstream end in a channel. Leung et al. (1998) recommended using the boiling-length-average (BLA) approach to account for the AFD effect.

[®] CANFLEX (CANDU FLEXible) and CANDU (CANada Deuterium Uranium) are registered trademarks of Atomic Energy of Canada Ltd. (AECL)

2. EVALUATION OF FUEL-STRING DRYOUT POWER

The fuel-string dryout power is calculated by subdividing the channel into nodes, and comparing the BLA heat fluxes against the predicted CHF values based on the correlation at each node until a tangent point is reached. As suggested by Leung et al. (1998), the BLA heat flux is calculated by averaging the power introduced to the coolant over the axial distance from the boiling initiation point to the location of interest. The CHF at each node is expressed as

$$CHF_{BLA} = CHF_{ref.BLA} K_{rfd} \quad (1)$$

where $CHF_{ref.BLA}$ is the reference CHF value and K_{rfd} is the modification factor for the RFD effect. The reference CHF correlations were derived from experimental data obtained with full-scale 6-m simulators of 12 fully aligned 37-element and CANFLEX bundles equipped with appendages and end-plates. Each bundle string was electrically heated; each had a non-uniform AFD, corresponding to the downstream-skewed cosine profile, and RFD, corresponding to NU fuel of mid-burnup level. Figure 1 shows the AFD of the simulators in the full-scale bundle tests, and Figure 2 shows the RFD of the simulators in the 37-element and CANFLEX bundle tests. Both the AFD and RFD have been normalised to a bundle average surface heat flux of 1 (the average surface heat flux for a CANFLEX bundle is 5% lower than a 37-element bundle for the same bundle power). The tests covered uniform and non-uniform variations in pressure-tube diameter to simulate various levels of diametral creep. Figure 3 illustrates the representative variations in pressure-tube diameter for various channels in a CANDU 6 reactor.

The modification factor, K_{rfd} , for the 37-element bundles was proposed by Yin et al. (1991). It is expressed as:

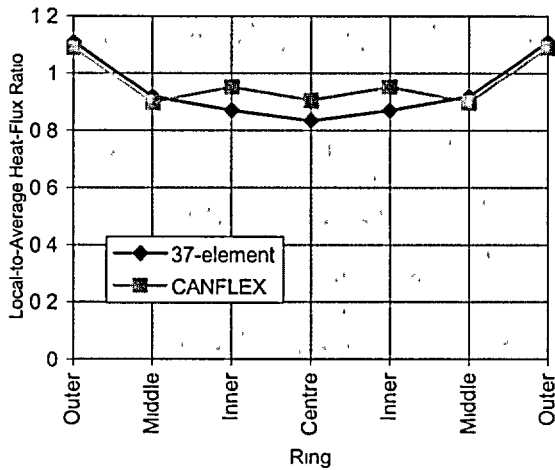


Figure 3: Radial Heat-Flux Profiles of the Full-Scale Bundle Simulators.

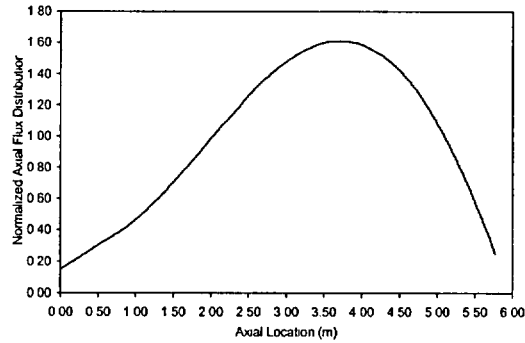


Figure 1: Axial Heat-Flux Profile of the Full-Scale Bundle Simulators.

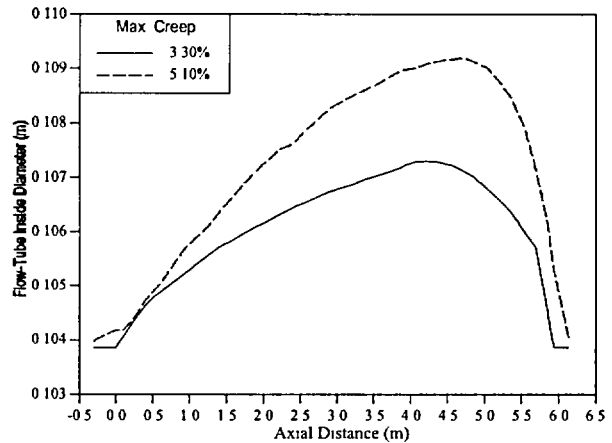


Figure 2: Axial Variations in Pressure-Tube Diameter in the Full-Scale Bundle Tests.

$$K_{rfd} = \frac{K_{rfdo}}{K_{rfdo,NU}} \quad (2)$$

where

$$K_{rfdo} = \frac{CHF \text{ for Flux Shape of Interest}}{CHF \text{ for Optimum Flux Shape}} \quad (3)$$

Yin et al. (1991) introduced a bundle-imbalance factor, Z , which represents the maximum deviation in the local-to-bundle-average heat-flux ratio of the bundle of interest from an optimum bundle¹. The factor is defined as

$$Z = \max(R_i / R_{i,o}) \quad (4)$$

where R_i and $R_{i,o}$ are the ratios of local heat-flux to bundle-average heat-flux for Ring i of the RFD of interest and of the optimum RFD, respectively. Based on the same methodology, a bundle-imbalance factor has been derived for the CANFLEX bundle. Analysis of experimental CHF data obtained with Freon-cooled CANFLEX bundles of various RFDs has provided the optimum RFD as 0.9892/1.080/0.8884/0.8884 (outer-ring/middle-ring/inner-ring/centre-rod). Yin et al. (1991) stated that the fractional reduction in CHF from the optimum value (i.e., $1 - K_{rfdo}$) is approximately the same as the fractional deviation from the optimum RFD (i.e., $Z - 1$). Hence, the K_{rfdo} for the bundle of interest is expressed as:

$$K_{rfdo} = 2 - Z \quad (5)$$

The value of $K_{rfdo,NU}$ is 0.9174, based on the experimental CHF data for CANFLEX bundles of various RFDs.

3. DRYOUT POWER FOR THE CANFLEX SEU FUEL-BUNDLE STRING

The current assessment focuses on the dryout power for the 0.9% SEU fuel bundle at conditions of interest (i.e., pressures of 9 and 11 MPa, mass-flow rates of 17-21 kg/s and an inlet-fluid temperature of 265°C). The dryout power for the CANFLEX SEU fuel-bundle string is calculated by accounting for the variations in RFD and AFD, using the methodologies described in Section 2.

3.1 Impact of RFD Variation

The element power in each ring was calculated using the WIMS computer code for the

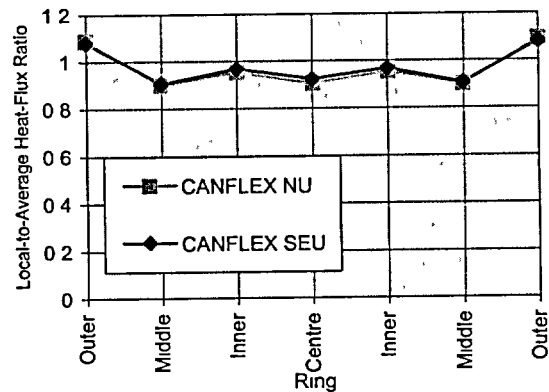


Figure 4: Radial Heat-Flux Profiles for SEU Fuel Bundles.

¹ An optimum bundle gives the highest dryout power, with dryout occurring on all rings simultaneously, i.e., $Z=1$.

CANFLEX bundles of NU and 0.9% SEU fuel. Figure 4 shows the local-to-average heat-flux ratio for elements in each ring based on the calculated element power at mid-burnup (corresponding roughly to the axial location of dryout). In general, the RFDs are similar for NU and 0.9% SEU fuel bundles at mid-burnup. The local heat-flux ratio for elements at the outer ring is slightly lower for the SEU than for the NU fuel bundle.

The average dryout-power enhancements for the CANFLEX 0.9% SEU fuel-bundle string over the CANFLEX NU fuel-bundle string were calculated for the same NU AFD and inlet-flow conditions in various crept² channels. The dryout power for the fuel-bundle string with the 0.9% SEU RFD is about 0.6% higher than that with the NU RFD, and is insensitive to pressure-tube creep.

3.2 Impact of AFD Variation

The assessment examines two different fuelling schemes (4-bundle shift and 2-bundle shift), and compares the dryout power for those schemes against the dryout powers for the typical 8-bundle-shift fuelling scheme currently used in the CANDU 6 reactor. Figure 5 shows the variation in AFD for various fuelling schemes. Table 1 lists the average dryout-power enhancements for various fuelling schemes of SEU fuel bundles, compared to the 8-bundle-shift fuelling scheme for NU fuel bundles. Overall, an enhancement of dryout power has been shown with a change in fuelling scheme, and it is slightly higher for the 4-bundle shift than the 2-bundle shift. In addition, the enhancement varies with channel creep³ and system pressure (see Figure 6). The effect of mass flux on the enhancement is relatively minor.

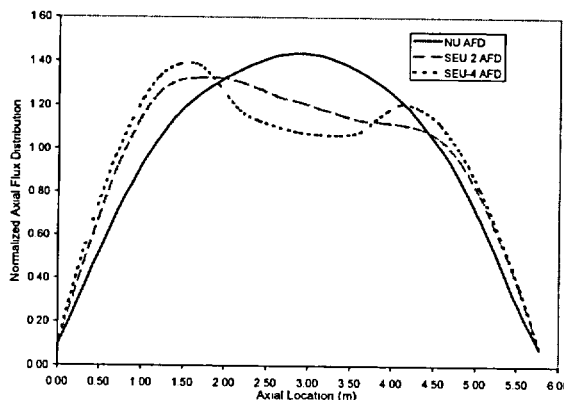


Figure 5: Axial Heat-Flux Profiles for the CANFLEX Bundles.

Table 1: Dryout-Power Enhancement for Various Fuelling Schemes of CANFLEX 0.9% SEU Fuel Bundles over the 8-Bundle-Shift Fuelling Scheme of CANFLEX NU Fuel Bundles

Maximum Creep (%)	Dryout-Power Enhancement over the 8-Bundle-Shift CANFLEX NU Fuel Bundles (%)	
	CANFLEX 0.9% SEU Fuel Bundles (2-Bundle Shift)	CANFLEX 0.9% SEU Fuel Bundles (4-Bundle Shift)
0	6.21	7.60
3.3	10.77	13.24
5.1	11.32	13.56

² In all cases, it was assumed that the effect of pressure-tube creep on RFD is small.

³ In assessing the effect of AFD on dryout power, it was assumed that the effect of pressure-tube creep on AFD was small.

4. DRYOUT-POWER ENHANCEMENT OVER THE 37-ELEMENT NU FUEL-BUNDLE STRING

The dryout-power values for the CANFLEX 0.9% SEU fuel bundle with various fuelling schemes have been compared against those for the 37-element NU fuel bundle with the 8-bundle-shift fuelling scheme (the fuel carrier in the current CANDU 6 reactor). This comparison includes the geometry effect (between 37-element and CANFLEX fuel bundles), in addition to the RFD and AFD effects. The dryout power for the bundle string is calculated using the methodology described in Section 2. Table 2 lists the average dryout-power enhancements over the 37-element NU bundle string for various fuelling schemes with the CANFLEX NU and 0.9% SEU fuel bundles. Depending on the degree of channel creep, the CANFLEX NU bundle enhances the dryout power from 2.2 to 15.4%, compared to the 37-element NU fuel bundle. The CANFLEX 0.9% SEU fuel bundles results in an even larger average enhancement over the current assessed conditions: 8.4 to 26.8% for the 2-bundle-shift and 9.8 to 29% for the 4-bundle-shift fuelling scheme. Similar to the results shown in the comparison of various CANFLEX bundles (Figure 6), the level of enhancement depends strongly on the channel creep and system pressure but not on mass flux, as illustrated in Figure 7. The corresponding range of enhancement in CCP must be calculated with an analytical tool for regional overpower protection (ROP) (such as the NUCIRC code). It is estimated to be about 4 to 13% for the 2-bundle-shift fuelling scheme over the pressure-tube creep range from 0 to 5.1%.

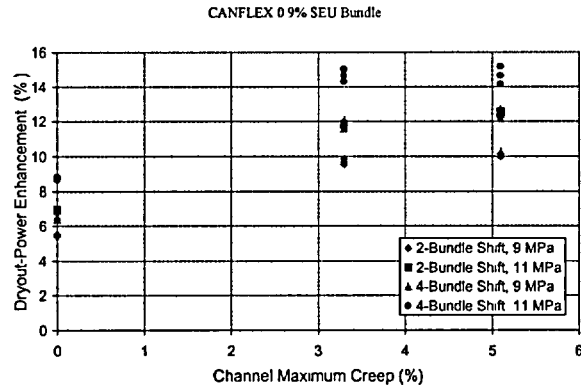


Figure 6: Dryout-Power Enhancement of the CANFLEX 0.9% SEU Fuel Bundles over the CANFLEX NU Fuel Bundles.

Table 2: Dryout-Power Enhancement for Various Fuelling Schemes of CANFLEX NU and 0.9% SEU Fuel Bundles over the 8-Bundle-Shift Fuelling Scheme of 37-Element NU Fuel Bundles

Maximum Creep (%)	Dryout-Power Enhancement over the 8-Bundle-Shift 37-Element NU Fuel Bundles (%)		
	CANFLEX NU Fuel Bundles (8-Bundle Shift)	CANFLEX 0.9% SEU Fuel Bundles (2-Bundle Shift)	CANFLEX 0.9% SEU Fuel Bundles (4-Bundle Shift)
0	2.23	8.43	9.83
3.3	7.99	18.76	21.23
5.1	15.43	26.75	28.99

5. CONCLUSIONS AND FINAL REMARKS

- The effect of AFD and RFD on dryout power for a string of CANFLEX 0.9% SEU fuel bundles has been assessed. The assessment is based primarily on the full-scale bundle data for CANFLEX NU fuel bundles of the mid-burnup RFD, and includes a modification factor to account for the RFD effect on CHF. The AFD effect is accounted for using the BLA heat-flux approach.
- The variation of RFD from NU to 0.9% SEU fuel results in an increase in dryout power of about 0.6% for the mid-burnup level.

- The variation of AFD from various fuelling schemes has a strong impact on dryout power. Depending on the degree of channel creep and system pressure, the dryout-power enhancement varies from 6.2 to 11.3% for the 2-bundle-shift and 7.6 to 13.6% for the 4-bundle-shift fuelling scheme with the CANFLEX 0.9% SEU fuel bundles as compared to CANFLEX NU fuel bundles.
- Use of the CANFLEX 0.9% SEU fuel bundles with a 2-bundle-shift fuelling scheme would increase dryout power from 8.4 to 26.8% over the range of pressures and channel creeps of interest, compared to the 37-element NU fuel bundles with an 8-bundle-shift fuelling scheme (a slightly larger improvement is shown for the 4-bundle-shift fuelling scheme). The equivalent improvement in CCP must be determined using an ROP analysis code (such as the NUCIRC code). It is estimated to be about 4 to 13%.
- The predictions are based on extensions of various correlations to cases beyond their database (e.g., AFD and RFD). Experimental data are needed to verify and confirm the estimated enhancements.

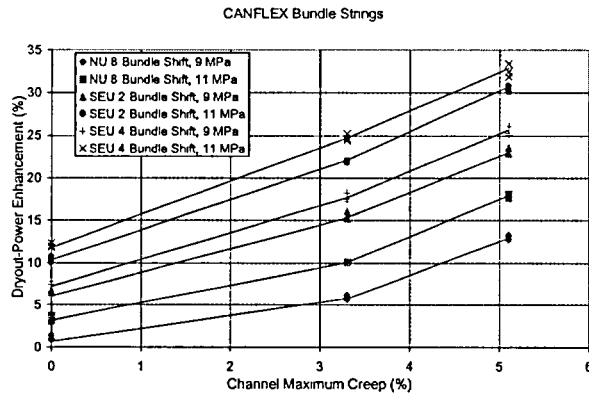


Figure 7: Dryout-Power Enhancement of the CANFLEX 0.9% SEU Fuel-Bundle String over the 37-Element NU Fuel-Bundle String.

6. REFERENCES

- Groeneveld, D.C., Doerffer, S., Leung, L.K.H., Rudzinski, K.F. and Yin, S.T., CHF Separate-Effects Studies at Chalk River Laboratories, *Proc. of the 17th Annual CNS Simulation Symposium on Nuclear Engineering*, Kingston, Canada, 1992 Aug. 16-18.
- Leung, L.K.H., Groeneveld, D.C. and Hotte, G., A Generalized Prediction Method for Critical Heat Flux in CANDU Fuel-Bundle Strings, *Proc. of the 11th International Heat Transfer Conference*, Kyongju, Korea, Aug. 23-28, Vol. 6, pp. 15-20, 1998.
- Yin, S.T., Groeneveld, D.C. and Wakayama, M., The Effect of Radial Flux Distribution on Critical Heat Flux in 37-Rod Bundles, *Proc. of the 12th National Heat Transfer Conference*, Minneapolis, July 28-31, Vol. 5, pp. 277-283, 1991.

ACKNOWLEDGEMENT

The authors would like to thank Dr. S.C. Sutradhar, W.W. Inch and P.G. Boczar for their comments and support of this study.

Increasing CANDU Operating Margins with CANFLEX Fuel

Prepared for

**6th COG/IAEA Technical Committee Meeting on
Exchange of Operational Safety Experience of PHWRs,
Trois Rivieres, Quebec
September 11-15**

by

Wayne W.R. Inch, Atomic Energy of Canada Limited, Canada

Joseph H. Lau, Atomic Energy of Canada Limited, Canada

Paul D. Thompson, Point Lepreau Generating Station, New Brunswick Power, Canada

Patrick J. Reid, Candesco Research Corporation, Canada

Increasing CANDU Operating Margins with CANFLEX Fuel

by

Wayne W.R. Inch, Atomic Energy of Canada Limited, Canada

Joseph H. Lau, Atomic Energy of Canada Limited, Canada

Paul D. Thompson, Point Lepreau Generating Station, New Brunswick Power, Canada

Patrick J. Reid, Candesco Research Corporation, Canada

ABSTRACT

The CANFLEX[®] fuel bundle is the latest design in the evolution of CANDU[®] fuel. Its 43-element fuel bundle assembly and its patented critical-heat-flux (CHF) enhancement appendages offer, over the range of operating conditions, 5 to 8% higher critical channel powers (CCP) than the standard 37-element bundle. The maximum linear-element rating in a CANFLEX bundle is 20% lower than that of a 37-element bundle, reducing the consequences of most design-basis accidents. It is fully compatible with operating CANDU reactors, designed to have hydraulic and neutronic characteristics that are similar to those of the existing fuel. This feature allows operators to introduce CANFLEX bundles during normal on-power refuelling

A rigorous verification process has been followed to qualify CANFLEX for use in a CANDU reactor. Extensive out-reactor testing combined with analysis has been used to show that CANFLEX meets the fuel design requirements. The design requirements, assessments and performance test results were documented in a Fuel Design Manual and were subject to an industry-wide formal Design Review. The final step prior to implementation was a demonstration irradiation in a power reactor. A 2-channel, 24-bundle demonstration irradiation of CANFLEX was started on 1998 September 03 at New Brunswick Power's Point Lepreau Generating Station. All 24 bundles have completed their planned irradiation. Several of the irradiated bundles have been examined to verify bundle integrity and condition. The post-irradiation examination data shows that the in-reactor performance of the CANFLEX fuel has met all design criteria and that it is fully compatible with existing CANDU reactors.

CANFLEX fuel development is part of an overall strategy on plant ageing, which recognized that certain processes were taking place within the heat-transport system which, if left unabated, could result in a decrease in the margin to fuel-sheath dryout. Because of the increase in CCP brought about by the improved CANFLEX design, it was recognized that this new fuel, when used in combination with other remedial actions, could counterbalance the adverse effects of aging within the heat-transport system.

This paper will report on the CANFLEX qualification program, the results of the demonstration irradiation and present the CANFLEX thermalhydraulic performance data. The paper will also discuss the various increases in safety margins with the use of CANFLEX fuel. Finally, it will show potential economic benefits of this new fuel concept and identify future developments and their potential economic impact.

CANFLEX[®] (CANDU FLEXible) is a registered trademark of Atomic Energy of Canada Limited and the Korea Atomic Energy Research Institute.

CANDU[®] (Canada Deuterium Uranium) is a registered trademark of Atomic Energy of Canada Limited

INTRODUCTION

Since the early 1990's, Atomic Energy of Canada Limited (AECL) and the Korea Atomic Energy Research Institute (KAERI) have pursued a collaborative program to develop, verify, and prove a new fuel design that would introduce advanced fuel cycles into CANDU reactors and provide enhanced performance with natural uranium (NU) fuel to provide higher operating margins in existing CANDU reactors.

In 1998 September, New Brunswick Power (NBP), at the Point Lepreau Generating Station (PLGS), began a two-year demonstration irradiation of CANFLEX fuel bundles, as final verification of the CANFLEX design in preparation for full-core conversion. This document provides a summary of the CANFLEX qualification and performance assessment program and discusses the benefits existing plants can derive from using this fuel design.

CANFLEX BUNDLE DESIGN

The CANFLEX design is a 43-element fuel-bundle assembly offering improved operating and safety margins, compared with the standard 37-element fuel bundle, for operating CANDU reactors[1-7]. The CANFLEX bundle design includes critical heat flux (CHF) enhancement devices leading to 5 to 8% higher critical channel power (CCP) in a full-length fuel channel, compared with that of 37-element fuel bundles. The lower heat rating of the CANFLEX fuel elements at current bundle powers leads to lower fuel temperatures. Hence less free fission-gas inventory is produced under normal operating conditions compared with the free fission-gas inventory produced in standard 37-element fuel elements at a similar bundle power.

The CANFLEX bundle consists of 2 fuel element sizes: small-diameter elements in the outer and intermediate rings, and larger-diameter elements in the inner and centre rings (Figure 1). Special buttons are attached to the elements at 2 planes, to provide improved heat-transfer and hence CHF enhancement (Figure 2). To maintain compatibility of the new bundle design with the design of existing CANDU 6 reactor and fuel handling systems, the basic overall dimensions of the CANFLEX fuel bundle were designed to be the same as those of the 37-element fuel bundle. The small-diameter elements of the outer ring result in a slightly larger end-plate diameter compared with end-plate diameter of the standard 37-element bundle. Consequently, the bearing pad heights of the bundle are designed to be larger than those of the 37-element bundle. This feature makes the CANFLEX bundle fully compatible with the sidestop/separator assembly of the CANDU 6 fuelling machine. The sidestop/separator assembly is an important component in the fuelling machine. The fuel bundle dimensions must be compatible with this assembly.

CANFLEX fuel is designed to have hydraulic and neutronic characteristics that are similar to those of the existing fuel. This feature allows operators to introduce CANFLEX bundles during normal on-power refuelling. The fuel bundle, in all other respects, is designed to be equivalent to the 37-element bundle, to be "transparent" to all reactor systems. To verify this, tests were performed for pressure drop, bundle strength under a number of situations such as radial cross-flow, and a test of the long-term fretting performance.

CANFLEX QUALIFICATION AND PERFORMANCE ASSESSMENT

The CANFLEX bundle has undergone an extensive verification program [8,9]. The verification program has been conducted following the strategy laid out in the Design Verification Plan (DVP). The verification work consisted of analysis and testing, drawing on the capabilities of AECL's facilities in Canada and KAERI's facilities in Korea. The DVP identifies the performance requirements, specifies the test or analysis required to verify that the requirement is met, and identifies responsibility and procedures. All testing and analysis conformed to the quality standard CAN/CSA-N286.2 or equivalent [10]. The DVP called for preparation of a Test Specification, Test Procedure, Acceptance Criteria and identified the required documentation.

Thermalhydraulic Testing of CANFLEX to Establish Thermalhydraulics Performance Data

To fully characterize the thermalhydraulic performance of CANFLEX, CHF experiments were performed in Freon-134a in the MR-3 facility at CRL, on both the 37-element and the CANFLEX simulated fuel strings. The pressure-drop characteristics of the CANFLEX bundle were determined in both Freon tests and hot and cold water.

Full-scale CANFLEX bundle tests were performed to obtain licensing data in the high-pressure steam-water loop at the Stern Laboratories [14,16]. The test string consisted of a 6-m-long, 43-element, bundle simulator. A wide range of steam-water flow conditions was covered in the CHF experiment: an outlet-pressure range from 6 to 11 MPa, mass-flow-rate range from 7 to 25 kg/s, and inlet-fluid-temperature range from 200°C to 290°C. Most of the data are directly relevant to analyses of the regional overpower trip (ROPT) set point in the reactor.

The dryout power enhancement of CANFLEX over 37-element fuel established from the water CHF testing, ranges from 8 to 18% for the range of conditions of interest at the same inlet-fluid temperature (Figure 3). Single and two-phase pressure-drop tests were performed at lower pressures and fluid temperatures, as well as at higher mass-flow rates (Figure 4). The pressure drop data corresponded closely to those previously obtained with a simulated string of 37-element bundles at the same test facility.

The water CHF and pressure drop data have been used to derive a CHF correlation and pressure drop loss coefficients for the NUCIRC [17] computer code. NUCIRC applies the correlations to the range of channel geometries, power shapes and operating conditions specific to a given reactor. Pre-release versions of NUCIRC with the CANFLEX correlations show that a typical CANDU 6 reactor will operate with 5 to 8% higher critical channel powers when fuelled with CANFLEX compared to the standard 37-element bundles. NUCIRC Version 2.01 which will contain the CANFLEX calculation options, is currently being verified and should be formally released late in fiscal year 2000/01.

Out-reactor Flow Testing

AECL and KAERI have subjected the CANFLEX fuel bundle to a set of out-reactor flow tests to simulate reactor conditions and verify that the design is compatible with existing reactor hardware. In addition to the heat transfer and pressure drop tests the following mechanical flow tests have been successfully completed:

- **Strength Test:** Strength tests showed that the fuel can withstand the hydraulic loads during refuelling, when the fuel string is supported only by the sidestops.. Post-test bundle geometry measurements showed no significant distortion.
- **Impact Test:** Impact tests showed that the CANFLEX bundle can withstand the bundle impact during refuelling.
- **Cross Flow:** Cross flow tests demonstrated that, during refuelling, when the bundle is in the cross flow region, the bundle withstands the flow-induced vibration for a minimum of 18 h.
- **Fuelling Machine Compatibility:** Fuelling machine compatibility tests showed that the bundle is dimensionally compatible with the fuel handling system.
- **Flow Endurance:** The 3000-h flow endurance test demonstrated that the CANFLEX bundle will maintain structural integrity during operation; fretting wear on the bearing pads, inter-element spacers and pressure tube will remain within design limits.

In-reactor Testing

CANFLEX bundles, AJK, AJM and AJN, were irradiated in the U-1 and U-2 loops in the NRU research reactor to demonstrate performance under expected in-reactor conditions. Typical power changes during refuelling and peak outer element midplane powers exceeding 70kW/m were used for the irradiation conditions in the NRU tests. For the high burn-up NRU irradiations, burn-ups of greater than 480MWh/kgU were achieved. Once the bundles were removed, detailed post-irradiation examinations (PIE) were performed. The irradiation in NRU reactor confirmed the performance of the CANFLEX bundles under in-reactor operating conditions.

Reactor Physics Testing and Analysis

The ZED-2 facility at CRL was used to measure the fine-structure, reaction rates, and reactivity coefficients for CANFLEX natural-uranium bundles, to validate the reactor physics lattice code WIMS-AECL [18]. The data showed excellent agreement with code predictions. A fuel management computer code was used to simulate reactor operation over 600 full-power days, to determine peak bundle powers, power changes during refuelling, burnups, and residence times. Various fuelling schemes were studied. Fuel performance requirements were established for NRU irradiation tests. The analysis showed that the CANFLEX bundle meets or exceeds all power requirements.

Structural Analysis

The CANFLEX design was analyzed for sheath strains, fission-gas pressure, end-plate loading, thermal behavior, sliding wear, element bow and end-flux peaking. The CANFLEX design met the performance requirements.

Formal Design Review

The Verification Program results were summarized in the Fuel Design Manual. This document captures all the design requirements and points to the individual analysis or test which shows that the requirement has been met. In 2000 February, AECL's Chief Engineer conducted a formal design review to assess the CANFLEX verification and qualification program, and the bundle's readiness for full-core

implementation. Industry experts from New Brunswick Power, Hydro Quebec, Ontario Power Generation, the two domestic fuel fabricators, and subject-area experts reviewed the CANFLEX Fuel Design Manual and other CANFLEX documentation. Reviewers provided written comments that the Design Team addressed. Closure was achieved for the majority of issues, however, a number of actions were assigned, including the completion of outstanding work, such as PIE of the DI bundles and completion of the thermalhydraulics licensing report.

CANFLEX DEMONSTRATION IRRADIATION

Demonstration Irradiation Plan

The final step in qualifying the fuel for full-core implementation was a demonstration irradiation in a power reactor. The principle objective was to show compatibility with all reactor systems rather than to establish CANFLEX performance data.

PLGS applied its standard process for special fuel irradiations for the CANFLEX demonstration irradiation [19]. This process involves preparation of an Information Report which is the basis on which both management and regulatory approvals are built. The demonstration irradiation plan called for Zircotec Precision Industries to manufacture 26 CANFLEX bundles to the Quality Assurance levels normally applied to 37-element fuel supplied to PLGS- 24 bundles for fuelling in PLGS and 2 for archiving. All configurations of CANFLEX bundles mixed with 37-element bundles in a single channel during transition and full-core refuelling were to be tested. The following objectives were set and applied to select candidate sites:

- Some fuel should be exposed to as high a power as possible within the allowable operating envelope.
- Some fuel should be exposed to as wide a power variation as possible within the allowable envelope.
- At least one channel should have normal dwell with a full CANFLEX fuel string.
- Some fuel should be exposed to normal fuelling-induced power ramps.
- At least one selected channel will be in the flow-assist-fuelling region.
- Some fuel should be exposed to high burnup within the allowable operating envelope.
- Some fuel should be exposed to long in-reactor residence time.
- Some fuel should be in an instrumented channel.
- Some fuel should be exposed to the largest amount of acoustic excitation that is possible.
- One high-powered channel and one low-powered channel were to be selected for CANFLEX fuelling.

On discharge and transportation to the bays, the CANFLEX bundles were to be visually examined. Two bundles would be selected and shipped to the Chalk River Laboratories (CRL) for PIE, consisting of:

- Visual examination, bundle and element profilometry;
- Disassembly and element profilometry;
- Gamma scanning;

- Fission-gas and void volume measurements;
- End-plate weld and button-weld strength tests;
- Metallography and ceramography;
- Chemical burnup analysis (high-performance liquid chromatography);
- Alpha, beta and gamma autoradiography; and
- Hydrogen analysis of sheath, button and end plate.

The demonstration irradiation will be fully documented, including station data and PIE reports.

CANFLEX Demonstration Irradiation Status

Once Atomic Energy Control Board (AECB) approval for the DI was secured in the late summer of 1998, PLGS fuel engineers selected channel S08 for the high-power channel and channel Q20 for the low-power channel (Figure 5-6). As part of the routine on-power fuelling in 1998 September, 8 CANFLEX bundles were fuelled into each of the two channels. In 1999 March, the low-power channel Q20 was refuelled and the first 4 DI CANFLEX bundles were discharged into the fuel bays. PLGS had planned a fuel-channel inspection in S08 during a summer maintenance shutdown, and it was decided to leave the CANFLEX fuel in the channel during the shutdown to demonstrate its compatibility with all maintenance handling systems and operations. Thus the high-power channel S08 was refuelled after reactor start-up in 1999 August, discharging 4 CANFLEX fuel bundles and establishing a full channel of 12 CANFLEX fuel bundles. In 2000 January, the final fuelling in Q20 was successfully completed, discharging 4 CANFLEX bundles and restoring the channel to full 37-element configuration. In 2000 February, S08 was refuelled, discharging 8 CANFLEX bundles. In 2000 August the last of the DI bundles was discharged thereby completing the irradiation of 24 CANFLEX bundles at PLGS.

The power history of bundles irradiated in the high power channel S08 (Figure 7) show a relatively high burnup of over 220 MWh/kgU, compared to a more standard burn-up of 175 MWh/kgU. From an operational perspective, the CANFLEX fuel behaved exactly as 37-element fuel would have: there were no significant differences in any monitored aspect of station behavior which could be attributed to CANFLEX fuel. During the above-mentioned summer shutdown, channel S08 underwent Spacer Location And Repositioning (SLAR) and Channel Inspection and Gauging Apparatus for Reactors (CIGAR) inspection. The fuel handling associated with these procedures was uneventful and the results of the CIGAR inspection did not indicate any unusual wear in the channel that was related to the use of CANFLEX fuel.

Irradiated Fuel In-bay Inspection

Of the 24 CANFLEX bundles irradiated, 20 bundles have been visually inspected in the fuel bays at Pt. Lepreau (the remaining 4 bundles discharged in August require 2 months of cooling before a full inspection can be made). The inspection team included fuelling experts from the station, a member of the CANFLEX design team and a member of the AECL fuel inspection group, who will conduct the PIE in the cells. The examination was done using an underwater periscope; photography was achieved using a

television camera attached to the periscope and digital imaging. The inspection team concluded that the bundles were in very good condition. All observations, photographs and irradiation data have been sent to the design team for review and disposition. The following summarizes observations and current status of disposition:

- **Element Gap:** Gaps were observed between adjacent elements. This led the inspection team to suspect spacer interlocking. Examination of the bundles during PIE found no evidence of interlocking as discussed in the next section. As had been observed in 37-element fuel bundles, the CANFLEX bundles were found to have element settling where limited distortions of some elements occurred due to a combination of applied loads, irradiation-induced creep and fabrication tolerances in the inter-element spacings. The design team awaits completion of the PIE to disposition this finding.
- **Marks on the sides of CHF Buttons:** Marks on the sides of a small fraction of the buttons raised concerns that material loss or corrosion was taking place during irradiation. Inspection of the two archive bundles held from the production run of the DI fuel, revealed CHF buttons that had features that appear similar to those seen in the bays at PLGS, i.e., an area with a raised periphery, at the side of some CHF buttons. Based on a comparison of the marks from the irradiated fuel and the unirradiated fuel, it was concluded that the features are an artifact of the fabrication and/or brazing process.
- **Marks on End Caps:** The inspection team saw scrape marks on some of the end-caps on some bundles. These appear to have been made when the side stops or separator feelers were inserted or withdrawn. Similar marks have been observed on 37-element bundles when side stops become worn. The design team concluded that the issue is not related to CANFLEX.
- **Bearing Pad Wear:** Some wear was observed on outboard bearing pads consistent with 37-element experience. All mid-plane pads of the CANFLEX bundles received very light wear. One mid-plane bearing pad showed higher wear on the CANFLEX bundle but a similar wear pattern was noted on one of the 37-element bundles inspected at the same time. The design team concluded that bearing pad wear was consistent with current irradiated fuel experience.
- **Marks on one location on the end-plates:** Marks were observed on the outer circumference of the end-plates. Similar marks were found on the archived bundles. It was traced to the manufacturing process which was used to fabricate the end-plates.

Full inspection reports have been prepared and the Design teams disposition of the findings will be documented for inclusion in the Demonstration Irradiation Report.

Post-Irradiation Examination

Two CANFLEX DI fuel bundles were shipped to CRL for post-irradiation examination (PIE) (Figure 8). Bundle FLX019Z, irradiated in Q20 position 8, was shipped to CRL on 1999 December 22. Bundle FLX019Z reached a calculated bundle burnup of 144 MWh/kgU and reached a peak outer-element linear power (OELP) of 38 kW/m. Bundle FLX007Z, irradiated in S08 position 8, was shipped to CRL on 2000 March 30 from PLGS. Bundle FLX007Z reached a calculated bundle burnup of 221 MWh/kgU and reached a peak OELP of 45 kW/m.

The visual and non-destructive examinations have been completed for both bundles and the destructive examinations are in progress. The following is a brief summary of the PIE results to date:

- No unusual features or anomalies were found visually.
- End-plate distortion was minor.
- Element settling was found; element settling has also been observed in the 37-element bundle in past PIE (Figure 9). No marks were found on spacers or elements to indicate spacer interlocking and no locked spacers were found. The spacers on one archived bundle were intentionally locked and the profilometry showed very different and distinct element bowing (Figure 10)
- Bearing and spacer pad wear was minor.
- Typical pellet-interface ridging was found for FLX007Z but it was not distinctive for the lower power bundle FLX019Z (Figure 11).
- Element gamma scans were normal and no Cs migration to the pellet-interface was evident (Figure 12).
- Fission gas volumes (1.4 to 1.7 ml at STP) and releases (less than 0.1%) were small.
- No unusual features or anomalies have been found in the metallographic and ceramographic examination of FLX019Z (e.g., typical fuel microstructure Figure 13).

The plant data, fuel-bay inspections, PIE and assessment work will be documented in a full report in 2001. This will conclude the demonstration irradiation program for the CANFLEX bundle.

INCREASING CANDU OPERATING MARGINS WITH CANFLEX FUEL

Implementing CANFLEX fuel in existing CANDU 6 reactors will increase the critical channel powers (CCP) by 5 to 8%. The actual CCP gain depends on individual channel conditions such as channel creep shape, power shape and local flow conditions. CCP is calculated using the computer code NUCIRC. The increase in CCP margin can be used by station operation to offset the margin reductions due to reactor ageing, such as the effect of heat transport system fouling and of diametral creep of the pressure tubes. Alternatively, the increase in margin could be utilized to increase the core power output, particularly in a new reactor.

The ~20% reduction in the linear element rating of the CANFLEX bundle (compared to the 37-element bundle) results in a substantial reduction of the fission product inventory in the fuel-to-sheath gap (i.e., gap-inventory). For example, at the same maximum bundle power, the iodine gap-inventory in the maximum-rated element in a CANFLEX bundle is estimated to be 3 times lower than the maximum-rated element in a 37-element bundle. This reduction provides several benefits. For accidents in which a number of fuel elements are predicted to fail and their fission product gap-inventory released, the radiological consequences will be reduced with the use of the CANFLEX bundles. This further enhances the safety performance of the reactor. The lower gap-inventory and lower power will also lead to lower activity burden in the heat transport circuit in the event of fuel failures during normal operation. While the performance of the CANDU fuel has been excellent, and the failure rate has been very low, on-power fuelling and failed fuel detection and location systems are designed to provide the means for an operator to

locate and remove defected fuel. The lower gap-inventory and lower power allows a longer action time for the operator. The lower gap-inventory will also reduce the radiological contamination in the heat transport circuit that arises from activity release from failed fuel. Consequently, the man-rem exposure during reactor maintenance is expected to be less, resulting in occupational health and cost benefits.

CANFLEX Implementation

AECL contracted Candesco to develop an implementation plan. The goal of the work was to identify the required scope of effort and define an optimized timetable for implementation of CANFLEX fuel in a CANDU 6 reactor. The approach taken was to define the program tasks required for implementation in detail and then, in consultation with the appropriate technical specialists within AECL's organization, to define the resource requirements for these tasks. Careful attention was paid to assumptions regarding the order of the tasks so that the resulting schedule was optimized in respect to elapsed time, while ensuring that it was still realistic.

The plan consists of the following main components:

- Regulatory interaction
- Finalizing design issues
- Safety and licensing
- Operational planning and implementation

Some basic assumption were made in defining this program plan. They are as follows:

- The utility implementing CANFLEX will perform all required modifications of Operating Manuals and/or operating procedures
- The utility implementing CANFLEX will develop the plan for managing the reduction in 37-element fuel inventories and provision of CANFLEX fuel in a timely manner
- The software tools needed to perform the licensing and design analyses with appropriate CANFLEX-specific models will be available.
- Code verification and validation will be addressed for tools used in safety analysis outside the context of this program

According to the plan, first loading of CANFLEX fuel in-reactor could take place within 20 months from the project start and trip setpoints could begin to be increased within 32 months from project start. The uncertainties on these time intervals are ± 3 and ± 6 months, respectively.

Economic Model of CANFLEX Implementation

To provide an economic basis for implementation, an economic model has been prepared to include all investments, effects on annual utility revenues and annual operating costs. Both the net present value (NPV) and internal rate of return are calculated for a range of implementation strategies and assumptions.

The economic model can assess the changes in revenue, operating costs, and investments that result from implementation of various plant-life-extension strategies available to offset the anticipated decline in reactor power due to ageing effects. The analysis includes all fiscal-year revenues, and all investment

costs are calculated to yield the annual projected cash flows. The differences between the cash flows are discounted to the decision date and are summed over the time period of application.

Implementation of CANFLEX fuel involves an initial investment in revising the safety analyses and operating procedures, leading to technical reviews and licensing submissions to obtain regulatory approval. The incremental costs of CANFLEX fuel are captured by the model. The resultant NPV quantifies the economic benefit of using a range of CANFLEX implementation strategies, to establish the sensitivity to various parameters. These various cases guide station management in selecting the most appropriate implementation strategy. Each station has unique and proprietary cost factors. The model accepts the reactor-specific costs as input assumptions and calculates the CANFLEX benefit. Current analysis using the latest thermalhydraulic performance data shows that the improvements in station revenue from the CANFLEX Mk4 bundle far outweigh the additional costs associated with its introduction and production. Each utility will implement CANFLEX according to its unique situation. AECL is working with utilities in Canada to determine implementation strategies for CANFLEX.

Safety Analysis And Licensing

At various stages of the CANFLEX fuel design, safety assessments were performed for key design basis accidents in a CANDU 6 reactor with 37-element fuel bundles replaced by CANFLEX bundles. These assessments were performed in order to provide interim feedback to design. The safety assessments identified the implications to the safety report when the CANFLEX fuel design is used in place of the existing 37-element bundles. This design-feedback process provides good assurance that there will not be unexpected impact of the design to safety.

Current operating licenses of Canadian reactors stipulate that only fuel of an approved design may be irradiated in the reactor. Use of any new fuel type in the reactor therefore requires regulatory approval. This approval depends on the existing safety report and supporting documentation to demonstrate that the change in fuel type does not compromise the safe operation of the reactor.

For the demonstration irradiation, a safety assessment was submitted to the regulators. The assessment showed that the presence of up to 24 CANFLEX fuel bundles in the core would not have a negative impact on the safe operation of the reactor. For full-core CANFLEX implementation, a separate licensing submission regarding full-core operation will be required. This licensing submission will also consider the transition between an all-37-element core and an all-CANFLEX core, since this process takes place over an extended period (about two years). The submission will cover all design basis accidents that will be affected by the change in the fuel types. As noted before, because the CANFLEX bundles have higher CCP performance and lower fission product gap-inventory compared to the 37-element bundles, larger safety margins are expected in most of the design basis accidents. It is also expected that the safety assessment in support of full-core CANFLEX implementation can also build extensively on the results of the assessment that was performed for the DI. AECL is working with CANDU utilities in Canada to establish the licensing program requirements for full-core implementation and the various roles and responsibilities.

CONCLUSIONS

CANFLEX fuel has been under development for over 10 years. CANFLEX fuel has been verified through extensive testing by AECL and KAERI and has been critically reviewed under a Formal Design Review. Results from the 20 CANFLEX bundles irradiated to date in PLGS verify the compatibility of this fuel type with existing reactor systems. The economic analysis based on the CHF-enhancement data indicates a significant payback to utilities operating CANDU reactors. The utilities now have an alternative fuel that can be deployed with confidence in CANDU design to provide a greater operating margin.

REFERENCES

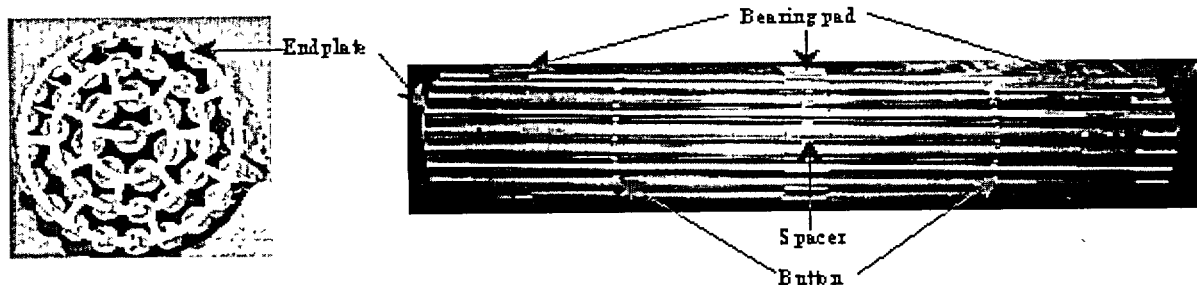
1. I.J. Hastings, A.D. Lane and P.G. Boczar, "CANFLEX - An Advanced Fuel Bundle for CANDU", Int. Conf. Availability Improvements in Nuclear Power Plants, Madrid, Spain, 1989 April 10-14, also AECL Report, AECL-9929, 1989.
2. A.D. Lane, D.F. Sears, I.E. Oldaker, B.M. Townes, A. Celli, H.C. Suk, C.H. Chung and K-S. Sim, "Recent Achievements in the Joint AECL/KAERI Program to Develop the CANFLEX Fuel Bundle", Proc. 10th KAIF/KNS Annual Conference, Seoul, Korea, 1995 April 6-7.
3. A.D. Lane, G.R. Dimmick, J.H.K. Lau, H.C. Suk, C.H. Chung and C.B. Choi, "CANFLEX: A New CANDU Fuel Bundle with Expanded Operating Capabilities", Proc. 11th KAIF/KNS Annual Conference, Seoul, Korea, 1996 April 11-12.
4. H.C. Suk, K.S. Sim, B.G. Kim, C.B. Choi, C.H. Chung, A.D. Lane, D.F. Sears, J.H.K. Lau, I.E. Oldaker and P.G. Boczar, "CANFLEX as a CANDU Advanced Fuel Bundle", presented at the Fifth International Topical Meeting on Nuclear Thermalhydraulics, Operations and Safety, Beijing, China, 1997 April.
5. K-S. Sim and H.C. Suk, "Some Considerations in the CANFLEX-NU Fuel Design", presented at the Fifth International Conference on CANDU Fuel, Canadian Nuclear Society, Toronto, Canada, 1997 September 21-25.
6. I.J. Hastings, P.G. Boczar and A.D. Lane, "CANFLEX - An Advanced Bundle Design for Introducing Slightly-Enriched Uranium into CANDU", presented at Int. Symp. on Uranium and Electricity (The Complete Nuclear Fuel Cycle), Saskatoon, Saskatchewan, 1988 September 18-21, Canadian Nuclear Society, also AECL Report, AECL-9766 (1988).
7. P.G. Boczar et al., "Recovered Uranium in CANDU: A Strategic Opportunity", presented at the INC Conf., Toronto, Canada, 1993 October 3-6.
8. P. Alavi, I.E. Oldaker, C.H. Chung and H.C. Suk, "Design Verification of the CANFLEX Fuel Bundle - Quality Assurance Requirements for Mechanical Flow Testing", presented at the Fifth International Conference on CANDU Fuel, Canadian Nuclear Society, Toronto, Canada, 1997 September 21-25.
9. C.H. Chung, S.K. Chang, H.C. Suk, I.E. Oldaker and P. Alavi, "Performance of the CANFLEX Fuel Bundle under Mechanical Flow Testing", presented at the Fifth International Conference on CANDU Fuel, Canadian Nuclear Society, Toronto, Canada, 1997 September 21-25.
10. Design Quality Assurance for Nuclear Power Plants, CAN/CSA-N286.2-96.
11. W.W.R. Inch, P. Thompson and H.C. Suk, "CANFLEX From Development Concept To A Proven Fuel", Proc. 13th KAIF/KNS Annual Conference, Seoul, Korea, 1998 April 14-16.

12. W.W.R. Inch, P. Thompson, P. Reid and H.C. Suk, "Demonstration Irradiation of CANFLEX in CANDU 6 Power Reactor", Proc. 14th KAIF/KNS Annual Conference, Seoul, Korea, 1999 April 8-9.
13. W.W.R. Inch, P.D. Thompson, M.A. Cormier, H.C. Suk, "Demonstration Irradiation of CANFLEX in a CANDU 6 Power Reactor", Proc. 15th KAIF/KNS Annual Conference, Seoul, Korea, 2000 April 18-20.
14. G.R. Dimmick, D.E. Bullock, A. Hameed and J.H. Park, "Thermalhydraulic Performance of CANFLEX Fuel", Proc. 5th International Conference on CANDU Fuel, Canadian Nuclear Society, Toronto, Canada, 1997 September 21-25.
15. G.R. Dimmick, W.W.R. Inch, J.S. Jun, H.C. Suk, G.I. Haddaller, R. Fortmann and R. Hayes, "Full-Scale Water CHF Testing of the CANFLEX Bundle", Proc. 6th CANDU Fuel Conference, Niagara Falls, Canada, 1999 September 26-30.
16. L.K.H. Leung, D.C. Groeneveld, G.R. Dimmick, D.E. Bullock and W.W.R. Inch, "Critical Heat Flux and Pressure Drop for a CANFLEX Bundle String Inside an Axially Non-Uniform Flow Channel", Proc. 6th International CANDU Fuel Conference, Niagara Falls, 1999 September 26-30.
17. G.D. Harvel, M. Soulard, R.F. Dam, P. White, R. Moffet, G. Hotte, "NUCIRC Simulations of a CANDU-Type Header Manifold Model", 5th CNS International Conference on Simulation Methods in Nuclear Engineering, Montreal Quebec, 1996.
18. J.V. Donnelly, "WIMS-CRNL, A User's Manual for the Chalk River Version of WIMS", AECL Report AECL-8955, 1986 January.
19. P.J. Reid, R.G. Steed, R.A. Gibb, R.W. Sancton, "A Standard Approach to Special Fuel Irradiations at Point Lepreau Generating Station", Proc. 19th Annual Conference of the Canadian Nuclear Society, Toronto, Ontario, Canada, 1998 October 18-21.



Figure 1: CANFLEX Design

CANFLEX (CANDU Flexible) Bundle



- CHF enhancement increases critical channel power by 5%-8%. Further improvements are possible
- 20% lower element ratings leads to lower Fission-product production
- Fully compatible with existing CANDU 6 reactors
- Fully qualified for use in CANDU 6 reactors

Figure 2: CANFLEX Pressure Drop Characteristics

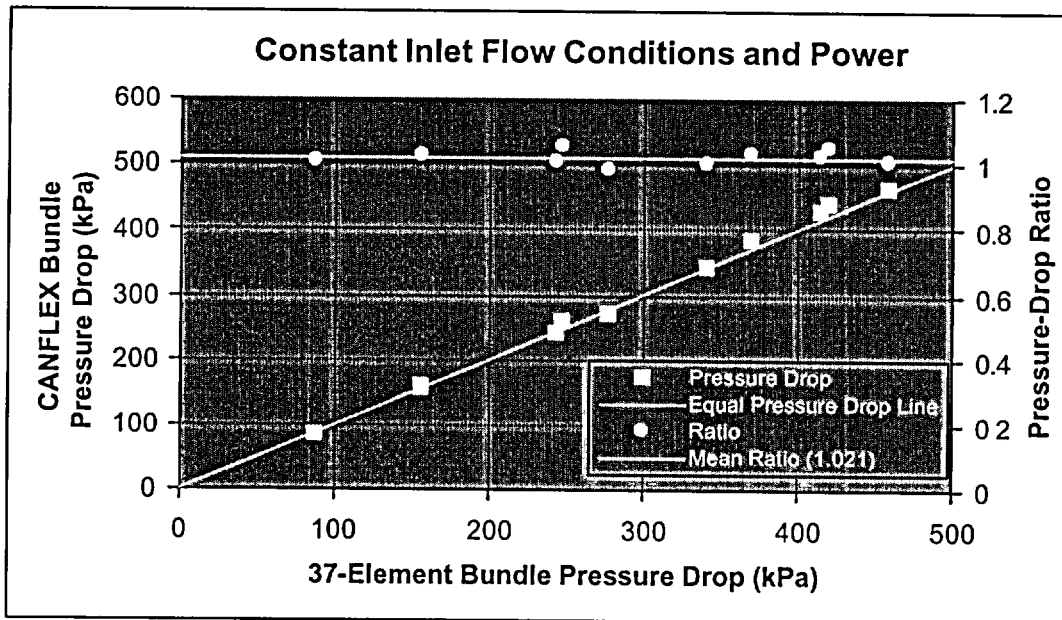


Figure 3: Dryout Power Enhancement of CANFLEX Relative to 37-Element

Pressure: 11 MPa, Mass-flow rate: 17-23 kg/s

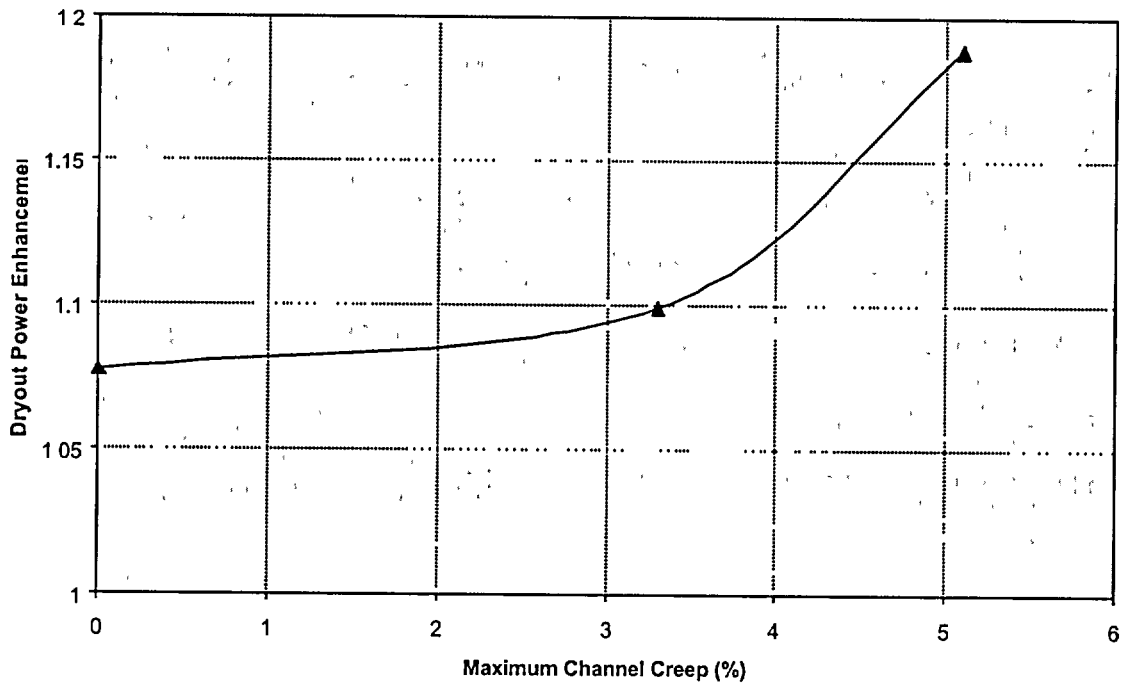


Figure 4: Fuelling History for High-power Channel

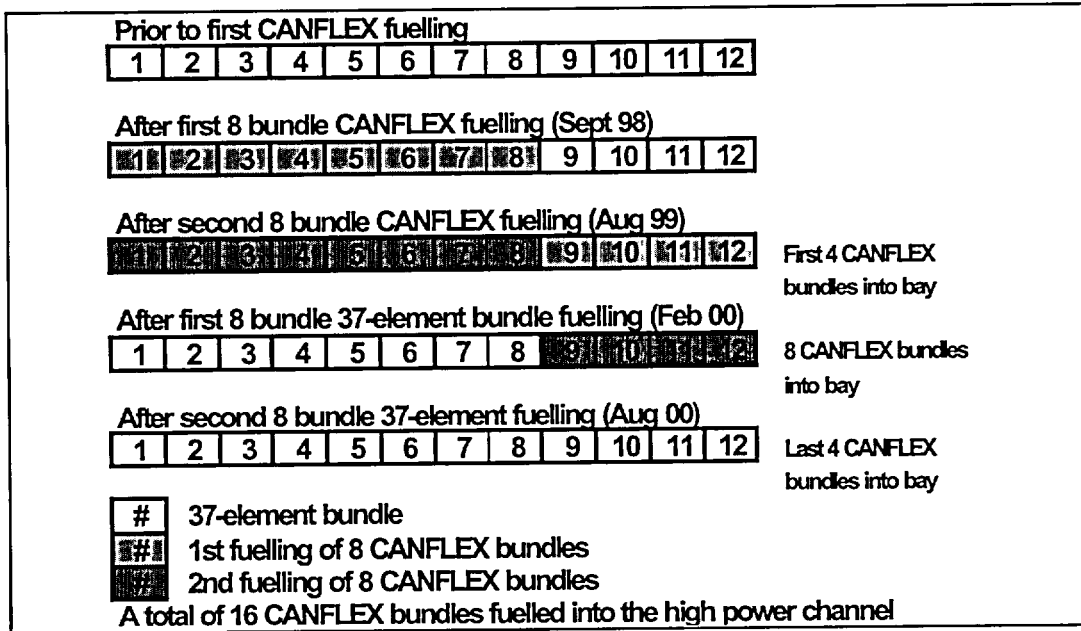


Figure 5: Power History for the DI CANFLEX Bundles in High-power Channel S08

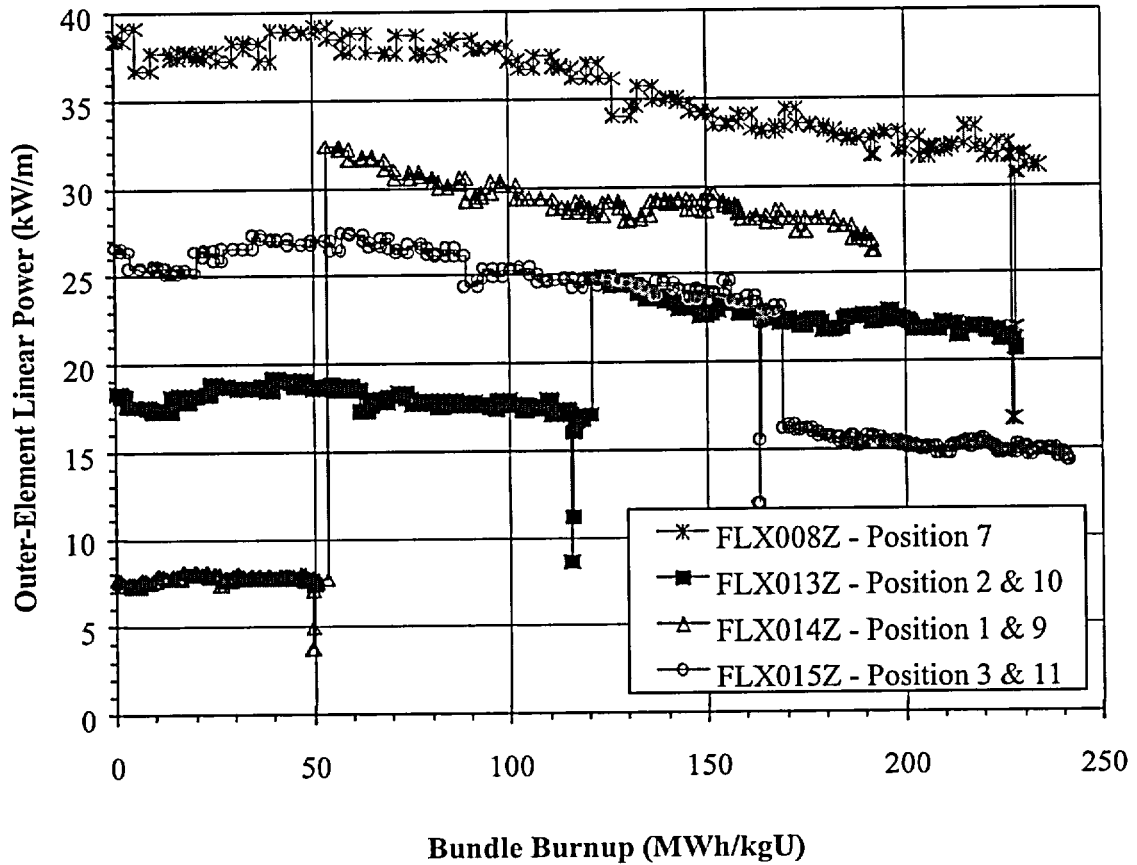


Figure 6: CANFLEX DI Element Diameter Profile

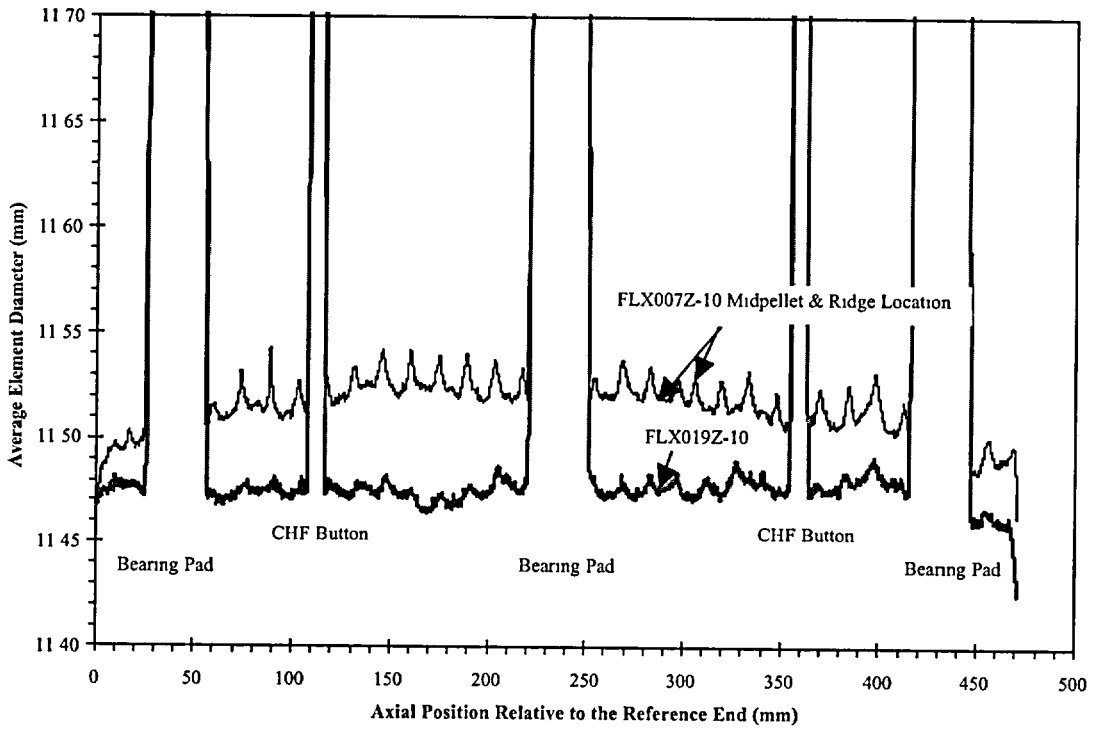


Figure 7: Gamma Scan Profile

Lepreau Canflex Bundle FLX007Z. Element 10. 2000 April 27.

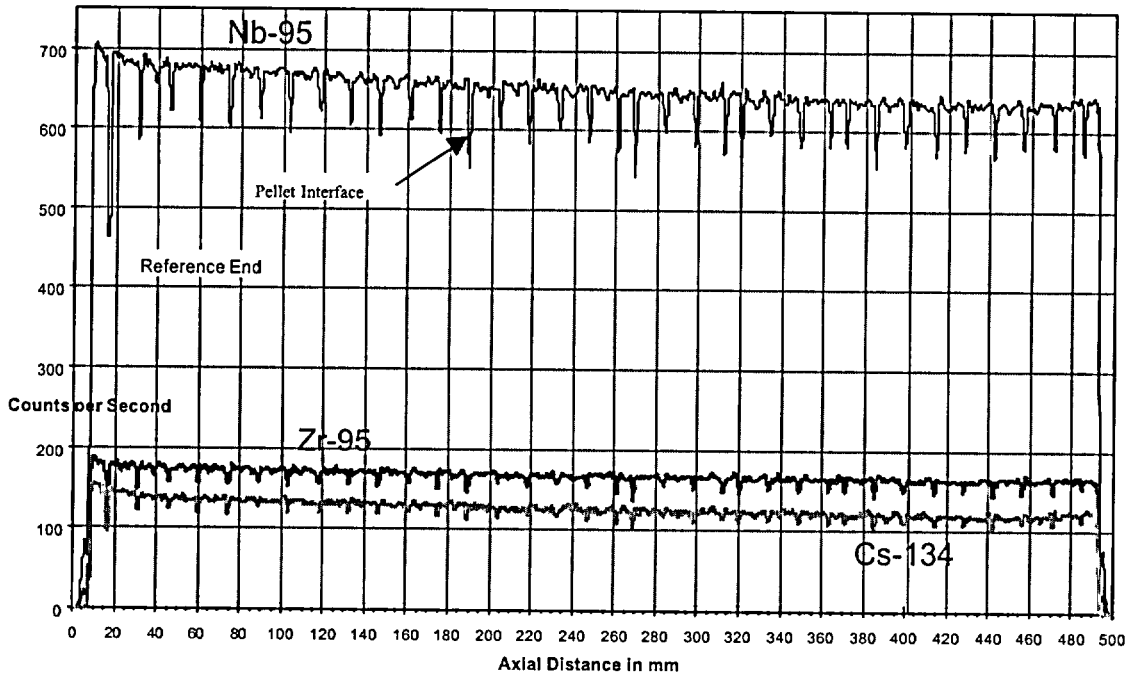
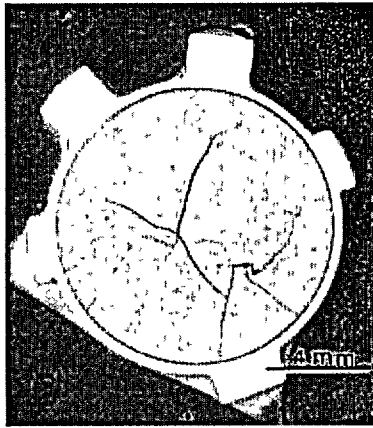
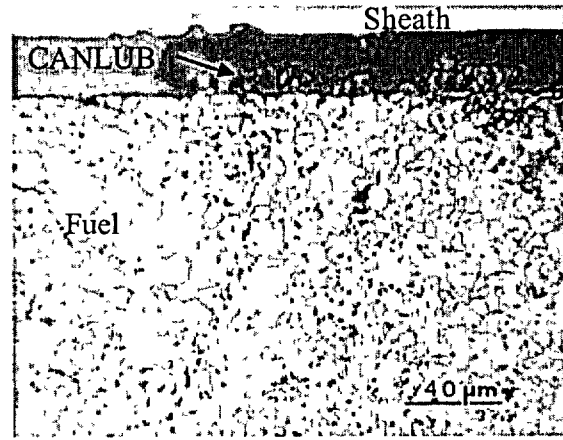


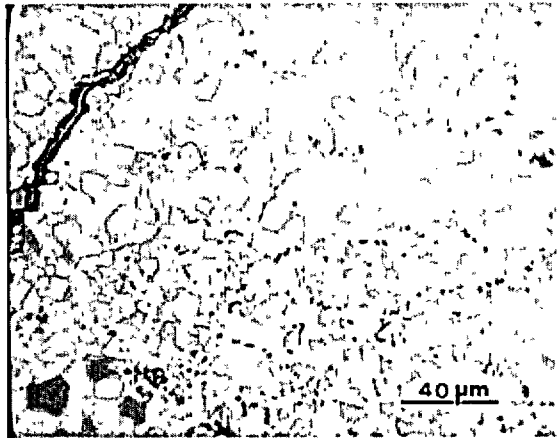
Figure 8: FIX019Z Element Fuel Microstructure Profile



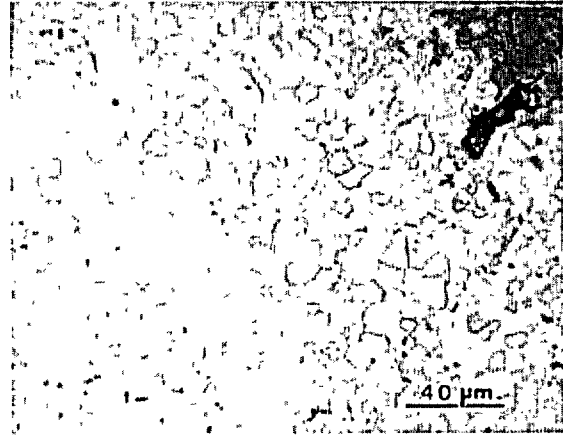
Macro Etched



Periphery



Mid-Radius



Centre

DRYOUT POWER OF A CANFLEX BUNDLE STRING WITH RAISED BEARING PADS

L.K.H. LEUNG*, J.S. JUN[†], G.R. DIMMICK*, D.E. BULLOCK*, W.W.R. INCH*, H.C. SUK[†]

*Fuel Channel Thermalhydraulics Branch
Chalk River Laboratories
Atomic Energy of Canada Limited
Chalk River, Ontario
CANADA K0J 1J0

[†]Korea Atomic Energy Research Institute
150 Dukjin-dong,
Yusong-ku, Taejon,
KOREA 305-353

Abstract

Dryout power data have been obtained with CANFLEX[®] bundle strings equipped with raised bearing pads (1.7 mm and 1.8 mm height as compared to 1.4 mm in the current Mk-IV design) at Stern Laboratories. The experiment covered a wide range of steam-water flow conditions in three flow tubes simulating uncrept, and 3.3% and 5.1% crept profiles. The dryout power follows consistent parametric trends: it increases with increasing mass-flow rate, and decreases with increasing pressure, inlet-fluid temperature and channel creep. Local and boiling-length-average (BLA) critical-heat-flux (CHF) values were evaluated from the dryout-power measurements. The dryout power and BLA CHF values of the high bearing-pad bundles are higher than those of the low bearing-pad bundles at the same channel inlet flow conditions. On average, the dryout powers for bundles with 1.7 mm and 1.8 mm bearing pads are about 8% and 10%, respectively, higher than those for the bundle with 1.4 mm bearing pads. Compared to the 37-element bundle, an enhancement in dryout power is shown with CANFLEX bundles for all bearing-pad heights, at flow conditions of interest for reactor licensing. The average dryout power enhancement varies from 4% for the CANFLEX bundle with 1.4 mm bearing pads in the uncrept channel to 27% for the CANFLEX bundle with 1.8 mm bearing pads in the 5.1% crept channel.

1. INTRODUCTION

Since 1991, Atomic Energy of Canada Limited (AECL) and the Korea Atomic Energy Research Institute (KAERI) have jointly developed the CANFLEX[®] ¹(CANDU[®] Flexible) bundle as an advanced nuclear-fuel carrier for CANDU pressurized-heavy-water reactors. Using AECL patented, non-load-bearing, heat-transfer enhancing buttons attached to the surface of elements, the CANFLEX fuel bundle is designed to improve thermalhydraulic performance over that of the current 37-element

¹ CANDU[®] and CANFLEX[®] are registered trademarks of Atomic Energy of Canada Limited (AECL)

bundle. The development of the CANFLEX (Mk-IV) fuel bundle is complete, and a demonstration irradiation of 24 bundles with natural-uranium fuel was performed between 1998 September and 2000 August at the Point Lepreau Generating Station (PLGS) in Canada [1]. A similar demonstration irradiation program is also being prepared for the Wolsong-1 reactor in Korea.

The CANFLEX fuel bundle contains about the same amount of uranium in weight as the 37-element bundle but uses 43 fuel pins. It is characterized by a moderately flat radial-power profile, with the outer and intermediate rings consisting of 21 and 14 elements of 11.5 mm O.D., and the inner ring and center rod consisting of 7 and 1 element(s) of 13.5 mm O.D. A full-scale out-reactor test of the CANFLEX design was performed under contract with Stern Laboratories (SL) to provide thermohydraulic data for the CANFLEX Mk-IV design [2]. The dryout power measurements were shown to be higher than those of the 37-element bundle in the 5.1% crept channel [3]. Dryout in the CANFLEX bundle was initiated at the bottom elements of the bundle. This is caused in part by the small subchannel sizes between the pressure tube and elements in the outer ring due to bundle eccentricity. Kobori [4] performed an experiment with a vertical 28-element bundle string and observed a dryout power improvement through the reduction of bundle eccentricity (i.e., to arrange the bundle in the concentric position within the flow tube). Similar to the CANFLEX bundle, dryout was initiated on elements in the outer ring at the small-subchannel region neighbouring to the flow tube. Therefore, a dryout power improvement would be anticipated through a reduction in the eccentricity of the CANFLEX bundle string inside the pressure tube.

One of the options to reduce the bundle eccentricity is to raise the bearing-pad height (from the Mk-IV design of 1.4 mm). This would result in an increase in local subchannel area and flow rate at the narrow-gap region and improve the heat transfer and dryout power. Based on the current CANDU 6 fuel bundle and fuel channel designs, the bearing-pad height is limited to a maximum of about 2.1 mm. Including the manufacturing tolerance, however, the maximum acceptable bearing-pad height is anticipated to be about 1.85 mm.

The full-scale bundle test has been extended to obtain dryout power measurements for the bundle string with two additional bearing-pad heights (1.7 and 1.8 mm). These measurements provide a means to quantify the dryout power improvement with the reduction in bundle eccentricity. The objectives of this paper are to

- Present the dryout power measurements obtained with the CANFLEX bundle string of raised bearing pads,
- Compare the dryout power values for CANFLEX bundle of various bearing-pad heights, and
- Quantify the dryout power improvement of the CANFLEX raised bearing-pad bundles as compared to the 37-element bundle in various crept channels.

2. FULL-SCALE CANFLEX BUNDLE TESTS

Full-scale CANFLEX bundle tests were performed to obtain licensing data in the high-pressure steam-water loop at SL [2]. The 6-m test string was designed and fabricated to simulate as closely as possible a string of 12 aligned CANFLEX bundles in a fuel channel, and includes endplates, bearing

pads, buttons and inter-element spacers. Each of the 43 heater rods consisted of Inconel-718 tubes, 481.0 mm heated length, joined by nickel-201 spool pieces to form a 12-segment, 6-m bundle string. The 12-segment heated length of the bundle string was joined to the power bus-bars by nickel-plated copper extensions with the same overall diameter as the Inconel tubes.

Appendages (i.e., spacers, bearing pads and more than 2,000 buttons) were spot-welded at various locations, as specified in the bundle design. The nominal bearing-pad height was 1.4 mm, which corresponds to the design value of the CANFLEX Mk-IV bundle. Thin metal shims (0.3 and 0.4 mm thick) were added to the bearing pads of six elements located at the bottom portion of the bundle to raise the bundle from the flow tube (Figure 1). This resulted in nominal bearing-pad heights of 1.7 and 1.8 mm, respectively. The modification was performed only on the bottom six elements to minimize the preparation procedure. This modification provides the same effect as reducing the bundle eccentricity and increasing the subchannel flow area at the dryout region.

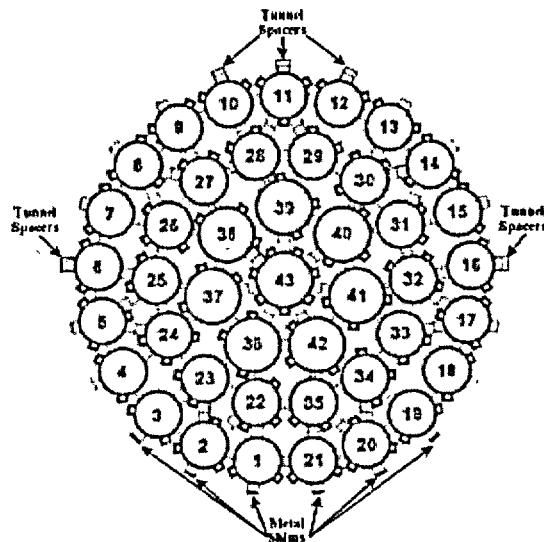


Figure 1: Modified CANFLEX bundle with raised bearing pads.

Additional spacers were introduced to maintain the bundle string at the eccentric position. These spacers, referred to as “tunnel spacers”, were formed into a “U” shape from small pieces of Inconel-718 sheet and were spot welded over the downstream bearing pads of Elements 6, 10, 11, 12 and 16 (see Figure 1). Figure 2 shows the shape and location of a tunnel spacer on the bearing pad. As these spacers are hollow and remote from the dryout locations, they will have an insignificant effect on the dryout power.

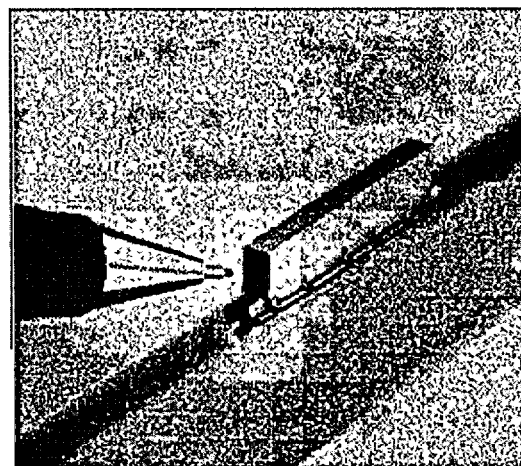


Figure 2: Shape and position of a tunnel spacer.

Power was applied to the bundle string through Joule heating. The sheath thicknesses of the elements were varied along the axial length and from ring to ring. This provided accurate simulations of non-uniform radial and axial power distributions. The radial power distribution simulated a bundle with natural-uranium fuel (local-to-average element power ratios are 1.034, 1.081, 0.873 and 1.056 for the center rod, inner ring, intermediate ring and outer ring). The axial power distribution corresponded to a downstream skewed-cosine profile [2]. Figure 3 presents the normalized axial-flux distribution (i.e., local to average heat-flux ratio) along the heated length. A ceramic flow tube electrically insulated the bundle string from the metal pressure boundary. Three different flow tubes were used in the test [2]; one had a uniform inside diameter of 103.86 mm and the other two had axially varying inside diameters, with a maximum diameter of 107.29 mm and

109.16 mm (3.3% and 5.1% larger than the uniform tube). The uniform flow tube simulated an uncrept pressure tube, while others simulated pressure tubes with various diametral creeps. Figure 4 shows the axial variations in inside diameter of the flow tubes for the crept channels.

Figure 5 shows the set-up of the test station. Fourteen taps were installed along the test section, and were connected to differential-pressure (DP) cells to provide pressure-drop measurements over the length of the bundle string. The taps at the inlet and outlet ends were also connected separately to pressure transmitters to measure the absolute pressures at those locations. K-type thermocouples and resistor temperature devices (RTDs) were used to monitor the fluid temperature at the inlet and outlet ends. The inside surface temperature of the heated sheath was measured with thermocouple-slider assemblies located inside the element. The sliders in all elements were moved axially and rotated at various locations to map out the surface-temperature distributions. Generally, dryout was established when a sharp surface temperature rise of about 5°C from the nucleate-boiling temperature was observed. Details of the experimental set-up and test procedure are described in [2].

A wide range of steam-water flow conditions was covered in the CHF experiment; an outlet-pressure range from 6 to 11 MPa, a mass-flow-rate range from 7 to 29 kg.s⁻¹, and an inlet-fluid-temperature range from 200 to 290°C. The majority of the data are directly relevant to the analyses of the regional overpower trip (ROPT) set point in the reactor. Single-phase and two-phase pressure-drop tests were performed at lower pressures and fluid temperatures, as well as at higher mass-flow rates. In addition, specific ONB (Onset of Nucleate Boiling) and OSV (Onset of Significant Void) runs were performed. The flow conditions corresponded closely to those previously obtained with the CANFLEX Mk-IV and 37-element bundles at the same test facility.

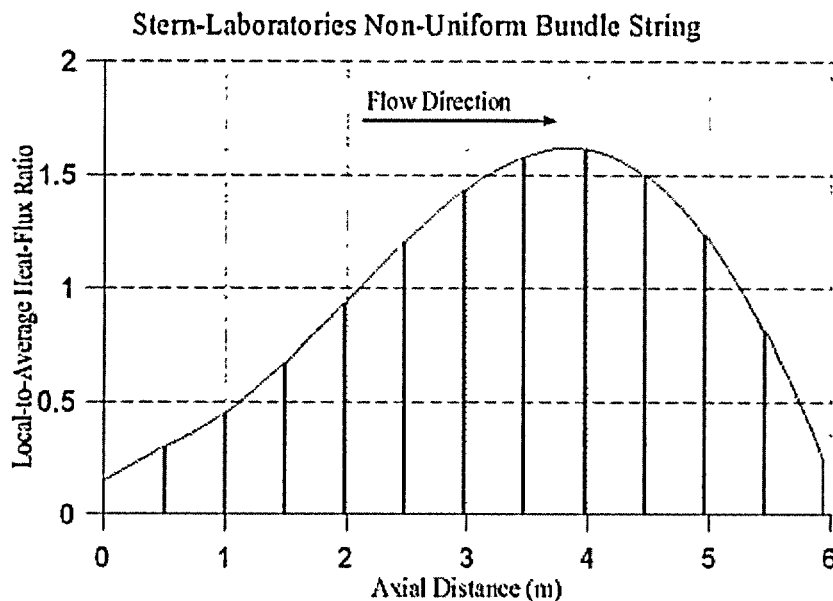


Figure 3: Axial heat-flux distribution of the full-scale bundle-string simulator.

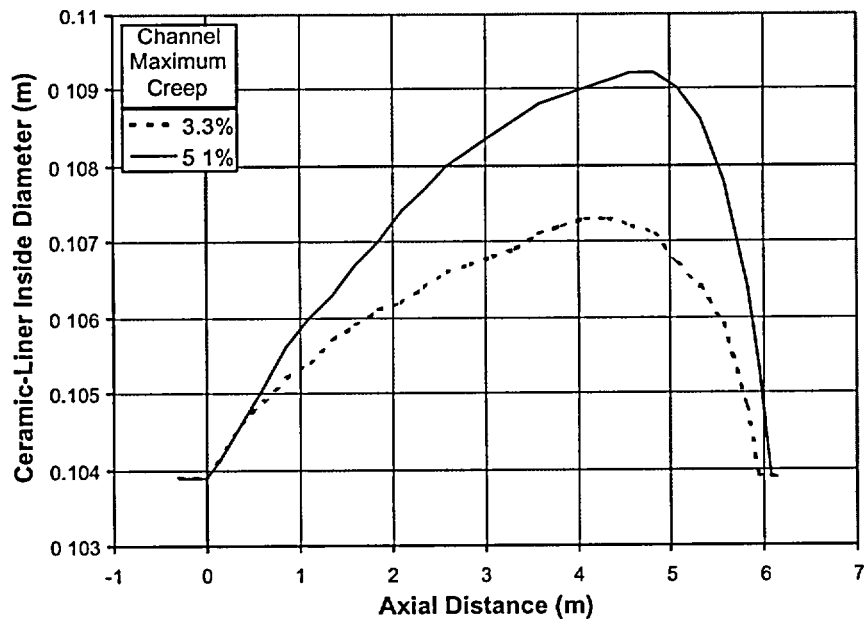


Figure 4: Axial variations of inside diameter in the crept channels.

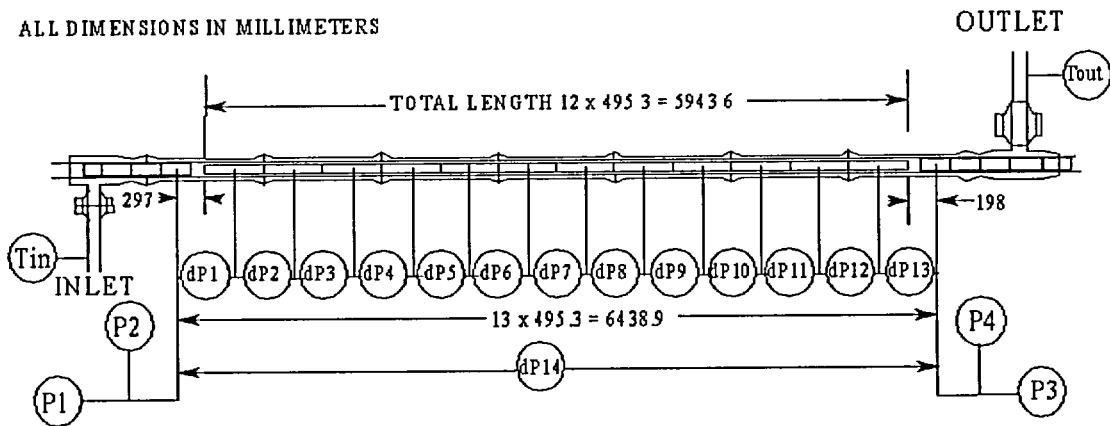


Figure 5: A schematic diagram of the test station in the high-pressure steam-water loop at Stern Laboratories.

3. DRYOUT POWER FOR CANFLEX BUNDLE STRINGS

Figure 6 illustrates the dryout power² measurements for the bundle string with 1.7 mm bearing pads in the uncrept channel. The dryout power increases with mass-flow rate and decreases with inlet-fluid temperature. Overall, the dryout power follows a relatively linear variation with the flow parameters over the test conditions. Similar variations in dryout power were observed for other bearing-pad heights with inlet-flow conditions. Several repeat points were obtained at various stages of the experiment (as indicated with multiple points at the same flow conditions). As shown in Figure 6, the repeatability of the measurements (multiple points at the same conditions) was excellent in the experiment. At conditions of interest for the uncrept channel (i.e., a mass-flow rate of 17 kg.s⁻¹ and an inlet-fluid temperature of 268°C), the dryout power for the CANFLEX bundle with 1.7 mm bearing pads is about 9.6 MW.

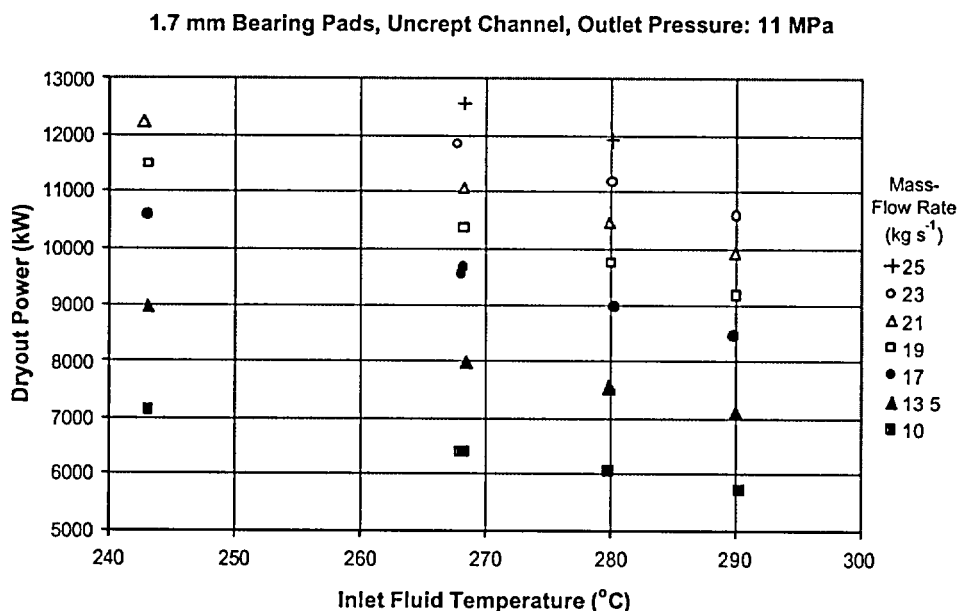


Figure 6: Dryout-power data for a CANFLEX bundle string with 1.7 mm bearing pads in the uncrept channel.

Figure 7 shows the dryout power variation for the 1.7 mm height bearing-pad bundle in a 5.1% crept channel. Overall, the measurements follow the same trend as exhibited in Figure 6 (i.e., dryout

² The dryout power represents the total power applied to the bundle string at which the onset of intermittent dryout (OID) occurs. This corresponds to only a single point at the sheath of an element, where the liquid film has broken down, while a continuous liquid contact is maintained at the remaining surfaces of the bundle string. Because of the high heat-transfer rate due to convection (at high flow velocity) and conduction (from the dry spot to the surrounding wet area), a gradual temperature rise is associated with this type of dryout.

power increases with mass-flow rate, and decreases with inlet-fluid temperature). However, the dryout powers are consistently lower than those for the uncrept channel at the same inlet-flow conditions. The dryout power for the 5.1% crept channel is 7 MW at the mass-flow rate of $17 \text{ kg}\cdot\text{s}^{-1}$ and inlet-fluid temperature of 268°C , as compared to 9.6 MW for the uncrept channel. Based on a constant fuel-string pressure drop, however, the mass-flow rate at dryout for the crept channel is higher than that for the uncrept channel and the dryout power reduction becomes less.

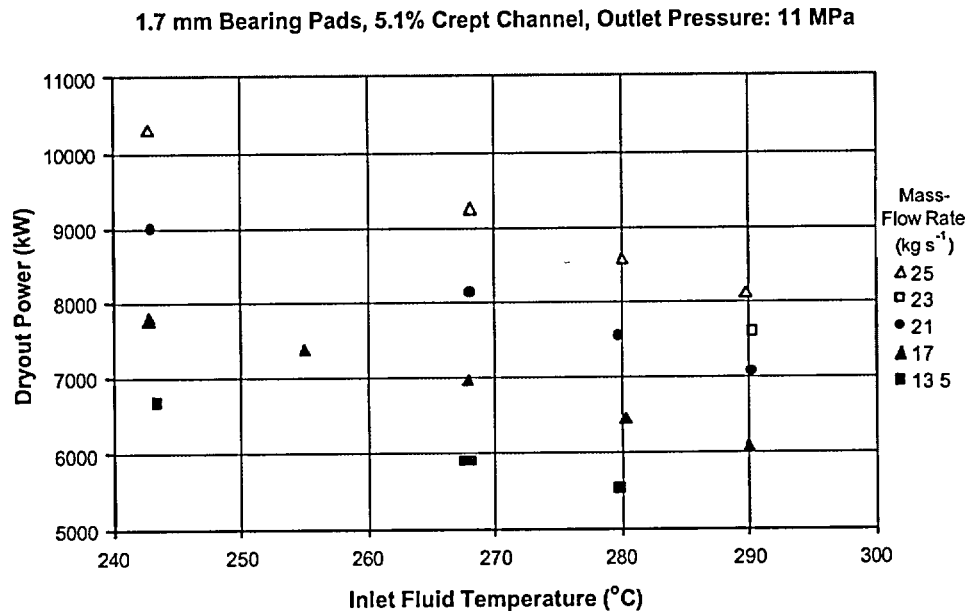


Figure 7: Dryout-power data for a CANFLEX bundle string with 1.7 mm bearing pads in the 5.1% crept channel.

Figure 8 shows the dryout power variation with creep at a pressure of 11 MPa and mass-flow rate of $21 \text{ kg}\cdot\text{s}^{-1}$. For given inlet conditions, the dryout power decreases with increasing creep. The dryout power reduction is slightly steeper at low creep values compared to higher creeps. This is to be expected as low values of creep have a higher relative effect on the bypass flow over the bundle (and hence the flow in the critical subchannel) compared to higher creeps. Similar variation is shown for various inlet temperatures and other pressures and mass-flow rates.

The effect of bearing-pad height on dryout power is shown in Figure 9 for the uncrept channel and Figure 10 for the 5.1% crept channel. Overall, the dryout power increases with bearing-pad height. The increasing trend is relatively linear within the current range of bearing-pad height. No significant differences on the dryout power variation with bearing pad height have been noticed between uncrept and 5.1% crept channels. On average, the dryout power increase as a result of increasing the bearing-pad height from 1.4 mm to 1.7 mm is about 8%, and from 1.4 mm to 1.8 mm is about 10%, at the inlet-fluid temperature of 268°C .

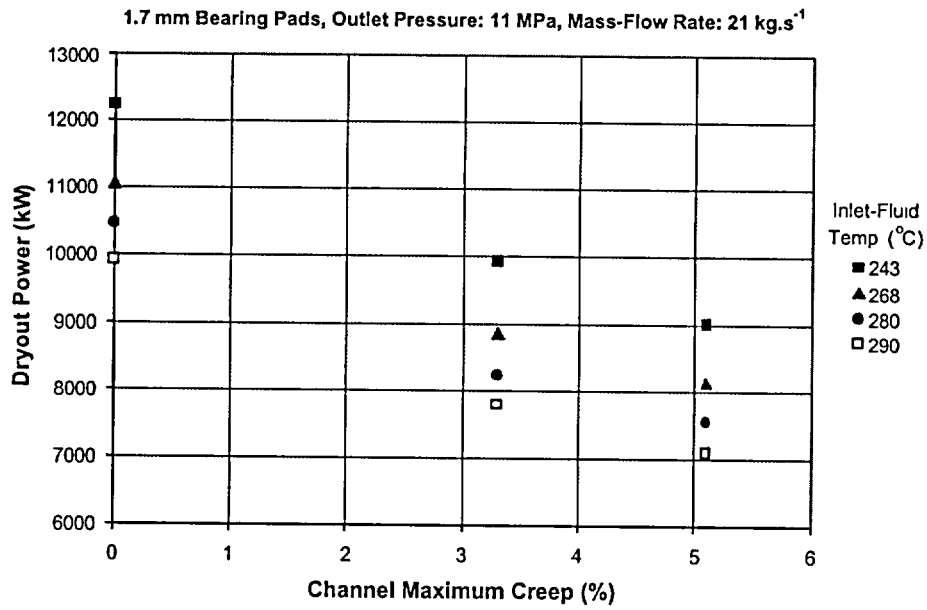


Figure 8: Effect of channel creep on dryout power.

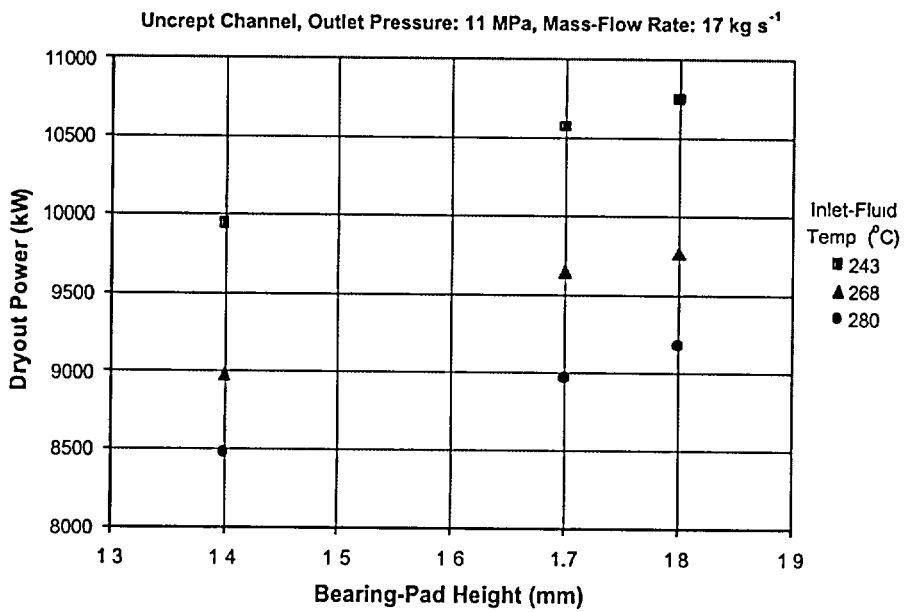


Figure 9: Effect of bearing-pad height on dryout power in the uncrept channel.

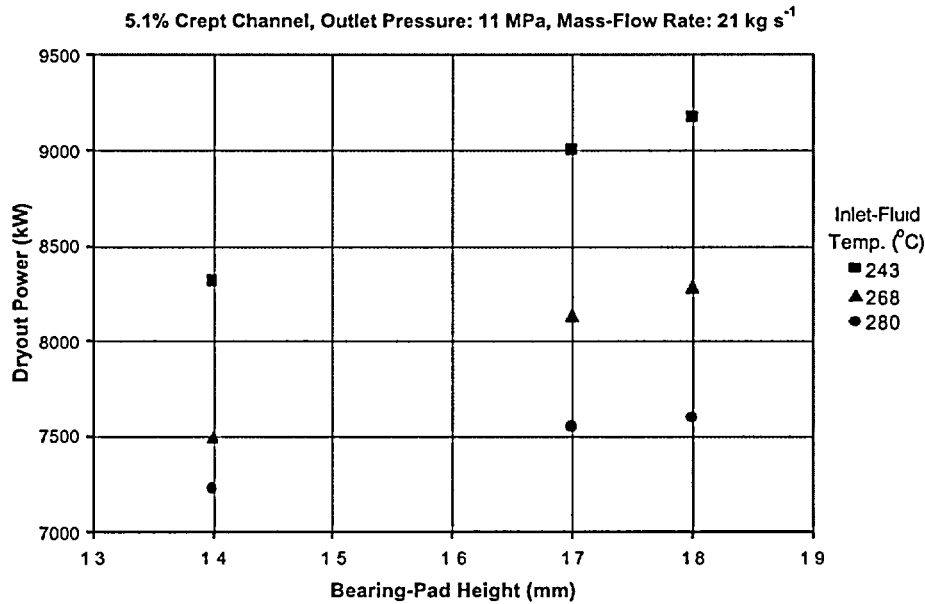


Figure 10: Effect of bearing-pad height on dryout power in the 5.1% crept channel.

4. CHF FOR CANFLEX BUNDLE STRINGS

Local and boiling-length-average (BLA) CHF values³ were evaluated with the dryout-power measurements and axial heat-flux distribution. Leung et al. [3] defined the BLA CHF as

$$CHF_{BLA} = \frac{1}{z_{DO} - z_{OSV}} \int_{z_{OSV}}^{z_{DO}} q_{local} dz$$

where z_{DO} and z_{OSV} are the locations at dryout and onset of significant void (OSV), respectively, q_{local} is the local heat flux in W/m², and z is the axial distance in metres. The OSV point was located from the pressure distribution established with the pressure-drop measurements along the channel. Figure 11 illustrates the pressure distribution and the OSV point in an uncrept channel. The pressure distribution follows a linear trend, which corresponds to the single-phase region, at the upstream section of the channel. It exhibits a non-linear trend at the downstream section, where two-phase (boiling) flow is encountered. The transition point between single-phase and two-phase flow is referred as the OSV point.

Figure 12 shows the CHF values based on the local and BLA heat-flux approaches for the same flow conditions in the 5.1% crept channel. The scatter among the CHF values is larger for the local than the BLA approach. Leung et al. [3] observed similar scatter among the CHF values for the CANFLEX bundle with the 1.4 mm height bearing pads. The BLA CHF values are more consistent than the local

³ Heat fluxes and flow conditions represent cross-sectional average values over the bundle.

CHF values with increasing dryout quality.

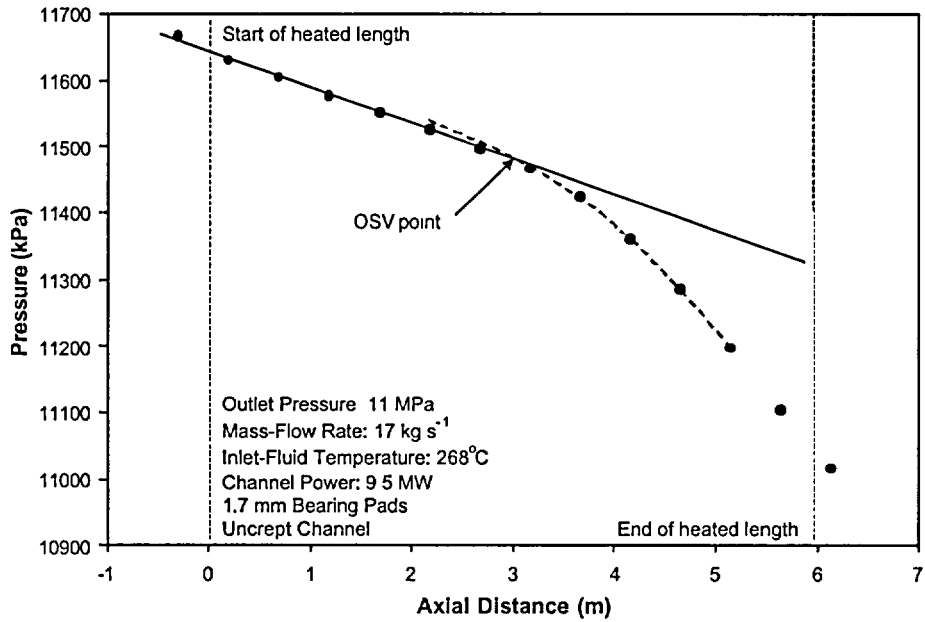


Figure 11: Pressure distribution along the channel.

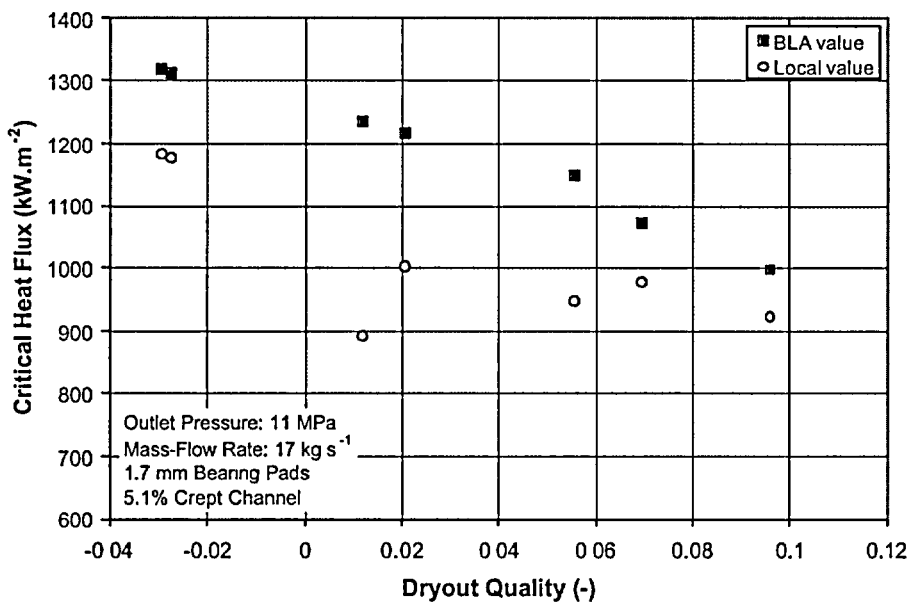


Figure 12: CHF values based on the local and BLA approaches.

Figure 13 compares the BLA CHF values for the CANFLEX bundle with 1.7-mm height bearing pads at various dryout qualities and mass-flow rates. In general, the BLA CHF increases with decreasing dryout quality and increasing mass-flow rate. The same trend was observed in data obtained with tubes, 37-element bundles, and CANFLEX bundles with other bearing pads. A number of data points were obtained at cross-sectional-average⁴ subcooled conditions (negative thermodynamic quality). Based on the BLA approach with boiling initiated at the OSV point, these data follow the same trend as exhibited among the saturated dryout data. Similar variations have been observed for other pressures in various crept channels.

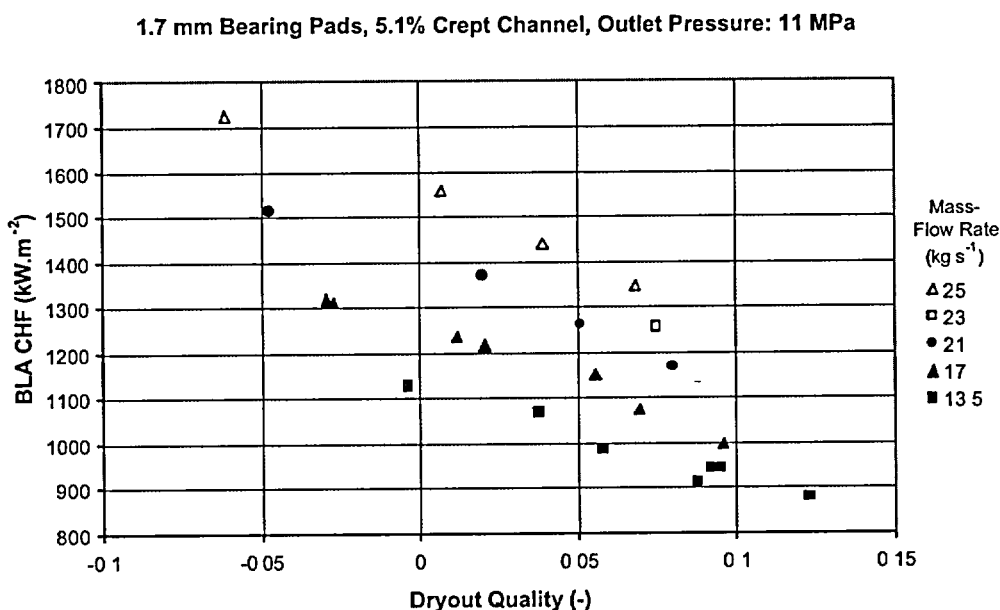


Figure 13: Variation of BLA CHF values with dryout quality and mass-flow rate.

5. COMPARISONS OF DRYOUT POWER BETWEEN CANFLEX AND 37-ELEMENT BUNDLE STRINGS

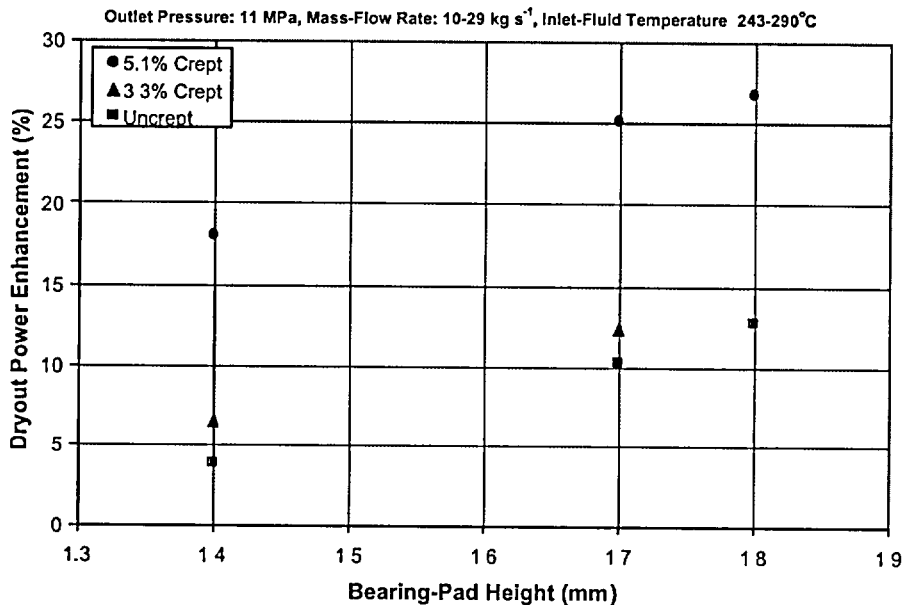
The dryout powers of CANFLEX bundles with various heights of bearing pads have been compared against those of the 37-element bundle⁵ at the same inlet-fluid temperature, mass-flow rate and outlet pressure. Leung et al. [3] presented a similar comparison for the CANFLEX bundle with 1.4 mm bearing pads in a 5.1% crept channel. Figure 14 shows the average dryout-power enhancements of various CANFLEX bundles⁶ as compared to the 37-element bundle at an outlet pressure of 11 MPa. Overall, the dryout powers of the CANFLEX bundles are higher than those of the 37-element

⁴ The quality at the critical subchannel is much higher than zero, and annular-film dryout is anticipated.

⁵ The dryout power for the 37-element bundle string is calculated with an optimized equation derived from the database.

⁶ Test was not performed for the CANFLEX bundle with a 1.8-mm bearing-pad height in the 3.3% crept channel.

bundle at conditions of interest for various crept channels. The dryout power enhancement increases with bearing-pad heights and channel creeps. On average, the enhancement varies from 4% for the 1.4-mm height bearing pads in an uncrept channel to 27% for the 1.8-mm height bearing pads in a 5.1% crept channel.



The effects of inlet-fluid temperature and mass-flow rate on the enhancement are generally small, but the effect of pressure is noticeable. The dryout power enhancement increases with increasing outlet pressures, generally being 4% higher for the uncrept channel and 9% higher for the 5.1% crept channel at 11 MPa compared to that at 9 MPa.

6. CONCLUSIONS AND FINAL REMARKS

- Bearing pads of several elements in the full-scale bundle simulator at Stern Laboratories have been modified to increase the height from 1.4 to 1.7 and 1.8 mm.
- Dryout power measurements have been obtained with CANFLEX bundles of various bearing-pad heights. The data are consistent and follow established parametric trends with various flow parameters.
- Local and BLA CHF values have been calculated with the dryout-power data. The scatter is much larger for the local CHF values than the BLA CHF values at the same local dryout conditions.
- The dryout power is consistently higher for the CANFLEX bundles with high bearing pads than those with low bearing pads. On average, the dryout power improvements are about 8% and 10%, respectively, for the 1.7 mm and 1.8 mm bearing pads, compared to 1.4 mm bearing pads.
- The dryout power is higher for the CANFLEX bundles than for the 37-element bundles at

conditions of interest. The average dryout power enhancement varies from 4% for the 1.4 mm bearing pads in the uncrept channel to 27% for the 1.8 mm bearing pads in the 5.1% crept channel at an outlet pressure of 11 MPa.

ACKNOWLEDGEMENT

The authors would like to thank the test engineers at Stern Laboratories for performing the experiment and providing the experimental data.

REFERENCES

- [1] Inch, W. and Suk, H.C., "Demonstration Irradiation of CANFLEX in Pt. Lepreau", Proc. of the IAEA Technical Committee Meeting on Fuel Cycle Options for LWRs and HWRs, Victoria, Canada, 1998.
- [2] Dimmick, G.R., Inch, W.W., Jun, J.S., Suk, H.C., Hadaller, G.I., Fortman, R.A. and Hayes, R.C., "Full Scale Water CHF Testing of the CANFLEX Bundle", Proc. of the 6th International Conference on CANDU Fuel, Vol. 2, pp. 103-113, Sept. 26-30, 1999.
- [3] Leung, L.K.H., Groeneveld, D.C., Dimmick, G.R., Bullock, D.E. and Inch, W.W., "Critical Heat Flux and Pressure Drop for a CANFLEX Bundle String Inside an Axially Non-Uniform Flow Channel", Proc. of the 6th International Conference on CANDU Fuel, Vol. 1, Sept. 26-30, 1999.
- [4] Kobori, T., "Critical Heat Flux Measurements in a Full Scale Rod Cluster", Bulletin of the JSME, Vol. 19, No. 131, pp. 540-546, 1976.

Status of the Development of CANFLEX 0.9% SEU

Prepared for the
7th International Conference on CANDU Fuel
September 23-27, 2001
Kingston, Ontario, Canada

by

Wayne W.R. Inch
Fuel Channel Thermalhydraulics
Chalk River Laboratories
Atomic Energy of Canada Ltd
Canada

Peter S.W. Chan
Reactor Core Physics
Sheridan Park
Atomic Energy of Canada Ltd
Canada

Zoran Bilanovic
Fuel Design
Sheridan Park
Atomic Energy of Canada Ltd
Canada

STATUS OF THE DEVELOPMENT OF CANFLEX 0.9% SEU

WAYNE W.R. INCH, PETER S.W. CHAN AND ZORAN BILANOVIC

Atomic Energy of Canada Ltd., Ontario, Canada

ABSTRACT

Atomic Energy of Canada Ltd. (AECL) participates in international collaboration programs on slightly enriched uranium (SEU) with the Korean Atomic Energy Research Institute, British Nuclear Fuel plc. and most recently with Nucleoelectrica Argentina S. A. (NASA). In Argentina, NASA has successfully converted Atucha I from natural uranium to 0.85% SEU. Significant fuel cycle cost reductions were realized, and NASA wishes to explore similar concepts to reduce operating costs of its Embalse reactor. This collaboration covers the first phase of a 3-phase program. If the study confirms the feasibility and benefits of SEU, then the program could move onto a demonstration irradiation and, potentially, full-core implementation of SEU fuel at Embalse.

This paper will provide an overview of the CANFLEX[®] 0.9% fuel concept. Reactor physics assessment of the conversion of a natural uranium core to an enriched core will be presented. The feasibility of conducting a demonstration irradiation of SEU fuel in a reactor core of natural uranium fuel will be covered. Preliminary assessments of the safety and licensing implications will be summarized.

INTRODUCTION

The use of 0.9% slightly enriched uranium (SEU) fuel offers significant benefits to CANDU[®] reactor operators. SEU fuel improves fuel cycle economics by increasing the fuel burnup, which enables large cost reductions in fuel consumption and in spent fuel disposal. SEU fuel offers enhanced operating margins that can be applied to offset aging effects, or to increase reactor power. These benefits can be realized using existing fuel production technologies and practices, and with almost negligible changes to fuel receipt and handling procedures at the reactor. The application of SEU is an important element in AECL's Next Generation reactor design.

Since the early 1990's, AECL and the Korean Atomic Energy Research Institute (KAERI) have pursued joint development of the CANFLEX[®] fuel bundle. Since 1994, AECL and British Nuclear Fuel plc (BNFL) have pursued an exchange of information co-operation program in SEU and recycled uranium (RU). In 2000, AECL and Nucleoelectrica Argentina S. A. (NASA) agreed to a collaborative program to study the feasibility of converting Embalse to SEU, in order to realize reduced operating costs and to provide a strategy for increasing reactor power.

CANFLEX[®] is a registered trademark of Atomic Energy of Canada Limited (AECL) and the Korean Atomic Energy Research Institute (KAERI).
CANDU[®] is a registered trademark of AECL.

A unique feature of the CANDU reactor design is its ability to use alternative fuel cycles other than natural uranium (NU), without requiring major modifications to the basic reactor design. These alternative fuel cycles, which are collectively known as advanced fuel cycles, utilize a variety of fissile materials, including SEU from enrichment facilities, and RU or plutonium obtained from the reprocessing of the spent fuel of light-water reactors (LWR). While the choice of a particular advanced fuel cycle depends on economics and resource conservation, as well as political considerations, the SEU fuel cycle is generally considered as the first logical step beyond the NU fuel cycle.

This paper provides early results of the physics and safety assessments concerning the converting of an operating CANDU 6 reactor from NU to SEU.

CANFLEX 0.9% SEU REFERENCE DESIGN

The CANFLEX design has been chosen as the fuel carrier for SEU. The maximum element linear-power rating of the CANFLEX fuel elements is 20% lower than that for 37-element bundles, leading to lower fuel temperatures. As a result, less free fission-gas inventory is produced under normal operating conditions, compared with the free fission-gas inventory produced in standard 37-element fuel elements at a similar bundle power. The lower fission-gas inventory results in lower element gas pressure, which enables higher burnups and reduces the consequences of most design-basis accidents.

Previous studies of CANDU SEU fuel cycles have shown that the optimal enrichment is between 0.9 wt% ^{235}U and 1.2 wt% ^{235}U . 0.9% SEU is chosen as the reference enrichment level for this study, because

- most of the benefits of the SEU fuel cycle are achieved between 0.9% and 1.0%,
- 0.9% SEU is below the threshold at which criticality considerations would have significant impact on fuel fabrication and fuel handling,
- the refuelling scheme is uniform 2- or 4-bundle shift, and transition from NU to SEU in a current CANDU can be easily accomplished with 0.9% SEU, and
- the neutronic properties of 0.9% SEU fuel are similar to those of the RU fuel, which is expected to be cheaper than equivalent SEU fuel.

RU, which is available as a by-product of conventional reprocessing of LWR fuel, can be considered as a subset of SEU. The fissile content of RU is nominally between 0.9% ^{235}U and 1.0% ^{235}U , depending on the initial fissile content and the discharge burnup of a particular batch of spent LWR fuel.

The reference fuelling scheme for CANFLEX 0.9% SEU fuel bundles is a 4-bundle shift where possible, and a 2-bundle-shift for the central channels. Since the fuel burnup for 0.9% SEU is twice that of NU fuel, the 4-bundle shift is equivalent to the current 8-bundle shift in fuelling rates, but 2-bundle shift would require a significantly higher fuelling rate. Alternate duty cycles are being assessed to reduce fuelling machine usage. Strategies are being explored to limit or eliminate the need for using 2-bundle shifts.

The reference design uses 0.9% enrichment in all 43 elements. Alternatively RU from spent PWR fuel can be considered as a lower-cost source of enrichment. The enrichment can be varied to tailor the burn-up, in order to address the specific needs of the application.

CANFLEX 0.9% SEU FEASIBILITY STUDY

CANFLEX is an appropriate vehicle for introducing SEU, because it reduces linear-power element ratings, thereby reducing fuel temperatures and gas releases, and facilitating the achievement of extended burnups. CANFLEX also provides a greater critical channel power margin than the 37-element bundle. The CANFLEX Mk-IV fuel bundle design has been qualified for the NU application.

The principle issues that must be considered with the use of SEU in CANDU are

- higher burnups, resulting in (1) longer residence time, (2) potential for higher fission gas production, and (3) greater decay heats in the spent fuel, all requiring design analysis and assessments.
- higher reactivity of the fuel, which requires different on-power fuelling schemes, resulting in different axial flux shapes that must be established through physics assessments, and that must be balanced with the duty-cycle for the fuelling machines. Bundle power, channel power and thermalhydraulic performance must be maintained.

The feasibility of transitioning the core from NU to SEU with no loss of reactor power, while maintaining safety and fuel performance standards, must be considered. To implement the fuel, it must be qualified; therefore, consideration must be given to a power reactor demonstration irradiation of SEU in a NU core. Finally, the overall economic impact of SEU on the capital and operating costs must be defined, as this will be the primary driver in switching to a new fuel type. Early work has concentrated on the reactor physics assessment and safety assessment, as presented in the following sections.

FEASIBILITY OF CONDUCTING A DEMONSTRATION OF CANFLEX SEU FUEL IN AN EXISTING CANDU 6 NU CORE

It is prudent to demonstrate the performance of SEU bundles under operating reactor conditions, prior to beginning the full-scale conversion from NU fuel to SEU fuel. This demonstration can be accomplished by irradiating a few SEU bundles in an operating reactor for a significant period of time. The discharged SEU fuel bundles would be examined closely in post-irradiation examination (PIE) hot cells, in order to confirm that the SEU fuel performance is within design specifications.

The demonstration irradiation (DI) of SEU bundles in a reactor currently operating with NU fuel requires careful planning, because the reactivity of the SEU fuel is significantly higher than that of the NU fuel. Hence, the presence of fresh SEU fuel could cause some local power peaking effects at the beginning of the DI. However, by choosing the appropriate channels and fuelling schemes for the DI, these local power perturbations can be mitigated. A reactor physics simulation of the DI of several SEU bundles in an operating CANDU 6 reactor has been conducted by using the RFSP-IST [4] and WIMS-AECL [5] codes to demonstrate that both the SEU fuel and the NU fuel can operate within current operating and safety limits during the DI period. An instantaneous fuel burnup distribution in a typical CANDU 6 core was used as a starting point of the DI simulation.

Channels L03, L11 and L20 in a CANDU 6 reactor have been identified as good candidates for the DI. Channels L03 and L20 are located outside the adjuster rod region, while L11 is a central channel inside the adjuster rod region. These channels are chosen primarily because of their moderate channel powers in the NU reactor. The fuel management scheme chosen for the DI channels is a 4-bundle shift with 0.9% CANFLEX SEU fuel for the first visit, and a 2-bundle shift with 37-element NU fuel for subsequent visits at the same channel. Hence, each DI channel contains four SEU fuel bundles. These SEU bundles are pushed through the channel using 2-bundle-shift NU fuel at 50 FPD intervals. All the SEU fuel bundles are discharged from the reactor after 300 FPD with an average discharge burnup of 13 MWd/kg.

In channel L03, the maximum channel power and maximum bundle power during the simulation period are 6.4 MW(th) and 890 MW(th), respectively, when the four SEU bundles are in the central locations, i.e., bundle positions 5,6,7 and 8 of the channel. Under these conditions the maximum element rating is below 47 kW/m, and the maximum element boost power is below 25 kW/m at a burnup of about 3.0 MWd/kg. Similar results are observed in the other two DI channels. There were no significant axial power distortions in the NU channels adjacent to the DI channels during the entire DI period when the SEU bundles were in different axial locations in the DI channels. The results of the DI simulation indicate that the DI of 12 SEU bundles can be carried out in an operating CANDU 6 reactor without affecting the reactor operation, and without posing a risk to either the SEU or the NU fuel.

Figure 1 shows the channel powers in the DI channel L03 and its NU neighbour K03, during the DI period. The corresponding maximum bundle powers are shown in Figure 2. Channel L03 has been refuelled six times using 2-bundle-shift NU fuel, and channel K03 has been refuelled twice using 8-bundle-shift NU fuel during this period. The maximum channel and bundle powers are all within operating limits.

PHYSICS ASSESSMENT OF THE TRANSITION TO AND OPERATION OF A 0.9% SEU-FUELLED CORE

The RFSP-IST and WIMS-AECL codes were used to simulate the transition from NU to 0.9% SEU in an operating CANDU 6 reactor. The starting point of the RFSP transition simulation corresponds to an actual reactor core configuration and fuel burnup distribution from an operating CANDU 6 reactor, with a full core of 37-element NU bundles. All these NU bundles are replaced by CANFLEX 0.9% SEU bundles using on-power fuelling over a simulation period of 726 FPD.

Fuelling Scheme For the Transition. The fuelling scheme used is a 4-bundle shift for the first introduction of the SEU fuel in a channel, and 2-bundle shifts with SEU fuel for all subsequent fuelling in the same channel. The refuelling simulations are carried out at intervals of 2 FPD, using both bulk and spatial control options with distributed xenon properties. The fuelling schemes for the transition study have been chosen for the following reasons:

- Using 2-bundle-shift fuelling at the beginning of the transition would give a very small increase in reactivity, because of the relatively low neutron flux levels at these positions at the ends of the channels. This would require the fuelling of more than 6 channels per FPD at the onset, resulting in excessive demand on the fuelling machine.

- The maximum distortion of the axial bundle power profile occurs in the period when there is a mixture of 4 SEU and 8 NU bundles in different channels in the reactor. It is highly desirable to get over this period as fast as possible.
- The use of a 4-bundle-shift fuelling scheme at the onset results in reasonable fuelling machine usage and acceptable axial bundle power profiles. However, the 4-bundle-shift scheme cannot be used for subsequent fuelling in the same channel, because the refuelling power ripple becomes excessive.
- The combination of a 4-bundle shift for the first introduction of the SEU fuel in a channel and a 2-bundle shift for all subsequent fuelling in the same channel appears to give the best results in terms of fuelling machine usage, axial bundle power profiles, and refuelling power ripples.

The fuelling rate is about 11.2 bundles per FPD for the first 100 FPD, and gradually declines to the equilibrium fuelling rate of about 8.8 bundles per FPD after 500 FPD.

Acceptance Requirements. The channels to be refuelled in each time step were carefully chosen to meet the following conservative requirements over the entire simulation period:

- the maximum channel power should not exceed 6.9 MW(th),
- the maximum bundle power should not exceed 850 kW(th),
- the average zone control level should remain between 30% and 70%, and
- individual zone control levels should remain between 10% and 90%.

CANDU 6 reactors are currently licensed to operate at a maximum channel power of 7.3 MW(th) and maximum bundle power of 935 kW using 37-element fuel bundles. The requirements used in the transition simulations are within these limits, with large conservative margins.

Furthermore, the CANFLEX design could potentially allow an increase in these limits.

Bundle and Channel Powers. Although the simulation period covered 726 FPD, the maximum channel power, maximum bundle power and fuelling rate became relatively stable after 500 FPD, when most of the NU bundles had been discharged from the core. At 726 FPD, it is estimated that the reactor will have been operating at equilibrium SEU core conditions for a significant period of time.

Figure 3 shows the maximum channel power as a function of FPD in the transition simulation. The power is kept between 6.7 MW(th) and 6.9 MW(th) essentially for the entire simulation. The maximum channel power was below 6.7 MW(th) for a few cases, but it was never allowed to exceed 6.9 MW(th), a self-imposed conservative requirement. However, thermalhydraulic assessments may be required for those channels with significant axial power distortions to determine the appropriate CCP limits.

During the first 150 FPD of the transition, the presence of four or six SEU bundles at the upstream end of the fuel channels created very significant distortions in the axial power profile. However, by keeping the maximum channel power below 6.9 MW(th), it was possible to keep the maximum bundle power at or below 850 kW(th), similar to the situations in the current NU reactor. The axial bundle power profile in the equilibrium SEU core is naturally flatter than that in an equilibrium NU core. As the transition progressed, more NU bundles were replaced by SEU bundles. The maximum bundle power began to decrease steadily, until the axial bundle

power shape approached that in an equilibrium SEU core. The variation of maximum bundle power as a function of FPD in the transition is shown in Figure 4. At 726 FPD, the maximum bundle power is about 800 kW, significantly lower than that in an equilibrium NU core.

The axial bundle power distributions at different stages during the transition in channel L03 are shown in Figure 5. This channel is outside the adjuster rod region, and it was refuelled eight times within this period. The introduction of the first four SEU bundles produces a severe axial power distortion. However, as more SEU fuel bundles are introduced at later stages, the distortion subsides. The axial power shape approaches the smooth inlet-skewed equilibrium SEU power shape after FPD 300. This flattened inlet-skewed power shape is a consequence of the simple 2-bundle-shift scheme used with SEU fuel. It is more desirable than the centre-peaked NU power shape, because it gives higher critical channel power (CCP) margins. Adjuster rods are not required, nor are they desirable for shaping the axial power profile in an SEU core. They can cause significant axial power distortions during the transition.

Figure 6 shows the axial bundle power distributions in Channel L11 at different stages during the transition. This channel is inside the adjuster region and it is also close to two zone controllers. Channel L11 was refuelled 8 times in this period. It can be seen that the axial power shape in channel L11 is already distorted before this channel is refuelled the first time. This distortion is created by the introduction of SEU fuel bundles in the adjacent channels. The introduction of the first 4 SEU bundles in L11 produces a severe double-humped axial power distortion. Introduction of SEU bundles in neighbouring channels at this time would further increase the axial power distortion in Channel L11. However, as more SEU fuel bundles are introduced in Channel L11 at later stages, the distortion decreases slowly. A smooth, but still double-humped axial power shape prevails after FPD 500. Because the SEU bundle power profile is naturally flat, the adjuster rods over flatten the axial power shape in an SEU core, creating an undesirable double-humped axial power shape.

Performance of Fuel Elements in Transition Core. The severity of the double-humped axial power distortion in inner-region channels suggests that a small number of fuel elements could be subjected to high power ratings and high power boosting during the transition. The outer elements in the NU 37-element bundles are most susceptible to excessive power boosting when they are pushed from bundle positions 7 and 8 (from inlet-end) to positions 9 and 10 during refuelling. The analysis of all outer elements in the NU 37-element bundles found no cases where both the normal power rating threshold and the power boost threshold were exceeded. The analysis concluded that the overall risk of fuel failure should be minimal. However, there were a small number of elements whose power boost ratings exceed the SCC threshold. All the elements in the three inner fuel rings are below the SCC defect threshold curves for normal operation and for power boost. Hence, there is no risk of fuel defect for these elements.

The NU elements are subjected to high operating powers and high refuelling power boosting only during the first 150 FPD of the transition, when the axial power shape is severely distorted. Furthermore, only the NU fuel elements in the inner core region are at risk. Therefore, several methods can be deployed to ensure good fuel performance:

- Raise the central adjuster rods (banks 6 and 7) before the start of the transition, and keep them locked out of the core until the equilibrium SEU core condition is reached. It should be noted that with SEU fuel, adjuster rods are not needed to flatten the flux and power

distributions. Hence, if they are not needed for another purpose, they can be removed altogether.

- Fuel the channels in the inner 10-by-10 square with CANFLEX NU bundles before the start of the transition, if the locking out of the central adjuster rods is not an option. The lower element rating in the CANFLEX design will keep the NU fuel element ratings below the SCC defect thresholds.
- Monitor the axial channel power shape carefully, especially during the first 150 FPD. The element ratings can be kept below the SCC defect thresholds by refuelling the inner channels judiciously.

The element ratings of all the CANFLEX SEU fuel elements for nominal power operation during the transition are significantly below the SCC defect threshold. The power boost ratings for all CANFLEX SEU fuel elements in the inner three fuel rings are also below the SCC power boost defect threshold curve. The power boost ratings of a very small number of ring-4 SEU fuel elements are slightly above the SCC defect threshold curve. Because the normal power ratings of all the CANFLEX SEU fuel elements are significantly below the SCC defect threshold curve, there is negligible risk of fuel failure for the CANFLEX SEU fuel.

The results of the RFSP simulations suggest that the reactor appears to operate at conditions similar to those in an equilibrium SEU core after 500 FPD. Therefore, power and burnup distributions for the period after 500 FPD are used to assess SEU fuel element ratings and power boost ratings in an equilibrium SEU core. Figure 7 shows the linear element rating for the ring-4 elements in the CANFLEX SEU fuel bundles for the period after 500 FPD. The power boost ratings for these fuel elements due to refuelling operations are shown in Figure 8. The results show that all the SEU CANFLEX fuel elements operate at power ratings and boost ratings significantly below the SCC defect threshold curves. Therefore, fuel failure for SEU CANFLEX fuel is not expected in an equilibrium SEU core.

Physics Summary Comments. Although this study shows that no change in the reactor operating procedure or hardware is required for the transition from an equilibrium NU core to an equilibrium SEU core, it is clear that the adjuster rods are not desirable during the transition. The option of locking some of the central adjuster rods out of the core during the transition period, even permanently, should be given serious consideration.

CANFLEX 0.9% SEU SAFETY IMPLICATIONS

The implementation of CANFLEX SEU fuel in a CANDU 6 reactor would have an overall beneficial effect in terms of safety margins during postulated reactor accidents. The main reason for this benefit is the reduction of more than 20% in the outer element linear powers of the fuel bundle, compared with the outer elements of a 37-element NU bundle. The effect of this reduction in element linear powers is that fuel temperatures, sheath temperatures and fission product release will all be lower for most design basis accidents. The higher fuel burnup would mean that the total inventory of long-lived fission products would be greater for CANFLEX-SEU fuel than for 37-element fuel; however, the distribution of the fission products would be different. Because of the lower fuel temperatures, the concentration of fission products in the fuel-to-sheath gap, as well as the grain boundaries, would be lower for CANFLEX-SEU fuel.

The effects of the above features of CANFLEX-SEU fuel upon the consequences of various postulated accidents in a CANDU reactor are outlined below.

Large Break Loss of Coolant Accident (LOCA). During a postulated LOCA, it is expected that the resultant power pulse within a CANFLEX-SEU core will be marginally greater than the power pulse within a CANFLEX-NU core, which, in turn, is greater than the power pulse within a 37-element fuelled core. The increase in the power pulse will be more than offset by the reduction in the outer element linear powers. The lower initial fuel temperatures will result in lower peak fuel centerline temperatures, thereby increasing the margins to fuel centerline melting. In addition, lower fuel temperatures will result in lower fuel string axial expansion, increasing channel integrity margins. Similarly, peak sheath temperatures of CANFLEX-SEU are expected to be lower than the peak sheath temperatures of 37-element fuel. The lower fuel and sheath temperatures will result in lower fission product release to the fuel-to-sheath gap, which will lead to fewer fuel failures and lower doses during a postulated large break LOCA. Because of the lower sheath temperatures, pressure tube temperatures will also be lower, resulting in less pressure tube/calandria tube contacts, and thus providing greater safety margins for channel integrity.

Large Break LOCA with Loss of Emergency Core Cooling (LOECC). In this postulated severe accident the CANFLEX-SEU bundle design could result in the potential for greater hydrogen generation within the containment structure, relative to the 37-element fuel. The higher burnup fuel will contain a greater long-lived fission product inventory than the current 37-element design, resulting in greater long-lived fission product release during a postulated LOCA/LOECC event. However, the inventory of short-lived fission products will be lower, since this inventory is strongly dependent upon element linear powers. A consequence of a flatter axial power profile is lower peak bundle powers within the channel—if low enough, then the elements could reach peak sheath temperatures that are below the metal/water reaction threshold, thus mitigating the production of hydrogen.

Small Break LOCA. The lower element linear powers, lower bundle powers, and an inlet skewed axial power distribution will all lead to greater margins with respect to fuel dryout during a postulated small break LOCA. This would substantially decrease the chances of fuel and channel failures.

Single Channel Events. For postulated single channel events, such as the complete channel flow blockage and feeder stagnation break, the lower element linear powers and peak bundle powers would result in a delay of channel failure for CANFLEX-SEU fuel, compared with 37-element fuel. The result would be marginally more molten material being generated at the time of pressure tube rupture. For the feeder off-stagnation break and end-fitting failure accidents, the two key parameters are fuel temperatures, and fission product content and distribution. The higher fuel burnup for SEU fuel will result in more long-lived fission products than would be found in 37-element fuel. However, the lower element linear powers would result in lower overall fuel-to-sheath gap and grain boundary inventories of fission products. This would mean that the initial release of fission products from SEU fuel would be lower. However, the long-term release may be greater, simply because of the greater total inventory of fission products compared with 37-element fuel. The mitigation measures would be the lower fuel temperatures of CANFLEX-SEU fuel that would reduce the oxidative release of fission products from the fuel matrix.

CONCLUSIONS

The CANFLEX 0.9% SEU fuel design has been established, and the fuel qualification and feasibility of applying it in existing CANDU 6 reactors is underway. The results of a 726 FPD RFSP simulation show that it is feasible to convert an existing CANDU 6 reactor from a full core of NU 37-element fuel to a full core of 0.9% SEU CANFLEX fuel, by on-power fuelling. The maximum channel power, the maximum bundle power, and the operating range of the zone controllers are all within the limits established for the current NU reactor. There is no risk of fuel failure for the SEU CANFLEX fuel elements in the transition core and in the equilibrium core. The results of DI simulations show that 12 SEU bundles can be irradiated in an operating CANDU 6 reactor without adversely affecting the reactor operation. The implementation of CANFLEX-SEU fuel into a CANDU 6 reactor would have an overall beneficial effect in terms of safety margins during postulated reactor accidents.

REFERENCES

1. I.J. HASTINGS, A.D. LANE and P.G. BOCZAR, "CANFLEX - An Advanced Fuel Bundle for CANDU", Int. Conf. Availability Improvements in Nuclear Power Plants, Madrid, Spain, 1989 April 10-14, and also AECL Report, AECL-9929 (1989).
2. A.D. LANE, G.R. DIMMICK, J.H.K. LAU, H.C. SUK, C.H. CHUNG and C.B. CHOI, "CANFLEX: A New CANDU Fuel Bundle with Expanded Operating Capabilities", Proc. 11th KAIF/KNS Annual Conference, Seoul, Korea, 1996 April 11-12.
3. B. ROUBEN, "Overview of Current RFSP-Code Capabilities for CANDU Core Analysis", Transactions of the American Nuclear Society, TANSO 72, 339, 1995.
4. J.V. Donnelly, "WIMS-CRNL, A User's Manual for the CRNL Version of WIMS", AECL-8955, January 1986.

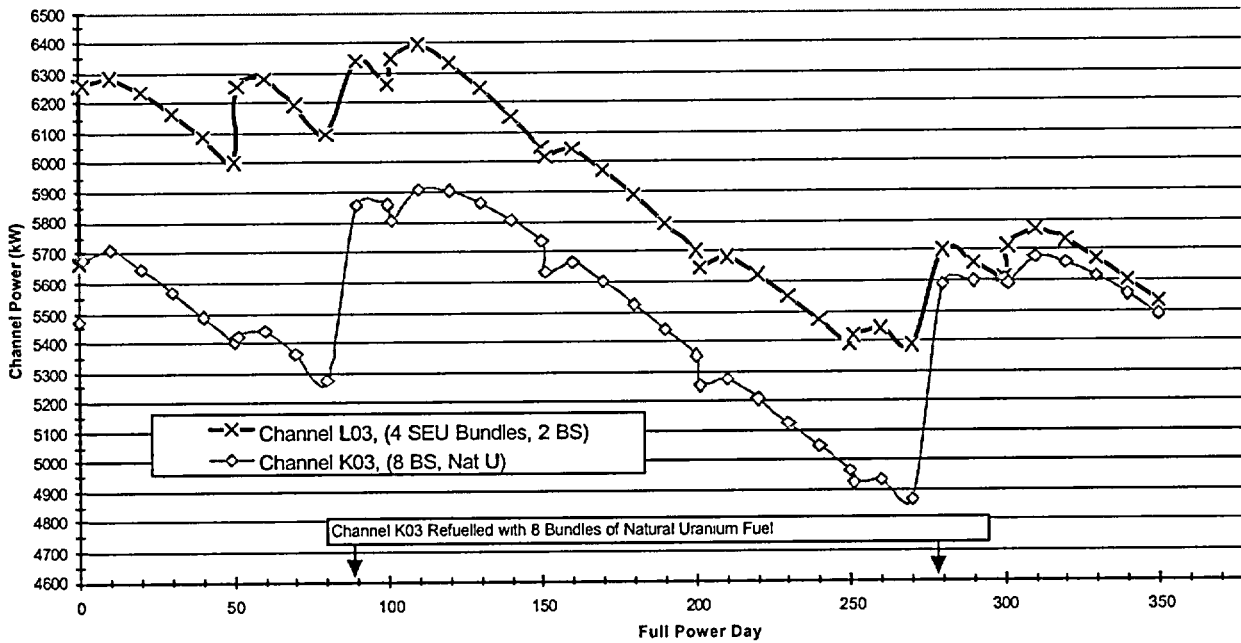


FIGURE 1. CHANNEL POWERS VS. FULL POWER DAY IN L03 AND K03 DURING DI SIMULATION

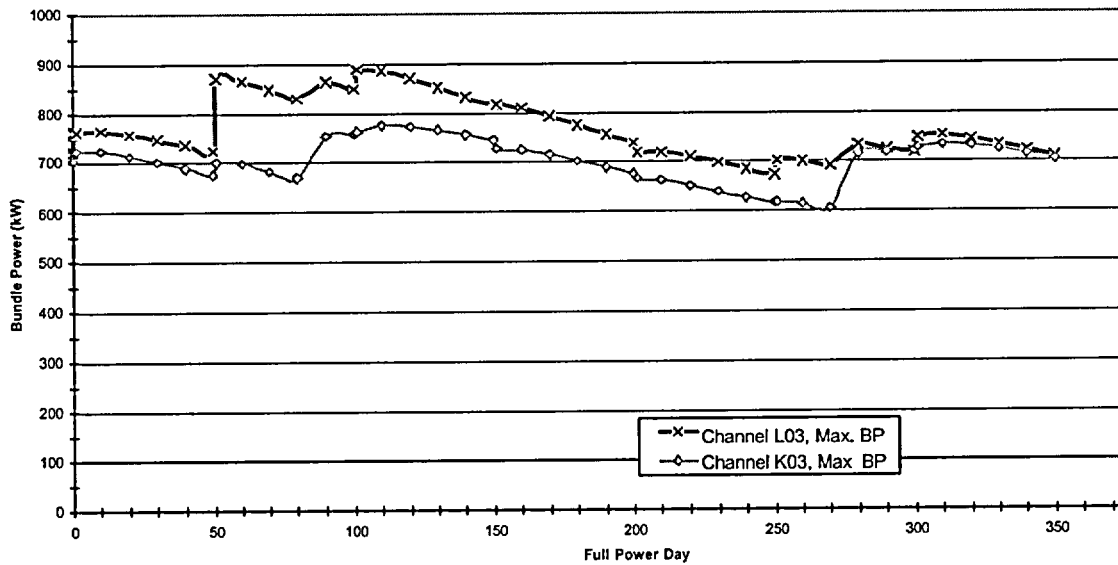


FIGURE 2. MAXIMUM BUNDLE POWERS VS. FULL POWER DAY IN L03 AND K03 DURING DI

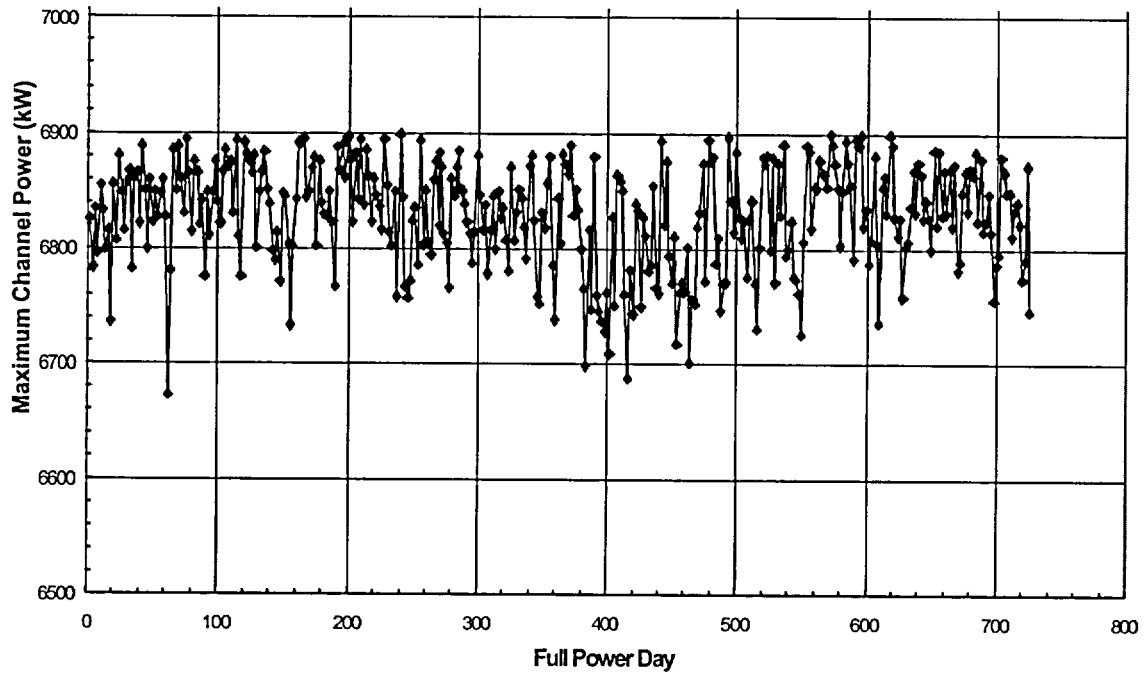


FIGURE 3. MAXIMUM CHANNEL POWER VS. FULL POWER DAY IN C6 NU/SEU TRANSITION CORE

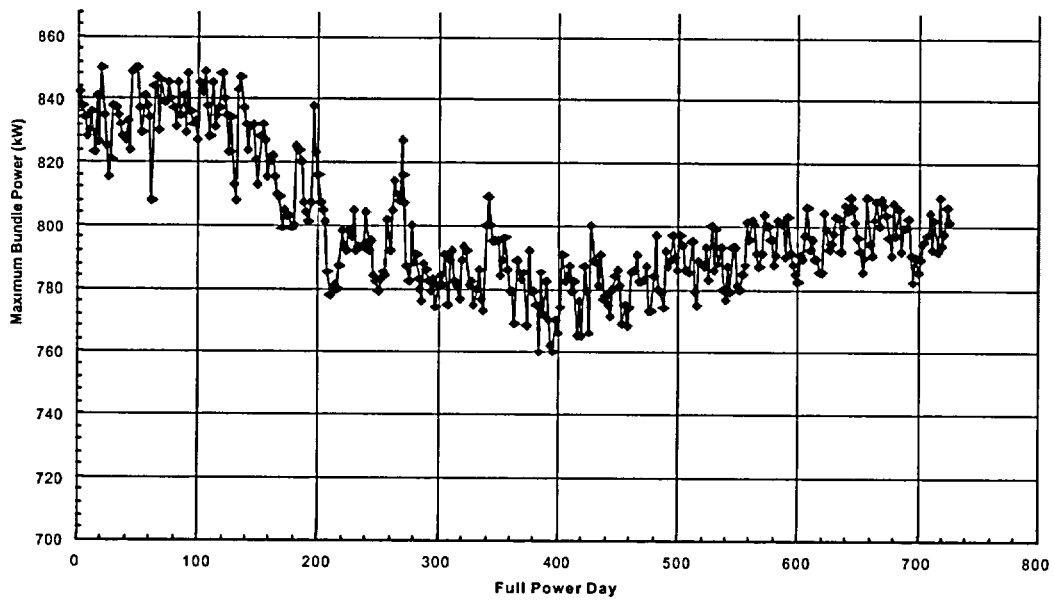


FIGURE 4. MAXIMUM BUNDLE POWER VS. FULL POWER DAY IN C6 NU/SEU TRANSITION CORE

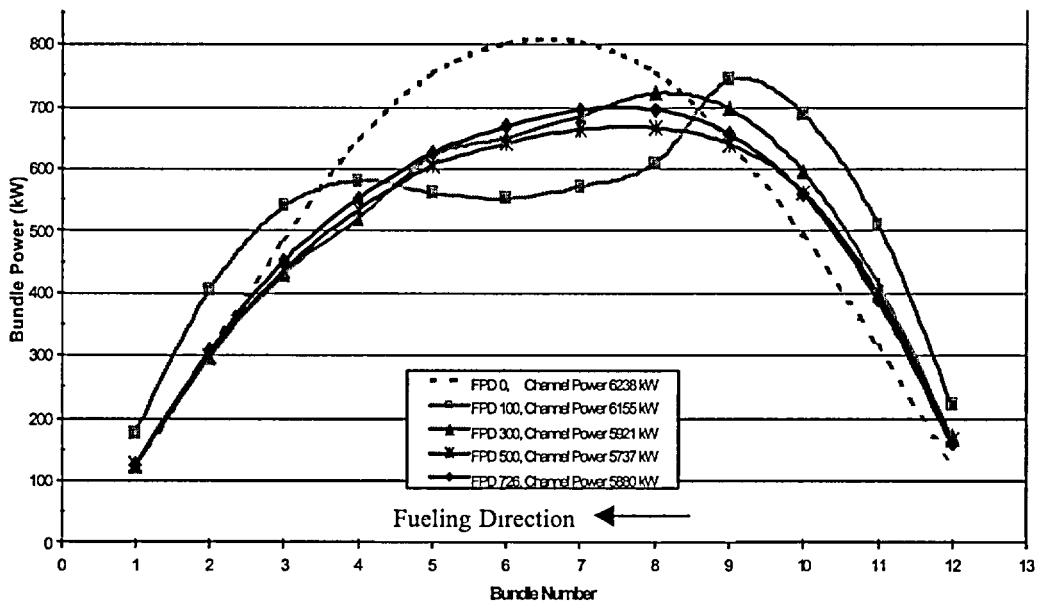


FIGURE 5. BUNDLE POWER DISTRIBUTION IN CHANNEL L03 DURING TRANSITION

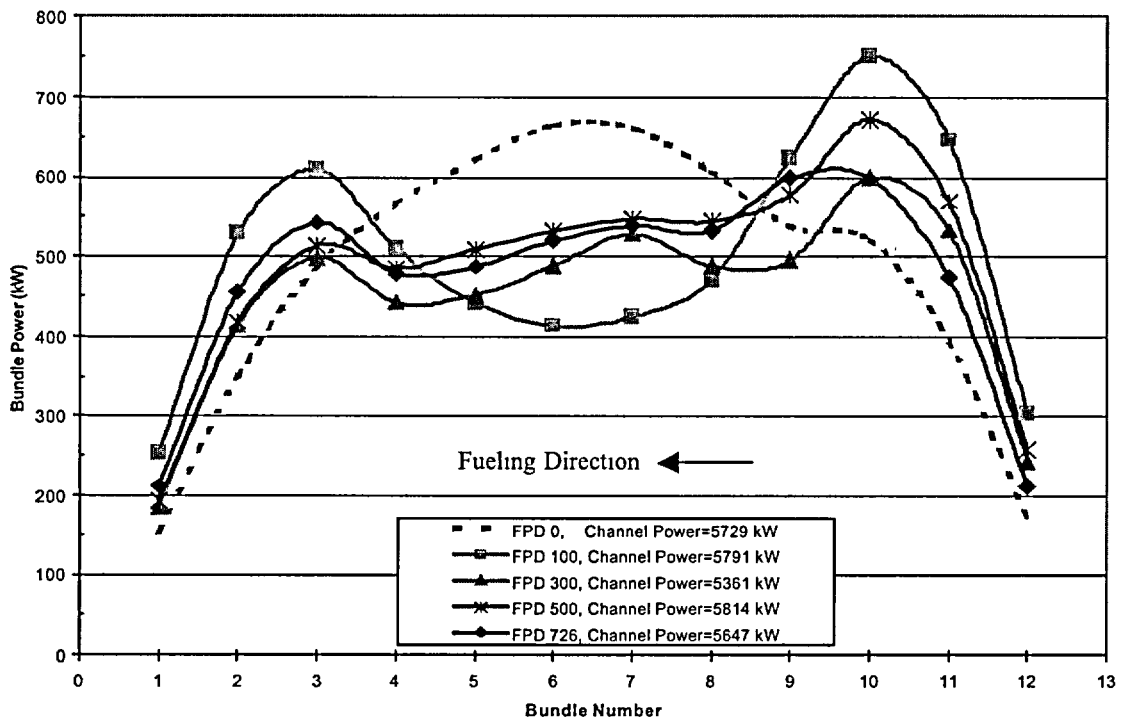


FIGURE 6. BUNDLE POWER DISTRIBUTION IN CHANNEL L11 DURING TRANSITION

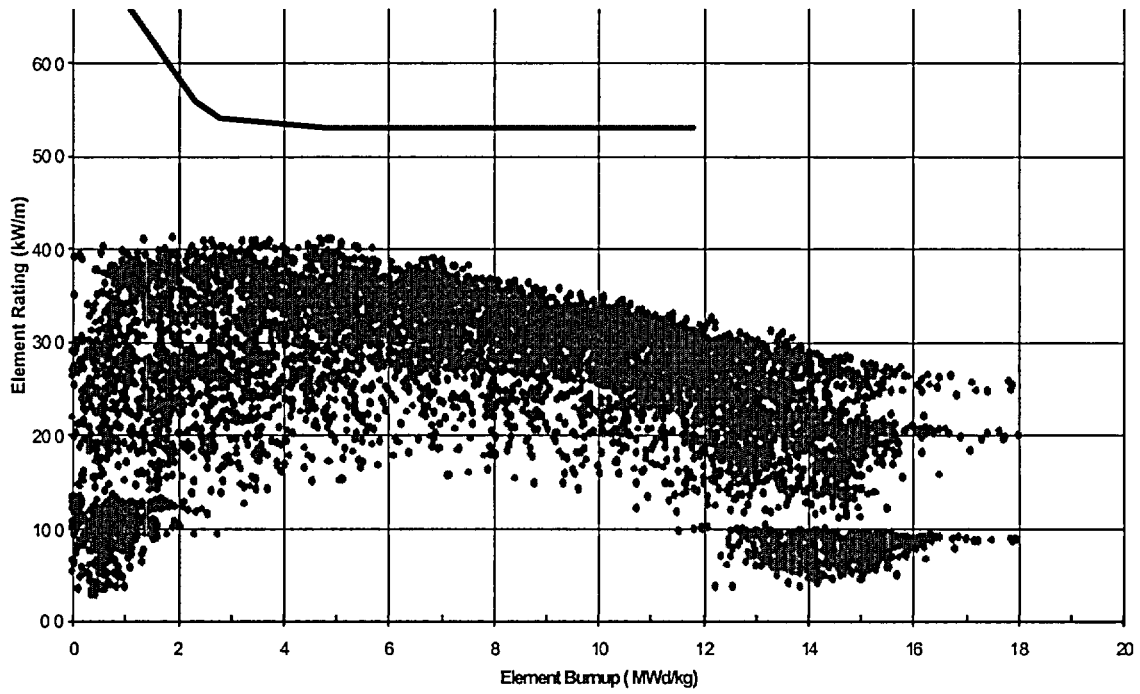


FIGURE 7. SEU (CANFLEX BUNDLE) RING 4 ELEMENT RATING VS. BURNUP

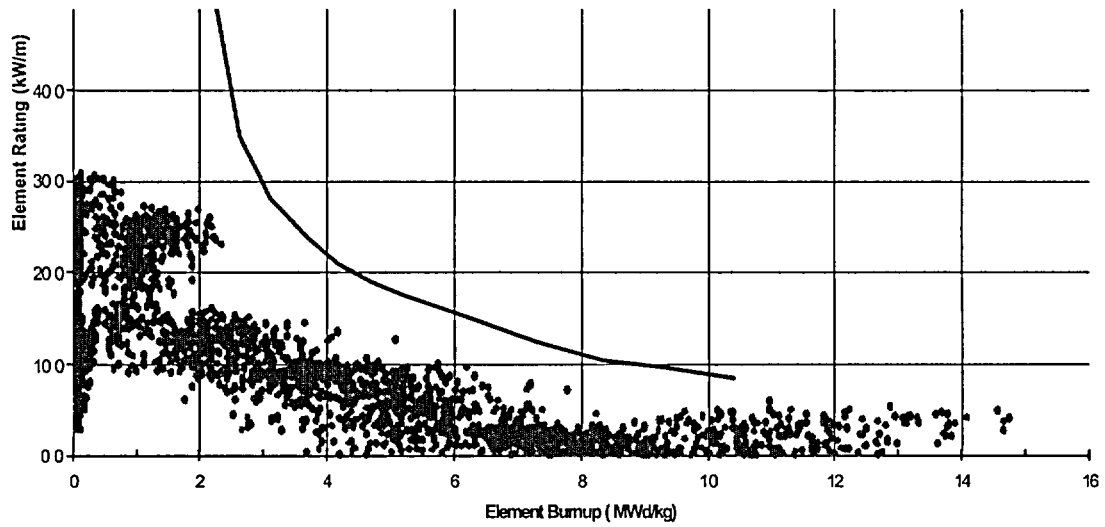


FIGURE 8. SEU (CANFLEX BUNDLE) RING 4 ELEMENT BOOST VS. BURNUP

CANFLEX Mk-IV Qualification Program and Readiness for Implementation

Prepared for the

7th International Conference on CANDU Fuel

September 23-27, 2001
Kingston, Ontario, Canada

by

Wayne W.R. Inch
Fuel Channel Thermalhydraulics
Chalk River Laboratories
Atomic Energy of Canada Ltd
Canada

Parva Alavi
Fuel Design Branch
Sheridan Park
Atomic Energy of Canada Ltd
Canada

CANFLEX MK-IV QUALIFICATION PROGRAM AND READINESS FOR IMPLEMENTATION

WAYNE W.R. INCH AND PARVA ALAVI

Atomic Energy of Canada Ltd

ABSTRACT

A formal design verification process was followed to qualify the CANFLEX[®] Mk-IV fuel bundle for use in CANDU[®] 6 reactors. Extensive out-reactor testing, combined with analysis, was used to show that CANFLEX meets the CANDU 6 fuel design requirements. The design requirements, assessments and performance tests results were documented in the Point Lepreau Generation Station (PLGS) Fuel Design Manual, which was subjected to an industry-wide formal Design Review. The final step before the implementation of CANFLEX fuel was to conduct a demonstration irradiation of these bundles in a power reactor to show compatibility with the fuel channel and fuel handling systems.

The Demonstration Irradiation (DI) has been successfully completed with 24 CANFLEX bundles at PLGS. Sixteen bundles were irradiated in a high-power channel (S08) to burnups ranging from 163 to 242 MWh/kgU, and to maximum outer-element linear powers of 25 to 39 kW/m. A further eight bundles were irradiated in a low-power channel. All bundles were visually inspected in the PLGS spent fuel bay, and two were subjected to full Post Irradiation Examination at the Chalk River Laboratories hot cells. The bundles were in good condition with no defects. All observations have been formally dispositioned.

All activities identified in the Design Verification Plan have been fully completed, all questions from the Design Review Panel have been resolved, and all observations from the DI bundle inspections have been formally dispositioned. The CANFLEX Fuel Design Manual has been revised to include results from the new analysis, testing and inspections that have been concluded through the final stages of the review process. AECL's Office of the Chief Engineer has concluded that the CANFLEX Mk-IV fuel bundle design is qualified for implementation in a CANDU 6 reactor. Discussions are underway with utilities in Canada and Korea, to quantify the benefits from implementing this new fuel design.

This paper will provide an overview of the verification process, with a focus on the most recent activities that are intended to resolve questions arising from the Design Review. This paper will describe the activities undertaken to address all observations from the inspections performed on the DI bundles. Finally, this paper will show the readiness of this new product for implementation, and the potential benefits that current stations can derive from its application.

INTRODUCTION

Since the early 1990's, Atomic Energy of Canada Limited (AECL) and the Korea Atomic Energy Research Institute (KAERI) have pursued a collaborative program to develop, verify and

CANFLEX[®] is a registered trademark of Atomic Energy of Canada Limited (AECL) and the Korean Atomic Energy Research Institute (KAERI).

CANDU[®] is a registered trademark of AECL.

prove a new fuel design that would introduce advanced fuel cycles such as slightly enriched uranium (SEU), recycled uranium (RU) and others into CANDU[®] reactors, and would provide enhanced performance with natural uranium (NU) fuel, through higher operating margins in existing CANDU reactors [1,2,3].

From 1998 September to 2000 August, New Brunswick Power (NBP), at the Point Lepreau Generating Station (PLGS), conducted a two-year demonstration irradiation (DI) of CANFLEX[®] fuel bundles, as the final verification of the CANFLEX design, and as a prerequisite to full-core conversion. Recently, the Korean Electric Power Corporation (KEPCO) announced a program in Korea to prepare for a DI in Wolsong Unit 1, followed by a potential full-core CANFLEX implementation.

This paper provides a summary of the CANFLEX qualification and performance assessment program. This paper also provides a summary of the disposition of all findings from the DI, and discusses the readiness of CANFLEX Mk-IV for full-core implementation.

CANFLEX BUNDLE DESIGN

The CANFLEX design is a 43-element fuel-bundle assembly that offers improved operating and safety margins, compared to the standard 37-element fuel bundle, for operating CANDU reactors. The CANFLEX bundle design includes critical heat flux (CHF) enhancement devices that lead to higher critical channel power (CCP) in a full-length fuel channel, compared to 37-element fuel bundles. The lower heat rating of the CANFLEX fuel elements at current bundle powers leads to lower fuel temperatures. As a result, less free fission-gas inventory is produced under normal operating conditions, compared with the free fission-gas inventory produced in standard 37-element fuel elements at a similar bundle power.

The CANFLEX bundle consists of two fuel element sizes: small diameter elements in the outer and intermediate rings, and larger diameter elements in the inner and centre rings. Special buttons are attached to the elements at two planes, to provide improved heat-transfer, and hence, critical heat flux enhancement. To maintain the compatibility of the new bundle design with the design of existing CANDU 6 reactor and fuel handling systems, the basic overall dimensions of the CANFLEX fuel bundle were designed to be the same as those of the 37-element fuel bundle. The small diameter elements of the outer ring result in a slightly larger end-plate diameter, compared with the end-plate diameter of the standard 37-element bundle. Consequently, the bearing pad heights of the bundle are designed to be larger than those of the 37-element bundle. This makes the CANFLEX bundle fully compatible with the sidestop/seperator assembly of the CANDU 6 fuelling machine. The sidestop/seperator assembly is an important component in the fuelling machine—the fuel bundle dimensions must be compatible with this assembly.

CANFLEX fuel is designed to have hydraulic and neutronic characteristics that are similar to those of the existing fuel. This feature allows operators to introduce CANFLEX bundles during normal on-power refuelling. The fuel bundle, in all other respects, is designed to be equivalent to the 37-element bundle, i.e., to be "transparent" to all reactor systems. To verify this transparency, tests were performed for pressure drop and bundle strength under a number of situations such as radial cross flow; a test of the long-term fretting performance was also performed.

CANFLEX VERIFICATION PROGRAM

The CANFLEX bundle has undergone an extensive verification program [4]. The verification program has been conducted following the strategy laid out in the Design Verification Plan (DVP). The verification work consisted of analysis and testing, and drew on the capabilities of AECL's facilities in Canada and KAERI's facilities in Korea [5]. The DVP identifies the performance requirements, specifies the test or analysis required to verify that the requirement is met, and identifies responsibility and procedures. All testing and analysis conformed to the quality standard CAN/CSA-N286.2 or equivalent [6]. The DVP called for the preparation of a Test Specification outlining the test procedure, acceptance criteria and required documentation.

Thermalhydraulic Testing of CANFLEX to Establish Licensing Data

To characterize the thermalhydraulic performance of CANFLEX, pressure drop, CHF and post dryout (PDO) experiments were performed in Freon-134a in the MR-3 facility at CRL. The pressure-drop characteristics of the CANFLEX bundle were determined in both Freon tests, and hot and cold water.

Full-scale CANFLEX bundle tests were performed to obtain licensing data in the high-pressure steam-water loop at Stern Laboratories [7,8]. The test string consisted of a 6-m-long, 43-element bundle simulator. A wide range of steam-water flow conditions was covered in the CHF experiment, with an outlet pressure range of 6 to 11 MPa, mass flowrate range of 7 to 25 kg/s, and inlet fluid temperature range of 200°C to 290°C. CANFLEX was found to provide CHF enhancement over 37-element bundles for all conditions with increasing enhancement as the channel creep increases. The water CHF data have been used to derive a CHF correlation for the NUCIRC computer code, which is used to calculate critical channel powers [9]. NUCIRC Version 2.01 has been verified with the CANFLEX thermalhydraulic relationships.

Out-Reactor Flow Testing

AECL and KAERI have subjected the CANFLEX fuel bundle to a set of out-reactor flow tests, in order to simulate reactor conditions, and to verify that the design is compatible with existing CANDU 6 reactor hardware. In addition to the heat transfer and pressure drop tests, the following mechanical flow tests have been successfully completed:

- **Strength Test:** Strength tests showed that the fuel can withstand the hydraulic loads imposed during refuelling. Post-test bundle geometry measurements showed no significant distortion.
- **Impact Test:** Impact tests showed that the CANFLEX bundle can withstand bundle impact loads during refuelling.
- **Cross Flow:** Cross flow tests demonstrated that, during refuelling, when the bundle is in the cross-flow region, the bundle withstands the flow-induced vibration for a minimum of 4 h.
- **Fuelling Machine Compatibility:** Fuelling machine compatibility showed that the bundle is dimensionally compatible with the fuel handling system.
- **Flow Endurance:** Flow endurance tests demonstrated that the CANFLEX bundle maintains structural integrity during operation. Fretting wear on the bearing pads, inter-element spacers and pressure tube remained within design limits over the 3000-h test time.

In-Reactor Testing

CANFLEX bundles AJK, AJM, AJN and AKT were irradiated in the NRU research reactor at Chalk River Laboratories (CRL) Canada, to demonstrate performance under expected in-reactor conditions. Typical power changes during refuelling and peak bundle powers during operation were calculated, in order to establish the irradiation conditions for the NRU tests. Actual peak powers experienced were over 25% greater than in a CANDU 6. Once the bundles were removed, detailed post-irradiation examination (PIE) was performed. All design requirements were met.

Reactor Physics Testing and Analysis

The ZED-2 facility at CRL was used to measure the fine structure, reaction rates, and reactivity coefficients for CANFLEX NU bundles, in order to validate the reactor physics lattice code WIMS-AECL. The data showed excellent agreement with code predictions. A fuel management computer code was used to simulate reactor operation over 600 full-power days, in order to determine peak bundle powers, power changes during refuelling, burnups and residence times. Various fuel schemes were studied. Fuel performance requirements were established for NRU irradiation tests. The analysis showed that the CANFLEX bundle meets or exceeds all power requirements.

Structural Analysis

The CANFLEX design was analyzed for sheath strains, fission-gas pressure, end-plate loading, thermal behaviour, mechanical fretting, element bow, end-flux peaking and a range of other mechanical characteristics. Acceptance criteria, established from years of operating experience with 37-element fuel and previous 37-element testing, were met by the CANFLEX design.

Formal Design Review

The Verification Program results were summarized in the Fuel Design Manual. This document captures all the design requirements, points to the individual analysis or test, and shows that the requirements have been met. In 2000 February, AECL's Chief Engineer conducted a formal design review to assess the CANFLEX verification and qualification program, and the bundle's readiness for full-core implementation. Industry experts from New Brunswick Power, Hydro Quebec, Ontario Power Generation, the two domestic fuel fabricators and subject-area experts reviewed the CANFLEX Fuel Design Manual and other CANFLEX documentation. Reviewers provided written comments, which were dispositioned. The reviewers' comments were incorporated into the CANFLEX fuel design manual. The design review has been closed, and the CANFLEX Mk-IV fuel bundle design has been declared qualified for full-core implementation in CANDU 6 reactors.

CANFLEX DEMONSTRATION IRRADIATION

As a final verification of the CANFLEX design, in preparation for full-core implementation, a DI was performed at the Point Lepreau Generation Station (PLGS) [10,11,12]. The aim of the DI program is two-fold: (i) to confirm the performance of the CANFLEX bundle design in a power reactor operating environment, and (ii) to qualify the production-type CANFLEX bundles. The DI bundles were manufactured as close as practical to the mass-production route, according

to the Canadian Quality Assurance Program Standard of CAN3-Z299.2. PLGS fuel engineers selected two channels (S08 and Q20) for the DI. Channel S08 has a higher channel power and coolant flow rate than channel Q20 (6473 kW versus 4688 kW, and 23.7 kg/s versus 17.1 kg/s). All configurations of CANFLEX bundles mixed with 37-element bundles in a single channel during transition and full-core refuelling were tested. Upon discharge and transportation to the PLGS spent fuel bays, the CANFLEX bundles were visually examined. Two bundles were selected, and were shipped to CRL for post irradiation examinations. The DI was fully documented, including station data and PIE reports.

Details on the Demonstration Irradiation

In 1998 September, New Brunswick Power (NBP), at PLGS, began a two-year 24-bundle DI program. In 2000 August, the last of the DI bundles were discharged, completing the irradiation of 24 CANFLEX bundles at PLGS. From an operational perspective, the CANFLEX fuel behaved exactly as 37-element fuel would have, and there were no significant differences in any monitored aspect of station behaviour that could be attributed to CANFLEX fuel. During the summer shutdown, channel S08 underwent Spacer Location And Repositioning (SLAR) and Channel Inspection and Gauging Apparatus for Reactors (CIGAR) inspection. The fuel handling associated with these procedures was uneventful, and the results of the CIGAR inspection did not indicate any unusual wear in the channel that was related to the use of CANFLEX fuel. The high-power channel, S08, had a relatively high burnup of over 250 MWh/kgU, compared to the more standard burn-up of 175 MWh/kgU.

Irradiated Fuel In-bay Inspection

All 24 CANFLEX bundles that were irradiated have been visually inspected in the fuel bays at PLGS. The inspection team included fuelling experts from the station, a member of the CANFLEX design team, and a member of the AECL fuel inspection group—who will conduct the PIE in the cells. The examination was done using an underwater periscope; photography was achieved using a television camera attached to the periscope and digital imaging. The inspection team concluded that the bundles were in very good condition. All observations, photographs and irradiation data were sent to the design team for review and disposition. Full inspection reports have been prepared. [13].

Post-irradiation Examination

Two CANFLEX DI fuel bundles were shipped to CRL for post-irradiation examination (PIE). Bundle FLX019Z, irradiated in channel Q20 position 8, was shipped to CRL on 1999 December. This bundle reached a calculated bundle burnup of 144 MWh/kgU, and a peak outer-element linear power (OELP) of 29 kW/m. Bundle FLX007Z, irradiated in channel S08 position 8, was shipped to CRL on 2000 March 30 from PLGS. This bundle reached a calculated bundle burnup of 223 MWh/kgU, and a peak OELP of 37 kW/m.

The visual, non-destructive and destructive examinations have been completed for both bundles. No unusual features or anomalies were found visually. The following is a brief summary of the PIE results:

- Outer element straightness was found to be consistent with that of irradiated 37-element bundles.

- Bearing and spacer pad wear and end plate distortion was minor, and was also consistent with irradiated 37-element fuel.
- Typical pellet-interface ridging was found for FLX007Z, but it was not distinctive for the lower power bundle FLX019Z.
- Element gamma scans are normal, and no Cs migration to the pellet interface was evident, consistent with lower internal fission gas release.
- Fission gas volumes (1.4 to 1.7 mL at STP) and release (less than 0.1%) were small.
- No unusual features or anomalies have been found in the metallographic and ceramographic examination of bundle FLX019Z or FLX007Z (e.g., typical fuel microstructure).

Formal Disposition of DI Observations

All observations from the in-bay inspections and PIE have been formally dispositioned by the design team through root cause assessment. Some further tests and the comparison of the observations against 37-element experience were performed. Five observations were dispositioned as follows:

- (a) Marks on the sides of the CHF buttons: These marks appeared on the sides of about 1% of the buttons on the outer elements of bundles inspected in the bay. The apparent material loss on the CHF buttons was not expected. Inspection of the two archive DI bundles revealed that these buttons also had the same features as those seen in the PLGS bay; i.e., an area with a raised periphery at the side of some buttons. Based on a comparison of the marks from the irradiated fuel and the unirradiated fuel, it was concluded that this feature is a manufacturing artifact due to beryllium that was side-coated on the CHF buttons and subsequently brazed at high temperature. ZPI agreed that the artefact observed was related to a small batch production, and would not occur in a mature manufacturing line. No design action is required.
- (b) Scuff marks on end caps: These marks were not caused during manufacturing or handling. It was determined that the scuff marks were caused by the separator feeler (also called the Sensor and/or Retractor) rather than the sidestops. Chipping of the chrome plating on the feeler tip has been observed on several of the separator assemblies at the CANDU 6 stations. This results in sharp edges that would be likely to cause scratching. Similar marks have been observed on 37-element bundles in the past, because of worn components. It is concluded that the scuff marks are not related to CANFLEX design. No design action is required.
- (c) Marks on one location on all end plates: These marks were present on all CANFLEX end plates at the element 19 location. Similar marks were also found on the archived bundles. These were typical machining and deburring marks caused by the Electric Discharge Machining method used to manufacture the small prototype lot. Stamping with a die would normally be used to make end plates. Thus, no design action is required.
- (d) Near-full-surface bearing pad wear: With the exception of one mid-plane bearing pad, all end bearing pads of the DI bundles had normal wear. In general, the wear on the mid bearing pads was light, and was less than those of the 37-element bundles. Because of the surface contour of the bearing pad, the sliding wear made when a pad transverses through the channel is normally reflected in a pattern of non-full-surface wear. The near-full-surface wear was observed on one mid bearing pad of CANFLEX bundle FLX008Z, and 37-element bundle

C00131Z, both from channel S08. The near-full-surface wear does not indicate a performance problem, and is not CANFLEX-specific.

CIGAR inspections of channel S08, during the summer shutdown, detected no additional flaws and no significant degradation of pre-existing flaws that could be attributed to the irradiation of CANFLEX bundles. Based on this observation, it is concluded that the flow-induced vibration and fretting behaviour of the CANFLEX bundles in S08 is similar to the 37-element fuel bundles. The bearing pad wear was within the current irradiated fuel experience, and no design action is required.

(e) Large gap between outer elements: The CANFLEX bundles were found to have element settling in high power and high crept positions. Gaps of about 3 mm were observed between outer elements, predominantly along the sides of bundles at either the 9 or 3 o'clock positions. Sideways and outward bowing was observed on some outer elements. These large gaps between adjacent elements along the sides of the bundles led the inspection team to suspect spacer interlocking.

Bundle FLX007Z, irradiated in S08 position 8, and was shipped to CRL for PIE. This bundle achieved a discharged burnup of 223 MWh/kgU, and a peak rating of 37 kW/m. PIE found no evidence of spacer interlocking. Spacer pad wear on the top surface of the spacers was normal, and the proper mating of spacers was indicated.

Analyses on the DI bundles using as-fabricated dimensions indicated that relatively large gaps existed between spacers on the intermediate elements. From the analysis, it is concluded that (1) interelement spacers are undersized, particularly on intermediate elements; and (2) centre bearing pads are undersized (1.1 mm in height), relative to end bearing pads (1.4 mm). The large gaps between spacers, combined with centre pads that were lower than the end pads, likely contributed to the amount of fuel element deformation observed on the DI bundles. Design has proposed to (1) tighten the manufacturing specification on minimum heights for all spacer groups, in order to reduce the current gaps, but to leave sufficient gap to maintain bundle assembly and to allow passage through the bent tube gauge; and (2) set minimum bearing pad heights as 1.4 mm uniformly along the bundle, in order to reduce the amount of element deformation in-reactor. As a normal quality assurance principle, to provide feedback from the irradiation experience to design, the identified changes have been formally incorporated into Revision 5 of the CANFLEX Design Drawing.

READINESS OF CANFLEX MK-IV FOR FULL-CORE IMPLEMENTATION

Potential Benefits to Existing Stations from the Implementation of CANFLEX Fuel

Implementing CANFLEX fuel in existing CANDU 6 reactors will increase the critical channel powers (CCP). The actual CCP gain depends on individual channel conditions, such as channel creep shape, power shape and local flow conditions. CCP is calculated using the computer code NUCIRC. The increase in the CCP margin can be used by station operations to offset the margin reductions resulting from reactor aging, such as the effect of heat transport system fouling and of diametral creep of the pressure tubes. Alternatively, the increase in margin could be utilized to increase the core power output, particularly in a new reactor.

The ~20% reduction in the linear element rating of the CANFLEX bundle (compared with the 37-element bundle) results in a substantial reduction of the fission product inventory in the fuel-to-sheath gap (i.e., gap inventory). For example, at the same maximum bundle power, the iodine gap inventory in the maximum-rated element in a CANFLEX bundle is estimated to be three times lower than for the maximum-rated element in a 37-element bundle. This reduction provides several benefits. For accidents in which a number of fuel elements are predicted to fail and their fission-product gap inventory released, the radiological consequences will be reduced with the use of the CANFLEX bundles. This further enhances the safety performance of the reactor. The lower fission-product gap inventory and lower power will also lead to a lower activity burden in the heat transport circuit, in the event of fuel failures during normal operation. The lower fission-product gap inventory will also reduce the radiological contamination in the heat transport circuit arising from activity release from failed fuel. Consequently, the man-rem exposure during reactor maintenance is expected to be less, resulting in occupational health and cost benefits.

Implementation Plan

AECL, in discussion with utilities in Canada, have prepared an Implementation Plan for full-core conversion of an operating plant from 37-element fuel bundles to CANFLEX. The plan consists of the following main components:

- **Design approval:** AECL and KAERI have completed the fuel qualification program and independent design reviews. AECL's Implementation Plan calls for the design information to be presented to the CNSC, to seek acceptance that CANFLEX is an approved fuel type for normal operating conditions. All the design information is compiled into a Fuel Design Manual (FDM). The FDM contains all the design requirements for the fuel, a summary of the test results or analysis results that show CANFLEX meets these requirements, and provides references to detailed reports. All CANFLEX reports are contained in a report series, and will be provided to utilities under license.
- **Regulatory interaction, safety and licensing:** The regulatory approval process is planned to occur in two stages: (1) approval for CANFLEX loading into the reactor, and (2) approval to raise trip set-points. The division of the safety submissions in support of conversion into two separate approval steps allows the program schedule to be optimized, by first demonstrating that CANFLEX can be implemented while maintaining the safe operation of the reactor, and second, that the reactor operating set-points can be safely raised. Thus, the safety analysis objectives are to (i) demonstrate that the use of CANFLEX fuel will not result in unacceptable consequences to the design basis accidents considered in the Safety Report, and (ii) quantify the improved trip set-points that CANFLEX allows, and gain regulatory approval for their implementation once the core conversion has progressed sufficiently far to credit them.
- **Operational planning and implementation:** Since one of the design requirements of CANFLEX fuel is that it interfaces as 37-element fuel does to other reactor systems, only minimal changes should be required to operational documentation and procedures. This group of activities includes the completion of all tasks at site to change over from 37-element fuel to CANFLEX. Examples of these activities include the following: (1) review operational documents and procedures, and make the required revisions for the use of CANFLEX fuel; (2) revise core-tracking methodology, including the possibility of using

RFSP fuel management computer code with WIMS for fuelling simulations; and (3) manage fuel procurement and the fuel inventory.

Readiness of Design and Licensing Tools and Methods for CANFLEX

A formal review of the design and licensing tools has been completed. The review identified, for all computer codes used in licensing and support work, whether or not the current methodologies covered the CANFLEX design, and whether or not the current Code Validation Program (CVP) covered the CANFLEX application. With the exception of ELESTRES- IST, it was determined that all codes are capable of performing the licensing calculations for CANFLEX, and the CVP covers CANFLEX. ELESTRES is being modified and validated to address the smaller diameter elements in the CANFLEX bundle. This work will be finished by March 2002. As well, a CANFLEX CHF Look-Up Table and a CANFLEX PDO correlation are being developed for the next release of CATHENA, in order to update the current methodology.

CONCLUSIONS

The CANFLEX fuel design has been verified through extensive testing and analyses by AECL and KAERI, and has been critically reviewed under a Formal Design Review. Results from the 24 CANFLEX bundles irradiated to date in PLGS confirm the compatibility of this fuel type with existing reactor systems. AECL has developed a detailed implementation plan to convert existing CANDU 6 reactors from 37-element fuel bundles to CANFLEX bundles. The economic analysis based on the CHF-enhancement data indicates a significant payback to utilities operating CANDU reactors. The utilities now have an alternative fuel that can be deployed with confidence, in order to provide greater operating margins.

REFERENCES

1. I.J. HASTINGS, A.D. LANE and P.G. BOCZAR, "CANFLEX - An Advanced Fuel Bundle for CANDU", Int. Conf. Availability Improvements in Nuclear Power Plants, Madrid, Spain, 1989 April 10-14, and also AECL Report, AECL-9929 (1989).
2. A.D. LANE, G.R. DIMMICK, J.H.K. LAU, H.C. SUK, C.H. CHUNG and C.B. CHOI, "CANFLEX: A New CANDU Fuel Bundle with Expanded Operating Capabilities", Proc. 11th KAIF/KNS Annual Conference, Seoul, Korea, 1996 April 11-12.
3. H.C. SUK, K.S. SIM, B.G. KIM, C.B. CHOI, C.H. CHUNG, A.D. LANE, D.F. SEARS, J.H.K. LAU, I.E. OLDAKER and P.G. BOCZAR, "CANFLEX as a CANDU Advanced Fuel Bundle", presented at the Fifth International Topical Meeting on Nuclear Thermalhydraulics, Operations and Safety, Beijing, China, 1997 April.
4. P. ALAVI, I.E. OLDAKER, C.H. CHUNG and H.C. SUK, "Design Verification of the CANFLEX Fuel Bundle - Quality Assurance Requirements for Mechanical Flow Testing", presented at the Fifth International Conference on CANDU Fuel, Canadian Nuclear Society, Toronto, Canada, 1997 September 21-25.
5. C.H. CHUNG, S.K. CHANG, H.C. SUK, I.E. OLDAKER and P. ALAVI, "Performance of the CANFLEX Fuel Bundle under Mechanical Flow Testing", presented at the Fifth

International Conference on CANDU Fuel, Canadian Nuclear Society, Toronto, Canada, 1997 September 21-25.

6. CSA (CANADIAN STANDARDS ASSOCIATION), "Design Quality Assurance for Nuclear Power Plants", CAN/CSA-N286.2-96, Canadian Standards Association, Rexdale, Ontario.
7. G.R. DIMMICK, W.W.R. INCH, J.S. JUN, H.C. SUK, G.I. HADDALLER, R. FORTMANN and R. HAYES, "Full-Scale Water CHF Testing of the CANFLEX Bundle", Proc. 6th CANDU Fuel Conference, Niagara Falls, Canada, 1999 September 26-30.
8. L.K.H. LEUNG, D.C. GROENEVELD, G.R. DIMMICK, D.E. BULLOCK and W.W.R. INCH, "Critical Heat Flux and Pressure Drop for a CANFLEX Bundle String Inside an Axially Non-Uniform Flow Channel", Proc. 6th International CANDU Fuel Conference, Niagara Falls, 1999 September 26-30.
9. G.D. HARVEL, M. SOULARD, R.F.DAM, P. WHITE, R. MOFFET and G. HOTTE, "NUCIRC Simulations of a CANDU-Type Header Manifold Model", 5th CNS International Conference on Simulation Methods in Nuclear Engineering, Montreal Quebec, 1996.
10. W.W.R. INCH, P. THOMPSON, P. REID and H.C. SUK, "Demonstration Irradiation of CANFLEX in CANDU 6 Power Reactor", Proc. 14th KAIF/KNS Annual Conference, Seoul, Korea, 1999 April 8-9.
11. W.W.R. INCH, P.D. THOMPSON, M.A. CORMIER, and H.C. SUK, "Demonstration Irradiation of CANFLEX in a CANDU 6 Power Reactor", Proc. 15th KAIF/KNS Annual Conference, Seoul, Korea, 2000 April 18-20.
12. P.J. REID, R.G. STEED, R.A. GIBB and R.W. SANCTON, "A Standard Approach to Special Fuel Irradiations at Point Lepreau Generating Station", Proc. 19th Annual Conference of the Canadian Nuclear Society, Toronto, Ontario, Canada, 1998 October 18-21.
13. P.J. VALLIANT, A.M. MANZER, G.L. MONTIN, D.F. SEARS and R.G. STEED, "PLGS CANFLEX Demonstration Irradiation: Highlights of In-Bay Inspections and Hot-Cell Examinations", 7th International Conference on CANDU Fuel, Kingston, Ontario, 2001 September 23-27.

NATURAL CIRCULATION IN AN INTEGRAL CANDU TEST FACILITY*

P.J. Ingham, J.C. Luxat**, A.J. Melnyk***, T.V. Sanderson
Safety Thermalhydraulics Branch
AECL Whiteshell Laboratories
Pinawa, Manitoba, Canada
ROE ILO

Abstract

Over 70 single- and two-phase natural circulation experiments have been completed in the RD-14M facility, an integral CANDU thermalhydraulic test loop. This paper describes the RD-14M facility and provides an overview of the impact of key parameters on the results of natural circulation experiments. Particular emphasis will be on phenomena which led to heat up at high system inventories in a small subset of experiments. Clarification of misunderstandings in a recently published comparison of the effectiveness of natural circulation flows in RD-14M to integral facilities simulating other reactor geometries will also be provided.

1. INTRODUCTION

Under certain postulated accident conditions decay heat is removed from the core of a nuclear reactor by single- or two-phase natural circulation of the primary coolant. An important nuclear safety consideration is to establish that decay heat can be adequately removed in these situations.

Experiments have been conducted in the RD-14M integral test facility located at AECL's Whiteshell Laboratories, Manitoba, Canada, to gain a better understanding of the probable behaviour of natural circulation in a CANDU® type heat transport system. The data collected from these tests is used to identify and examine relevant phenomena and assist in model development. An electronic database of all experiments has been developed to aid in the validation of computer models used for safety analysis and licensing.

2. FACILITY DESCRIPTION

Figure 1 shows a simplified schematic of RD-14M, a multiple-heated channel, full- elevation, scaled, integral test facility, possessing most of the key components of a CANDU Primary Heat Transport System (PHTS). The facility is arranged in the standard CANDU two-pass figure-of-eight configuration. The facility is designed to produce similar fluid mass flux, transit time and pressure and enthalpy distributions as those typical of CANDU reactors under both forced and natural circulation conditions [1].

The reactor core is simulated by ten, 6 m-long horizontal test sections. Each test section has simulated endfittings and seven electrical heaters, or fuel element simulators (FES), designed to have many of the characteristics of a CANDU fuel bundle. Test sections are connected to headers via full-length insulated feeders. Feeders are equipped with trace heating tapes to minimise heat losses

* Funded by the CANDU Owners Group (COG) through the Safety Thermalhydraulics Working Party 5

** Nuclear Safety Technology, Ontario Hydro Nuclear, Toronto, Ontario, Canada, MSG 1X6

*** Emission Management Technology, AECL Chalk River Laboratories, Deep River, Ontario, Canada, KOJ 1JO

* CANDU is a registered trademark of Atomic Energy of Canada Limited (AECL)

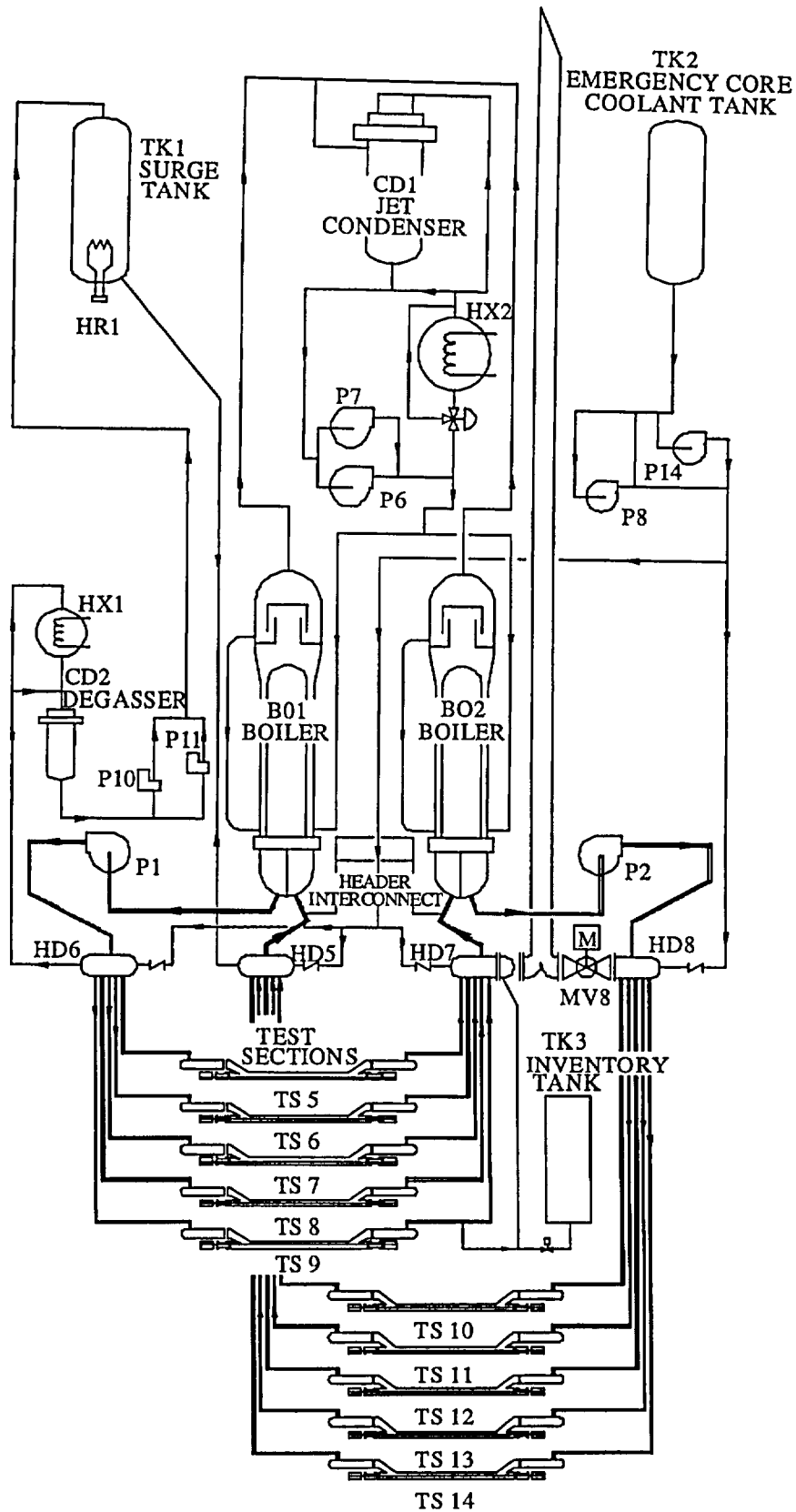


FIG. 1. Schematic of the RD-14M integral CANDU test facility

under natural circulation conditions. Pipework connecting outlet headers can also be valved in to study the effect of outlet header interconnect geometry on mitigating oscillatory behaviour at full and low power conditions.

Above header piping is also CANDU-typical including two full-height, U-tube steam generators or boilers (BO1 and B02) and two bottom-suction centrifugal pumps (P1 and P2). Steam generated in the secondary, or shell, side of the steam generators is condensed in a jet condenser (CD1) and returned as feedwater to the boilers. For natural circulation experiments conducted post 1990 a customised secondary system, designed to operate at reduced power levels typically encountered under natural circulation conditions, was utilised.

The primary-side pressure is controlled by a pressurizer/surge tank (TK1) using a 100-kW electric heater (HR1). The facility operates at typical CANDU primary system pressures and temperatures (typically 10 MPa(g) and 310°C at the outlet header).

For the natural circulation experiments described in this paper, fluid removed from the primary circuit at header 7 (HDR7) is cooled and stored in an inventory tank (TK3). Level monitoring of the inventory tank provides a record of the quantity of primary fluid removed.

The RD-14M facility is extensively instrumented. FES sheath and centre line temperatures up to 1 000°C can be measured axially in five of the seven heaters in each simulated fuel channel to provide a comprehensive picture of the FES temperature distribution. In addition flow, temperature, pressure and the void fraction of the fluid entering and leaving each test section is measured. Gamma densitometers are used to measure the void fraction of fluid at the entrance and exit to both steam generators and at the discharge of both pumps. Fluid temperature, pressure and flow rates are measured at regular intervals throughout the facility. In addition, over 50 differential pressure measurements provide an accurate picture of the pressure distribution throughout the facility. Key secondary-side measurements such as pressure, steam flow rate and temperature, feed water temperature and flow rate and internal shell-side recirculation rate are also recorded. Overall, approximately 600 instruments are scanned and recorded using a dedicated data acquisition system.

3.0 NATURAL CIRCULATION EXPERIMENTS

3.1 Test conditions

To date over 70 natural circulation experiments have been completed in RD-14M. Various parameters have been investigated as summarised in Table I.

3.2 Test procedure

Prior to the start of each test single-phase natural circulation was established and maintained for several hours at the required test conditions. When steady-state conditions were reached, data collection was initiated and several minutes of steady-state data were collected. The primary inventory was then reduced through a series of discrete drains, from header 7 into the inventory tank. Drains were separated by periods where no perturbations were intentionally introduced to allow steady-state conditions to re-establish. The drains continued until a process protection trip on high FES sheath temperatures, 600°C, was reached terminating the experiment. Slower drain rates with longer periods between drains were used in tests conducted after 1990.

TABLE I. RD-14M NATURAL CIRCULATION EXPERIMENTAL TEST CONDITIONS INVESTIGATED

CONDITION VARIED	RANGE INVESTIGATED
POWER	160, 100 and 60 kW/pass
SECONDARY-SIDE PRESSURE	4.5, 4.0, 1.0, and 0.1 MPa(g)
SURGE TANK	on/off
DRAIN RATE	0.03 to 0.2 L/s
SECONDARY-SIDE SYSTEM	High / Low Power
OUTLET HEADER INTERCONNECTS	Dynamic and Geometric Scaled
ECI ADDITION	15-33 L/s
MAKE-UP WATER ADDITION	0.08 kg/s
ECI ISOLATION VALVES	open/closed
TRACE HEATING	on/off

4. NATURAL CIRCULATION BEHAVIOUR

In all RD-14M natural circulation tests the individual channel flows were uni-directional at the start of the test. Once draining started and saturation pressure was reached void was detected in the hot leg regions of the loop. The presence of void increased flow rates throughout the loop due to an increase in the buoyancy driving force. As the primary inventory was further reduced a maximum flow rate through the steam generators was eventually reached. Subsequent reduction in the primary inventory resulted in a decrease in flow rates. In tests conducted at the higher pressures and powers, unidirectional flow was maintained throughout this stage. It is suspected that the reduction of flow resulted from a degradation in the steam generator buoyancy driving force component arising from the penetration of void into the cold leg regions of the steam generators. This phenomenon has also been postulated to explain similar behaviour in integral PWR experiments [2]. In RD-14M high pressure, high power tests (>4 MPa(g) and at 160 kW/pass), further reduction of the primary inventory lead to the establishment of an adverse pressure gradient in the steam generators. This adverse pressure gradient eventually offset the forward buoyancy driving component in the highest elevation feeders resulting in flow reversal in these channels in some tests at about 85% inventory. In all cases, core cooling was maintained even after the onset of bi-directional flow. Tests conducted at these conditions have been captured using existing simple models [3].

In tests carried out at lower secondary-side pressures ($P \leq 1.0$ MPa(g)), flows were highly oscillatory at high primary inventories and exhibited highly dynamic behaviour. Flow reversed preferentially in some channels at primary inventories of 95-90% as a result of statistically characterised lags between steam generator and feeder pressure drop components. Channels having long horizontal feeder sections immediately adjacent the end-fittings generally had the largest lags and were most vulnerable to flow reversal.

In all tests, at high and low pressures, continued reduction in primary inventory was accompanied by additional channel flow reversals. While bi-directional flow in the channels caused a break down in net flow through the loop as measured through the steam generators, it did not cause a simultaneous breakdown in core or channel cooling as shown in Figure 2. This suggests that reflux-condensation in the steam generators became the prime heat rejection mechanism at lower inventories. Similar behaviour is also reported for PWR integral tests [2].

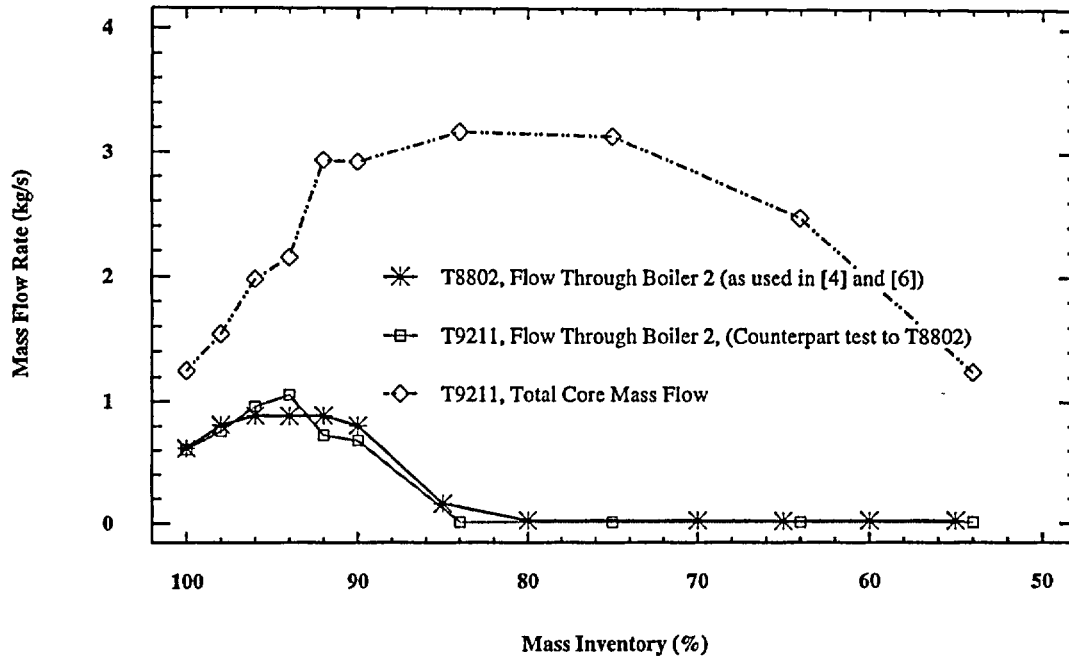


FIG. 2. Comparison of above header and total core flow in RD-14M

In the overwhelming majority of tests FES heatup did not occur until primary fluid inventories were reduced to less than 70%. A small subset of tests carried out at powers of 160 kW/pass and a secondary-side pressure of 1.0 MPa(g) has been the focus of particular interest as FES heatup occurred at primary fluid inventories greater than 85%.

4.1 Dryout at high primary fluid inventories

Dryout at primary inventories greater than 85% resulting in FES temperature excursions in excess of 600°C only occurred in 3 natural circulation experiments carried out at primary powers of 160 kW/pass and a secondary side pressure of 1.0 MPa(g). Six other tests conducted under similar conditions did not experience dryout at inventories greater than 70%. In all cases dryout did not occur until the flow in at least 2 of the 5 channels in a pass was reversed.

At these test conditions, the net buoyancy driving force component from the steam generators becomes negligible by about 90% inventory. Individual channel flow is driven by the feeder buoyancy component, which is made up of the liquid filled inflow feeder and a highly voided outflow feeder. In these 3 tests, dryout occurred following a continuous reduction in the pressure drop in the inflow feeder which caused a proportional reduction in the flow through the channel. Inflow feeder gamma densitometer and pressure drop measurements indicate this reduction was caused by void penetration of the inflow feeder (VPIF). Gamma densitometers are located on the feeder piping near the inlet and outlet of each channel. Since void is observed in the feeder, as inferred from pressure drop measurements, prior to being detected by the gamma densitometers, the void does not seem to have originated in the test section (Fig. 3).

All 9 tests showed evidence of void in an inflow feeder at some time following the onset of flow reversal. In fact, a review of natural circulation experiments conducted at other test conditions showed

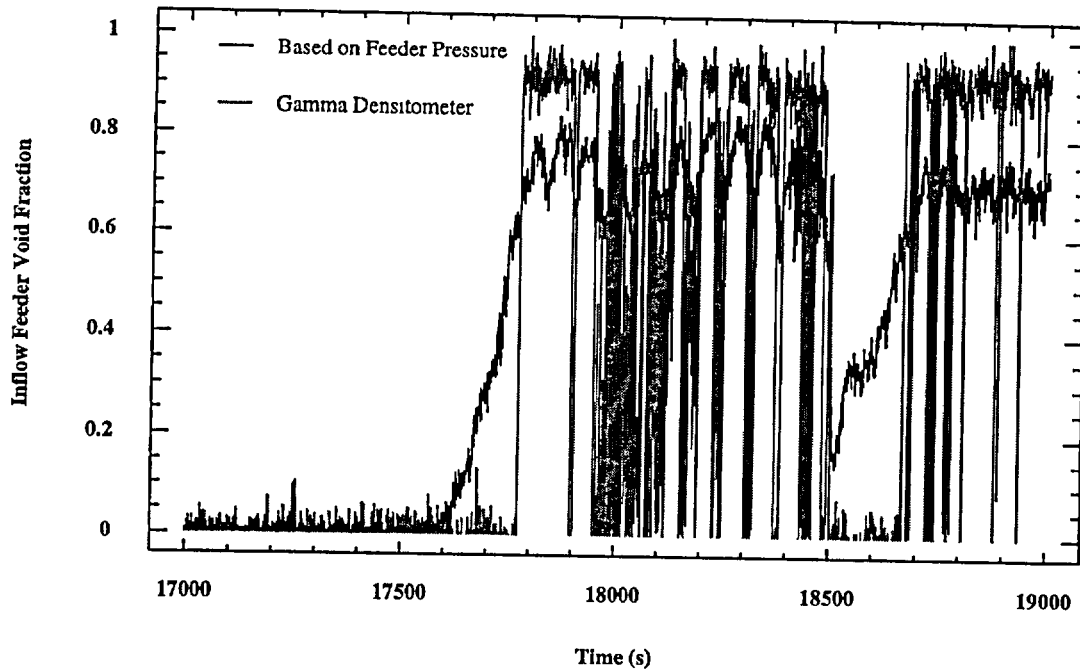


FIG. 3. Appearance of void in the inflow feeder

VPIF to be a common phenomenon. However, in all but these 3 tests the extent of void penetration of the inflow feeder was limited to an intermediate level and only resulted in a partial degradation of channel flow. In some cases, inflow feeders appeared to refill after a period of several minutes, in other cases inflow feeders remained partially voided for several hours. In these latter situations flow through the channels was reduced but did not totally break down. In the three tests experiencing dryout at high inventories, void penetrated the inflow feeder until there was no net buoyancy driving flow in one channel. Flow in all other channels remained sufficient to provide channel cooling. In tests T8809, T8810 and T9308, VPIF, and subsequent dryout, was induced by a depressurization caused by a draining operation as shown in Figure 4.

To obtain more information on conditions leading to dryout at high primary inventories and to establish limits of FES temperature excursions additional tests were carried out. These tests were conducted at power levels of 160 kW/pass and a secondary side pressure of 1.0 MPa(g). FES trips were set at 800 °C as an extrapolation of these earlier results suggested that the FES temperatures would have approached an asymptotic limit close to 700 °C had a process protection trip at 600 °C not occurred. Primary inventories were limited to greater than 80%. Primary coolant draining and/or small changes to the secondary side (10%) were used to induce dryout. Although 69 of the previous 70 natural circulation experiments had trace heating applied to the inlet and outlet feeder piping in these tests feeder trace heating was initially off.

Results from these tests showed that without trace heating only limited VPIF of Test Section 7 (TS7) and TS12 inflow feeders could be induced (Figure 5) and FES temperature excursions were limited to less than 300 °C. Turning on the trace heating resulted in immediate but limited VPIF in some inflow feeders (Figure 5). Further VPIF phenomena were then readily induced by secondary side perturbations (Figure 6). A maximum FES temperature of 675 °C was reached prior to quenching in TS 11 at a primary inventory greater than 85% (Figure 7).

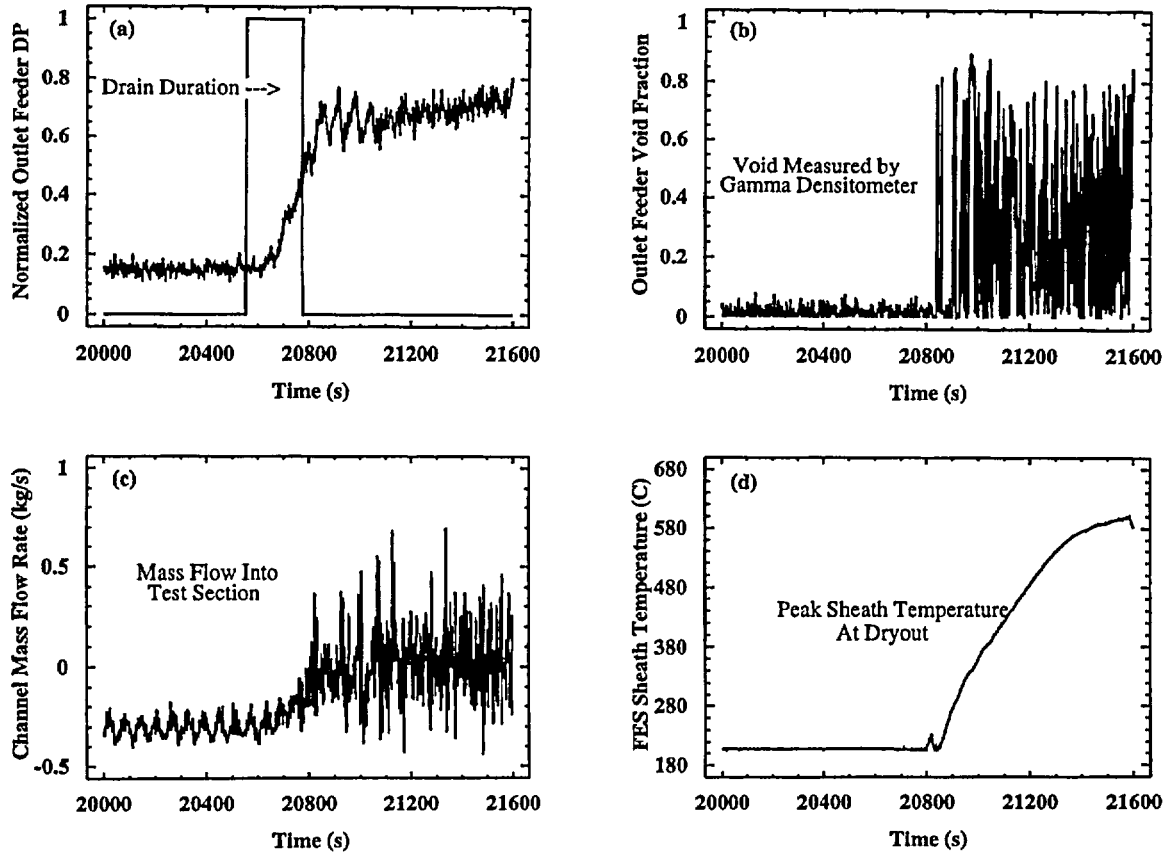


FIG. 4. RD-14M test T9308 (a) VPIF induced by draining, (b) void measured at the inflow of the test section, (c) mass flow through the channel is reduced, (d) dry out occurs at 87% mass inventory

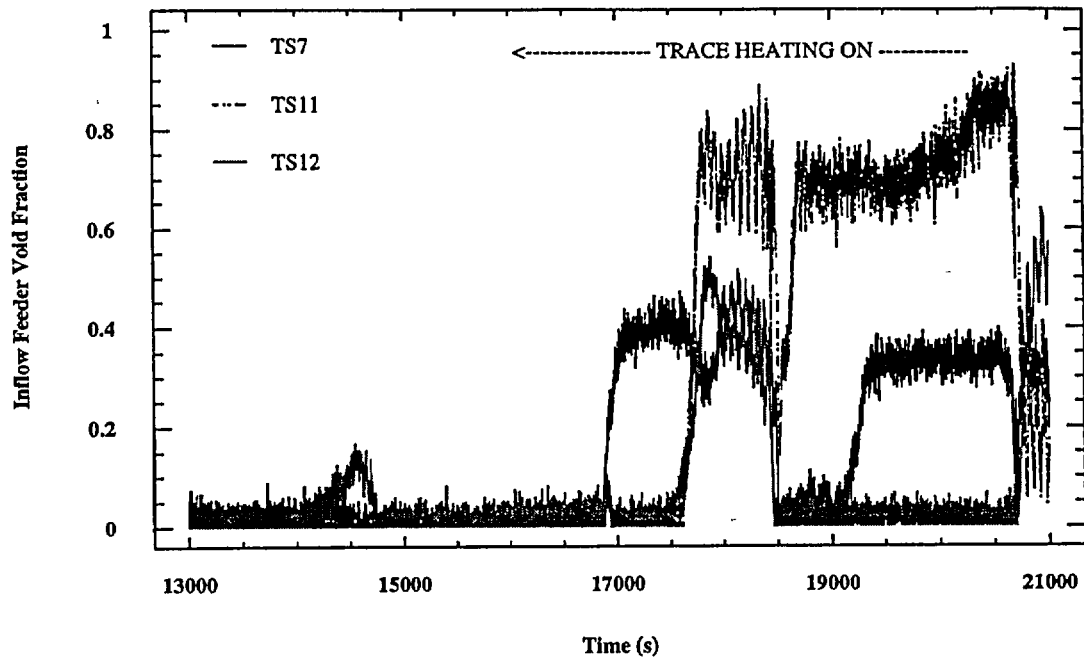


FIG. 5. The effect of feeder trace heating on VPIF

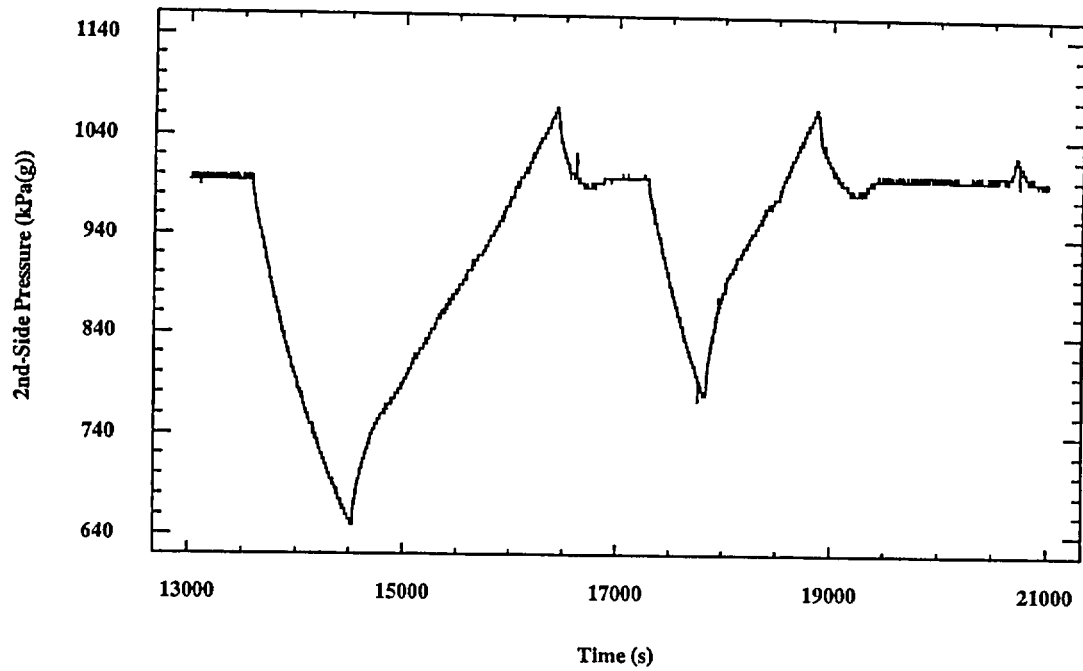


FIG. 6. Secondary side pressure transient

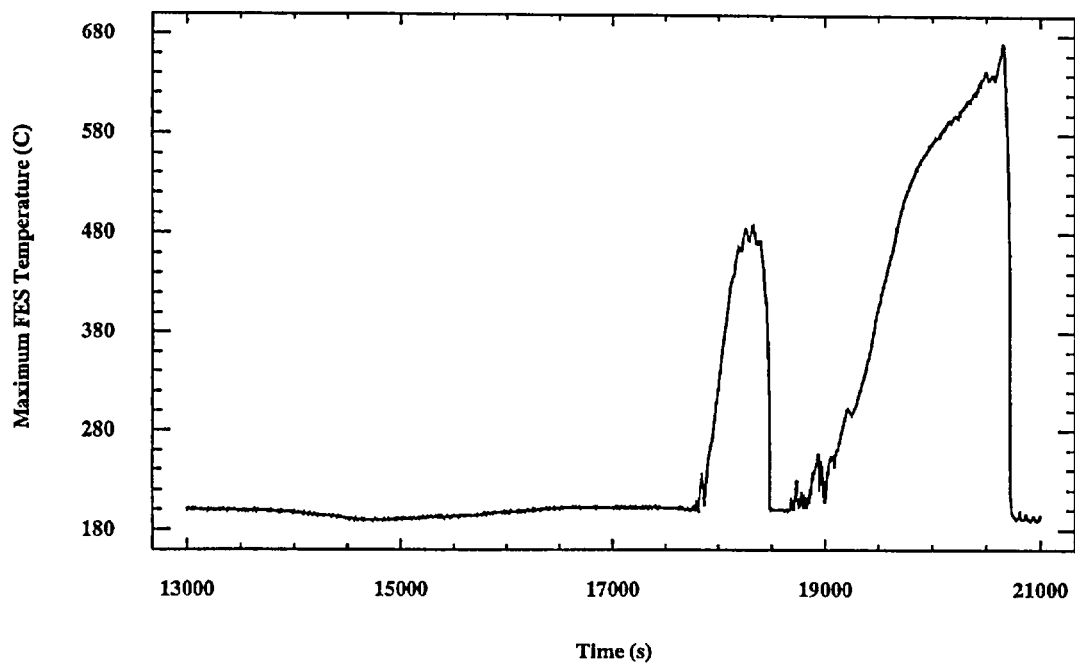


FIG. 7. Test section 11 FES temperature transient

4.2 VPIF mechanisms

It still is not clear why dryout occurred in only T8809, T8810 and T9308. However, it should be noted that T88 tests had a drain rate three times that of subsequent tests and an unplanned secondary side pressure transient during the drain prior to dryout occurred in T9308. It should also be noted that dryout only occurred at these test conditions in a reversed channel following the second channel flow reversal. Under this circumstance fluid entering the inflow feeder is at saturation temperature. A brief explanation of the various hypotheses as to the cause of VPIF follows.

Steam bubble entrainment and flashing were mechanisms considered. For steam bubble entrainment, the drag forces exceed buoyancy forces causing steam bubbles to be dragged from the header into the feeder. This mechanism should be self limiting and self correcting as a result of reduction in drag forces caused by flow reduction and bubble coalescence. Flashing would imply that void production is solely due to depressurization. This is highly unlikely since all saturated feeders should be effected instead of only a few. Flow induced flashing was also considered. This is attributable to frictional pressure drop and is highly unlikely due to the very low flow rates. This is a self correcting and non sustainable mechanism.

Liquid starvation is a mechanism where an adverse distribution of void in the headers exists such that insufficient liquid is available at the header/feeder interface to offset the flow from the feeder into the channel. Depending on the availability of liquid from the header, the liquid level in the feeder and consequently the flow into the channel will drop until a new steady-state is reached, or in extreme cases, until total flow breakdown occurs and dryout results.

Test data suggests the void entering the feeders originates from the headers and indicates that the void distribution inside the header is extremely complex. Both axial and radial variations must occur with more void present at lower elevations within the header. No direct measurements of void in the RD-14M headers are currently available. However, recent separate effect tests using an instrumented RD-14M inlet header, although not conducted at conditions expected during natural circulation, confirm these variations are possible. Work is presently continuing to extend the study of the distribution of void in RD-14M headers to conditions more typical of natural circulation.

4.3 Complicating factors affecting VPIF mechanisms

Trace heating has a marked effect on VPIF. The trace heating used for natural circulation tests in RD-14M is fixed at the start of the test and is not controllable. Following the onset of bi-directional flow, the added energy may exceed the actual heat losses and void may be generated in the inflow feeder. Trace heating also inhibits void collapse. Experiments are planned to examine this effect.

Feeder metal mass temperature can also effect VPIF. As the primary pressure drops with each subsequent drain, the saturation temperature of the fluid is reduced, possibly below the temperature of the metal pipe. Additional void production may result as stored energy from the pipe walls is transferred to the fluid. Pressure vessel requirements have resulted in an increase in the relative metal to fluid mass ratio from that expected in typical CANDU headers and feeders. Experiments are planned to study this effect as well.

5. CLARIFICATION OF A RECENT COMPARISON OF NATURAL CIRCULATION FLOWS IN OTHER INTEGRAL FACILITIES

Differences in the geometrical configuration between the CANDU PHTS and other reactor systems make direct comparison of natural circulation results difficult. Although many similarities in natural circulation phenomena between CANDU and PWR's have been identified, the multiple, horizontal-channel reactor core allows phenomena like individual channel flow reversal to occur which do not have a counterpart in other systems.

Recently, a quantitative comparison of the effectiveness of natural circulation flows in the CANDU type RD-14M facility and integral facilities simulating PWR and WWER geometries was published [4]. The RD-14M data presented in this comparison was inappropriately extracted and interpreted from an early paper for test T8802 [5]. The authors of this comparison incorrectly assumed the core flow for the RD-14M test was equivalent to the reported flow through only one of the steam generators [6]. Because of the figure-of-eight configuration, this assumption is a factor of two too low under strictly unidirectional flow conditions. The error in this assumption becomes even greater following the onset of channel flow reversal. The RD-14M experimental data used is not consistent with the author's analysis methodology. As a consequence, the magnitudes of RD-14M natural circulation flows are severely underestimated.

Core mass flow rates for the RD-14M test used in this comparison, T8802, cannot be calculated due to insufficient instrumentation in this early test. However, a more recent, better instrumented test, T9211, was conducted at the same nominal conditions as T8802. Test T9211 was the only test conducted using similar conditions and test procedure. Experimental results for T9211 are comparable to T8802 as shown in Figure 2. The similarity between these two tests is also illustrated in Table II where initial conditions, boundary conditions and key experimental results are compared. Important results to note include the similarity of inventory for the first and second flow reversals, breakdown of flow through the boilers and break down of flow in one of the channels (dry out).

The core mass flow rate is obtained by adding the mass flow rate through each channel. Individual channel mass flows are determined by correcting single-phase inflow feeder flow rate measurements made at steady-state conditions at each inventory for density.

To make an accurate comparison of RD-14M with other facilities, the total core mass flow as shown in Figure 2 should have been used in Ref. [4] instead of the flow through only one of the steam generators. As illustrated in Figure 2, both the effective range and the magnitude of the core mass flow rates are significantly larger than the values used in assessing RD-14M results. The referenced comparison implies significant core flow rates only occur over a narrow range of primary inventories (82 to 100%), whereas in reality effective core flow rates were measured at inventories as low as 48%. Similarly, the actual maximum core mass flow rate is a factor of three higher than that in the data used in the referenced comparison. It is unfortunate that the differences in facility configurations and the nature of the data used in this comparison were misunderstood. The impact of these oversights is a gross underestimation of the core cooling effectiveness of natural circulation in CANDU geometries. Superimposition of the correct data on the published comparison clearly demonstrates that natural circulation flows in a CANDU type facility are quantitatively as high, if not higher, than flows encountered in integral facilities representing PWR and WWER geometries.

TABLE II. INITIAL CONDITIONS, BOUNDARY CONDITIONS AND KEY EXPERIMENTAL RESULTS FOR COUNTERPART EXPERIMENTS T8802 AND T9211

PARAMETER / RESULT	T8802	T9211
INITIAL PRIMARY PRESSURE (MPa(g))	8.0	7.0
SECONDARY-SIDE PRESSURE (MPa(g))	4.3	4.0
PASS 1 - TOTAL POWER (kW)	100.0	101.9
PASS 2 - TOTAL POWER (kW)	101.5	101.7
INITIAL HEADER 5 TEMPERATURE (°C)	264.2	259.5
INITIAL HEADER 6 TEMPERATURE (°C)	246.9	242.9
INITIAL HEADER 7 TEMPERATURE (°C)	264.8	260.4
INITIAL HEADER 8 TEMPERATURE (°C)	248.0	244.1
TRACE HEATING (kW)	22.0	22.0
BOILER FEEDWATER TEMPERATURE (°C)	57.1	164.9
% MASS INVENTORY OF FIRST CHANNEL TO REVERSE (CHANNEL NUMBER) - PASS 1	84% (HS5)	91% (HS7)
% MASS INVENTORY OF SECOND CHANNEL TO REVERSE (CHANNEL NUMBER) - PASS 1	84% (HS7)	82% (HS7)
% MASS INVENTORY OF FIRST CHANNEL TO REVERSE (CHANNEL NUMBER) - PASS 2	89% (HS10)	91% (HS12)
% MASS INVENTORY OF SECOND CHANNEL TO REVERSE (CHANNEL NUMBER) - PASS 2	84% (HS11 & HS14)	82% (HS14)
% MASS INVENTORY WHERE FLOW THROUGH BOILERS BREAKS DOWN ^a	84%	82%
% MASS INVENTORY AT DRY OUT ^b (CHANNEL NUMBER)	48% (HS7)	48% (HS8)

^a Breakdown of flow through the boilers based on stalling of above header turbine flow meters. These meters stall at flows below 0.4 L/s.

^b Dry out based on first channel to have at least two fuel element simulator temperatures exceed 600°C.

6. SUMMARY

The key features of RD-14M, an integral CANDU test facility, have been described. An overview of the general behaviour observed in RD-14M natural circulation experiments has been discussed. Void penetration of inflow feeders (VPIF) has been identified as the mechanism responsible for early heatup in a small subset of tests. For these tests, heatup is limited to FES temperatures less than 700°C and is followed by quenching. VPIF probably originates in the RD-14M headers and is strongly coupled with both header conditions and feeder trace heating.

Natural circulation flows in RD-14M, when accurately compared on a quantitative basis to those found in integral facilities representing PWR and WWER geometries, are as good if not better.

In essence, RD-14M natural circulation results are understood and explainable. They provide a valuable experimental data base for development and validation of physical models.

7.0 REFERENCES

- [1] INGHAM, P.J., et al, "Scaling Laws for Simulating the CANDU Heat Transport System, Proc. 2nd Intern. Conf. Sim. Meth in Nucl. Engrg., Montreal, Canada (1986)
- [2] DUFFEY, R.B., SURSOCK, J.P., "Natural Circulation Phenomena Relevant to Small Breaks and Transients", Nucl. Engrg. Des., 102,115-128. (1987)
- [3] WAN, P. T., et al, "Modelling of RD-14M Partial-Inventory Thermosiphoning Tests Using the OHAT Code", 4th Intern. Sim. Meth. Conf., Montreal, Canada, (1993)
- [4] D'AURIA, F. and GALASSI, G.M., "Code Validation and Uncertainties in System Thermalhydraulics", Progress In Nuclear Energy, Vol. 33. No.1/2. Pp175-216, (1998)
- [5] MELNYK, A.J., AECL, D'AURIA, F., University of Pisa, personal communication, 1997 February 20
- [6] INGHAM, P.J., et al., "Natural Circulation Experiments in RD-14M with Emergency Coolant Injection", ANS Intern. Top. Meetg.-Safety of Thermal Reactors, Portland, Oregon, USA (1991)